Espectroscopia óptica para análises diretas: O futuro dos diagnósticos analíticos

Edilene Cristina Ferreira

Tese apresentada ao Instituto de Química da
UNESP de Araraquara como parte dos requisitos para
obtenção do título de Livre Docente

Araraquara, 2022

Dedico

A meus pais, João e Créria, responsáveis por tudo que sou;
Aos meus irmãos Ednaldo e Elisângela, companheiros de uma vida;
Ao meu esposo Ronaldo Montes, meu amor e companheiro de todas as horas;
À minha filha Giovanna, por me dar a oportunidade de experimentar o amor incondicional!

Agradecimentos

Primeiramente, agradeço a Deus por iluminar meus caminhos, provendo sempre tudo de que necessito, e me concedendo forças para perseverar em meus propósitos;

A minha família por todo apoio e incentivo à minha formação e carreira;

Minha gratidão a cada professor e pesquisador com os quais eu tive oportunidade de trabalhar e que foram de imensurável importância para o meu desenvolvimento científico e pessoal: Dra. Ana Rita A. Nogueira, Dr. Gilberto Batista de Souza, Dr. Luiz A. Rocha Batista (in memoriam), Prof. Dr. Joaquim de Araújo Nobrega, Dra. Débora M. B. P. Milori e Prof. Dr. Jesús Anzano;

Ao Instituto de Química da UNESP de Araraquara, pela minha formação e pela acolhida, quando retornei à instituição como profissional.

Aos funcionários do IQAr (docentes e técnicos administrativos) por todo apoio e aos alunos que me permitem aprender e crescer a cada dia, tanto no aspecto profissional quanto humano;

Ao Prof. Dr. José Anchieta Gomes Neto, por me acolher em seu espaço de trabalho, pela amizade, ensinamentos, discussão de resultados e parceria;

Ao Prof. Dr. Clóvis A. Ribeiro e Profa. Dra. Marisa S. Crespi, por todo apoio e companheirismo;

Ao Grupo de Espectroanalítica e Automação (GEA). A todos os alunos que integravam o GEA, no momento do meu ingresso, agradeço pela acolhida e pela oportunidade de aprender com seus trabalhos. Agradeço também a todos os colaboradores contemporâneos, meus alunos de graduação, pós-graduação, pós-doutorandos e alunos de intercâmbio que ao passarem pelo GEA deixam boas lembranças e importantes contribuições científicas. O entusiasmo e persistência de vocês são imprescindíveis para a construção do conhecimento científico;

Ao meu irmão Ednaldo José Ferreira, pelo companheirismo, pelos ensinamentos sobre estatística e técnicas de aprendizado de máquina, discussão de resultados e pela parceria;

Ao Dr. Giorgio S. Senesi, pela parceria e amizade.

Às agências de fomento, que através do apoio financeiro me proporcionam a chance de concretizar ideias, desenvolver e transmitir conhecimento científico.

“A luz é a sombra de Deus”

Albert Einsten

Resumo

O papel da espectroscopia óptica para o desenvolvimento da ciência e evolução do conhecimento sobre a composição da matéria é irrefutável e a evolução das técnicas espectroscópicas tem permitido avanços inimagináveis para diversos setores. Apesar da acelerada evolução instrumental, os métodos consolidados/oficiais, que utilizam espectroscopia óptica, ainda requerem o pré-tratamento da amostra. Ainda que atualmente se disponha de novos métodos e tecnologias para o pré-tratamento de amostras, esta etapa da sequência analítica continua sendo a mais demorada, mais susceptível a introdução de erros, a que envolve maior custo e que gera maior quantidade de resíduos químicos. Contudo, a evolução instrumental tem proporcionado o desenvolvimento de técnicas de espectroscopia óptica que dispensam o pré-tratamento da amostra, possibilitando análise direta, rápida e sem geração de resíduos químicos. Essas técnicas são simplesmente baseadas na interação da luz com a matéria para produzir espectros que contêm informações acerca da composição da amostra. Considerando o fato de que a amostra é analisada em sua forma natural, ou seja, sem pré-tratamento químico, os espectros agregam informações riquíssimas sobre a sua composição. O grande desafio analítico para aplicação dessas técnicas recai sobre o desenvolvimento de estratégias adequadas para extrair as informações contidas nos espectros, sejam para fins qualitativos ou quantitativos. Nessa perspectiva, o trabalho de pesquisa aqui apresentado tem por objetivo ilustrar as estratégias utilizadas para viabilizar diagnósticos analíticos rápidos e ambientalmente amigáveis, utilizando técnicas espectroscópicas de análise direta.

LISTA DE FIGURAS

Figura 1: Esquema de um gerador de luz laser 14
Figura 2: Esquema de um gerador de luz laser pulsado – a) cavidade bloqueada pelo modulador e b) modulador aberto 15
Figura 3: Esquema de uma montagem LIBS básica 19
Figura 4: Comparação ilustrativa dos espalhamentos Rayleigh e Raman (Stokes e anti-Stokes) 20
Figura 5: Componentes instrumentais básicos para espectroscopia Raman 21
Figura 6: Componentes instrumentais básicos para NIRS 23

SUMÁRIO

1. Introdução 8
2. Contextualização 9
2.1 História da Espectroscopia Óptica 9
2.2 O LASER - inovação para a espectroscopia óptica 13
2.3 Técnicas de análise direta 16
2.3.1 Espectroscopia de emissão óptica em plasma induzido por laser (LIBS) 16
2.3.2 Espectroscopia Raman 19
2.3.3 Espectroscopia na região do infravermelho próximo (NIRS) 22
3 Ciência de dados: estratégia à extração de informações espectrais 24
4 Contribuições das pesquisas com espectroscopia óptica para os diagnósticos diretos, simples e rápidos 27
4.1 Determinação quantitativa de Cu em solos empregando um sistema LIBS portátil e redes neurais artificiais 28
4.2 Uso de comitês de preditores e a técnica LIBS para certificação de cafés 29
4.3 Uma nova forma de estimar o grau de humificação da matéria orgânica do solo, usando LIBS 29
4.4 Estendendo a aplicação de LIBS para estimar o pH de amostras de solo 30
4.5 Aplicação da LIBS para determinação da textura de solos 31
4.6 Potencial da LIBS para análise da qualidade café moído e não torrado 32
4.7 Determinação de Ca em fertilizantes a base de biocarvão, utilizando Na como padrão interno 33
4.8 Determinação de K em fertilizantes a base de biocarvão por LIBS na presença de elementos facilmente ionizáveis 33
4.9 Determinação de P em fertilizantes utilizando LIBS associada à um sistema de descarga elétrica. 34
4.10 Predição dos teores de grãos defeituosos (pretos, verdes e ardidos) em misturas com grãos bons, utilizando a técnica LIBS 35
4.11 Avaliação da autenticidade de arroz marrom por SD-LIBS 35
4.12 Determinação da origem botânica de arroz utilizando SD-LIBS 36
4.13 Incineração seca para o aumento de sinal na técnica LIBS 36
4.14 Detecção e quantificação de adulterantes em mel, utilizando LIBS 37
4.15 Uso da emissão diatômica de CN para determinação de N usando LIBS 38
4.16 Avaliação de método de calibração baseado em um único padrão de calibração para determinar P e Al por SD-LIBS 39
4.17 Espectroscopia Raman para discriminação de milho transgênico 39
4.18 Identificação geográfica protegida de mel por SD-LIBS 40
4.19 Determinação de fósforo em fertilizantes a base de biocarvão usando SD-LIBS..... 41
5 Conclusões 41
6 Referências 42
7 Anexos 46

1. Introdução

A espectroscopia óptica está amplamente difundida em diversas áreas do conhecimento, inclusive em nosso cotidiano. Quando os olhos humanos detectam a cor de um objeto irradiado pela luz branca do sol, um tipo de espectroscopia está se concretizando. O objeto absorve alguns comprimentos de onda que compõem a luz branca e transmite um residual não absorvido, que é visto como cor. Assim, a cor exibida pelo objeto está intrinsecamente relacionada aos diferentes comprimentos de onda absorvidos, que por sua vez, estão relacionados à composição química do objeto [1,2]. É nessa perspectiva de investigar e interpretar a matéria, a partir de sua interação com luz, que se fundamenta a espectroscopia óptica.

A interação da luz com a matéria ocorre porque ambas possuem características elétricas e magnéticas. Os átomos constituintes da matéria apresentam características elétricas devido à presença de cargas (elétrons) e magnéticas, devido ao movimento dessas cargas, enquanto a radiação eletromagnética se propaga através de campos elétricos e magnéticos [2].

A interação luz-matéria pode ser monitorada através de diferentes fenômenos luminosos (emissão, absorção, espalhamento), e a interpretação desses fenômenos viabiliza inferências sobre a composição da matéria [3].

Atualmente, alguns arranjos instrumentais para espectroscopia óptica priorizam a análise de soluções. Dessa forma, grande parte das demandas analíticas requerem o pré-tratamento da amostra antes da análise. Em geral, os procedimentos utilizados para o pré-tratamento da amostra demandam tempo, reagentes químicos e geram resíduo, além de descaracterizar a composição original da amostra. Então, para interpretar a matéria de forma mais ampla, é necessário recorrer a diferentes técnicas analíticas e submeter a mesma amostra a pré-tratamentos específicos requeridos para cada tipo de análise. Desse modo, custos elevados são outorgados aos setores que requerem diagnósticos/laudos químicos para as tomadas de decisões. Além disso, a morosidade dos métodos faz com que o conhecimento dos laudos ocorra somente alguns dias após a coleta das amostras, ocasionando o retardamento das intervenções, o que pode impactar diretamente a economia de um setor em transformações dinâmicas, que necessita de ações rápidas.

A interação direta luz-matéria, utilizada pelas espectroscopias ópticas de análise direta, pode proporcionar mais amplo acesso à composição original da matéria. O desafio científico está em como explorar a informação luminosa coletada após a

interação. Em adendo ao maior acesso à informação química, as técnicas de espectroscopia óptica para a análise direta fornecem resultados rápidos, dispensam a utilização de reagentes e apresentam potencial para análise *in situ,* características altamente desejáveis para os mais diversos setores que dependem dos diagnósticos químicos.

Para a finalidade deste documento serão ilustrados os trabalhos que vêm sendo desenvolvidos na perspectiva de explorar técnicas de espectroscopia óptica para análise direta de amostras. Esses trabalhos têm como objetivo geral desenvolver conhecimento sobre as condições analíticas mais adequadas para análise e propor métodos simples, rápidos, condizentes com a química analítica verde, capazes de acessar, de forma mais ampla, a composição química de amostras e relacioná-la com as causas dos fenômenos naturalmente observados. Esta abordagem compreende a espectroscopia de emissão óptica em plasma induzido por laser (LIBS, do inglês *Laser-Induced Breakdown Spectroscopy*), o "carro chefe" dos estudos, além da espectroscopia Raman e espectroscopia na região do infravermelho próximo (NIRS, do inglês *Near Infrared Spectroscopy*), as quais temos começado a utilizar mais recentemente.

2. Contextualização

Descreve-se neste tópico um apanhado sobre os principais aspectos que permitem melhor compreender o propósito da linha de pesquisa abordada nesta tese.

2.1 História da Espectroscopia Óptica

A compreensão dos princípios que regem a espectroscopia óptica se deu a partir do entendimento sobre a natureza da luz e, consequentemente, sobre a forma de manipulação dessa entidade física.

Desde a antiguidade, a luz despertava a curiosidade humana, o que permitiu o desenvolvimento de conhecimentos e teorias sobre a sua natureza. Há aproximadamente 400 anos a.C. foi proposto por Pitágoras que partículas eram emitidas pelos olhos quando um objeto era visto [4]. Já no século XVII, na tentativa de explicar a propagação da luz, o físico inglês Isaac Newton propôs a teoria corpuscular, a qual foi publicada em seu famoso livro *Opticks* em 1704. Para Newton, a luz era constituída por pequenos corpúsculos que se propagavam em linha reta e que ao se depararem com um objeto, tinham suas trajetórias interrompidas, gerando a sombra.

Através da teoria corpuscular e das leis da mecânica quântica, que preveem a reversão de movimento após colisão, Newton explicava o fenômeno de reflexão da luz como sendo a reversão de movimento dos corpúsculos, após colidirem com uma superfície espelhada [5]. A teoria corpuscular tartareava apenas para explicar o fenômeno da refração.

Em 1680, o holandês Christiaan Huygens propôs a teoria ondulatória da luz. Para Huygens, as ondas de luz se propagavam devido à presença de uma substância invisível, inodora e sem massa que preenchia todo espaço, a qual chamou de “éter luminífero” [6]. Com essa teoria, Huygens explicava bem os fenômenos de reflexão, refração e interferência da luz, mas a teoria ondulatória de Huygens foi negligenciada por quase 100 anos, devido à influência científica que Newton exercia na época. Todavia, em 1802, a teoria de Newton foi desafiada pelos experimentos de Thomas Young, que validavam uma concepção ondulatória para a luz. Young mostrou que um feixe de luz ao se deparar com fendas estreitas realizava um desvio (difração), o qual não podia ser explicado pela teoria corpuscular de Newton. Young também demonstrou que luz proveniente de duas fendas, ao se sobreporem, interferem uma na outra para se reforçarem ou se destruírem, dependendo da diferença do caminho das duas ondas. Assim, retomava-se o princípio sobre a natureza ondulatória da luz [7].

Os experimentos de Augustin Jean Fresnel sobre a difração da luz, publicados em 1818 reforçavam a natureza ondulatória da luz e explicavam sua propagação retilínea em meios homogêneos e isotrópicos [8]. Juntamente com Dominique François Arago, Fresnel demonstrou que não há interferência entre dois raios de luz com polarizações perpendiculares, conceito que permitiu a Thomas Young concluir sobre a onda transversal (direção da vibração perpendicular à direção da propagação) [7,9].

Por volta de 1821, Michael Faraday demonstrou que a variação temporal de campo magnético produzia campo elétrico e, em 1850, fortalecendo a concepção ondulatória, Jean Bernard Léon Foucault provou que a velocidade da luz na água era inferior à velocidade da luz no vácuo e calculou a velocidade da luz no ar, obtendo o valor de 298 000 km/s [6-7].

Apesar de todo o conhecimento desenvolvido até 1860, ainda não era possível consolidar a natureza da luz como onda, pois as ondas conhecidas na época eram as mecânicas, as quais dependem de um meio físico para se propagarem e a ideia de Huygens sobre o “éter luminífero” era muito frágil para sustentar a teoria ondulatória. Então, em 1860, James Clerck Maxwell, baseado nos trabalhos de Faraday, mostrou que eletricidade e magnetismo estavam intimamente relacionados. Maxwell mostrou,

através suas equações matemáticas, que ao fazer uma corrente elétrica oscilar, era possível produzir campos elétricos e magnéticos que se propagavam a altas velocidades. Assim, Maxwell concluiu que a luz consiste de ondas eletromagnéticas transversais que não requerem meio para propagação e se propagam à velocidade fixa, a velocidade previamente determinada por Foulcalt. Em 1888, Heinrich Rudolf Hertz desenhou um detector e um oscilador que permitiram gerar e detectar ondas eletromagnéticas, comprovando as teorias de Maxwell [6-7].

No fim do século XIX, a teoria ondulatória parecia ser completamente apropriada para explicar a natureza da luz. Entretanto, em 1900, a utilização da teoria quântica de Max Planck, para explicar a distribuição de energia de um corpo negro, fez com que Albert Einstein introduzisse o conceito de quanta de energia, o que mais tarde foi denominado fóton. Dessa forma, retomava-se a perspectiva sobre a natureza corpuscular da luz e desenvolvia-se a teoria da dualidade partícula-onda [6-7].

O conceito dual da luz é de extrema relevância para a compreensão da interação da luz com a matéria, uma vez que alguns fenômenos como absorção e emissão são mais bem compreendidos se a luz é considerada como partícula (fóton), enquanto outros, como o espalhamento e reflexão são mais bem compreendidos ao considerar a luz como onda [3].

Paralelamente à evolução do conhecimento acerca da natureza da luz, iniciavam-se descobertas que culminariam no surgimento da espectroscopia óptica. Em 1648, Johannes Marcus Marci publica o livro *Thaumantius*. Neste documento, disponível na Linda Hall Library (Kansas City), Marci discorre sobre o arco-íris celestial e a natureza das suas cores, sua origem e causas, explicando-o corretamente como resultado da difração da luz. Aproximadamente 20 anos mais tarde, Isaac Newton comprovou a produção de um espectro colorido a partir da difração da luz branca em um prisma e a recomposição da luz difratada, empregando um segundo prisma. A partir de seus experimentos, Newton foi capaz de explicar o fenômeno da difração de forma mais rigorosa que Marci [10].

O conhecimento sobre as energias associadas às diferentes frequências que compõem o espectro visível surgiu em 1777 com os experimentos do químico sueco Carl Wilhelm Scheele. Utilizando um prisma, Scheele difratou a luz branca e com as diferentes frequências difratadas da região visível irradiou porções de cloreto de prata. O experimento mostrou que a redução dos íons Ag^+ e, portanto, o escurecimento observado, era mais efetivo para as porções irradiadas pelas frequências próximas à frequência que produz a cor violeta no espectro visível. Assim, Sheele concluiu que a

radiação violeta era a mais energética do espectro. A radiação ultravioleta foi descoberta em 1801 de forma independente por Johann Wilhelm Ritter e William Hyde Wollaston os quais, conduzindo experimentos similares aos de Sheele, observaram que a reação de redução dos íons Ag^+ se dava de forma mais efetiva quando o cloreto de prata era exposto a uma frequência da radiação invisível, difratada ao lado da frequência que produz a cor violeta no espectro visível [11-12].

Quase concomitantemente, no ano de 1800, o astrônomo William Herschel, conduzindo um experimento similar ao de Sheele, mas utilizando termômetros no lugar de cloreto de prata, observou que a temperatura aumentava pela incidência da luz e que o aumento era mais efetivo quão mais próximo o termômetro estivesse das frequências que produzem cor vermelha no espectro visível. Herschel também comprovou que a radiação invisível difratada além do vermelho aumentava a temperatura do termômetro de forma mais efetiva do que a frequência da radiação vermelha, evidenciando a existência do infravermelho. Os experimentos de Herschel permitiram entender que as radiações vermelha e infravermelha não possuem energia para promover reações que envolvem transição eletrônica, mas fornecem energia necessária para aumentar a vibração de moléculas [11-12].

A partir dos experimentos de Newton, acreditava-se que o espectro solar era totalmente contínuo, então, em 1802, trabalhando com um feixe de luz muito estreito, obtido a partir uma fenda de cerca de 0,01 mm, William Hyde Wollaston mostrou que o espectro solar continha sete linhas negras a ele sobrepostas. Nessa mesma perspectiva, Joseph von Fraunhofer, um jovem alemão construtor de instrumentos ópticos, usando prismas e grades de difração desenvolveu, em 1814, o primeiro espectroscópio, um marco para a espectroscopia óptica, e com ele identificou 574 linhas escuras no espectro solar. Além do mapeamento das linhas escuras sobre o espectro contínuo, Fraunhofer também notou que a radiação emitida devido ao decaimento de átomos excitados, ao passar por um prisma, gerava um espectro discreto, composto por linhas brilhantes que pareciam coincidir com as linhas negras sobrepostas ao espectro contínuo da luz solar. Mais tarde, em 1859, Gustav Kirchhoff e Robert Bunsen criaram um espectroscópio, instrumento que permitiu explicar que as linhas negras observadas por Fraunhofer eram provenientes do fenômeno de absorção atômica. O espectroscópio de Bunsen e Kircchoff também propiciou a descoberta de novos elementos químicos como Rb e Cs [11-13].

Nas últimas décadas, o avanço da eletrônica tem propiciado o desenvolvimento de instrumentação espectroscópica cada vez mais sofisticada e miniaturizada, conferindo facilidade de manuseio e agilidade para obtenção de resultados analíticos.

2.2 O LASER - inovação para a espectroscopia óptica

A compreensão sobre a natureza da luz e processos de absorção e emissão atômicas permitiu o desenvolvimento de diferentes formas de produção e manipulação de luz, inclusive a luz LASER (do inglês *Light Amplifcation by Stimulated Emission of Radiation*), amplamente aplicada em diversos setores como saúde, indústria, pesquisa, etc.

A luz laser é originada a partir da interação da radiação eletromagnética com átomos e moléculas que constituem meios materiais e sua forma peculiar de geração acaba conferindo propriedades características a esse tipo de luz [6].

A base conceitual que culminou no desenvolvimento do laser foi proposta em 1916 por Albert Einstein ao descrever que a emissão estimulada de luz é um processo que deve ocorrer juntamente com a absorção e a emissão espontânea. A emissão estimulada consiste na desativação do estado excitado de um átomo por um fóton de frequência específica para interagir com um elétron excitado e induzir sua transição para um nível de energia menor. O estímulo para desativação do estado excitado é feito antes que ocorra o decaimento natural do átomo e o fóton proveniente da emissão estimulada apresenta características idênticas ao fóton estimulador, ou seja, mesma frequência, fase, polarização e direção [7].

Um gerador de luz laser consiste basicamente de três partes: um meio material ativo, uma fonte externa de energia e uma cavidade óptica ou ressonador (Fig 1).

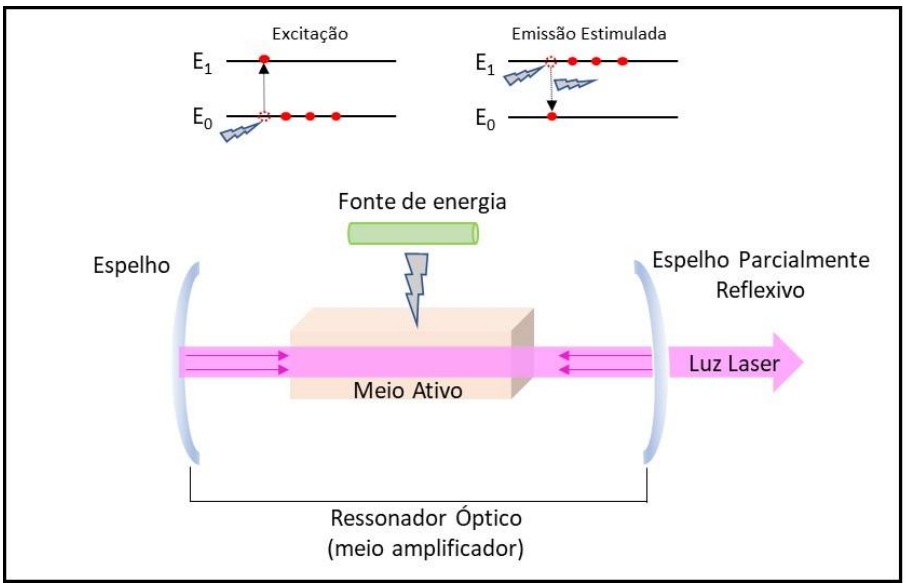


Figura 1: Esquema de um gerador de luz laser
Fonte: Autora

O meio ativo que pode ser sólido, líquido ou gasoso, porta os átomos ou moléculas que proverão elétrons a serem excitados e que, posteriormente decairão através de estímulo externo. Um bom meio ativo é constituído por espécies químicas cujos elétrons permanecem por tempos relativamente longos no estado excitado. O maior tempo para o decaimento natural permite acumular espécies no estado excitado, as quais podem ser estimuladas a decair, pela ação de um fóton externo. O espaçamento quântico nos átomos ou nas moléculas, pelos quais os elétrons transitam na excitação e relaxação, é característico do meio ativo e possui também "*gaps"* de energia característicos. Assim, considerando a equação que relaciona a energia (E) com a frequência da luz (ν), **E= h ν** (onde h é a constante de Planck), é possível prever a frequência da luz laser a ser gerada por um determinado meio ativo [14].

A fonte de energia externa é responsável por iniciar o processo de geração da luz, excitando as espécies do meio ativo. Uma fonte luminosa, capaz de fornecer fótons para excitação das espécies é comumente utilizada. O bombeamento do meio ativo com fótons excita os elétrons e, quando a maioria dos átomos apresentam elétrons no estado excitado, diz-se que ocorreu uma inversão de população. O decaimento dos elétrons a níveis de menor energia resulta em fótons que vão se acumulando na cavidade óptica ou ressonador. A cavidade contém espelhos em suas extremidades que refletem os fótons, os quais percorrem a cavidade, viajando de um lado para o outro provocando mais emissão estimulada, em um processo denominado amplificação. O tamanho da cavidade óptica tem a função de selecionar a frequência

da onda a ser gerada. Somente os fótons que se propagam ao longo do eixo principal do laser é que vão sofrer as várias reflexões no interior da cavidade ressonante. Uma abertura ou a reflexão parcial de um dos espelhos da cavidade permite a saída de luz do gerador continuamente. A luz laser que emerge do gerador, apresenta quatro importantes propriedades: monocromaticidade, alta intensidade, direcionalidade, além de coerência espacial (ondas sucessivas em fase) e temporal (mesma direção e mesmo comprimento de onda) [6,14].

O processo acima descrito refere-se à produção de um feixe contínuo de luz laser. Entretanto, algumas aplicações espectroscópicas demandam lasers de maior irradiância (potência radiante/área) no ponto focal, que somente é obtida, utilizando laser pulsado. Para obtenção do laser pulsado é preciso prevenir a emissão estimulada, armazenando mais átomos no estado excitado e limitando o fluxo do decaimento espontâneo. Para essa finalidade, uma estratégia denominada *Q-switching* é normalmente utilizada. O *Q-switching* consiste em colocar um modulador na cavidade óptica para fechar a saída do fluxo de luz e impedir que os fótons viajem de um lado para o outro da cavidade, como esquematizado na Figura 2.

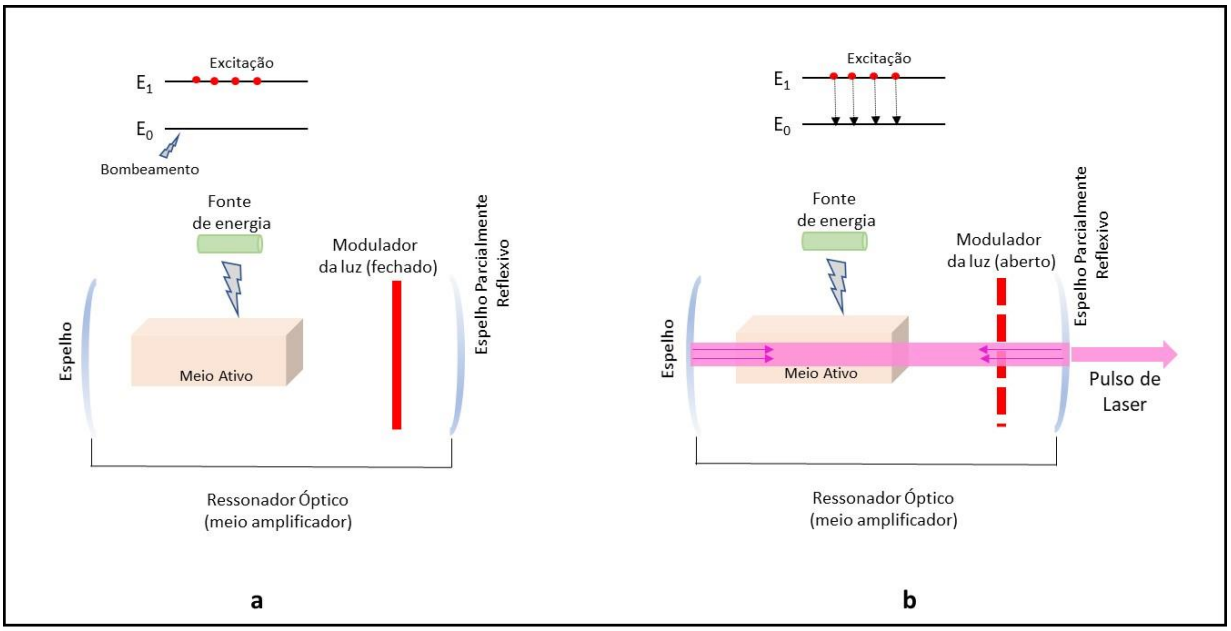


Figura 2: Esquema de um gerador de luz laser pulsado – a) cavidade bloqueada pelo modulador e b) modulador aberto
Fonte: Autora

Nessa situação, o bombeamento do meio ativo produz um número de átomos no estado excitado maior do que é perdido por emissão espontânea, causando um aumento considerável na população do estado excitado. Após um certo tempo, com

uma população elevada de átomos no estado excitado, a emissão estimulada torna-se muito provável e todos os átomos armazenados no nível superior caem abruptamente, emitindo fótons estimulados. Assim, a cavidade do laser é preenchida com fótons estimulados ao mesmo tempo em que o nível superior se esvazia. O resultado é a emissão de um pulso curto e altamente energético através do espelho de saída com poder irradiante capaz de exceder o limite de ruptura de superfícies sólidas (10^6 – 10^9 W cm^{-2}) [15].

Antes dos anos 60, a instrumentação analítica assistida por lasers era considerada exótica. Porém, de forma gradativa, este tipo de instrumentação foi se tornado popular por oferecer características interessantes para obtenção de diagnósticos analíticos rápidos de diferentes naturezas.

2.3 Técnicas de análise direta

A possibilidade de conduzir as análises espectroscópicas de forma rápida, direta e sustentável é uma demanda emergente. Atualmente, diversas técnicas analíticas apresentam em sua concepção o potencial para realizar análises com essas características e obter um panorama bastante amplo sobre a composição das amostras. Apesar dos espectros provenientes da análise direta permitirem o acesso a muitas informações sobre a composição da amostra, a escolha de condições adequadas para as medidas espectrais é muito importante para que se obtenha informações espectrais fidedignas da amostra. Então, para melhor compreensão dos trabalhos que têm sido desenvolvidos serão abordados, nesse tópico, os princípios básicos das técnicas espectroscópicas que têm sido utilizadas.

2.3.1 Espectroscopia de emissão óptica em plasma induzido por laser (LIBS)

Os avanços tecnológicos da década de 80 permitiram o desenvolvimento e a proliferação de fontes de lasers compactos e de detectores e instrumentação ótica potencialmente eficientes. As fontes de laser, atualmente disponíveis, são bastante poderosas, podendo proporcionar energia de centenas de milijoules em pulsos de curta duração (6 a 10 ns). Essa tecnologia tem permitido a evolução de técnicas analíticas, como a espectroscopia de emissão óptica em plasma induzido por laser conhecida pelo acrônimo LIBS [16].

A LIBS é uma técnica de espectroscopia óptica multielementar que utiliza pulsos de laser de alta energia para criar um plasma. Na análise direta de amostras sólidas, o pulso do laser promove amostragem do material, removendo massas da ordem μg-ng. O superaquecimento instantâneo da porção removida promove fusão e vaporização em curtíssimo espaço de tempo (ns-ps). A ação do pulso do laser sobre a massa vaporizada promove ruptura dielétrica (*breakdown*), ionização e atomização. Os elétrons livres, gerados a partir dos processos de ionização, absorvem fótons do laser e ganham energia cinética (processo denominado *Bremsstrahlung* inverso), favorecendo os processos de colisão com átomos neutros. As colisões resultam em mais ionização e este processo de ionização em "cascata" culmina na formação de um plasma. O plasma se expande rapidamente, enviando uma onda de choque ao seu redor e seu núcleo pode atingir temperaturas tão elevadas quanto 20.000 K. Após 0,5 ou 1,0 μs, as espécies neutras no plasma entram em equilíbrio local termodinâmico e, a partir desse instante, estados eletrônicos superiores de átomos e íons começam a ser populados por elétrons, de acordo com o equilíbrio de Boltzmann [17-19].

À medida que o plasma esfria, ocorre emissão de luz branca e brilhante denominada *continuum*, a qual é causada por processos de *Bremsstrahlung* (perda de energia cinética dos elétrons livres). Concomitantemente, os átomos neutros e íons excitados começam a decair, liberando a energia absorvida na forma de radiação eletromagnética. Para um pulso de laser, com duração aproximada de 9 ns, observa-se o decaimento da intensidade da emissão contínua a partir de aproximadamente 10 ns e quase que a extinção desta emissão, a partir de 10 μs. Assim, a otimização do tempo, que se deve aguardar para iniciar a aquisição do sinal a partir do pulso do laser (*delay time*), permite separar a emissão contínua da emissão das espécies de interesse. A otimização do tempo de aquisição do sinal analítico também é muito importante para evitar a coleta de sinais de baixa intensidade. Uma vez que o plasma vai esfriando até sua completa extinção, processos de recombinação dos átomos e íons vão ocorrendo e a recombinação ocasiona a perda do sinal do analito [16].

Os comprimentos de onda das radiações emitidas pelas espécies que decaem são características das mesmas e, portanto, um registro das emissões em função do comprimento de onda permite inferir sobre a composição química elementar da amostra. Já as intensidades da emissão podem ser utilizadas para fins quantitativos e semi-quantitativos [16-17].

A análise quantitativa por LIBS não é tão trivial quanto a qualitativa, pois alguns fenômenos intrínsecos ao processo de análise deterioram a esperada

proporcionalidade entre o sinal de emissão e a concentração do analito. Assim, sinais diferentes são obtidos para um analito presente em concentração idêntica em amostras diferentes. Esses efeitos são denominados efeitos de matriz e dificultam o estabelecimento de padrões de calibração para os métodos, dada a dificuldade em se encontrar materiais certificados com matrizes idênticas às das amostras, especialmente porque dentro de uma mesma classe de amostras, pode-se observar variações em suas composições físico-químicas. Além do efeito de matriz, a baixa sensibilidade das análises por LIBS, comparada à das técnicas analíticas elementares convencionais, e a baixa precisão constituem fatores que devem ser considerados para o desenvolvimento de métodos quantitativos [17].

A instrumentação de LIBS consiste basicamente em uma fonte de laser pulsado de alta energia, lentes para focalização do pulso de laser na superfície da amostra (visando obter altos índices de irradiância), lentes para coleta da luz emitida no plasma, fibras ópticas para condução da luz emitida e espectrômetro. O laser normalmente utilizado em LIBS é o Nd:YAG, que consiste em um cristal de granada de ítrio e alumínio dopado com neodímio (Nd:$Y_3Al_5O_{12}$). A granada é um grupo mineral de nesossilicatos isoestrutrais e a YAG é a granada mais comumente utilizada em lasers de estado sólido. No caso do Nd:YAG, o íon dopante, Nd^{3+} é o elemento laser ativo [6]. O espectrômetro consiste de duas partes: i) dispositivo de difração, para separação das frequências emitidas pelas diversas espécies no plasma, ii) dispositivo de detecção de fótons e conversão em sinais elétricos, sendo os dispositivos de carga acoplada (CCDs ou iCCDs) os mais utilizados. Um computador é utilizado para o controle dos disparos dos pulsos do laser, sincronização do espectrômetro, processamento dos sinais e exibição dos espectros de emissão (intensidade x comprimento de onda). Um esquema básico de uma montagem LIBS é mostrado na Figura 3.

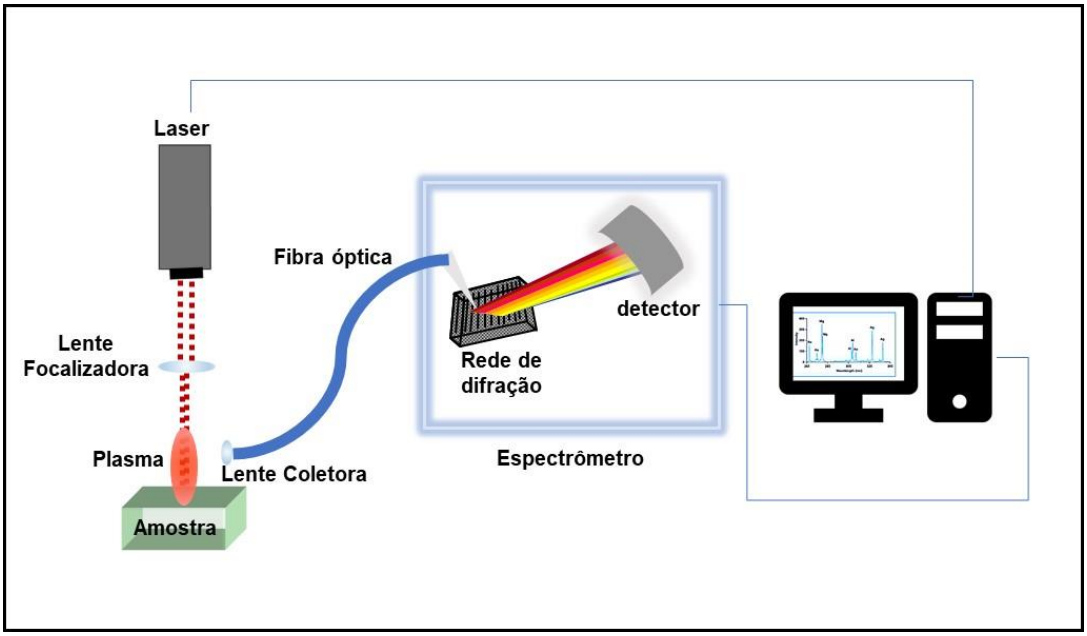


Figura 3: Esquema de uma montagem LIBS básica
Fonte: Autora

Por apresentar estruturas rotacionais finas, as moléculas diatômicas também podem ser monitoradas por LIBS. A exploração de espécies diatômicas em espectros LIBS amplia o potencial da técnica ao permitir o acesso à composição orgânica das amostras. Algumas bandas de emissão molecular diatômicas atribuídas às moléculas de C2, CN, CH, NH e OH podem ser correlacionadas à liberação direta de moléculas orgânicas originais ou a grandes fragmentos orgânicos primários [20].

A possibilidade de acessar informações elementares e algumas informações orgânicas a partir de uma simples interação laser-amostra, em tempos curtos de análise (da ordem de ms), faz de LIBS uma ferramenta analítica fantástica para atender às demandas por diagnósticos rápidos e ambientalmente amigáveis.

2.3.2 Espectroscopia Raman

A denominação da técnica Raman originou-se do nome do físico indiano Chandrasekra Venkata Raman, que comprovou a ocorrência de espalhamento inelástico de luz visível, após sua incidência sobre um líquido espalhador. Assim, a técnica Raman está baseada no espalhamento inelástico, de luz monocromática, que ocorre a partir da troca de energia com vibrações moleculares [21].

Quando um fóton impacta uma molécula pode ocorrer dois tipos de espalhamento: elástico e inelástico. Se após impactar a molécula o fóton retorna ao

meio com sua energia original, diz-se que esse fóton sofreu um espalhamento elástico. Esse espalhamento é chamado Rayleigh e, aproximadamente, 1 fóton em 1000 é espalhado de forma elástica. O espalhamento Rayleigh não é útil para caracterização molecular [22].

O espalhamento Raman ocorre quando a molécula é excitada por fótons e os fótons emitidos, no decaimento, apresentam frequências maiores ou menores, comparadas com a frequência monocromática que produziu a excitação (somente 1 fóton em 10^6 sofre espalhamento Raman) [22]. Assim, o espalhamento Raman pode ser classificado como espalhamento Stokes ou anti-Stokes. O espalhamento Stokes ocorre quando há absorção de energia no processo de espalhamento e a frequência da radiação espalhada fica menor que a frequência da radiação incidente. Já no espalhamento anti-Stokes, a radiação espalhada apresenta frequência maior que a radiação incidente, devido à retirada de energia do meio espalhador pela luz [23]. No diagrama de energia mostrado na Figura 4, são comparados os espalhamentos Rayleigh e Raman (Stokes e anti-Stokes).

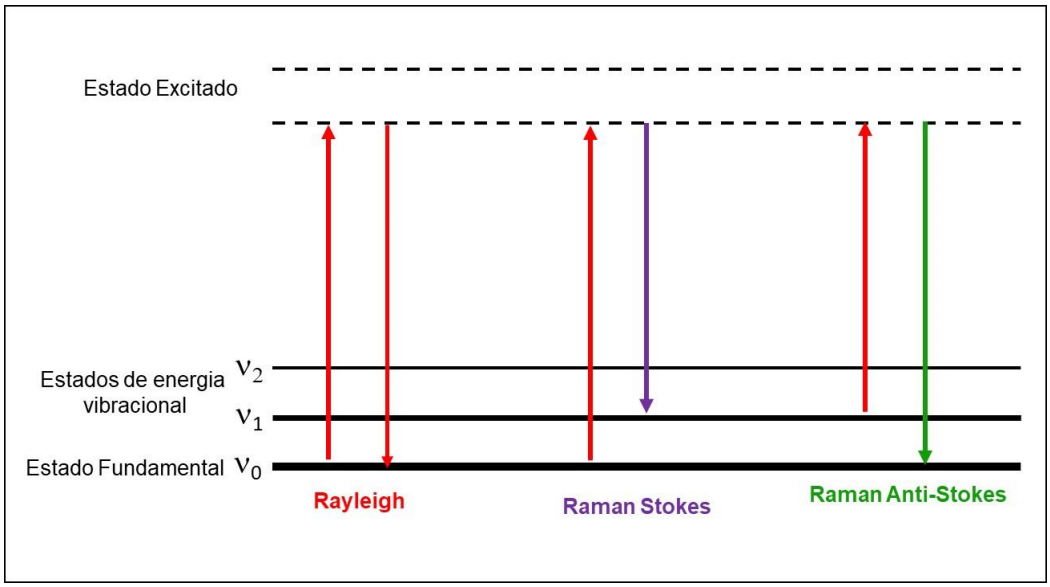


Figura 4: Comparação ilustrativa dos espalhamentos Rayleigh e Raman (Stokes e anti-Stokes)
Fonte: Autora

Na análise por Raman, os fótons provenientes de uma fonte monocromática, ao incidirem sobre uma molécula, sofrem espalhamentos inelásticos, tendo alterada suas energias e, portanto, suas frequências. As alterações nas frequências são dependentes das espécies moleculares analisadas e a intensidade de sinal é diretamente

proporcional a concentração dos constituintes moleculares. Assim, o espectro Raman (intensidade de luz espalhada versus número de onda) representa a composição molecular da amostra analisada [22]

A espectroscopia Raman requer basicamente um laser monocromático de emissão contínua, para induzir o espalhamento, óptica para coleta da radiação espalhada, a qual deve incluir um filtro para eliminar espalhamento Rayleigh, um elemento para difração da radiação espalhada (normalmente uma rede de difração), um detector para captura dos fótons e conversão em sinal elétrico, sendo geralmente utilizado um dispositivo de carga acoplada (CCD) e um computador para o processamento dos sinais [24]. Na Figura 5, é mostrado um esquema básico de uma montagem Raman.

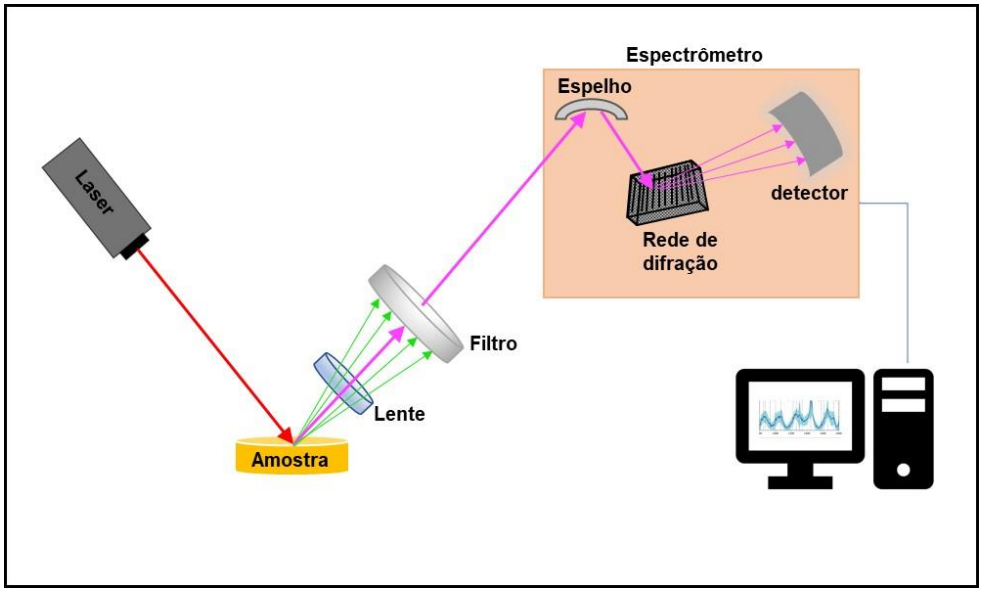


Figura 5: Componentes instrumentais básicos para espectroscopia Raman
Fonte: Autora

Considerando as baixas probabilidades de ocorrência do espalhamento Raman, e a relação da quantidade de luz espalhada (I) com o comprimento de onda da luz (λ): $I \propto 1/\lambda^4$, demonstrada por Lord Rayleigh, a escolha do laser, como fonte de radiação é muito relevante.

O meio ativo de lasers que emitem na região do visível é geralmente um gás, como argônio ou criptônio. Apesar de proporcionarem altas potências radiantes, esse tipo de laser apresenta limitações relacionadas à grande dimensão física e à excitação de fluorescência, o que causa altos sinais de fundo. Os lasers com emissão na região do infravermelho próximo possuem meio ativo sólidos, os quais permitem a construção

do laser em menores dimensões, viabilizando a portabilidade da técnica. Por esse motivo, os lasers mais comumente empregados na espectroscopia Raman são os com emissão em 1064, 830 e 785 nm, que apesar de proporcionarem espalhamentos Raman em menor quantidade não excitam emissões fluorescentes tão intensas [24].

O potencial da Raman para acessar a composição orgânica de amostras, também faz da técnica uma ferramenta muito interessante para emissão de diagnósticos analíticos rápidos, obtidos através de análises diretas, limpas, não invasivas e não destrutivas.

2.3.3 Espectroscopia na região do infravermelho próximo (NIRS)

A espectroscopia na região do infravermelho (IRS, do inglês *Infrared Spectroscopy*) originou-se em 1800 com a descoberta da radiação infravermelha por William Herschel. Contudo, a técnica só se concretizou em 1882, quando Abney e Festing obtiveram espectros de absorção no IR para mais de 50 compostos [25].

A IRS é um tipo de espectroscopia vibracional, cuja energia dos fótons empregados para interação com a matéria promove somente transições em baixos níveis de energia vibracionais e rotacionais das moléculas que compõem a matéria.

As fontes de luz utilizadas emitem a número de ondas (λ^{-1}) compreendidos no intervalo entre 12800 a 10 cm^{-1}. Esse intervalo é subdivido em três regiões: 12800 – 4000 cm^{-1} (NIR - do inglês *Near Infrared*), 4000 – 200 cm^{-1} (MIR- do inglês *Medium Infrared*) e 200 – 10 cm^{-1} (FIR - do inglês *Far Infrared*) [26].

A interação entre a radiação IR e uma molécula pode ser primeiramente compreendida, considerando o modelo de um oscilador harmônico para moléculas diatômicas, constituídas por duas massas esféricas conectadas por uma mola. Este modelo explica a variação da energia potencial após a absorção de um fóton, quando uma molécula abandona o estado de equilíbrio.

Embora, de forma geral, o oscilador harmônico ajude na compreensão de espectroscopias vibracionais, ele falha na explicação de NIRS por considerar transições somente entre níveis vibracionais adjacentes, para as quais a variação do número quântico vibracional (ν) é ±1.

Se somente a variação $\Delta\nu=\pm1$ ocorresse, apenas uma banda seria observada no espectro NIR de uma molécula diatômica, pois a diferença de energia entre dois estados vibracionais adjacentes é sempre a mesma [26]. Entretanto, em um espectro

NIR, são observadas bandas de sobretons, provenientes de transições para números quânticos vibracionais maiores que um ($\nu_0 \rightarrow \nu_n$, onde n>1) e também as bandas de combinações, provenientes da absorção de um fóton por dois modos vibracionais [28]. Ademais, diferentemente do oscilador harmônico, que considera absorção de energia contínua, o oscilador anarmônico considera absorção de energias discretas (*quantum*), o que explica melhor o fenômeno da absorção e excitação da molécula. Assim, as moléculas só absorvem radiação IR quando a energia da radiação é exatamente igual à diferença energética entre dois estados vibracionais, ou a de seus harmônicos ou a de combinações de duas ou mais vibrações. Dessa forma, somente algumas frequências da radiação incidida sobre uma molécula são absorvidas. Além disso, para que uma vibração seja ativa, é necessário, além da coincidência energética, haver interação entre a molécula e o campo elétrico da radiação eletromagnética incidente. Esta interação somente ocorre se os deslocamentos no modo vibracional provocarem alteração no momento de dipolo da molécula. A magnitude da variação de dipolo determina a intensidade espectral da banda [27].

Os componentes instrumentais básicos para medidas espectrais na região NIR consistem em fonte de radiação, emitindo na região NIR, suporte para a amostra, óptica para separação de frequências, detector e processador de sinais. Um esquema contendo os componentes básicos da técnica pode ser visualizado na Figura 6.

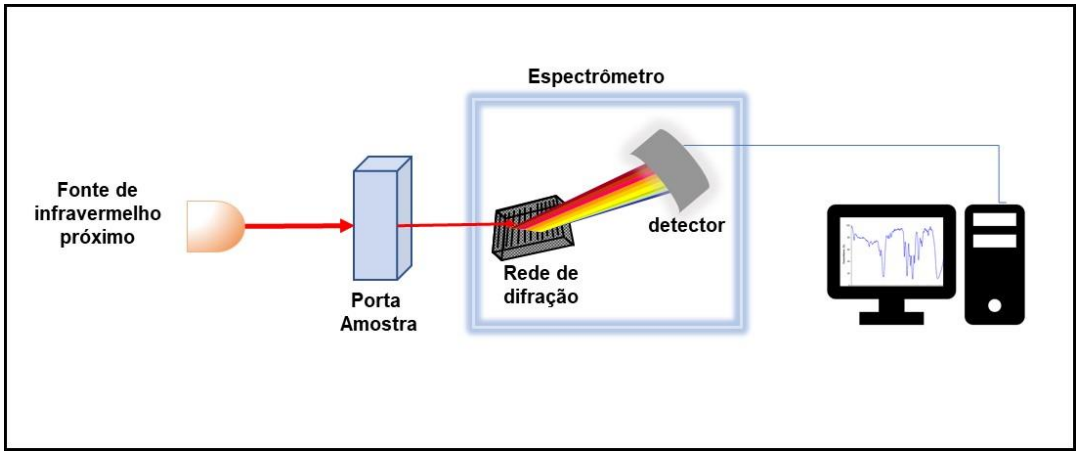


Figura 6: Componentes instrumentais básicos para NIRS
Fonte: Autora

Lâmpadas de tungstênio-halogênio são fontes de radiação comumente empregadas em NIRS. Essas lâmpadas fornecem radiação intensa e estável, além de abrangerem uma ampla faixa espectral (13000-4000 cm^{-1}) [3]. A recente tendência de

miniaturização instrumental também tem feito dos diodos emissores de luz (LEDs, do inglês *Light Emitting Diodes*) fontes convenientes para NIRS [27].

Como suporte de amostra é normalmente utilizada uma cela de sílica fundida ou quartzo, transparente à radiação NIR, com caminho óptico, variando de 0,1 a 10 cm [3].

Em NIRS, a óptica instrumental pode ser do tipo AOTF (do inglês, *Acousto-Optical TunablevFilters*), que consiste na utilização de um elemento dispersor, em posição fixa, para separar a radiação eletromagnética em suas frequências componentes. Sem partes móveis na óptica, o instrumento alcança altas velocidades de varredura (cerca de 2000 comprimentos de onda por segundo) em uma ampla faixa na região do NIR [27].

Assim como Raman, NIRS fornece informações relevantes sobre as estruturas químicas presentes na composição orgânica das amostras, proporcionando diagnósticos rápidos, através de análise diretas, limpas, não invasivas e não destrutivas.

3 Ciência de dados: estratégia à extração de informações espectrais

As técnicas espectroscópicas atualmente disponíveis permitem explorar amostras de forma bastante abrangente. A simplicidade, rapidez e baixo custo por análise permitem medições de um grande número de amostras e proporcionam informações para um elevado número de variáveis, com graus mistos de dependência. Por outro lado, os dados obtidos são, geralmente, complexos, com redundâncias e irrelevâncias que dificultam a aplicação de modelos de calibração tradicionais. Nesse contexto, ressalta-se a importância de uma abordagem pautada na *ciência de dados* para extração de informação útil dos dados. A ciência de dados combina vários conhecimentos, incluindo estatística, método científico, inteligência artificial e análise de dados para extrair valor dos dados [28].

O aumento do volume de dados para extração de valores não é uma particularidade analítica. O volume de dados, gerado mundialmente, cresce exponencialmente a cada dia, nas mais diferentes atividades humanas, tornando notória a urgência da temática “dados” nas mais diversas áreas do conhecimento humano. O chamado “*Big Data”*, por exemplo, é uma tentativa de contextualização de um cenário que reúne um conjunto de dados extremamente diversificado e que,

necessita de ferramentas especiais para organizar, extrair e transformar as informações nele contidas, possibilitando uma análise ampla em tempo hábil [29]. Nesse campo, a inteligência artificial tem ganhado ênfase, particularmente por uma subárea de pesquisa bastante intensa nos últimos anos: o Aprendizado de Máquina (ML do inglês, *Machine Learning*). De forma simplificada, o ML pode ser definido como o campo científico que dá às máquinas a capacidade de aprender sem serem estritamente programadas [30]. O arcabouço de ML constitui uma ferramenta valiosíssima para lidar com dados espectroscópicos derivados de análise direta.

A eficácia e o sucesso do tratamento e modelagem dependem diretamente da quantidade e da qualidade dos dados disponíveis, bem como dos modelos de aprendizagem desenvolvidos [31]. Com relação à qualidade dos dados, além da otimização de condições experimentais, para maioria das aplicações é necessário lançar mão de técnicas de pré-processamento espectral. As técnicas de processamento espectral consistem em uma variedade de métodos matemáticos para correção de efeitos físicos oriundos de fenômenos luminosos indesejáveis, para aprimorar a qualidade dos dados a serem utilizados nos modelos de calibração [32]

Em posse de volumes de dados adequadamente tratados, pode-se recorrer aos algoritmos de ML para ajustar modelos de previsões qualitativas e quantitativas. Os algoritmos de aprendizado supervisionado utilizam um conjunto de exemplos (dados de treinamento) para ajustar um modelo suficientemente bom para inferir/generalizar sobre as classes às quais pertencem ou concentrações de analitos às amostras (dados de teste/validação) que não participaram da etapa de treinamento. Para variáveis dependentes (alvos), caraterizadas por classes (rótulos) nominais, há (atualmente) uma numerosa família de algoritmos de classificação. Similarmente, algoritmos diversos estão disponíveis para tarefas de regressão, caracterizadas por variáveis dependentes quantitativas contínuas ou discretas. Como exemplos dos muitos algoritmos disponíveis para métodos de aprendizagem supervisionados de regressão e de classificação, citam-se: o PLS (do inglês, *Partial Least Square*), ANN (do inglês, *Artificial Neural Network*), KNN (do inglês, *K-Nearest Neighbors*), SVM (do inglês, *Support Vector Machine*), Árvores de Decisão, LDA (do inglês, *Linear Discriminant Analysis*) e PLS-DA (do inglês, *Partial Least Square Discriminant Analysis)* [33].

O método de aprendizado não supervisionado é mais comumente utilizado para a exploração dos dados espectroscópicos. Nesse caso, os algoritmos tornam viáveis as análises de agrupamentos das amostras com base em métricas de similaridade. Após a determinação dos agrupamentos, uma análise é necessária para determinar o que

cada grupo significa no contexto do problema analisado [34]. Como exemplo de algoritmo não supervisionado, cita-se a análise de componentes principais, PCA (do inglês, *Principal Component Analysis*) [33].

Apesar de os algoritmos de ML poderem induzir funções de previsão precisas, a densidade espectral de atributos redundantes, irrelevantes e apenas correlacionados com o alvo tornam a tarefa de modelagem deveras complexa. Além disso, a alta dimensionalidade dos dados espectroscópicos pode induzir à inexatidão das previsões, devido ao enviesamento dos modelos de calibração causado pela colinearidade de variáveis (presença de diversas variáveis que apresentam algum grau de correlação). Nesse sentido, métodos para seleção de variáveis são essenciais para aumento da precisão, acurácia e interpretabilidade do modelo [35]

Uma das principais estratégias a ser utilizada para seleção de variáveis é o conhecimento causal acerca do fenômeno abordado. Por exemplo, para determinar Fe, a partir de espectros de emissão óptica, deve-se escolher linhas espectrais referentes a processos de emissão desse elemento.

Há, porém, situações em que não se tem conhecimento sobre as variáveis causais e, nesse caso, algoritmos de seleção de variáveis relevantes podem ser úteis tanto na pré-seleção para ajuste de um modelo de previsão exato, quanto para auxiliar na elucidação de causa-efeito acerca do fenômeno investigado. Para auxiliar na identificação das variáveis causais pode-se recorrer às abordagens de seleção de variáveis, também chamadas de mineração de dados. Essas abordagens, utilizam algoritmos particularmente interessantes para serem aplicados em conjuntos de dados com grande número de amostras e variáveis, pois permitem otimizar as variáveis de entrada e, assim, aumentar a precisão, sensibilidade e especificidade dos modelos de calibração [36].

Um exemplo prático sobre o uso das duas estratégias acima citadas (conhecimento de efeitos causais e algoritmos de mineração de dados) é o trabalho de Lin e colaboradores (2011), que teve por objetivo discriminar tecidos de pulmão cancerígenos e limítrofes (baixo potencial maligno), utilizando a técnica LIBS [37]. A partir do conhecimento de efeitos causais, os autores pré-selecionaram linhas de Ca (por poderem refletir calcificação no tecido tumoral), Na e K (por serem elementos que controlam a homeostase eletrolítica nos tecidos), Mg (por apresentar baixa intensidade), C (por ser o principal elemento constituinte da matéria orgânica em tecidos biológicos) e CN (por refletir diferença nos conteúdos de matéria orgânica como proteína, açúcar e gordura, o que pode ser uma resposta à diferença do metabolismo

fisiológico). Nessa perspectiva, um conjunto de 12 linhas de emissão foram selecionadas. Para a obtenção das variáveis de entrada do modelo de calibração, uma nova seleção foi feita, utilizando o algoritmo *Random Forest,* o qual selecionou apenas 3 linhas. Tendo definido as variáveis de entrada, um modelo de classificação baseado no algoritmo *RF-Boosting Tree* foi ajustado, proporcionando discriminação dos tecidos com de sensibilidade 99.3% e especificidade de 98.6%.

Em parte das pesquisas apresentadas no presente documento, a ciência de dados tem sido utilizada em dados provenientes de técnicas espectroscópicas de análise direta, permitindo o desenvolvimento de métodos analíticos simples e rápidos e, em alguns casos, permitindo elucidar variáveis causais que regem diferentes fenômenos.

4 Contribuições das pesquisas com espectroscopia óptica para os diagnósticos diretos, simples e rápidos

A pesquisa descrita nos itens subsequentes aborda a análise direta por espectroscopia óptica (com ênfase em LIBS) para diferentes diagnósticos, com destaque aos diagnósticos requeridos pelo agronegócio. Os métodos desenvolvidos fornecem resultados rápidos e consonantes com a Química Analítica Verde, ciência que preconiza o desenvolvimento de metodologias analíticas diretas alternativas que não necessitam de solventes ou reagentes, para a minimização do impacto das metodologias analíticas ao meio ambiente [38].

A exploração das preciosas informações químicas, contidas nos espectros gerados pela interação direta luz-amostra, tem possibilitado extrair informações que transcendem as triviais aplicações de uma técnica analítica. Por exemplo, a LIBS (técnica de análise elementar) foi aplicada para determinar o grau de humificação, o pH e a textura de amostras de solo [39-41]

Ademais tem sido possível gerar conhecimento sobre as causas químicas de fenômenos expressos por diferentes tipos de amostras, por exemplo, o conhecimento de que o teor de carboidratos em milho é importante para a identificação de sementes transgênicas e não transgênicas [42].

Particularmente para a técnica LIBS, os principais desafios (efeito de matriz e baixa sensibilidade) para o desenvolvimento de métodos quantitativos tradicionais

(calibração univariada modelada pelo método dos mínimos quadrados), também têm sido abordados.

De forma geral, para encontrar a estratégia de calibração mais adequada ou de melhor desempenho, segue-se uma ordem de crescente complexidade dos métodos disponíveis, ou seja, escolhe-se um método multivariado, somente quando o univariado não se mostra adequado. Segue-se a mesma lógica para seleção do método multivariado, iniciando-se por métodos estatísticos mais simples até os mais rebuscados, envolvendo ML.

Os inconvenientes relativos à baixa precisão da técnica têm sido minimizados pela medida de um grande número de espectros para composição de médias.

Alguns dos trabalhos científicos produzidos sob a perspectiva acima descrita, publicados em periódicos internacionais, serão apresentados para a finalidade desta tese. Os detalhes em termos experimentais e de discussão dos resultados podem ser obtidos diretamente nas publicações que se encontram em anexo. Uma breve descrição/contextualização sobre cada trabalho, será feita nos itens subsequentes para melhor situar o leitor.

4.1 Determinação quantitativa de Cu em solos empregando um sistema LIBS portátil e redes neurais artificiais (Anexo 1)

O objetivo central dessa proposta era utilizar a técnica LIBS para determinação de Cu em amostras de solos provenientes de diferentes regiões do país. Dispunha-se de 60 amostras de solo com texturas e composições químicas bem diversificadas e teores de Cu de referência. As composições distintas entre amostras ocasionavam efeito de matriz, o que é bastante comum nas análises por LIBS. O efeito de matriz resulta na obtenção de sinais analíticos distintos, para duas amostras diferentes com a mesma concentração do analito. Esse fator dificulta o desenvolvimento de métodos quantitativos, dada a dificuldade em selecionar padrões de calibração que apresentem respostas ao estímulo instrumental similares às apresentadas por amostras do conjunto de validação/teste. Assim, a hipótese dessa investigação foi aplicar um método de inteligência artificial para “aprender” com as características das diferentes matrizes e, assim, ajustar um modelo de calibração capaz de “ignorar” o efeito de matriz para fornecer previsões exatas sobre teor de Cu em diferentes amostras.

Foi demonstrado que o efeito de matriz e possíveis interferências espectrais resultavam na obtenção de curvas de calibração tradicionais com baixas correlações (R= 0,09 e 0,11, para as linhas atômicas de Cu 324,7 e 327,4 nm respectivamente). Contudo, para o método avaliado, o qual utilizou redes neurais artificiais do tipo multicamadas, esses efeitos apresentaram baixa influência, viabilizando determinações acuradas.

4.2 Uso de comitês de preditores e a técnica LIBS para certificação de cafés (Anexo 2)

A qualidade global do café é aferida por um painel de provadores treinados. Assim, um certo grau de subjetividade pode acometer os diagnósticos. Para solucionar esse problema analítico, visualizou-se a possibilidade de utilizar a LIBS para desenvolver um método analítico rápido, limpo e livre de subjetividade. A partir dos dados de espectrais de LIBS, um novo método de predição foi desenvolvido para classificar cafés de acordo com as denominações de classes estabelecidas pela Associação Brasileira da Indústria do Café (ABIC): inferior, tradicional, superior e gourmet.

Foram utilizadas 41 amostras comerciais de cafés, provenientes de diferentes regiões do Brasil e certificados pela ABIC de acordo com as classes previamente descritas. Após a aquisição e pré-processamento dos espectros, 25 intervalos de comprimentos de onda na asa do pico, de intensidade máxima em 680 nm, foram comparados em relação ao desempenho preditivo, utilizando um algoritmo de árvore de decisão (J48) e dois comitês de preditores (RSM-IPCS e RBM).

Os resultados mostraram que, em geral, os três métodos tiveram desempenhos satisfatórios para região espectral compreendida no intervalo de 670-690 nm, sendo alcançada acurácia de 83,33% pelo comitê de preditores RSM-IPCS. Para as demais regiões espectrais avaliadas, o desempenho de classificação foi melhor, utilizando os dois comitês de preditores avaliados.

4.3 Uma nova forma de estimar o grau de humificação da matéria orgânica do solo, usando LIBS (Anexo 3)

A importância de acessar o grau de humificação da matéria orgânica do solo reside no fato de que esse parâmetro é um indicativo da recalcitrância da matéria orgânica do solo e fornece uma estimativa da capacidade de sequestro de carbono por

solos submetidos a diferentes manejos. Para avaliar o grau de humificação da matéria orgânica do solo, Milori e colaboradores (2006) [43], utilizando a técnica de fluorescência induzida por laser (LIFS, do inglês *Laser Induced Fluorescence Spectroscopy*), introduziram o conceito do índice de humificação H_{LIFS}, que consiste na razão entre a área integrada sob os espectros de fluorescência de amostras de solos e o teor de carbono total na amostra (H_{LIFS} = área de fluorescência / %carbono). Embora este método seja baseado em análises diretas de fluorescência, ele depende do teor de carbono total, o qual é determinado por outra técnica, aumentando assim o tempo e o custo das análises.

Nesse trabalho buscou-se investigar o potencial da LIBS para estimar o índice de humificação da matéria orgânica do solo. Para tal propósito, um valor equivalente à área de fluorescência LIFS foi determinado a partir dos espectros LIBS (A-LIBS), e esse valor foi normalizado pelo teor de carbono total na amostra de laboratório, o qual foi determinado, usando o mesmo espectro LIBS. Linhas de emissão de Al, Mg e Ca foram utilizadas como variáveis de entrada para o modelo por exibirem correlações com as emissões de fluorescência. O modelo gerado permitiu a predição de valores de A-LIBS altamente correlacionados com a área LIFS (R=0.94), evidenciando o potencial de LIBS para determinação do índice de humificação da matéria orgânica do solo.

4.4 **Estendendo a aplicação de LIBS para estimar o pH de amostras de solo** (Anexo 4)

A biodisponibilidade dos nutrientes para as plantas depende da solubilização de minerais na solução do solo e este processo é dependente do pH. O pH de solos é normalmente determinado por meio de medidas potenciométricas em suspensão aquosa de solo. Em alguns procedimentos, solução de $CaCl_2$ é utilizada para minimizar interferências devido a partículas suspensas na fase aquosa e aos teores variáveis de sais presentes. Assim, eliminar a etapa de preparo da amostra já seria um excelente atrativo para desenvolver um novo método de determinação de pH. Nessa perspectiva, surgiu a ideia de aplicar LIBS para executar medidas de pH. A possibilidade de determinar o pH, a partir de um espectro LIBS, tornaria a análise bem mais abrangente, visto que já constavam na literatura, métodos para determinação de nutrientes e contaminantes em amostra de solo. Logo, a partir de um espectro LIBS, poder-se-ia extrair a concentração de nutrientes, contaminantes e pH.

Como variáveis de entrada, foram selecionadas as intensidades de 32 linhas de emissão dos elementos: Al, Ca, H e O. A seleção foi feita com base em conhecimento sobre efeitos causais desses elementos no o pH do solo. A partir dessas variáveis, um modelo baseado em mínimos quadrados parciais foi construído e otimizado em relação ao número de variáveis latentes. Os resultados da validação mostraram boa concordância entre os valores preditos pelo modelo obtido e os de referência.

4.5 Aplicação da LIBS para determinação da textura de solos (Anexo 5)

A análise da textura do solo é fundamental para o manejo adequado dos sistemas agrícolas e para os estudos ambientais. A textura do solo (teores de argila, areia e silte) é geralmente determinada pelos métodos da pipeta ou do hidrômetro, mas esses métodos requerem preparo da amostra com reagentes químicos e podem levar horas, o que inviabiliza a análise de um grande número de amostras. Assim, na mesma perspectiva do uso de LIBS para análises rápidas, e visando ampliar os diagnósticos obtidos a partir de uma única medida, surgiu a ideia de aplicar a técnica para determinar a textura do solo.

Dois modelos baseados no algoritmo de regressão por mínimos quadrados parciais (PLSR, do inglês, *Partial Least-Squares Regression*) foram avaliados para o ajuste de modelos de predição da textura de 60 diferentes amostras solos. A diferença entre os dois modelos foi o conjunto de variáveis de entrada. Para o modelo A, o conjunto foi composto por todas as variáveis compreendidas no intervalo espectral de 188 a 980 nm, enquanto para o modelo B foram selecionadas linhas de emissão dos elementos Si, Na, Fe, Ti, Ca, K, Al, Co, Mg, V, Ba e Be. O critério utilizado para a seleção das variáveis foi a correlação dos sinais espectrais com os teores de argila, areia e silte nas amostras. Dessa forma, foi possível compreender o papel dos elementos na designação da textura.

Ambos os modelos forneceram bons resultados de validação, apresentando coeficientes de correlação entre teor predito e teor de referência, superiores a 0,85 e erro quadrático médio (RMSE, do inglês, Root Mean Squared Error) menor que 8%. Em média, o desempenho do modelo B foi um pouco melhor do que o modelo A. Apesar do PLSR ser particularmente útil, quando o número de variáveis de previsão é maior que o número de observações, os resultados corroboram a importância da seleção de variáveis causais.

Este método foi patenteado sob Número de registro: BR1020130085316.

4.6 Potencial da LIBS para análise da qualidade café moído e não torrado (Anexo 6)

A mistura de grãos defeituosos à grãos bons de café causam um impacto negativo à qualidade global da bebida. Os principais grãos defeituosos que têm sido utilizados nas misturas com grãos bons são os grãos pretos, verdes e ardidos (PVA).

Neste trabalho, um estudo exploratório foi conduzido, utilizando as técnicas LIBS e NIRS, com o objetivo de avaliar o potencial da LIBS para identificação de PVAs, uma vez que o potencial de NIRS para análise da qualidade global de cafés já é bem estabelecido.

As duas técnicas foram utilizadas para medir espectros de amostras de grãos bons, e PVAs (separadamente) e, após adequado processamento dos espectros, a existência de correlações entres sinais espectrais e as classes dos grãos foram avaliadas, utilizando PCA e análise de variância. Nos espectros NIRS, todas as bandas espectrais foram consideradas para análise, enquanto nos espectros LIBS, apenas as linhas de elementos e moléculas diatômicas que compõem estruturas de compostos orgânicos (C, N, H, O, CN e C2).

Os resultados mostraram que as bandas espectrais obtidas por NIRS, correspondentes a lipídeos, açúcares e proteínas (4244–4350 cm^{-1}), ácidos carboxílicos (~5260 cm^{-1}) e água (5280–5286 cm^{-1}) contribuem para uma clara distinção das classes de grãos avaliadas. Análise dos espectros LIBS mostrou que os sinais de CN (388.5 nm), C2 (516.6 nm), N (744.2 nm) e N (746.8 nm) contribuem, majoritariamente, para a discriminação das classes estudadas.

Um estudo também foi conduzido para verificar correlações entre os sinais obtidos por LIBS e por NIRS. Os resultados desses estudos mostraram que há altas correlações ($R > 0,9$) entre os sinais de emissão de N, CN, C e C2 obtidos por LIBS e bandas de proteínas, lipídeos e ácidos carboxílicos, obtidas por NIRS. A partir desses estudos, confirmou-se o potencial da LIBS para análise de qualidade do café adulterada por PVAs e, também se visualizou a possibilidade de empregar a técnica para estimar classes de compostos orgânicos nas amostras de PVAs.

4.7 Determinação de Ca em fertilizantes a base de biocarvão, utilizando Na como padrão interno (Anexo 7)

A incorporação de nutrientes em biocarvão pode agregar a esse precioso produto a característica de fertilizante de liberação controlada.

Na produção do fertilizante, o tipo de biomassa utilizada para obtenção do biocarvão e o método de incorporação dos nutrientes resultam em diferentes produtos, os quais requerem controle/padronização. Considerando que se trata de um material de difícil decomposição, a determinação dos nutrientes por técnicas analíticas convencionais, as quais demandam o preparo da amostra, não é uma tarefa trivial. Nesse contexto, surgiu a ideia da aplicação da LIBS para análise direta e o elemento Ca foi inicialmente escolhido para avaliação.

As amostras foram preparadas a partir de três diferentes biomassas (eucalipto, fibra de bananeira e cascas de amendoim) e a incorporação do nutriente foi feita na biomassa crua, por meio do contato desta com solução aquosa de íons Ca^{2+}. As biomassas enriquecidas com Ca^{2+} foram pirolisadas para a obtenção do fertilizante. Para minimizar os efeitos de matriz, os padrões de calibração foram preparados por compatibilização, misturando-se quantidades predefinidas de CaO a biocarvão de eucalipto.

Os resultados mostraram que a compatibilização de matriz não foi eficaz para a minimização dos efeitos de matriz, sendo necessário agregar a esta estratégia a padronização interna. Após normalizar os sinais de Ca com o de Na, foi possível minimizar o efeito de matriz e alcançar a exatidão nas determinações.

4.8 Determinação de K em fertilizantes a base de biocarvão por LIBS na presença de elementos facilmente ionizáveis (Anexo 8)

Em continuidade ao desenvolvimento de métodos para análise direta de nutrientes nos fertilizantes a base de biocarvão, nesse trabalho, foi descrita uma proposta para aumentar a sensibilidade da LIBS e viabilizar o desenvolvimento de método para determinação de K.

A proposta para o aumento da sensibilidade foi baseada na adição de elementos facilmente ionizáveis. A hipótese para essa proposta era de que a presença de elementos facilmente ionizáveis causaria um aumento na densidade eletrônica do

plasma, aumentando, assim, as probabilidades de colisões entre as espécies presentes no plasma e consequentemente a sua temperatura, proporcionando processos de excitação mais eficientes a todas as espécies presentes no plasma. Para testar a hipótese, sais contendo os íons K^+, Li^+, Na^+, Cu^{2+} e Mg^{2+} foram misturados as amostras e os espectros resultantes foram avaliados. Os resultados confirmaram a hipótese, indicando que não houve variação aparente do sinal espectral, quando os sais de Cu e Mg foram adicionados. Entretanto, quando foram utilizados os sais de Na, K e Li, as intensidades das linhas de emissão mostraram significativo aumento.

Assim, a proposta foi aplicada para determinação de K nos fertilizantes, utilizando adição de Li_2CO_3 para o aumento da sensibilidade. Essa estratégia, viabilizou a obtenção de bons sinais e o ajuste de um modelo de calibração linear univariado, o qual foi aplicado para determinação de K em três diferentes fertilizantes, produzindo resultados exatos.

4.9 Determinação de P em fertilizantes utilizando LIBS associada à um sistema de descarga elétrica (Anexo 9)

Nesse trabalho, foram descritas estratégias para minimizar dois dos inconvenientes da LIBS que influenciam as análises quantitativas – a reduzida sensibilidade e o efeito de matriz. O problema analítico abordado como prova de conceito foi a determinação de P em fertilizantes comerciais. As estratégias, anteriormente desenvolvidas no grupo de pesquisa para aumento da detectabilidade do sistema LIBS disponível, não permitiam melhorar os sinais analíticos de P ou N (importantes nutrientes agrícolas). Assim, a proposta de um sistema de descarga elétrica (*homemade*) para ser acoplado ao sistema LIBS foi desenvolvida. Esse sistema, chamado de SD (do inglês *Spark Discharge*) basicamente consiste em dois eletrodos de tungstênio posicionados a uma distância de 4 mm entre eles e 2 mm acima da superfície da amostra e um sistema elétrico armazenador de carga.

A partir da amostragem feita pela incidência do pulso do laser, a amostra vaporizada entre os eletrodos fecha o circuito eletrétrico e faz com que o vapor/plasma receba uma “injeção” de elétrons, proveniente da descarga elétrica de capacitores previamente carregados. Nesse caso, o princípio envolvido no aumento da sensibilidade é o mesmo anteriormente descrito para o uso dos elementos facilmente ionizáveis (aumento da densidade eletrônica do plasma). Entretanto, esse sistema é muito mais eficiente e limpo, pois não requer a adição de reagentes às amostras. Cabe

destacar que o desenvolvimento do sistema de descarga elétrica tem viabilizado muitas aplicações diferentes, as quais serão posteriormente descritas.

Para o desenvolvimento do método quantitativo, assim como nos dois trabalhos anteriormente descritos, a compatibilização de matriz foi utilizada como estratégia para minimizar o efeito de matriz. Dessa forma, foi possível ajustar um modelo de calibração linear univariado para determinação de P em amostras comerciais de fertilizantes com adequada exatidão.

4.10 Predição dos teores de grãos defeituosos (pretos, verdes e ardidos) em misturas com grãos bons, utilizando a técnica LIBS (Anexo 10)

Nas cooperativas brasileiras de café, o método utilizado para estimar os teores de PVAs misturados aos grãos bons de café arábica são baseados em inspeção visual e separação/contagem. Esse método além de subjetivo é moroso.

Considerando i) a necessidade de método rápido e livre de subjetividade e ii) os resultados sobre o potencial da LIBS para identificação de PVAs, apresentados no item 6.6 (anexo 6), buscou-se, neste trabalho, desenvolver métodos analíticos, utilizando LIBS para determinação do teor de PVAs misturados a grãos bons.

Espectros foram adquiridos a partir de misturas, contendo diferentes teores (m/m) de PVAs. Nos espectros pré-processados foram selecionadas variáveis referentes às linhas de C, N, O, CN e C2, previamente constatadas como potenciais para discriminação das classes de defeitos PVAs. Do conjunto inicial de variáveis, mais três seleções foram feitas com o objetivo de estabelecer subconjuntos de variáveis capazes de discriminar um defeito individual dos demais.

A partir dos subconjuntos, três modelos de calibração, baseados em regressão linear múltipla, foram ajustados para a predição dos defeitos. Os três modelos foram eficientes para as predições pretendidas, exibindo baixos erros na validação.

4.11 Avaliação da autenticidade de arroz marrom por SD-LIBS (Anexo 11)

Muitos países têm adotado rotulagem controlada para alimentos com base na denominação de origem protegida. Essa rotulagem confere garantia de qualidade, tradição e autenticidade dos produtos.

Neste trabalho, o potencial de SD-LIBS foi investigado com o objetivo de desenvolver um método simples, rápido e limpo para a certificação de origem de arroz marrom proveniente de duas regiões produtoras, localizadas na província de Corrientes- Argentina (Berón de Astrada e Mercedes). Foram obtidos espectros para um total de 66 amostras (35 de Mercedes e 31 de Berón de Astrada), os quais foram divididos em conjunto de calibração e conjunto de validação

As variáveis de entrada utilizadas para o ajuste do modelo de calibração foram selecionadas, utilizando o algoritmo extreme gradiente boosting e a linhas selecionadas correspondem aos elementos Fe, Ca, Mg, Na e C. Esses resultados sugerem que as regiões produtoras conferem ao arroz teores distintos dos elementos citados.

Para classificação, foram avaliados três algoritmos de aprendizado de máquina (LDA, k-NN, SVM e RF). O modelo baseado em k-NN mostrou o melhor desempenho para a classificação almejada.

4.12 **Determinação da origem botânica de arroz utilizando SD-LIBS** (Anexo 12)

A certificação de origem botânica também imprime autenticidade, tradição e garantia de qualidade a produtos alimentícios. Neste trabalho, avaliou-se a possibilidade de utilizar SD-LIBS para certificação da origem botânica de amostras de arroz.

Setenta e duas amostras de quatro variedades de arroz foram analisadas por SD-LIBS. A seleção de variáveis foi parametrizada por linhas de altas intensidades não colineares e sustentada por conhecimentos descritos na literatura. Assim, linhas espectrais de C, Ca, Fe, Mg, N e Na foram selecionadas como variáveis de entrada para o ajuste de modelo de predição baseado no algoritmo SVM.

Os resultados mostraram acurácia global de 96,4% na predição das amostras do conjunto de validação, sendo o método desenvolvido simples, rápido, limpo e mais eficiente, quando comparado a outros métodos previamente descritos.

4.13 **Incineração seca para o aumento de sinal na técnica LIBS** (Anexo 13)

Os estudos relatados, neste trabalho, tiveram como objetivo minimizar os inconvenientes relacionados à baixa sensibilidade da técnica LIBS, através de uma proposta simples, independente de modificações instrumental, envolvendo um simples

preparo da amostra e mantendo alinhados com os pressupostos da Química Analítica Verde, os possíveis métodos desenvolvidos sob essa perspectiva.

A hipótese da proposta era que com a incineração da amostra por via seca ocorreria simplificação de suas estruturas químicas componentes, as quais durante a análise por LIBS, demandariam menos energia para os processos de rupturas no plasma. Assim, ter-se-ia um excedente de energia para favorecer os processos de excitação das espécies no plasma e o sinal seria maior.

Para avaliar a hipótese formulada, amostras de composição bem contrastantes (folhas de citrus, solo e liga de aço) foram escolhidas. As amostras foram aquecidas a seco em forno mufla e analisadas na sequência. Como prova de conceito, a estratégia foi aplicada para determinação de Sr em folhas de plantas.

A hipótese foi confirmada com a observação de amplificação geral dos sinais de emissão nas três classes de amostra estudadas. Apesar do grau de amplificação dos sinais ter sido diferente, observou-se que suas intensidades estão diretamente relacionadas com a natureza química da amostra. A estratégia viabilizou a determinação de Sr em folhas, a qual não era possível antes do aquecimento.

4.14 **Detecção e quantificação de adulterantes em mel, utilizando LIBS** (Anexo 14)

O mel é um alimento de elevado valor agregado e, por isso, um produto susceptível à adulteração. A certificação de qualidade do mel requer métodos analíticos rápidos e, nesse contexto propôs-se avaliar o potencial da LIBS para detectar e quantificar adulterantes em mel.

O conjunto amostral consistiu de amostras de mel puro de diferentes origens botânicas, xaropes comumente utilizados para adulteração e amostras de mel fortificadas com os xaropes.

Espectros SD-LIBS foram capturados diretamente nas amostras líquidas e diversos métodos para processamento espectral e para seleção de variáveis foram sistematicamente avaliados.

Para a detecção da presença e do tipo de adulterante foi utilizado o algoritmo PLS-DA e para quantificação dos adulterantes, PLS.

A discriminação entre mel puro e adulterado pelo modelo (PLS-DA) foi bem sucedida, quando se utilizaram as variáveis selecionadas por iPLS no modo *forward* (FiPLS). Os resultados dessa seleção mostram que linhas de emissão de Fe atômico

apresentaram maiores coeficientes de regressão para a discriminação das classes (adulterado, não adulterado), sugerindo a importância desse elemento para detectar adulteração. Após a detecção da adulteração, o tipo de adulterante pôde ser identificado por meio de um segundo modelo PLS-DA, sendo as principais variáveis relacionadas a essa identificação as linhas de emissão de Ca e Fe.

Para a avaliação do teor de adulterante presente, o modelo PLS que apresentou as melhores métricas foi o que utilizou os espectros pré-processados pela 1ª derivada mais correção de sinal ortogonal e centralização na média e as variáveis espectrais selecionadas por *backward* iPLS (BiPLS).

Os métodos desenvolvidos para detectar e quantificar adulterantes em mel permitem verificar a autenticidade do produto em 1 mL da amostra em menos de 3min sem geração de resíduos e expandem o potencial da LIBS, dedicada à análise de sólidos, à análise de outras amostras viscosas como maionese, leite condensado, etc

4.15 Uso da emissão diatômica de CN para determinação de N usando LIBS (Anexo 15)

O desenvolvimento de métodos para determinação de nutrientes em fertilizantes a base de biocarvão, anteriormente descritos (itens 7 e 8), limitou-se aos elementos Ca e K, pois a sensibilidade instrumental não permitia a visualização de linhas que pudessem ser utilizadas para determinação de N. Cabe destacar que as melhores linhas de emissão desse elemento ocorrem a comprimentos de onda superiores a 600 nm, o que constitui uma limitação ao instrumento utilizado, o qual cobre a faixa espectral de 200 a 600 nm. Contudo, após o desenvolvimento do SD (descrito no item 12) foi possível detectar bandas de emissão referentes à molécula diatômica de CN e pôde-se, então, retomar a ideia de desenvolver método para determinação de N nos fertilizantes de biocarvão.

Para essa proposta, o interior da câmara de amostragem foi purgado, utilizando um fluxo de argônio de 10 L/min, visando minimizar a influência do N atmosférico. Das cinco bandas de CN visualizadas, nos espectros SD-LIBS dos fertilizantes, a banda a 388,3 nm foi a que apresentou a melhor correlação linear com os teores de N em padrões e amostras, e por isso, foi utilizada no desenvolvimento do método.

Utilizando a compatibilização de matriz para produção dos padrões de calibração, implementada pela utilização de biocarvão de eucalipto, foi possível delinear uma curva

de calibração linear e univariada. O modelo ajustado permitiu determinar N com exatidão em três diferentes amostras de fertilizantes.

4.16 Avaliação de método de calibração baseado em um único padrão de calibração para determinar P e Al por SD-LIBS (Anexo 16)

Neste trabalho uma nova estratégia de calibração foi proposta utilizando um único padrão de calibração e duas diferentes voltagens (V_1 e V_2), aplicadas através do dispositivo SD, para produzir duas diferentes intensidades de sinal (I_1 e I_2).

A proposta requer que tanto o padrão quanto a amostra sejam submetidos a duas voltagens diferentes (V_1, V_2), consecutivamente, e que as intensidades a diferentes voltagens sigam relação linear. Dessa forma, medindo-se os sinais de amostra e padrão em duas voltagens diferentes, pode-se calcular a concentração do analito na amostra de acordo com a equação 1:

$$\mathbf{C_{Amostra} = C_{Padrão} .(I_1 + I_2)_{Amostra} / (I_1 + I_2)_{Padrão}} \qquad \text{Equação 1}$$

O desempenho desta proposta, chamada de OP-MVC (do inglês *One Point Multi-Voltage Calibration*), foi avaliado para a determinação de Al e P em folhas de plantas e fertilizantes, respectivamente. Os resultados obtidos não apresentaram diferença estatística, quando comparados aos valores de Al certificados e os valores P, medidos por espectrometria de absorção atômica em chama de alta resolução e fonte contínua.

A proposta representa uma redução para as dificuldades associadas ao preparo de vários padrões de calibração, para calibração externa, quando o modelo univariado se mostra eficiente para a solução do problema analítico.

4.17 Espectroscopia Raman para discriminação de milho transgênico (Anexo 17)

Apesar do aumento na produção de culturas geneticamente modificadas, a aceitabilidade pelos consumidores é ainda bastante questionável, principalmente no que diz respeito à segurança de consumo. Nesse sentido, a cadeia do milho carece de métodos rápidos e de baixo custo para detectar culturas geneticamente modificadas.

Considerando o exposto, neste trabalho avaliou-se a aplicabilidade da espectroscopia Raman para discriminar milho transgênico e não transgênico. Os espectros foram obtidos para amostras de sementes de milho, de procedência controlada, representativas de quatorze pares de transgênicos e não transgênicos.

Diversos pré-processamentos espectrais e a abordagem Wrapper para seleção de variáveis (com pesquisa usando diferentes algoritmos) foram sistematicamente avaliados para o ajuste de um modelo classificador, baseado em LDA.

Utilizando as variáveis selecionadas pela abordagem Wrapper, juntamente com algoritmo genético, foi possível obter um classificador com acurácia preditiva de 87,5%,

A análise das variáveis selecionadas para este modelo sugere que a modificação genética provoca alteração nos teores de algumas classes de compostos, como os carboidratos e carotenoides. Assim, foi possível concluir que a expressão química da modificação genética pode ser detectada pela espectroscopia Raman e que a estratégia pode ser considerada para outros produtos geneticamente modificados.

.

4.18 Identificação geográfica protegida de mel por SD-LIBS (Anexo 18)

As propriedades nutricionais e terapêuticas do mel estão intrinsicamente relacionadas à sua origem geográfica. Assim, o desenvolvimento de métodos rápidos e diretos para autenticação da origem geográfica do mel, é de grande importância para combater fraudes.

Nesse trabalho, buscou-se desenvolver um método para classificar amostras de mel de acordo com a região produtora. Foram utilizadas amostras de mel multifloral, provenientes de quatro províncias argentinas, as quais foram analisadas diretamente utilizando SD-LIBS. Diferentes tipos de pré-processamento espectral foram avaliados em conjunto com três algoritmos para classificação (PLS-DA, k-NN e SVM).

O melhor desempenho de classificação foi obtido usando uma sequência de três estratégias para o pré-processamento espectral (suavização + ponderação dos mínimos quadrados generalizada + centralização na média) e os algoritmos k-NN e SVM, sendo que ambos os classificadores obtidos apresentaram acurácia preditiva de 100%.

O modelo ajustado com PLS-DA também alcançou um alto percentual de acerto nas classificações (94%) e além disso, contribuiu para identificar os elementos que influenciavam na distinção das classes, apontando o N, como o mais importante

elemento para discriminar as classes estudadas. Esse resultado sugere a ocorrência de diferenças proteicas entre as amostras provenientes das diferentes regiões geográficas.

4.19 Determinação de fósforo em fertilizantes a base de biocarvão usando SD-LIBS (Anexo 19)

Após a proposta do SD (anexo 9) e o sucesso do acoplamento SD-LIBS para determinação de N em de fertilizantes a base de biocarvão (anexo 15), um método usando SD-LIBS foi desenvolvido para determinação de P em fertilizantes de biocarvão.

Assim como para Ca, K e N (anexos 7,8 e 15, respectivamente), a calibração inicialmente avaliada foi a univariada com compatibilização de matriz, usando biocarvão de eucalipto para produção dos padrões de calibração. A ideia desenvolvida neste trabalho foi muito similar a apresentada para determinação de Ca (anexo 7), exceto pelo uso do SD. Contudo, para determinação do Ca, além da compatibilização de matriz, foi necessário lançar mão da padronização interna. No caso do P, aqui estudado, somente a compatibilização de matriz já permitiu alcançar a exatidão, o que sugere que Ca e P interagem de formas distintas com o biocarvão. Esses achados mostram o grau de complexidade dos efeitos de matriz em LIBS e a importância de se buscar novas estratégias para minimização desse efeito.

5 Conclusões

O potencial investigativo da interação luz-matéria é imenso, mas de forma geral, as técnicas analíticas consolidadas que utilizam esta interação como princípio analítico não exploram esse potencial de forma ampla.

Por requererem o preparo da amostra, algumas técnicas espectroscópicas acabam por destruir a informação química original da amostra. Além disso, os métodos analíticos conduzidos sob essa perspectiva são morosos, demandam tempo e geram resíduos químicos.

Em um mundo globalizado, onde a informação em tempo real é essencial, o retardamento de diagnósticos analíticos pode significar sérias perdas econômicas. Assim, a busca por métodos rápidos e ambientalmente amigáveis é imprescindível. As técnicas espectroscópicas de análise direta atendem às demandas globais, mas

requerem expertise em termos de princípios analíticos, para que se possa atuar nos fatores que afetam a obtenção de bons resultados, e a associação de conhecimentos na área de dados, para possibilitar a extração da informação espectral desejada.

Os resultados dos trabalhos apresentados nesta tese evidenciam que a associação das técnicas espectroscópicas de análise direta, ciência de dados e o desenvolvimento de estratégias para obtenção de resultados espectrais fidedignos à amostra têm proporcionado importantes contribuições as demandas emergentes. Por meio dessa associação, muitos efeitos causais têm sido elucidados e, quando utilizados como parâmetros para obtenção de modelos de calibração, geram métodos mais acurados e com maior rastreabilidade. Conclui-se assim, que a continuidade dessa linha de pesquisa é essencial para o avanço da Química Analítica em direção às características dos diagnósticos que serão demandas oficiais em um futuro não muito distante.

6 Referências

1. ORNA, M. V. Chemistry and artists' colors: part I. Light and color. **Journal of Chemical Education**, v. 57, n. 4, p. 256-258, 1980. DOI: http://dx.doi.org/10.1021/ed057p256.

2. WEINER, J.; HO, P.-T. **Light - matter Interaction**: fundamentals and applications. New Jersey: John Wiley & Sons, 2003. v. 1. ISBN 9783527617883. DOI: http://dx.doi.org/10.1002/9783527617883.

3. SKOOG, D. A; CROUCH, S. R.; HOLLER, F. J. **Princípios de análise instrumental**. 6. ed. Porto Alegre: Bookman, 2009. ISBN 9788577804603.

4. BALL, D. W. Light: particle or wave? **Spectroscopy**, v. 21, n. 6, 2006. Disponível em: https://www.spectroscopyonline.com/view/light-particle-or-wave. Acesso em: 08 ago. 2022.

5. NEWTON, I. **Opticks.** London: Octavo, 1998. ISBN 9781891788048.

6. BAGNATO, V. S. **Laser e suas aplicações em ciência e tecnologia**. São Paulo: Livraria da Física, 2008. ISBN 9788588325982.

7. RIBEIRO, A. R.; COELHO, L.; BERTOLAMI, O.; ANDRÉ, R. Luz: história, natureza e aplicações. **Para físicos e amigos da física**, v. 39, p. 6-13, 2015. Disponível em: https://www.spf.pt/magazines/GFIS/119/article/982/pdf. Acesso em: 08 ago. 2022.

8. ARAGO, F.; HUYGENS, C.; YOUNG, T.; CREW, H.; FRESNEL, A. J. **The wave theory of light**: memoirs by huygens, young and fresnel. [*S. l.*]: Franklin Classics, 2018. ISBN 9780342418954.

9. ROSA, C. A. P. **História da ciência**: a ciência moderna. 2. ed. Brasília: FUNAG, 2012. v. 2. ISBN 9788576313946. Disponível em: http://funag.gov.br/loja/download/1020-Historia_da_Ciencia_-_Vol.II_Tomo_I_-_A_Ciencia_Moderna.pdf. Acesso em: 08 ago. 2022.

10. CHRISTIAN, G. D.; DASGUPTA, P. K.; SCHUG, K. A. **Analytical chemistry**. 7th ed. New Jersey: John Wiley & Sons, 2013. ISBN 9780470887578.

11. FILGUEIRAS, C. A. L. A espectroscopia e a química: da descoberta de novos elementos ao limiar da teoria quântica. **Química Nova na Escola**, n. 3, p. 22-25, maio 1996.

12. TILMON H. PEARSON, T. H; IHDE, A. J. Chemistry and the spectrum before Bunsen and Kirchhoff. **Journal of Chemical Education**, v. 28, n. 5, p. 267-271, May 1951. DOI: http://dx.doi.org/10.1021/ed028p267.

13. THOMAS, N. C. The early history of spectroscopy. **Journal of Chemical Education**, v. 68, n. 8, p. 631-634, Aug. 1991. DOI: http://dx.doi.org/10.1021/ed068p631.

14. BAGNATO, V. S. Os fundamentos da luz laser. **Física na Escola**, v. 2, n. 2, p. 4-9, 2001. Disponível em: http://www.sbfisica.org.br/fne/Vol2/Num2/a02.pdf. Acesso em: 08 ago. 2022.

15. OPTICS 4 ENGINEERS. **Laser:** fundamentals - Q-switching. [20--]. Disponível em: http://www.optique-ingenieur.org/en/courses/OPI_ang_M01_C01/co/Contenu_12.html. Acesso em: 25 maio 2022.

16. CREMERS, D. A; RADZIEMSKI, L. J. **Handbook of laser-induced breakdown spectroscopy**. 2nd ed. New Jersey: John Wiley & Sons, 2013. ISBN 9781119971122.

17. MIZIOLEK, A. W.; PALLESCHI, V.; SCHECHTER, I. **Laser induced breakdown spectroscopy (LIBS)**: fundamentals and applications. Cambridge, UK: Cambridge University Press, 2006. ISBN 9780511541261.

18. CAPITELLI, F.; COLAO, F.; PROVENZANO, M. R.; FANTONI, R.; BRUNETTI, G.; SENESI, N. Determination of heavy metals in soils by laser induced breakdown spectroscopy. **Geoderma**, v. 106, n. 1-2, p. 45-62, Mar 2002. DOI: http://dx.doi.org/10.1016/S0016-7061(01)00115-X.

19. RUSAK, D. A.; CASTLE, C.; B. W. SMITH, B. W; WINEFORDNER, J. D. Fundamentals and applications of laser-induced breakdown spectroscopy. **Critical Reviews in Analytical Chemistry**, v. 27, n. 4, p. 257-290, Oct. 2006. DOI: http://dx.doi.org/10.1080/10408349708050587.

20. MOROS, J.; LASERNA, J. Laser-induced breakdown spectroscopy (LIBS) of organic compounds: a review. **Applied Spectroscopy**, v. 73, n. 9, p. 963-1011, Sept. 2019. DOI: http://dx.doi.org/10.1177/0003702819853252.

21. BOHNING, J. J.; MISRA, T. N.; CHOUDHURY, M. **The Raman Effect**: an international historic chemical landmark. Washington, DC: American Chemical Society; Calcutta: Indian Association for the Cultivation of Science, 1998. Disponível em: https://www.acs.org/content/dam/acsorg/education/whatischemistry/landmarks/ramaneffect/the-raman-effect-commemorative-booklet.pdf. Acesso em: 08 ago. 2022.

22. KIM, H. H. Endoscopic Raman spectroscopy for molecular fingerprinting of gastric cancer: principle to implementation. **BioMed Research International**, v. 2015, p. 1-9, May 2015. DOI: http://dx.doi.org/10.1155/2015/670121.

23. RODRIGUES, A. G.; GALZERANI, J. C. Espectroscopias de infravermelho, Raman e de fotoluminescência: potencialidades e complementaridades. **Revista Brasileira de Ensino de Física**. v. 34, n. 4, p. 4309, dez. 2012. DOI: http://dx.doi.org/10.1590/S1806-11172012000400009.

24. FERRARO, J. R.; NAKAMOTO, K.; BROWN, C. W. **Introductory Raman spectroscopy**. 2nd ed. Cambridge, US: Academic Press, 2003. ISBN 9780080509129.

25. DAVIES, T. The history of near infrared spectroscopic analysis: past, present and future “From sleeping technique to the morning star of spectroscopy”, **Analusis**, v. 26, n. 4, p. 17-19, 1998. DOI: http://dx.doi.org/10.1051/analusis:199826040017.

26. BURNS, D. A.; CIURCZAK, E. W. **Handbook of near-infrared analysis**. 3th ed. Boca Raton: CRC Press, 2007. ISBN 9780429123016.

27. PASQUINI, C. Near infrared spectroscopy: fundamentals, practical aspects and analytical applications. **Journal of Brazilian Chemical Society**, v. 14, n. 2, p. 198-219, Apr. 2003. DOI: http://dx.doi.org/10.1590/S0103-50532003000200006.

28. KELLEHER, J. D.; TIERNEY, B. **Data science**. Cambridge, US: MIT Press, 2018. ISBN 9780262535434.

29. SAGIROGLU, S.; SINANC, D. Big data: a review. *In*: INTERNATIONAL CONFERENCE ON COLLABORATION TECHNOLOGIES AND SYSTEMS (CTS), San Diego, US, 2013. **Proccedings** […]. [S. l.]: IEEE, 2013. p. 42-47. DOI: http://dx.doi.org/10.1109/CTS.2013.6567202.

30. LIAKOS, K. G.; BUSATO, P.; MOSHOU, D.; PEARSON, S.; BOCHTIS, D. Machine learning in agriculture: a review. **Sensors**, v. 18, n. 8, p. 1-29, 2018. DOI: http://dx.doi.org/10.3390/s18082674.

31. SCHMIDT, J.; MARQUES, M. R. G.; BOTTI, S.; MARQUES, M. A. L. Recent advances and applications of machine learning in solid-state materials science. **Computational Materials**, v. 5, n. 83, p.1-36, Aug. 2019. DOI: http://dx.doi.org/10.1038/s41524-019-0221-0

32. GHOLIZADEH, A.; BORŮVKA, L.; SABERIOON, M. M.; KOZÁK, J.; VAŠÁT, R.; NĚMEČEK, K. Comparing different data preprocessing methods for monitoring soil heavy metals based on soil spectral features. **Soil & Water Research**, v. 10, p. 218-227, 2015. DOI: http://dx.doi.org/10.17221/113/2015-SWR.

33. ZHANG, J. M.; HARMAN, M.; MA, L.; LIU, Y. Machine learning testing: survey, landscapes and horizons. **IEEE Transactions on Software Engineering**, v. 48, n. 1, p. 1-36, Jan. 2022. DOI: http://dx.doi.org/10.1109/TSE.2019.2962027.

34. MONARD, M. C.; BARANAUSKAS, J. A. Conceitos sobre aprendizado de máquina. *In*: MONARD, M. C.; BARANAUSKAS, J. A. **Sistemas inteligentes Fundamentos e Aplicações**. Barueri, SP: Manole, 2003. p. 89-114. ISBN 85-204-168.

35. CHANDRASHEKAR, G.; SAHIN, F. A survey on feature selection methods. **Computers & Electrical Engineering**, v. 40, n. 1, p. 16-28, Jan. 2014. DOI: http://dx.doi.org/10.1016/j.compeleceng.2013.11.024.

36. BELLINGER, C; SHAZAN, M.; JABBAR, M.; ZAÏANE, O.; OSORNIO-VARGAS, A. A systematic review of data mining and machine learning for air pollution epidemiology. **BMC Public Health**, v. 17, n. 907, p. 1-19, Nov. 2017. DOI: http://dx.doi.org/10.1186/s12889-017-4914-3.

37. LIN, X.; SU, H.; GAO, X.; XU, Y. T.; WANG, Z. X.; WANG, Y. Discrimination of lung tumor and boundary tissues based on laser-induced breakdown spectroscopy and machine learning. **Spectrochimica Acta Part B: Atomic Spectroscopy**, v. 180, p. 106200, June 2021. DOI: http://dx.doi.org/10.1016/j.sab.2021.106200.

38. ARMENTA, S.; GARRIGUES, S.; LA GUARDIA, S. Green analytical chemistry. **TrAC Trends in Analytical Chemistry**, v. 27, n. 6, p. 497-511, June 2008. DOI: http://dx.doi.org/10.1016/j.trac.2008.05.003.

39. FERREIRA, E. C.; FERREIRA, E. J.; VILLAS-BOAS, P. R.; SENESI, G. S.; CARVALHO, C. M.; ROMANO, R. A.; MARTIN-NETO, L.; MILORI, D. M. B. P. Novel estimation of the humification degree of soil organic matter by laser-induced breakdown spectroscopy (LIBS). **Spectrochimica Acta. Part B: Atomic Spectroscopy**, v. 99, p. 76-81, Sept. 2014. DOI: http://dx.doi.org/10.1016/j.sab.2014.06.016.

40. FERREIRA, E. C.; GOMES NETO, J. A.; MILORI, D. M. B. P.; FERREIRA, E. J.; ANZANO, J. M. Laser-induced breakdown spectroscopy: extending its application to soil pH measurements. **Spectrochimica Acta. Part B: Atomic Spectroscopy**, v. 110, p. 96-99, Aug. 2015. DOI: http://dx.doi.org/10.1016/j.sab.2015.06.002.

41. VILLAS-BOAS, P. R.; ROMANO, R. A.; FRANCO, M. M. A.; FERREIRA, E. C.; FERREIRA, E. J.; CRESTANA, S.; MILORI, D. M. B. P. Laser-induced breakdown spectroscopy to determine soil texture: a fast analytical technique. **Geoderma**, v. 263, p. 195-202, Feb. 2016. DOI: http://dx.doi.org/10.1016/j.geoderma.2015.09.018.

42. DIB, S. R.; SILVA, T. V.; GOMES NETO, J. A.; GUIMARÃES, L. J. M.; FERREIRA, E. J.; FERREIRA, E. C. Raman spectroscopy for discriminating transgenic corns. **Vibrational Spectroscopy**, v. 112, p. 103183, Jan. 2021. DOI: http://dx.doi.org/10.1016/j.vibspec.2020.103183.

43. MILORI, D. M. B. P.; GALETI, H. V. A.; MARTIN-NETO, L.; DIECKOW, J.; GONZÁLEZ-PÉREZ, M.; BAYER, C.; SALTON, J. Organic matter study of whole soil samples using laser-induced fluorescence spectroscopy. **Soil Science Society of American Journal**, v. 70, p. 57-63, Jan. 2006. DOI: http://dx.doi.org/10.2136/sssaj2004.0270

7 Anexos

Anexo 1

Spectrochimica Acta Part B 63 (2008) 1216–1220

Contents lists available at ScienceDirect

Spectrochimica Acta Part B

journal homepage: www.elsevier.com/locate/sab

Artificial neural network for Cu quantitative determination in soil using a portable Laser Induced Breakdown Spectroscopy system ☆

Edilene C. Ferreira [a,*], Débora M.B.P. Milori [a], Ednaldo J. Ferreira [a], Robson M. Da Silva [a,b], Ladislau Martin-Neto [a]

[a] Embrapa Agricultural Instrumentation, Rua XV de Novembro, 1452, São Carlos, SP, CEP: 13560-970, Brazil
[b] University of São Paulo, São Carlos Chemistry Institute, Av. Trabalhador São-carlense, 400, São Carlos, SP, CEP: 13560-970, Brazil

ARTICLE INFO

Article history:
Received 16 October 2007
Accepted 21 August 2008
Available online 29 August 2008

Keywords:
LIBS
Soil samples
Calibration strategy
ANN

ABSTRACT

Laser Induced Breakdown Spectroscopy (LIBS) is an advanced analytical technique for elemental determination based on direct measurement of optical emission of excited species on a laser induced plasma. In the realm of elemental analysis, LIBS has great potential to accomplish direct analysis independently of physical sample state (solid, liquid or gas). Presently, LIBS has been easily employed for qualitative analysis, nevertheless, in order to perform quantitative analysis, some effort is still required since calibration represents a difficult issue. Artificial neural network (ANN) is a machine learning paradigm inspired on biological nervous systems. Recently, ANNs have been used in many applications and its classification and prediction capabilities are especially useful for spectral analysis. In this paper an ANN was used as calibration strategy for LIBS, aiming Cu determination in soil samples. Spectra of 59 samples from a heterogenic set of reference soil samples and their respective Cu concentration were used for calibration and validation. Simple linear regression (SLR) and wrapper approach were the two strategies employed to select a set of wavelengths for ANN learning. Cross validation was applied, following ANN training, for verification of prediction accuracy. The ANN showed good efficiency for Cu predictions although the features of portable instrumentation employed. The proposed method presented a limit of detection (LOD) of 2.3 mg dm^{-3} of Cu and a mean squared error (MSE) of 0.5 for the predictions.

© 2008 Elsevier B.V. All rights reserved.

1. Introduction

Laser Induced Breakdown Spectroscopy (LIBS) is a type of atomic emission spectroscopy which employs a highly energetic laser pulse to simultaneously prepare the sample and excite the species. Usually, excited species return to their fundamental states emitting characteristic radiation. The qualitative analysis of emission spectrum provides the "fingerprint" of sample with regard to its elemental composition [1].

Using LIBS for element identifications is advantageous in that it allows direct and fast analysis, besides being almost non-destructive, since the ablated sample mass for laser pulse is in the order of micrograms [2,3].

The main features of LIBS, as for instance, the requirement for a small amount of sample and minimal sample preparation, are partially responsible for unsatisfactory figures of merit. Given that a small amount of material is removed for analysis, the accuracy and precision can be dependent on the sample homogeneity. Other conditions that affect the figures of merit are physical parameters, atmospheric conditions and sample matrix composition [4]. Nevertheless, if experimental conditions can be well controlled, especially those dependent of sample and sampling procedure, the LIBS can reach good precisions. Like other analytical techniques, some inconvenient conditions of analysis can be minimized by using appropriate calibration standards, which match with the samples. In LIBS, under determined analysis conditions, the physical parameters and atmospheric conditions can be fixed variables, however matrix effects prove more difficult to be controlled, owing to the fact that the LIBS signals from the same element often depend on the matrix in which it is embedded [2]. Thus, calibration has been an important issue to be considered for LIBS methods.

The simplest and better known calibration technique is based on the use of standard calibration curves. It consists in plotting interest intensity line as a function of known concentration from a set of calibration standards. Ideally, there will be a linear relationship between the element response and the mass or concentration over the

☆ This paper was presented at the Euro Mediterranean Symposium on Laser Induced Breakdown Spectroscopy (EMSLIBS 2007) held in Paris (France), 11–13 September 2007, and is published in the Special Issue of Spectrochimica Acta Part B, dedicated to that conference.

* Corresponding author. Tel.: +55 16 3374 2477; fax: +55 16 3372 5958.
E-mail addresses: edilene@cnpdia.embrapa.br (E.C. Ferreira), debora@cnpdia.embrapa.br (D.M.B.P. Milori), ednaldo@cnpdia.embrapa.br (E.J. Ferreira), robson@cnpdia.embrapa.br (R.M. Da Silva), martin@cnpdia.embrapa.br (L. Martin-Neto).

0584-8547/$ – see front matter © 2008 Elsevier B.V. All rights reserved.
doi:10.1016/j.sab.2008.08.016

entire range investigated, and a linear fit to the data should pass through the origin [5]. Nevertheless, calibration curves with a composition as close as possible to unknown samples are not feasible for most of the interest samples. In soil analysis, for instance, it is almost impossible to obtain matching standards calibration with samples. Moreover, soils from different regions present different chemical and physical compositions and, consequently, different matrices. Hence, it increases the difficulty in producing a set of calibration standards [5,6]. Moreover, the phenomenon of self-absorption may be considered as factor of linearity deviation in conventional calibration. This phenomenon is a consequence of loss of signal at high analite concentrations [5]. For this reason, linear models can be the most time unsatisfactory.

Methods employing calibration-free algorithm (without use of calibration curves) proposed by Ciucci et al. [7], have been applied to dribble matrix effects. Such approach is based on models proposed to account for the effect of relevant factors associated to the laser parameters, the sample and its environment [8]. However, this technique has not been widely considered as a method as it still needs to be better studied, since the quality of results has been sample dependent [5].

Chemometric methods have also been applied to different analytical methods. LIBS technique has increasingly been associated with these methods, in order to improve its analytical performance with respect to the standard calibration curve [6]. Chemometric techniques such as: principal component analysis (PCA), partial least-squares (PLS) and artificial neural network (ANN) have been applied to extract spectral information in different analytical techniques [9–13].

ANN is a massive parallel distributed processor that has a natural propensity for storing experimental knowledge, hence making it available for use. Due to its superior classification and prediction capabilities, ANNs have found their impact in spectral analysis [14–16].

This paper focuses on the use of ANN as a calibration strategy for Cu determination in soil samples using a portable LIBS system.

2. Theoretical

2.1. Laser Induced Breakdown Spectroscopy

LIBS is a simple analytical technique to determine the elemental composition, which utilizes a focused high energy laser pulse to create a plasma in a solid, liquid, or gaseous media. In analysis of solid or liquid samples, part of the energy in the plasma is used to ablate the material. After the ablation process, the plasma rapidly expands, sending a shock wave into the surrounding media. In the core of the plasma, effective temperatures can easily exceed 20,000 K. During this stage, material in the core of the plasma is vaporized, atomized and ionized, and the plasma is typically highly ionized. Usually after 0.5 to 1.0 μs, the neutral species in the plasma typically reach local thermodynamic equilibrium (LTE). From this time, upper electronic states of atoms and ions are populated in Boltzmann equilibrium [17,18].

As the plasma cools, continuum emission from the plasma (Bremsstrahlung emission) fades, typically much faster than emission lines from neutral and singly-ionized atomic lines. Thus, by adjusting an optimal temporal detector gating it is possible to collect elemental emission [19].

2.2. Artificial neural network

The ANN has been motivated right from its inception by recognizing that the human brain computes in an entirely different way from the conventional digital computer. The brain is a highly nonlinear information-processing system and parallel computer. It has the capacity to organize its structural constituents (neurons) to perform certain computations (e.g. pattern recognition, perception and motor control) many times faster than the fastest digital computer [20].

An ANN represents a computational paradigm that undertakes solving problems by imitating the structure of human brain. It involves a network of simple processing elements (artificial neurons), which can exhibit complex global behavior, determined by the connections (analogous to synapses in human brain) between the processing elements and element parameters. In other words, ANNs are nonlinear statistical models or decision making tools, whose practical use comes with algorithms designed to alter the strength (weights) of the connections in the network to produce a desired signal flow [21].

In Fig. 1 is illustrated a useful scheme of an ANN structured in layers, like that used in this work. Each layer has a set of neurons and each neuron has a mathematical function responsible for its activation. Sigmoidal functions are commonly used for all the neurons. The first layer receives a set of values, i.e. an input vector containing the values for measured, variables. The dimensionality of the vector corresponds to the number of neurons in the input layer. The weights are a set of numerical values (weight vector) associated with each neuron for representing its synaptic connections. The knowledge is codified in weights by means of an algorithm. The inner product between input vector and weight vector is applied to the activation function to produce the neuron output. The outputs of a layer are used as input for the next layer. As result, the output layer provides a value or a set of values, corresponding to propagation of a set of values from input layer to output layer (forward phase).

A task is learned for an ANN from a training dataset, which is a set of input vectors with their respective desired outputs. The procedure applied to perform the training process is called learning algorithm, whose function is to modify the weights of the network aiming to attain a desired goal [20]. During the training process, all the weights are changed to minimize the error between desired output and ANN output. The learning paradigm of ANNs involves developing mathematical models to extract important features from the training dataset [22].

After training process, a validating process should be performed to estimate the ANN performance on testing datasets. The ANN which yields good validation performance is an accurate model [22].

3. Experimental

Fifty nine Brazilian soil samples, provided by AIC (Agronomic Institute of Campinas), with reference values for Cu labile concentration, were used as calibration set. Each reference soil sample presents different composition with regard to sand, clay and silt amounts in their matrices. The use of different soil matrices for calibration was

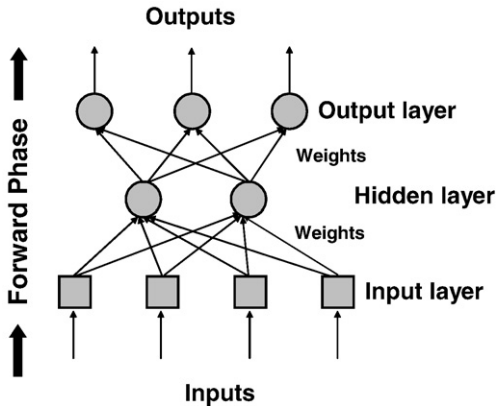


Fig. 1. A typical artificial neural network setup.

considered to obtain a model for Cu determination independently of the soil matrix. Table 1 provides Cu reference values and their respective standard deviation for all used samples.

The samples were submitted to a cryogenic grounding to reduce their heterogeneity. For the grounding process a cryogenic mill from SpexCertiprep model 6750 was used, which works at liquid nitrogen temperature (−196 °C). The grounding program used consisted of two grounding steps of 2 min each one, 3 min of pre-cooling and 2 min of cooling between grounding steps. With this procedure size of particles between 60 μm and 120 μm was obtained. The ground samples were used to make pellets. The pellets were prepared by applying 15 ton of pressure on the samples for 3 min.

Table 1
Reference values for labile Cu of 59 samples used as calibration set

Sample	Cu (mg dm^{-3})
AIC 237	2.4 (±0.4)
AIC 238	10 (±1)
AIC 239	1.1 (±0.1)
AIC 240	1.9 (±0.3)
AIC 241	0.9 (±0.2)
AIC 242	2.1 (±0.3)
AIC 243	1.0 (±0.2)
AIC 244	0.6 (±0.1)
AIC 245	9.3 (±0.2)
AIC 246	2.6 (±0.4)
AIC 247	0.7 (±0.1)
AIC 248	9 (±1)
AIC 249	9.4 (±0.9)
AIC 250	2.2 (±0.3)
AIC 251	1.9 (±0.3)
AIC 252	10 (±1)
AIC 253	1.0 (±0.1)
AIC 254	9.5 (±0.6)
AIC 255	2.2 (±0.3)
AIC 256	9.4 (±0.7)
AIC 257	1.6 (±0.2)
AIC 258	0.7 (±0.2)
AIC 259	2.8 (±0.4)
AIC 260	2.5 (±0.3)
AIC 261	0.2 (±0.1)
AIC 263	1.8 (±0.3)
AIC 264	2.4 (±0.3)
AIC 265	1.5 (±0.2)
AIC 266	4.7 (±0.7)
AIC 267	5.1 (±0.9)
AIC 268	1.5 (±0.2)
AIC 269	0.7 (±0.1)
AIC 270	2.7 (±0.4)
AIC 271	5.2 (±0.9)
AIC 272	1.8 (±0.2)
AIC 273	2.8 (±0.4)
AIC 274	1.8 (±0.2)
AIC 275	2.8 (±0.4)
AIC 276	2.4 (±0.2)
AIC 277	2.8 (±0.4)
AIC 278	3.2 (±0.5)
AIC 279	0.5 (±0.1)
AIC 280	2.6 (±0.3)
AIC 281	2.9 (±0.3)
AIC 282	1.5 (±0.2)
AIC 283	1.7 (±0.3)
AIC 284	1.6 (±0.3)
AIC 285	3.1 (±0.5)
AIC 286	1.4 (±0.3)
AIC 287	2.8 (±0.6)
AIC 288	0.7 (±0.2)
AIC 289	5.2 (±0.8)
AIC 290	2.6 (±0.3)
AIC 291	1.7 (±0.2)
AIC 292	3.1 (±0.4)
AIC 293	2.8 (±0.3)
AIC 294	1.7 (±0.2)
AIC 295	2.8 (±0.4)
AIC 296	2.6 (±0.2)

The LIBS spectra of each sample were captured by using a portable LIBS system (Porta-LIBS 2000) from StellarNet Inc. This system is comprised of a permanently aligned Nd-YAG laser (MK-367) from Kigre Inc. operating at 1064 nm, with a passive Q switch and 6 MW peak per 4 ns pulse (25 mJ) at 1 Hz pulse repetition rate; the laser spot on the sample is approximately 0.2 mm^2. Four spectrometers EPP2000 LSR fitted with a 2048 elements non-intensified CCD detector and optical fibers to collect and lead the plasma emission to the detection system. The four spectrometers cover a spectral bandwidth of 190–1000 nm with spectral resolution of 0.2 nm and a fixed delay time of 2 μs for spectra acquisition.

To improve the precision of results, 60 spectra were captured for each reference sample, being each spectrum corresponding to one shot in different regions of the pellets. A previous shot was also used to clean the surface of pellets, before capturing the spectrum. The captured spectra were considered in a range of 190 nm to 400 nm.

Spectra were corrected for noise and offset. The factor used for offset correction was obtained averaging 85 points from spectrum in the range of 202.2 nm to 210.2 nm, which corresponds to a region free of signal. The factor of correction obtained for each spectrum was then subtracted from the own spectrum. The noise was smoothed performing an average of 60 spectra previously corrected for offset.

Firstly the conventional calibration obtained by fitting models of linear regression was experimented. This procedure was accomplished aiming to verify the possibility of performing calibration with simple model. The linear model was experimented for two different Cu atomic lines: 324.7 nm and, 327.4 nm.

After performing models for conventional calibration, ANN was experimented. The dataset used for this aim was 59 spectra, with their respective Cu reference values. Instead of using all 2048 wavelengths, a pre-processing procedure was applied to reduce the number of variables (wavelengths) to avoid a low-performance of the ANN. This procedure consisted of two strategies for selection of the relevant wavelengths. The first one consisted in an empirical strategy aiming to find the wavelength with the best linear correlation with Cu concentration and smaller medium squared error (MSE). This task was performed by fitting a model using a simple linear regression (SLR).

The second strategy aimed to select a set of wavelengths with some important property for Cu predictions. This task was performed by using a feature selection approach based on wrapper [23]. The wrapper is an effective technique for feature selection, however it has a high computational cost and its performance depends on the algorithm embedded in it. Thus, a lower cost algorithm, called Instance Based (IB-*k*, where *k* is a required parameter) was used to improve the wrapper performance [23,24].

The set of wavelengths selected by these two strategies was used as the input for ANN, while the Cu values of each reference sample were the desired output.

The ANN adopted was a MultiLayer Perceptron (MLP), similar that depicted in Fig. 1, available in JAVA on Weka system, which provides several tools for machine learning and data mining [25]. For this proposal, the activation function used for all neurons activation was the hyperbolic tangent.

The MLP was trained by backpropagation algorithm [26]. The backpropagation parameters and the MLP topology were the following: learning rate = 0.1, momentum = 0.2, epochs = 3300 and one hidden layer with 7 elements (neurons).

The performance of the MLP was evaluated by the MSE and the Pearson's correlation coefficient calculated for predictions and reference values using only testing data.

For an adequate estimation of the MSE, a 10-fold cross validation methodology was applied. In this methodology, the dataset is partitioned into 10 equal sized sets, and then each set is used as the test set while a MLP is trained on the other nine sets. This process is repeated for each test set, for a total of ten times. This method makes possible that each sample may be seen as a testing instance for which the prediction error (MSE) can be calculated.

4. Results and discussions

Analytical calibration is an essential aspect for the quality of the analysis. Therefore, the first step in a new analytical method proposal is to define the appropriate material and method for calibration [27].

Obtaining appropriate material for analytical calibration can be quite complex. Direct analysis of soil samples by LIBS is a typical instance of such difficulty. Soil samples present intricate matrices, and the use of a single reference material to perform calibration curves does not reproduce the real situation, leading to errors in determinations.

The LIBS spectra obtained by the employed system present low spectral resolution (0.2 nm) and high noise levels (Fig. 2a). However, the average of 60 spectra had smoothed it considerable (Fig. 2b).

A conventional linear model for calibration was evaluated. Nevertheless, no good linear model was obtained. For the most intense atomic Cu lines 324.7 nm and 327.4 nm, the obtained *r*-values were 0.09 and 0.11 respectively. Thus, the simple analysis of *r*-value shows the lack of linearity. Possibly, due to the low spectral resolution of used instrument, lines like Ti (324.86 nm), V (326.77 nm, 327.11 nm and 327.61 nm) and Na (327.42 nm), which are elements present in these samples, could interfere in these intense Cu lines and consequently damage the linearity.

Nevertheless, the spectral resolution and the matrix effect (commonly present in LIBS spectra) have lower influence on MLP calibration methods, because MLP can use different information besides peak height if such information is considered important to predict the variable of interest [20]. Then aiming to use MLP to perform a strategy of calibration, data mining was employed to extract from spectra relevant wavelengths for Cu predictions.

The first strategy applied to wavelength selection indicated the wavelength 224.6 nm. The SLR model showed a MSE of 3 (mg dm^{-3})^2,

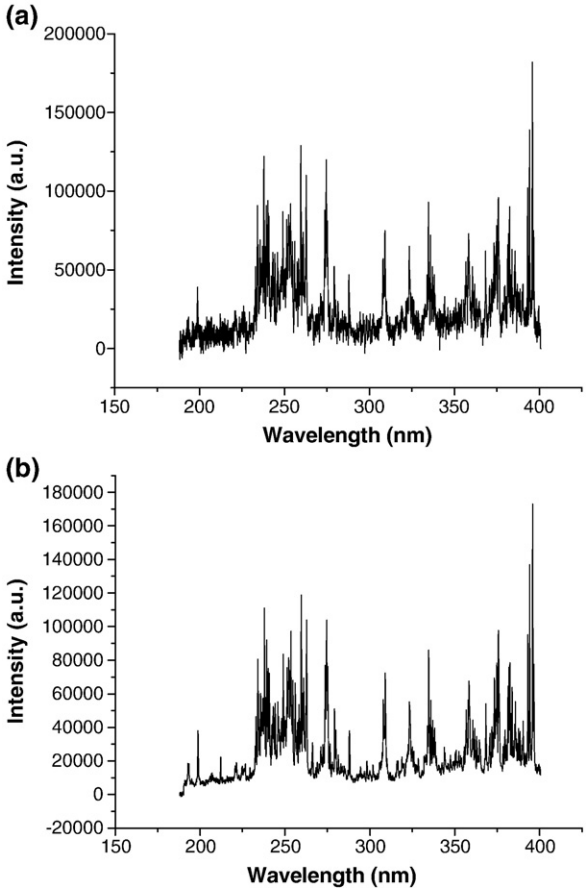


Fig. 2. Spectra captured by portable LIBS system. (a) Single shot (b) average of 60 shots.

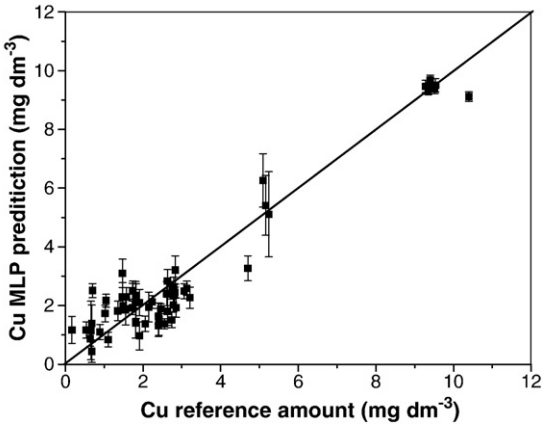


Fig. 3. Correlation between Cu certified values and Cu predicted by ANN (R=0.96).

and a Pearson's correlation coefficient (r) of 0.74. The wavelength 224.6 nm corresponds to intermediate region between the peaks at 224.4 nm and 224.7 nm (Cu I and Cu II respectively). Probably, these peaks present interference, but between them the SLR found the region with higher linear correlation. In fact, this was the best linear correlation with Cu concentration considering all wavelengths of spectrum. Note that in spite of this wavelength had presented higher *r*-value, the MSE (3) and the *r*-value (0.74) was considered inadequate for an appropriate linear model of calibration.

For the second strategy (wrapper approach) the parameter required for IB-*k* was defined as 5 (k=5) [24]. The selected wavelengths using this approach were: 207.3 nm, 221.3 nm, 247.4 nm, 270.2 nm and 399.1 nm. From this subset, only the wavelength 270.2 nm corresponds to a Cu line (Cu II 270.10 nm). Although the other selected wavelengths are uncorrelated to Cu lines, the set presented some degree of importance for predictions, according to the adopted approach. Possibly, there is some kind of correlation among Cu and the selected wavelengths in all evaluated soil. Nevertheless, the comprehension of this correlation is part of our ongoing research.

The 10-fold cross validation was applied using the dataset and the settings detailed in Section 3. For each fold, 53 samples were used in MLP training and six samples remain for test. This procedure was repeated ten times until that all samples were predicted. The predictions are depicted in Fig. 3.

Table 2
Comparison among reference values and MLP predicted values

Sample	Cu (mg dm^{-3}) reference value	Cu (mg dm^{-3}) MLP predicted value
AIC 238	10 (±1)	9.5 (±0.2)
AIC 245	9.3 (±0.2)	9.5 (±0.2)
AIC 248	9 (±1)	9.4 (±0.2)
AIC 249	9.4 (±0.9)	9.7 (±0.2)
AIC 252	10 (±1)	9.1 (±0.2)
AIC 254	9.5 (±0.6)	9.4 (±0.2)
AIC 256	9.4 (±0.7)	9.3 (±0.1)
AIC 259	2.8 (±0.4)	2.4 (±0.4)
AIC 266	4.7 (±0.7)	3.3 (±0.4)
AIC 267	5.1 (±0.9)	6.3 (±0.9)
AIC 271	5.2 (±0.9)	5 (±1)
AIC 273	2.8 (±0.4)	2.5 (±0.3)
AIC 277	2.8 (±0.4)	2.4 (±0.2)
AIC 278	3.2 (±0.5)	2.3 (±0.4)
AIC 280	2.6 (±0.3)	2.4 (±0.4)
AIC 285	3.1 (±0.5)	2.5 (±0.3)
AIC 287	2.8 (±0,6)	2.6 (±0.4)
AIC 289	5.2 (±0.8)	5 (±1)
AIC 292	3.1 (±0.4)	2.6 (±0.2)
AIC 293	2.8 (±0.3)	2.5 (±0.2)
AIC 295	2.8 (±0.4)	3.2 (±0.5)

It can be observed that the values predicted by MLP presented good correlation with reference values with $r=0.96$ calculated for all the samples in the 10-fold cross validation. The MSE estimated for MLP predictions was 0.5 $(\text{mg dm}^{-3})^2$ and the limit of detection (LOD) calculated for the proposed methodology, according to Sirven et al. [28] was 2.3 mg dm^{-3}.

In Table 2 is shown the Cu predicted and the Cu values from reference samples. Only samples which present Cu concentration above LOD were considered in this table. An estimation of the standard deviation was provided for the predictions. This estimation was obtained after a study of the sampling size, using a progressive sampling approach. The results showed that 20 shots are enough to get a smoothed spectrum and that the average of spectra does not show significant deviation for more than 20 shots. This study made possible three measurements from the same sample. Therefore, each testing sample was considered in triplicate, being each replicate an average of 20 spectra, from which the standard deviation for the prediction could be estimated.

The predictions results show the good performance of MLP for predictions of Cu concentration above 2.3 mg dm^{-3}. Therefore, the deficiency of the instrumental features employed, which made difficult to perform conventional calibration, could be compensated for the use of MLP.

5. Conclusions

The difficulty in establishing an efficient calibration for analytical methods is significantly increased when performing direct solid analysis due to the high level of complexity of the matrices. The complexity of the spectrum emission lines from LIBS, low sensitivity and low spectral resolution of some detectors make it difficult to detach interest lines. Moreover, the lack of linearity among Cu reference values and emissions lines intensities in the set of samples studied showed that linear models cannot be efficient strategy to perform quantitative analysis. The use of data mining and MLP for LIBS calibration methods proved to be an efficient strategy for Cu determination in soil. The MLP proposed presented good accuracy (MSE=0.5) for prediction of Cu in a heterogenic set of soil samples, however the use of low spectral resolution detector. The proposed method also presented LOD rather adequate for this proposal, which uses a portable LIBS instrument.

Acknowledgments

The authors express their gratitude for the grant from Fundação de Amparo a Pesquisa do Estado de São Paulo (FAPESP) and EMBRAPA—Agricultural Instrumentation, for financial support and structure of this work, and also to Dr. Gilberto Batista de Souza for concession of soil samples.

References

[1] C. Pasquini, J. Cortez, L.M.C. Silva, F.B. Gonzaga, Laser Induced Breakdown Spectroscopy, J. Braz. Chem. Soc. 18 (2007) 463–512.
[2] J.M. Anzano, M.A. Villoria, A. Ruíz-Medina, R.J. Laceras, Laser-Induced Breakdown Spectroscopy for quantitative spectrochemical analysis of geological materials: effects of the matrix a simultaneous determination, Anal. Chim. Acta 575 (2006) 230–235.
[3] D. Santos-Júnior, L.V.G. Tarelho, F.J. Krug, D.M.B.P. Milori, L. Martin-Neto, N.D. Vieira-Júnior, Espectrometria de emissão óptica com plasma induzido por laser (LIBS)—fundamentos, aplicações e perspectivas, Rev. Anal. 24 (2006) 72–81.
[4] B.C. Castle, K. Talabardon, B.W. Smith, J.D. Winefordner, Variables influencing the precision of Laser-induced Breakdown Spectroscopy measurements, Appl. Spectroc. 52 (1998) 649–657.
[5] D.A. Cremers, L.J. Radziemski, Handbook of Laser-induced Breakdown Spectroscopy, John Wiley & Sons Ltd, Chichester, 2006.
[6] J.-B. Sirven, B. Bousquet, L. Canioni, L. Sarger, Laser-induced Breakdown Spectroscopy of composite samples: comparison of advanced chemometrics methods, Anal. Chem. 78 (2006) 1462–1469.
[7] A. Ciucci, M. Corsi, V. Palleschi, A. Rastelli, A. Salvetti, E. Tognoni, A new procedure for quantitative analysis by laser induced breakdown spectroscopy, Appl. Spectrosc. 53 (1999) 960–964.
[8] V.S. Burakov, S.N. Raikov, Quantitative analysis of alloys and glasses by a calibration-free method using laser-induced breakdown spectroscopy, Spectrochim. Acta Part B 62 (2007) 217–223.
[9] D.L. Massart, B.G.M. Vandeginste, S.N. Deming, Y. Michotte, Chemometrics: A Textbook, Elsevier Science Publishers B V, Amsterdam, 1988.
[10] S. Wold, M. Sjöström, L. Eriksson, PLS-regression: a basic tool of chemometrics, Chemom. Intell. Lab. Syst. 58 (2001) 109–130.
[11] M. Blanco, I. Villarroya, NIR spectroscopy: a rapid-response analytical tool, TrAC Trends Anal. Chem. 21 (2002) 240–250.
[12] R.J.H. Waddell, N. NicDaéid, D. Littlejohn, Classification of ecstasy tablets using trace metal analysis with the application of chemometric procedures and artificial neural network algorithms, Analyst 129 (2004) 235–240.
[13] B.H. Menze, W. Petrich, F.A. Hamprecht, Multivariate feature selection and hierarchical classification for infrared spectroscopy: serum-based detection of bovine spongiform encephalopathy, Anal. Bioanal. Chem. 387 (2007) 1801–1807.
[14] K.H. Ott, N. Aranibar, B. Singh, G.W. Stockton, Metabonomics classifies pathways affected by bioactive compounds. Artificial neural network classification of NMR spectra of plant extracts, Phytochemistry 62 (2003) 971–985.
[15] T. Baczek, A. Buciñski, A.R., R. Kaliszan, Artificial Neural Network analysis for evaluation of peptide ms/ms spectra in proteomics, Anal. Chem. 76 (2004) 1726–1732.
[16] M.C. McCann, M. Defernez, B.R. Urbanowicz, J.C. Tewari, T. Langewisch, A. Olek, B. Wells, R.H. Wilson, N.C. Carpita, Neural network analyses of infrared spectra for classifying cell wall architectures, Plant Physiol. 143 (2007) 1314–1326.
[17] A.W. Miziolek, V. Palleschi, I. Schechter, Laser Induced Breakdown Spectroscopy, Cambridge University Press, New York, 2006.
[18] R. Barbini, F. Colao, R. Fantoni, A. Palucci, F. Capitelli, Application of laser-induced breakdown spectroscopy to the analysis of metals in soils, Appl. Phys. 69 (1999) 175–178.
[19] B.T. Fisher, H.A. Johnsen, S.G. Buckley, D.W. Hahn, Temporal gating for the optimization of Laser-induced Breakdown Spectroscopy detection and analysis of toxic metals, Appl. Spectrosc. 55 (2001) 1312–1319.
[20] S. Haykin, Neural Networks: A Comprehensive Foundation, second ed., Prentice Hall, New Jersey, 1999.
[21] G. Naomi, The Brain-shaped Mind: A Neural-Network View: What the Brain Can Tell us About the Mind, Cambridge University Press, New York, 2001.
[22] P. Inakollu, A study of the effectiveness of neural networks for elemental concentration from LIBS Spectra, Thesis submitted to the faculty of Mississippi State University in partial fulfillment of the requirements for the degree of master of Science in Computer Engineering, Mississippi, 2003, p. 50.
[23] R. Kohavi, G.H. John, Wrappers for feature subset selection, Artif. Intell. 97 (1997) 273–324.
[24] D. Aha, D. Kibler, M.K. Albert, Instance-based learning algorithms, Mach. Learn. 6 (1991) 37–66.
[25] I.H. Witten, E. Frank, Data Mining: Practical Machine Learning Tools and Techniques, second ed., Elsevier, San Francisco, 2005.
[26] D.E. Rummelhart, G.E. Hinton, R.J. Williams, Learning representations by back propagation errors, Nature 323 (1986) 533–536.
[27] U. Kurfürst, Solid Sample Analysis: Direct and Slurry Sampling Using GF-AAS and ETV-ICP, Springer, Berlin, 1998.
[28] J.-B. Sirven, B. Bousquet, L. Canioni, L. Sarger, S. Tellier, M. Potin-Gautier, I. Le Hecho, Qualitative and quantitative investigation of chromium-polluted soils by laser-induced breakdown spectroscopy combined with neural networks analysis, Anal. Bioanal. Chem. 385 (2006) 256–262.

Anexo 2

Ensemble of predictors and laser induced breakdown spectroscopy for certifying coffee

E.J. Ferreira, E.C. Ferreira, A.C.B. Delbem and D.M.B.P. Milori

The commercial demand and the economic value of roasted and ground coffee (RGC) are intrinsically related to its quality. Brazilian RGC has been certified for quality based on a score assigned by expert tasters. However, intrinsic costs and the lack of fast techniques make large-scale analysis prohibitive. Laser induced breakdown spectroscopy (LIBS) is a promising technique for RGCs, however it demands an accurate coupled-model for pattern recognition. In this reported work, two ensemble methods in ranges around 680 nm of LIBS spectra are employed to construct ensembles of decision trees for RGC classification. Results show accuracies above 84% for ensemble methods in some spectral ranges. The best performances were in the range 670–690 nm, making viable the design of dedicated equipment with low-cost devices.

Introduction: The Brazilian coffee industry and producers have shown a growing concern for quality certification of roasted and ground coffee (RGC), since the commercial demand and the economic value of the product are strongly related to it. Quality for coffees is a multifactorial metric related to organoleptic features, blend of different cultivars, purity, grains, among others. The Association of the Brazilian Coffee Industry (ABIC) has provided certification for Brazilian RGCs based on a well-defined score referred to as Global Quality (GQ), which is assessed using several organoleptic features assigned by expert coffee tasters. It has been useful to classify RGCs into four GQ classes: *Inferior*, for GQ below 4.5; *Traditional*, for GQ between 4.5 and 5.9; *Superior*, for GQ between 6.0 and 7.3; and *Gourmet*, for GQ above 7.3. However, an appropriate estimation of GQ demands a panel of expert tasters, with a high maintenance cost for large-scale analysis. This is why ABIC is looking for fast techniques to classify RGCs similarly to experts.

Ferreira *et al.* [1] proposed an ensemble method (EM), called the Random Subspace Method in Principal Components Space (RSM-PCS), for constructing a regression model to predict the GQ from electrical features provided by an electronic tongue. However, in practice the methodology for preparation of the RGC solutions, stabilisation, cleaning of microelectrodes and measurements demand high processing time, which makes that proposal unsuitable for large-scale analysis.

Laser induced breakdown spectroscopy (LIBS) is a fast analytical technique that requires a minimum or no sample preparation [2], with a significant potential for organic compounds and food analysis [3, 4]. Graphical analysis of LIBS spectra has indicated a region where RGCs seem to be distinctively organised according to some GQ classes. However, the information entropy varies in this region, making difficult the selection of a single descriptor for an accurate classification. There is now the challenge of recognising spectral patterns from this region, as well as restricting it to an operating range for higher classification accuracy. In this context, robust and accurate machine learning models, such as those based on ensembles of predictors, are promising for recognition of these patterns.

In this Letter, we propose the use of EMs to construct ensembles of predictors for classification of RGCs, according to their GQ classes, using a spectral range from LIBS spectra. Moreover, we investigate several ranges and propose the use of these models only in a specific range for a higher accuracy.

LIBS and GQ classes: LIBS is a fast analytical technique based on emission spectroscopy. It uses a highly energetic laser pulse for ablation of a small amount of a sample and the induction of a high-temperature plasma. The light emitted during the cooling of the plasma is spectroscopically analysed and the elements present in the sample show unique spectral responses [2].

Machine learning and statistical techniques have been successfully coupled with LIBS for several applications, such as soils, protein classification and food analysis [3–5]. A preliminary graphical analysis using LIBS for RGCs has indicated wavelengths with good potential for the distinction of some GQ classes in a region around 680 nm, right side of the hydrogen emission line (H_α), as a result of a still inexplicable physicochemical effect. Ongoing works are investigating causes responsible for it, including molecular emission effects and others. However, changes in information entropy make it difficult to select manually only one or more wavelengths (features) as accurate descriptors for all GQ classes, demanding an appropriate machine learning inducer, such as decision tree algorithms. In that sense, higher accuracies can be reached by using an ensemble of decision trees constructed by an appropriate EM.

Ensembles and methods: An ensemble is a model consisting of a set of predictors the individual predictions of which are combined in some way to produce the ensemble prediction. In general, the combination of accurate and diverse predictors produces a model more accurate than its individual predictors [6].

Many EMs for constructing ensembles have been developed. Ho [7] proposed an effective method based on a simple random selection of features, also called the random subspace method (RSM). RSM picks at random Z features (subspace size) to build each ensemble predictor. Ferreira *et al.* [1] proposed applying RSM in the principal components space (RSM-PCS) with advantages for their application.

A method derived from both RSM and RSM-PCS, referred to as RSM-IPCS, is proposed in [8]. To explore the synergy in the characteristics of these two EMs, RSM-IPCS builds a subset of predictors from the instance space, such as RSM, and another subset from the principal components space, such as RSM-PCS. This approach showed relevant results compared to both RSM and RSM-PCS.

Rodríguez *et al.* [9] proposed another EM referred to as the Rotation-Based Method (RBM). In this EM, the set of features is randomly split into K subgroups. For each subgroup, instances of a random subset of classes are eliminated; then a percentage P of instances is randomly removed. Principal components analysis is then applied to each subgroup as a rotation technique. Finally, each ensemble predictor is built from a training set transformed according to K local rotations. Both RBM and RSM-IPCS were chosen for this study because they have shown significant results with decision trees algorithms.

Experiments and settings: An Ocean Optics LIBS2500 system was used to acquire the RGC spectra. This system is composed of a Q-switched Nd:YAG laser at 1064 nm manufactured by Quantel (Big Sky Laser Ultra50) with a single-pulse energy 50 mJ and duration of 8 ns, 10 Hz repetition rate; an ablation chamber; a detection system with seven spectrometers with CCD arrays (2048-element linear) providing a spectral resolution of 0.1 nm and a spectral range of 188–980 nm. It was used only in the range of 618–716 nm.

Forty-one commercial samples of certified RGCs from different Brazilian regions were used, being 11 *Inferior*, 11 *Traditional*, 10 *Superior* and 9 *Gourmets*. Three pellets were prepared for each sample by applying 12-ton pressure. Twenty spectra were acquired from different regions of each pellet. A laser shot was used to clean the pellet surface before acquiring two accumulated spectra. An average of 60 spectra for the three pellets was used as the mean spectrum representing the sample. A 9-point unweighted sliding-average smooth was applied to the mean spectrum to minimise noise levels. For offset adjustment, the value in the 618 nm wavelength (offset point) was subtracted from all spectral points. To minimise signal fluctuations derived from the laser and/or other related effects, each mean spectrum was divided by its mean intensity. This procedure normalised variations observed on different days of acquisitions, attributing robustness and reproducibility to the proposal.

The experiments were performed in the Weka software [10] using the *Experimenter* environment. Twenty-five growing bandwidths at around 680 nm, i.e. 2 nm for the range 679–681 nm, 4 nm for 678–682 nm, 6 nm for 677–683 nm, and so on, up to 50 nm for 655–705 nm, were compared for performance using a decision tree algorithm – C4.5 [11] (J48 in Weka with default parameters) and the two proposed EMs: RSM-IPCS and RBM. The ensemble size was 50 decision trees, also induced by J48 (default parameters), being half for each space in RSM-IPCS. Performances were analysed for subspace sizes (Z-parameter) of 5, 10, 15, 20, 25 and 30% of the bandwidth dimensionality for RSM-IPCS (for both spaces). Likewise, 3, 4, 5, 7, 10, 20 subgroups (K-parameter) were considered for RBM. The covered variance for principal components was 100% for both EMs. All results were averaged using 10 runs of 15-fold stratified cross-validation and compared for significant differences in accuracy using a paired t-test with 95% confidence level.

Results: Only the best results, considering the settings for RSM-IPCS or RBM, are shown in Fig. 1. The best performances for the EMs were statistically significant compared to the best performance of J48. J48 showed the best result (80.56% ±21.88) for 20 nm bandwidth (670–690 nm); while the best accuracy for RSM-IPCS was 84.78% ±19.97 for 26 nm (667–693 nm). RBM showed the higher accuracy, 85.33% ±20.52, for 16 nm (672–688 nm); however, there was no real significance compared to the best performance of RSM-IPCS.

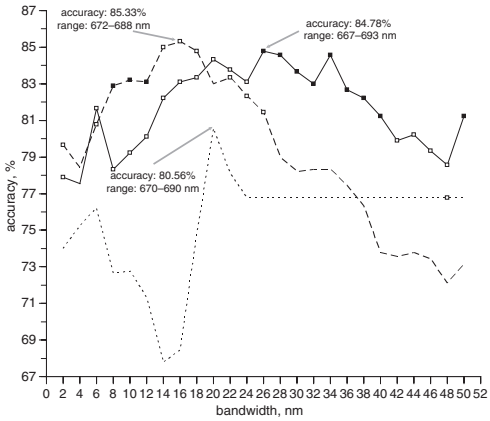


Fig. 1 *Performance comparisons in growing bandwidths at around 680 nm*
——— RSM-IPCS
– – – RBM
- - - - J48 (C4.5)

Methods were also compared in bandwidth (Fig. 1). A filled square on the line indicates that the method is statistically better than the other two in the respective bandwidth. An open square indicates that the method outperforms statistically only the one with the lowest accuracy in the respective bandwidth. RBM was statistically better than RSM-IPCS in three bandwidths. On the other hand, RSM-IPCS was statistically better than RBM for all bandwidths above 26 nm. In general, bandwidths too narrow or too wide did not provide satisfactory performance, although RSM-IPCS was shown to be less sensitive compared to others. The region between 14 and 26 nm bandwidth was promising for both EMs. On average, the three methods performed satisfactorily in the range of 670–690 nm, with emphasis on RSM-IPCS.

Conclusions: Two EMs were applied to construct ensembles of decision trees to classify RGCs according to their GQ classes using ranges from LIBS spectra. Both EMs constructed models with accuracies above 84%, being statistically better than J48. RSM-IPCS showed better results compared to both RBM and J48 for most ranges. In general, the three methods built models with a satisfactory accuracy in the range of 670–690 nm, especially RSM-IPCS with an accuracy of 84.33%. These results show that the coupling of ensemble models with a LIBS system creates a fast technique for large-scale analysis of RGCs, with relatively high accuracy. More importantly, the operating range (670–690 nm) makes possible the use of cheaper acquisition devices and minimises costs for the construction of dedicated equipment.

Acknowledgments: Financial support was given by Embrapa, and we acknowledge S. Lemos for providing some RGCs.

© The Institution of Engineering and Technology 2011
19 April 2011
doi: 10.1049/el.2011.1150

E.J. Ferreira, E.C. Ferreira and D.M.B.P. Milori (*EMBRAPA Instrumentação Agropecuária, CP 741, 13.560-970, São Carlos, SP, Brazil*)

E-mail: ednaldo@cnpdia.embrapa.br

A.C.B. Delbem (*Instituto de Ciências Matemáticas e de Computação, ICMC, USP, CP 668, São Carlos, SP 13560-970, Brazil*)

References

1 Ferreira, E.J., Pereira, R.C.T., Delbem, A.C.B., Oliveira, O.N., and Mattoso, L.H.C.: 'Random subspace method for analysing coffee with electronic tongue', *Electron. Lett.*, 2007, **43**, (21), pp. 1138–1140
2 Mansoori, A., Roshanzadeh, B., Khalaji, M., and Tavassoli, S.H.: 'Quantitative analysis of cement powder by laser induced breakdown spectroscopy', *Opt. Lasers Eng.*, 2011, **49**, (3), pp. 318–323
3 Vance, T., Pokrajac, D., Lazarevic, A., Marcano, A., Markushin, Y., McDaniel, S., and Melikechi, N.: 'Classification of LIBS protein spectra using multilayer perceptrons', *Trans. Mass-Data Anal. Images Signals*, 2010, **2**, (1), pp. 96–111
4 Ferreira, E.C., Menezes, E.A., Matos, W.O., Milori, D.M.B.P., Nogueira, A.R.A., and Martin-Neto, L.: 'Determination of Ca in breakfast cereals by laser induced breakdown spectroscopy', *Food Control*, 2010, **21**, pp. 1327–1330
5 Ferreira, E.C., Anzano, J., Milori, D.M.B.P., Ferreira, E.J., Lasheras, R.J., Bonilla, B., Montull-Ibor, B., Casas, J., and Martin-Neto, L.: 'Multiple response optimization of laser-induced breakdown spectroscopy parameters for multi-element analysis of soil samples', *Appl. Spectrosc.*, 2009, **63**, (9), pp. 1081–1088
6 Dietterich, T.G.: 'Ensemble methods in machine learning'. Proc. 1st Int. Workshop on Multiple Classifier Systems, Cagliari, Italy, 2000, (Springer Verlag), New York, *Lect. Notes Comput. Sci.*, pp. 1–15
7 Ho, T.K.: 'The random subspace method for construction decision forests', *IEEE Trans. Pattern Anal. Mach. Intell.*, 1998, **20**, (8), pp. 832–844
8 Ferreira, E.J., Delbem, A.C.B., Romero, R.A.F., and Oliveira, O.N.: 'Random subspaces of the instance and principal component spaces for ensembles'. Proc. Int. Joint Conf. on Neural Networks, Atlanta, GA, USA, 2009, pp. 923–926
9 Rodríguez, J.J., Kuncheva, L., and Alonso, C.J.: 'Rotation forest: a new classifier ensemble method', *IEEE Trans. Pattern Anal. Mach. Intell.*, 2006, **28**, (10), pp. 1619–1630
10 Witten, I.H., and Frank, E.: 'Data mining: practical machine learning tools and techniques' (Morgan Kaufmann, San Francisco, 2005)
11 Quinlan, J.R.: 'C4.5 programs for machine learning' (Morgan Kaufmann, San Mateo, 1993)

View publication stats

Anexo 3

Spectrochimica Acta Part B 99 (2014) 76–81

Contents lists available at ScienceDirect

Spectrochimica Acta Part B

journal homepage: www.elsevier.com/locate/sab

Novel estimation of the humification degree of soil organic matter by laser-induced breakdown spectroscopy

Edilene Cristina Ferreira [a,b,*], Ednaldo José Ferreira [a], Paulino Ribeiro Villas-Boas [a], Giorgio Saverio Senesi [c], Camila Miranda Carvalho [a,d], Renan Arnon Romano [a,d], Ladislau Martin-Neto [a], Débora Marcondes Bastos Pereira Milori [a]

[a] Embrapa Instrumentation, Rua XV de Novembro, 1452, CEP 13560-970 São Carlos, SP, Brazil
[b] São Paulo State University—UNESP, Analytical Chemistry Department, P.O. Box 355, 14801-970 Rua Prof. Francisco Degni, 55, CEP 14800-900 Araraquara, SP, Brazil
[c] Institute of Inorganic Methodologies and Plasmas, CNR, Bari 70126, Italy
[d] Physics Institute of São Carlos, University of São Paulo, IFSC-USP, Av. Trabalhador são-carlense, 400 Pq. Arnold Schimid, 13566-590 São Carlos, SP, Brazil

ARTICLE INFO

Article history:
Received 11 November 2013
Accepted 17 June 2014
Available online 28 June 2014

Keywords:
Soil organic matter
Humification degree
LIFS
LIBS

ABSTRACT

Soil organic matter (SOM) constitutes an important reservoir of terrestrial carbon and can be considered an alternative for atmospheric carbon storage, contributing to global warming mitigation. Soil management can favor atmospheric carbon incorporation into SOM or its release from SOM to atmosphere. Thus, the evaluation of the humification degree (HD), which is an indication of the recalcitrance of SOM, can provide an estimation of the capacity of carbon sequestration by soils under various managements. The HD of SOM can be estimated by using various analytical techniques including fluorescence spectroscopy. In the present work, the potential of laser-induced breakdown spectroscopy (LIBS) to estimate the HD of SOM was evaluated for the first time. Intensities of emission lines of Al, Mg and Ca from LIBS spectra showing correlation with fluorescence emissions determined by laser-induced fluorescence spectroscopy (LIFS) reference technique were used to obtain a multivaried calibration model based on the k-nearest neighbor (k-NN) method. The values predicted by the proposed model (A-LIBS) showed strong correlation with LIFS results with a Pearson's coefficient of 0.87. The HD of SOM obtained after normalizing A-LIBS by total carbon in the sample showed a strong correlation to that determined by LIFS (0.94), thus suggesting the great potential of LIBS for this novel application.

© 2014 Elsevier B.V. All rights reserved.

1. Introduction

Soil organic matter (SOM) represents the main reservoir of terrestrial carbon and can be considered an important alternative to reduce atmospheric carbon emissions. It is estimated that 2/3 of terrestrial carbon is contained in SOM. However, unlike the carbon in fossil fuels (inactive unless the burn occurs) the carbon in SOM can be converted to atmospheric carbon by soil micro-organisms and chemical decomposition, thus increasing the atmospheric CO_2 content [1,2]. Several research groups have observed that some practices of soil management can contribute to atmospheric carbon sequestration and to increase carbon stock in the soil [3–6]. Therefore, the study of soil management effects on SOM stability is useful to help establishing the most appropriate management aiming to minimize CO_2 emissions and improve soil quality.

Most carbon in SOM is contained in humic and non-humic substances; thus, carbon stability is related to the humification degree (HD) of SOM, in that highly humified SOM fractions, such as humic substances (HS), are more stable compared to less humified ones. In the humification process the concentration of recalcitrant chemical structures, such as complex conjugated aromatic rings and long aliphatic rings, increases [7], whereas non-humic fraction possesses a simpler chemical structure. Analytical techniques such as fluorescence spectroscopy and nuclear magnetic resonance (NMR) have been used to assess the HD of HS [8–14]. Further, analytical techniques able to identify specific radicals present on aromatic structures (e.g. semiquinones types), such as electron paramagnetic resonance (EPR), have been successfully applied [15,16].

Nevertheless, the determination of HD using the analytical techniques mentioned above generally requires a complex laboratory sample pretreatment, which may last up to fifteen days. Further, the laboratory procedure requires the preliminary isolation of HS, which represents only a fraction of the bulk SOM. Thereby, the adoption of these methods does not allow the estimation of whole SOM stability.

* Corresponding author at: Instituto de Química de Araraquara, Departamento de Química Analítica, UNESP, Rua Prof. Francisco Degni, 55, CEP 14800-900 Araraquara,SP, Brazil. Tel.: +55 16 33019616.
E-mail addresses: edilene@iq.unesp.br (E.C. Ferreira), ednaldo.ferreira@embrapa.br (E.J. Ferreira), paulino.villas-boas@embrapa.br (P.R. Villas-Boas), giorgio.senesi@ba.imip.cnr.it (G.S. Senesi), camilamc@gmail.com (C.M. Carvalho), renan.romano@gmail.com (R.A. Romano), ladislau.martin@embrapa.br (L. Martin-Neto), debora.milori@embrapa.br (D.M.B.P. Milori).

http://dx.doi.org/10.1016/j.sab.2014.06.016
0584-8547/© 2014 Elsevier B.V. All rights reserved.

Further, the presence of Fe^{3+} in HS represents a drawback in the application of NMR and EPR techniques [7].

To assess the HD of SOM, Milori et al. [17] have introduced a humification index, denominated H_{LIFS}, that is the ratio between the integrated area under the emissions fluorescence spectra recorded at an excitation wavelength of 465 nm, and the percentage of the total carbon in the whole soil sample (fluorescence area/carbon%). The authors showed a close and direct correlation of H_{LIFS} with aromaticity assessed by NMR and free radical semiquinone content assessed by EPR for soil humic acids (HAs). The authors thus proposed that H_{LIFS} can be used as an indicator of the chemical complexity of SOM and, possibly, of its stability/recalcitrance. Although this method has very interesting features based on the direct, fast and clean determination of fluorescence spectra, it depends on the percentage of total carbon, which is usually obtained through elemental (CHNS) analysis, thus increasing the time and cost of analysis.

Laser-induced breakdown spectroscopy (LIBS) is an emerging analytical technique capable of performing multi-elemental direct analysis without any laboratory sample pre-treatment and having the potential to perform analysis *in situ* [18,19]. In a LIBS experiment a high-energy laser pulse irradiates the target and the energy absorbed by the portion test causes a local heating of the material that results in its evaporation or sublimation. The high temperature of the ablated material generates a small plasma plume and, as a result of the plasma temperature, the ablated material breaks down into excited atomic and ionic species. During the plasma cooling, the excited species return to their lower energy state emitting electromagnetic radiation at characteristic wavelengths [20]. In a LIBS spectrum the measurement of the characteristic emission wavelengths provides qualitative information about the elemental composition of the sample, whereas the intensities of the signals can be used for quantitative determinations [19,20]. The LIBS potential for the analysis of organic compounds has also been explored recently [21–23] by using the emission lines of elements that are commonly present in organic compounds, such as the predominant C, H, P, O and N [23].

In the present work the potential of LIBS to provide the HD of bulk SOM was evaluated. To this purpose, the correlation between LIBS elemental emission line intensities and the fluorescence area of integrated laser-induced fluorescence spectra (LIFS) was investigated. A value equivalent to the LIFS fluorescence area determined from the LIBS spectrum intensities, named A-LIBS, was normalized by the total carbon content in the laboratory sample, which was determined using the same LIBS spectrum.

2. Materials & methods

Fifty-six soil samples, classified as red yellow argisol containing 67.5 g/kg of sand, 17.6 g/kg of silt and 14.8 g/kg of clay, were collected at five locations at six different depths: 0-5, 5-10, 10-20, 20-30, 30-50, and 50-80 cm from two different sugar cane management areas, either under raw cane (RC) mechanical harvesting, or under burned cane (BC) manual harvesting after a controlled burning procedure.

The soil laboratory samples were homogenized using a mortar and a pestle to obtain particle sizes smaller than 0.15 mm. To obtain soil pellets (portion test) an amount of 0.5 g of each laboratory sample was submitted to 8 tons of pressure. Three pellets were made for each laboratory sample. The LIFS and LIBS spectra were obtained from the pellets.

2.1. LIFS measurements

The LIFS spectra were measured on a lab-assembled instrument that includes a continuous wave laser at a wavelength of 405 nm, a bifurcated optical bundle fiber and a spectrometer. The laser emission was conducted on the pellet surface through six external optical fibers, and the fluorescence emission resulting from the decay of excited species was transferred to the spectrometer through a central optical fiber bundle. A computer assisted in recording the spectra and adjusting the measurement conditions. The measurement range was from 420 nm to 800 nm, the maximum intensity of emission was 4000 counts, and the integration time, average and boxcar selected were 400 ms, 3 and 3, respectively, for all measurements. Ten spectra were acquired for each portion test by focusing the continuous laser radiation on different 3.14 mm^2 sites of the pellet. As three pellets were examined for each laboratory sample, three sites were irradiated in two pellets and four sites in the third pellet. The ten obtained spectra were then averaged to have a representative spectrum for each sample.

2.2. LIBS measurements

As LIFS technique performs non destructive analysis, the surfaces of pellets remained unchanged; thus, the LIBS spectra were measured on the same pellets previously submitted to LIFS analysis.

Three pellets were examined for each laboratory sample and twenty sites were irradiated in each pellet, ten sites for each face. Thus, a total of sixty spectra were obtained from each sample. Each site was irradiated employing two consecutives laser pulses, so that the spectrum obtained corresponded to the instrumental average of two laser pulses. A previous laser pulse was always used to clear the pellet surface before obtaining the experimental spectrum. The average of spectra from each pellet (40 pulses) was considered as a single measurement, and the average (and respective standard deviation) of spectra of the three pellets for each laboratory sample was used for the proposed predictions.

The LIBS spectra were obtained using a system model LIBS2500 (Ocean Optics, USA). This system includes seven spectrometers that provide a resolution of ~0.1 nm (FWHM) for the spectral analysis ranging from 188 to 980 nm, a Q-switched Nd:YAG laser at 1064 nm (Quantel, Big Sky Laser Ultra50), an ablation chamber, a lens for laser focalization, and an optical system to collect plasma emission and address it to the spectrometers. A laser pulse of 50 mJ energy and a duration of 8 ns was used for all measurements. The laser fluence was 1.2×10^3 J cm^{-2} and the diameter of the spot on soil pellets was 73 mm. The delay time (relative to a Q-switch delay) and integration time used were 10 μs and 2 ms respectively, which are instrumental fixed conditions. The distance between the radiation collecting lens and plasma sampling was fixed at about 1 cm.

The obtained spectra were individually normalized by dividing each point of the spectrum by the area calculated under the corresponding spectrum. The area was calculated separately for each spectrometer and only the spectra recorded by the first four spectrometers were used. Therefore, the spectral evaluated wavelength ranged from 190.8 to 500.6 nm. After normalization, the spectral offset was corrected from the beginning of the spectrum with an average of 30 intensities values calculated from a pure noise region. Before performing spectra average, data of LIBS emissions resulting from measurements of each pellet were tested for normality and the Grubb's test was applied for outlier's exclusion. An average was obtained for each pellet and the sample values and respective standard deviations were obtained averaging the values of three pellets.

2.3. Total carbon determination

The carbon content of laboratory samples was obtained by two analytical techniques: CHNS analyzer and LIBS. The carbon determination by CHNS was performed using a 2400 CHNS analyzer series II from Perkin-Elmer. The soil laboratory samples were weighed directly in consumable tin capsules, which were closed and introduced in the instrument furnace. A 10-mg mass of each laboratory sample was measured using a microbalance PerkinElmer AD-6 Auto Balance Controller, which is connected to the 2400 CHNS for direct mass acquisition.

Carbon determination by LIBS was performed using a calibration method based on simple linear regression. Considering two different kinds of soil (oxisol and spodosol), Nicolodelli et al. (2014) [24] showed that Al ionic and atomic lines interferences with C (I) 193.03 nm are proportional to the partial interference of Al (I) 193.58 nm. Thus, the calibration model used in this work for carbon determination by LIBS consisted in correlating the ratio of C (I) 193.03 nm and Al (I) 193.58 nm with the carbon reference values determined by CHNS.

2.4. Estimation of SOM humification degree

Reference values of the humification degree (HD_{LIFS}) of SOM were obtained by dividing the integrated fluorescence areas from averaged LIFS spectra by the total carbon contents determined using the CHNS analyzer [17]. The LIBS estimation of the humification degree (HD_{LIBS}) of SOM consisted of two steps. In the first step, a value equivalent to the LIFS fluorescence area, the A-LIBS, was determined. To determine the A-LIBS a calibration model based on the algorithm instance based k-nearest neighbor (k-NN) [25] was used by correlating a number of selected emission lines in LIBS spectra with the LIFS fluorescence area. The LIBS emission lines used to build the calibration model were selected on the basis of ascertained correlations between emission intensities at a fixed wavelength and the fluorescence area. Thus, each wavelength (independent variable) was observed as a function of the fluorescence area (dependent variable). Only the wavelengths that exhibited a behavior similar to a linear, exponential or quadratic correlation were selected. The ten wavelengths selected by this procedure (see below) were then used to build the k-NN model. The k parameter required for the k-NN model was equal to five, and the mathematical model was generated using the Weka software [26].

In the second step, to obtain the HD_{LIBS} the A-LIBS value was divided by the total carbon content in the laboratory sample which was determined by the same LIBS spectrum. Thus, HD_{LIBS} of SOM could be determined using uniquely the LIBS spectrum.

3. Results and discussions

In LIBS measurements plasma characteristics may vary even for the same homogeneous sample and under the same experimental parameters, due to fluctuations of the laser energy and the laser–sample interaction, thus leading to large signal uncertainties [27]. Reducing LIBS signal uncertainties is thus very important to improve the accuracy and precision of measurements. In data processing, a common method for reducing the signal uncertainty is normalizing the data by the whole spectrum area [28–30]. Thus, before selecting the emission lines (variables), each spectrum was normalized by its corresponding area.

Fig. 1 shows the repetitions of LIBS spectra for the same pellet in the spectral region of some selected emission lines, together with the coefficient of variation (CV) obtained by considering the original spectra and the spectra normalized by the whole area. After spectral correction a considerable improvement in precision was obtained.

The considered LIBS spectra include 5782 variables; thus, the data matrix has a 5782-dimensional space. According to Bellman [31], with increasing the dimensionality the volume of space increases so fast that the available data become sparse, a problem for any method that requires statistical significance. Thus, a selection of wavelengths was performed as described previously. Ten wavelengths were selected: 198.96, 279.55, 280.26, 285.22, 317.95, 393.38, 394.42, 396.84, 396.91 and 422.65 nm, which according to NIST atomic spectra database [32] correspond, respectively, to Al (II), Mg (II), Mg (II), Mg (I), Ca (II), Ca (II), Al (I), Ca (II), Ca (II) and Ca (I).

The scatter plots of emission intensity at the selected wavelengths are shown in Fig. 2 as a function of the spectral area of LIFS. The selected lines of Al (II) and Al (I) (198.96 nm and 394.42 nm, respectively) showed a positive correlation, whereas the line emissions of Ca and Mg showed negative correlations with the spectral area of LIFS. These correlations indicate an increase of the HD of SOM. It is well known [33,34] that with increasing HD, the C content of HS increases and HS tend to complex more polyvalent metal ions like Al, and to be impoverished of ions like Ca and Mg.

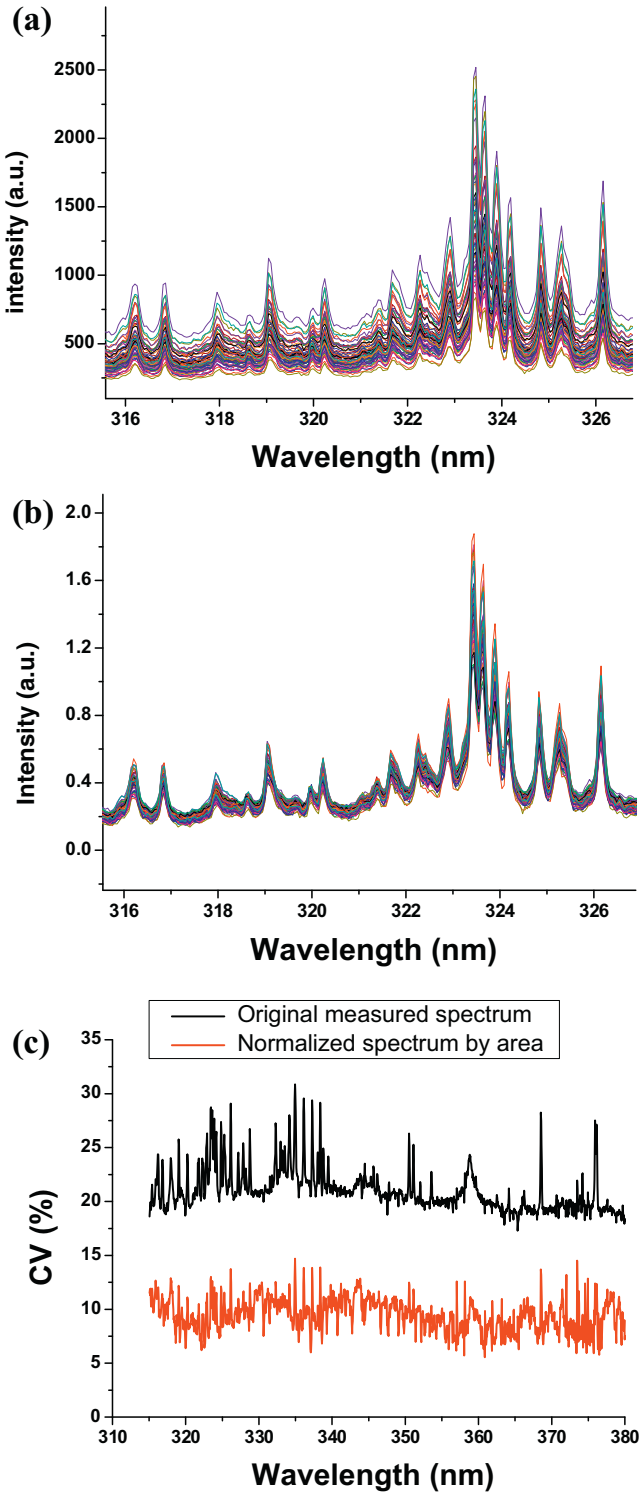


Fig. 1. Spectra obtained from 60 repetitions on each sample: (a) original measured spectra; (b) spectra individually normalized by their whole area and corrected for the offset; and (c) comparison between coefficients of variation (CV) of original measured spectra and individual spectra normalized for their whole area.

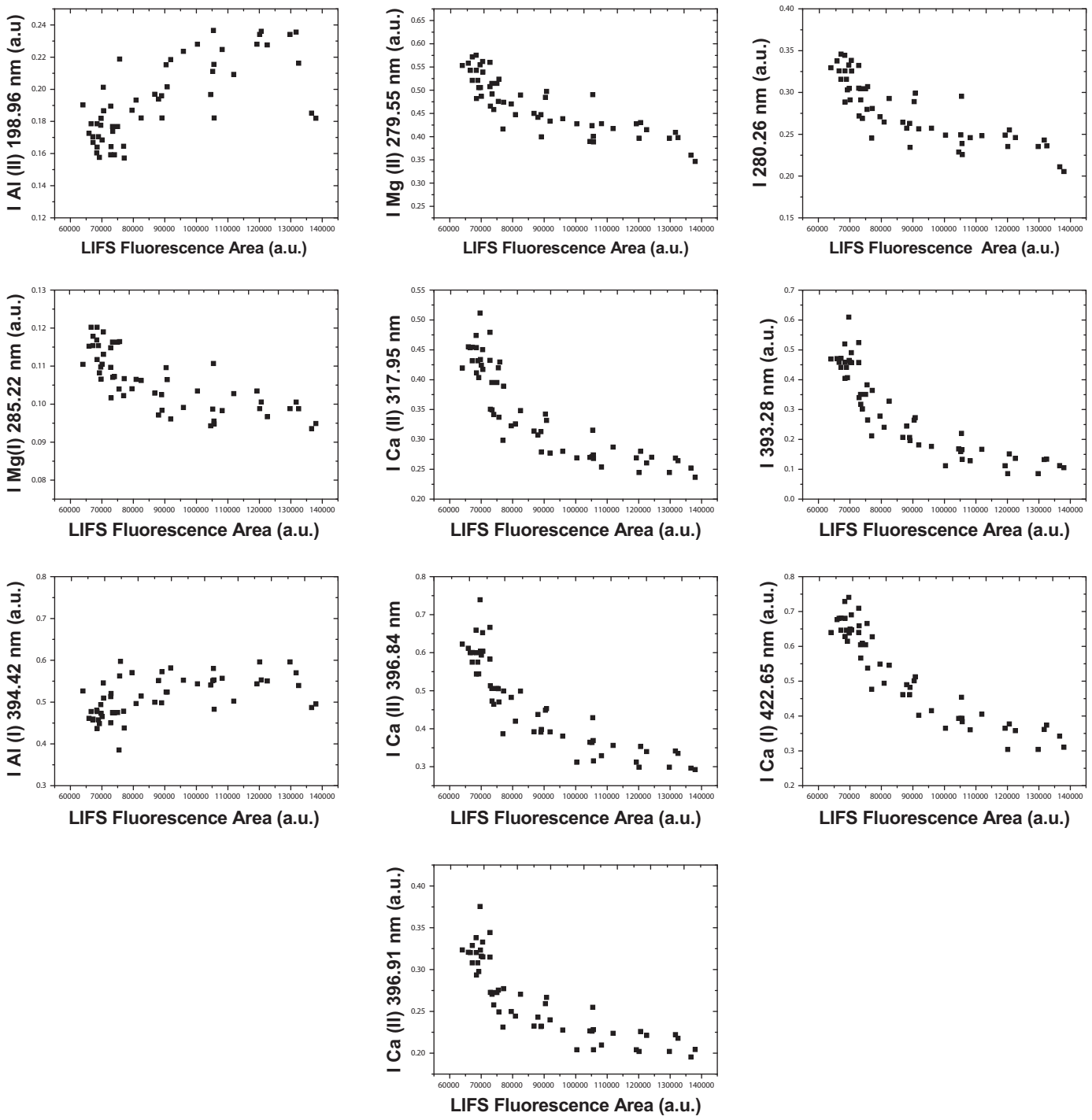


Fig. 2. Plots of correlation between LIFS fluorescence area and intensities of selected LIBS wavelengths (in arbitrary units) for the sixty soil samples studied.

By using selected variables a k-NN model was evaluated to predict A-LIBS. A 10-fold cross validation methodology was used to estimate the prediction errors and correlations between predicted and reference values. In this methodology, the dataset of samples was partitioned into 10 equal-size sets, and then each set was used as the test set while the k-NN was built with the other nine sets. This process was repeated for each test set for a total of ten folds. This method makes it possible that each sample may be considered as a testing instance for which the relative absolute error (RAE) can be assessed. The results of the method validation are shown in Fig. 3. The correlation between the reference LIFS fluorescence area and the A-LIBS predicted by the proposed method provided a Pearson's coefficient of 0.87, which indicates a strong correlation between the predicted and reference values. The assessed RAE was 33.5%, which was due to five laboratory samples presenting LIFS fluorescence area near the maximal value of data set. Due to the intrinsic characteristics of the k-NN model, the proposed method is recommended for fluorescence areas above the minimal value (64,000) and below the maximal value of data set (138,000).

In order to determine the HD_{LIBS}, the A-LIBS values were divided by the total carbon contents values in the samples, which were also determined by LIBS on the same spectra. The HD_{LIBS} values determined by LIBS were compared to HD_{LIFS} values determined by the reference

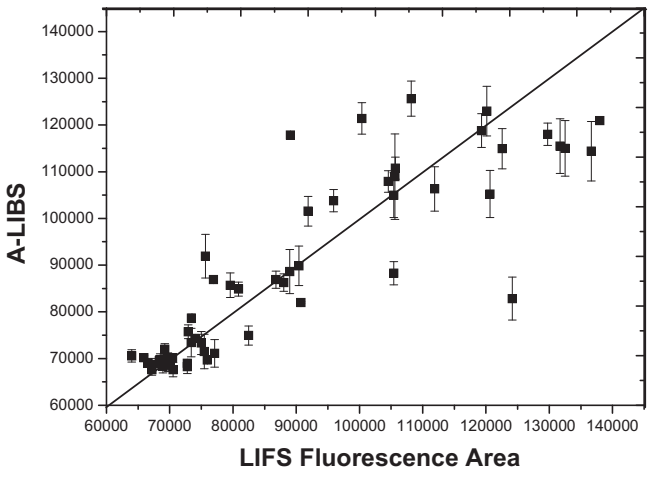


Fig. 3. Validation plot of the LIFS fluorescence area versus the predicted A-LIBS.

method (Fig. 4). The two indexes showed to be highly correlated ($R = 0.94$), thus underlying the promising potential of LIBS for this new application.

The LIBS application described above can thus provide an important contribution to the studies of SOM. In particular, the possibility of measuring the HD of SOM using a single technique would reduce the analytical time and increase the number of samples to be analyzed. Compared to the conventional techniques used to evaluate the HD of SOM (e.g. NMR, EPR and LIFS-CHNS), LIBS is faster, less costly and can provide in the same measurement also useful data on metal ions present in the samples.

4. Conclusions

In this work, the potential of LIBS was evaluated to assess the HD of SOM, which represents relevant information on the chemical recalcitrance of SOM. The data of the proposed method showed strong correlation ($R = 0.94$) with those obtained by the reference method, which however requires the use of two analytical techniques for the same determination. These results appear to be promising; however, for a better assessment of the robustness of the proposed method, it needs to be proved for different types of soil.

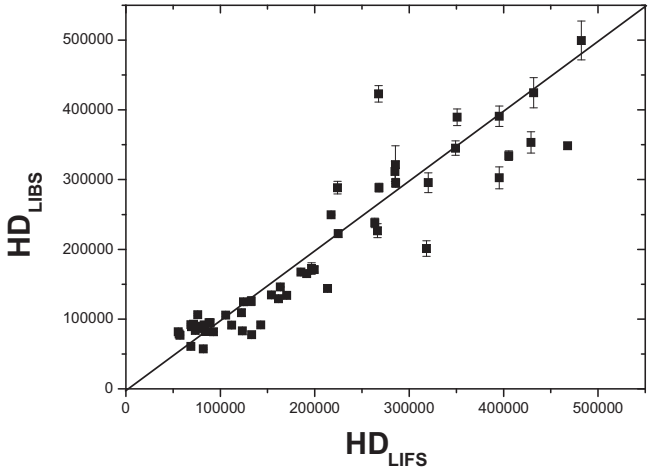


Fig. 4. Correlation between the HD determined by the LIFS reference method (HD_{LIFS}) and the LIBS proposed method (HD_{LIBS}).

This new application features all advantages of the LIBS technique, such as the possibility of performing multielemental determinations, the reduction of sample preparation, a fast and direct analysis, low cost, and the potential to be accomplished *in situ* using portable LIBS instruments.

References

[1] R. Lal, Sequestration of atmospheric CO_2 in global carbon pools, Energy Environ. Sci. 1 (2008) 86–100.
[2] K. Budge, J. Leifeld, E. Hiltbrunner, J. Fuhrer, Alpine grassland soils contain large proportion of labile carbon but indicate long turnover times, Biogeosciences 8 (2011) 1911–1923.
[3] R. Lal, Soil management and restoration for C sequestration to mitigate the accelerated greenhouse effect, J. Prog. Environ. Sci. 1 (1999) 307–326.
[4] Z. Ma, C.W. Wood, D.I. Bransby, Soil management impacts on soil carbon sequestration by switchgrass, Biomass Bioenergy 18 (2000) 469–477.
[5] R.F. Follett, Soil management concepts and carbon sequestration in cropland soils, Soil Tillage Res. 61 (2001) 77–92.
[6] C. Bayer, J. Mielniczuk, L. Martin- Neto, P.R. Ernani, Stocks and humification degree of organic matter fractions as affected by no-tillage on a subtropical soil, Plant Soil 238 (2002) 133–140.
[7] C.M. Favoretto, D. Gonçalves, D.M.B.P. Milori, J.A. Rosa, W.C. Leite, A.M. Brinatti, S.C. Saab, Determinação da humificação da matéria orgânica de um latossolo e de suas frações organo-minerais, Quim. Nova 31 (2008) 1994–1996.
[8] N. Senesi, Molecular and quantitative aspects of the chemistry of fulvic acid and its interactions with metal ions and organic chemicals: Part II. The fluorescence spectroscopy approach, Anal. Chim. Acta. 232 (1990) 77–106.
[9] C.M. Preston, Applications of NMR to soil organic matter analysis: history and prospects, Soil Sci. 161 (1996) 144–166.
[10] A. Jezierski, F. Czechowski, M. Jerzykiewicz, Y. Chen, J. Drozd, Electron paramagnetic resonance (EPR) studies on stable and transient radicals in humic acids from compost, soil, peat and brown coal, Spectrochim. Acta A Mol. Biomol. Spectrosc. 56 (2000) 379–385.
[11] D.M.B.P. Milori, L. Martin-Neto, C. Bayer, J. Mielniczuk, V.S. Bagnato, Humification degree of soil humic acids determined by fluorescence spectroscopy, Soil Sci. 167 (2002) 739–749.
[12] T. Ohno, Fluorescence inner-filtering correction for determining the humification index of dissolved organic matter, Environ. Sci. Technol. 36 (2002) 742–746.
[13] K. Kalbitz, J. Schmerwitz, D. Schwesig, E. Matzner, Biodegradation of soil-derived dissolved organic matter as related to its properties, Geoderma 113 (2003) 273–291.
[14] A.H. Rosa, M.L. Simões, L.C. de Oliveira, J.C. Rocha, L. Martin Neto, D.M.B.P. Milori, Multimethod study of the degree of humification of humic substances extracted from different tropical soil profiles in Brazil's Amazonian region, Geoderma 127 (2005) 1–10.
[15] N. Senesi, Molecular and quantitative aspects of the chemistry of fulvic acid and its interactions with metal ions and organic chemicals Part I. The electron spin resonance approach, Anal. Chim. Acta. 232 (1990) 51–75.
[16] M. González-Pérez, L. Martin-Neto, S. Saab, E.H. Novotny, D.M.B.P. Milori, V.S. Bagnato, L.A. Colnago, W.J. Melo, H. Knicker, Characterization of humic acids from a Brazilian Oxisol under different tillage systems by EPR, ^{13}C NMR, FTIR and fluorescence spectroscopy, Geoderma 118 (2004) 181–190.
[17] D.M.B.P. Milori, H.V.A. Galeti, L. Martin Neto, J. Dieckow, M. González-Pérez, C. Bayer, J. Salton, Organic matter study of whole soil samples using laser-induced fluorescence spectroscopy, Soil Sci. Soc. Am. J. 70 (2006) 57–63.
[18] A.W. Miziolek, V. Palleschi, I. Schechter, Laser Induced Breakdown Spectroscopy—Fundamentals and Applications, Cambridge University Press, Cambridge UK, 2006.
[19] D.W. Hahn, N. Omenetto, Laser-induced breakdown spectroscopy (LIBS). Part II: review of instrumental and methodological approaches to material analysis and applications to different fields, Appl. Spectrosc. 66 (2012) 347–419.
[20] D.A. Cremers, L.J. Radziemski, Handbook of Laser-Induced Breakdown Spectroscopy, Wiley & Sons Ltd., The Atrium, Southern Gate, Chichester, England, 2006.
[21] M. Baudelet, M. Boueri, J. Yu, S.S. Mao, V. Piscitelli, X. Mao, R.E. Russo, Time-resolved ultraviolet laser-induced breakdown spectroscopy for organic material analysis, Spectrochim. Acta B 62 (2007) 1329–1334.
[22] J. Anzano, R.J. Lasheras, B. Bonilla, J. Casas, Classification of polymers by determining of C1:C2:CN:H:N:O ratios by laser-induced plasma spectroscopy (LIPS), Polym. Test. 27 (2008) 705–710.
[23] P. Lucena, A. Doña, L.M. Tobaria, J.J. Laserna, New challenges and insights in the detection and spectral identification of organic explosives by laser induced breakdown spectroscopy, Spectrochim. Acta B 66 (2011) 12–20.
[24] G. Nicolodelli, B.S. Marangoni, J.S. Cabral, P.R. Villas-Boas, G.S. Senesi, C.H. Santos, R. A. Romano, A. Segnini, Y. Lucas, C.R. Montes, D.M.B.P. Milori, Quantification of total carbon in soil using laser-induced breakdown spectroscopy: a method to correct interference lines, Appl. Opt. 53 (2014) 2170–2176.
[25] D. Aha, D. Kibler, M.K. Albert, Instance-based learning algorithms, Mach. Learn. 6 (1991) 37–66.
[26] M. Hall, E. Frank, G. Holmes, B. Pfahringer, P. Reutemann, I.H. Witten, The WEKA Data Mining Software: An Update, SIGKDD Explor. 11 (2009) 10–18.
[27] L. Li, Z. Wang, T. Yuan, Z. Hou, Z. Li, W. Ni, A simplified spectrum standardization method for laser-induced breakdown spectroscopy measurements, J. Anal. At. Spectrom. 26 (2011) 2274–2280.

[28] D. Body, B.L. Chadwick, Optimization of the spectral data processing in a LIBS simultaneous elemental analysis system, Spectrochim. Acta B 56 (2001) 725–736.
[29] H. Kurniawan, M.M. Suliyanti, T.J. Lie, K. Kagawa, M.O. Tjia, Application of primary plasma standardization to Nd-YAG laser-induced shock wave plasma spectrometry for quantitative analysis of high concentration Au–Ag–Cu alloy, Spectrochim. Acta B 56 (2001) 1407–1417.
[30] S.Y. Oh, F.Y. Yueh, J.P. Singh, C.C. Herman, K. Zeigler, Preliminary evaluation of laser induced breakdown spectroscopy for slurry samples, Spectrochim. Acta B 64 (2009) 113–118.
[31] R.E. Bellman, Dynamic Programming, Courier Dover Publications, Mineola, New York, 2003.
[32] http://physics.nist.gov/PhysRefData/ASD .
[33] N. Senesi, E. Loffredo, The chemistry of soil organic matter, in: D.L. Sparks (Ed.), Soil Physical Chemistry, 2nd ed., CRC Press, Boca Raton, 1999, pp. 239–270, (Ch. 6).
[34] K. Kawaguchi, K. Kyuma, On the complex formation between soil humus and polyvalent cations, Soil Sci. Plant Nutr. 5 (1959) 54–63.

Anexo 4

Spectrochimica Acta Part B 110 (2015) 96–99

Contents lists available at ScienceDirect

Spectrochimica Acta Part B

journal homepage: www.elsevier.com/locate/sab

Laser-induced breakdown spectroscopy: Extending its application to soil pH measurements

Edilene Cristina Ferreira [a,*], José A. Gomes Neto [a], Débora M.B.P. Milori [b], Ednaldo José Ferreira [b], Jesús Manuel Anzano [c]

[a] São Paulo State University – UNESP, Analytical Chemistry Department, Rua Prof. Francisco Degni 55, CEP 14800-060, Araraquara, SP, Brazil
[b] Embrapa Agricultural Instrumentation, Rua XV de Novembro 1452, CEP 13560-970, São Carlos, SP, Brazil
[c] Laser Laboratory & Environment, Faculty of Sciences, University of Zaragoza, C/. Pedro Cerbuna 12, 50009, Zaragoza, Spain

article info

Article history:
Received 17 October 2014
Accepted 8 June 2015
Available online 14 June 2015

Keywords:
Soil pH determination
PLS
LIBS

abstract

Acid–base equilibria are involved in almost all the processes that occur in soil. The bioavailability of nutrients for plants, for instance, depends on the solubilization of mineral nutrients in the soil solution, which is a pH-dependent process. The determination of pH in soil solutions is usually carried out by potentiometry using a glass membrane electrode, after extracting some of the soil components with water or $CaCl_2$ solution. The present work describes a simple method for determining the pH of soil, using laser-induced breakdown spectroscopy (LIBS). Sixty samples presenting different textural composition and pH (previously determined by potentiometry) were employed. The samples were divided into a calibration set with fifty samples and a validation set with ten samples. LIBS spectra were recorded for each pelleted sample using laser pulse energy of 115 mJ. The intensities of thirty-two emission lines for Al, Ca, H, and O were used to fit a partial least squares (PLS) model. The model was validated by prediction of the pH of the validation set samples, which showed good agreement with the reference values. The prediction mean absolute error was 0.3 pH units and the root mean square error of the prediction was 0.4. These results highlight the potential of LIBS for use in other applications beyond elemental composition determinations. For soil analysis, the proposed method offers the possibility of determining pH, in addition to nutrients and contaminants, using a single LIBS measurement.

© 2015 Elsevier B.V. All rights reserved.

1. Introduction

Acid–base equilibria are involved in almost all soil processes, and the physical, chemical, and biological properties of soil are all influenced by pH [1]. The bioavailability of plant nutrients depends on the solubilization of minerals or other nutrients in the soil solution, and this process is pH dependent. The pH can also affect the activity of microorganisms, altering the rate of decomposition of soil organic matter and consequently the release of nutrients [2]. The determination of soil pH is therefore crucial for agricultural soil use. For example, the correction of soil pH (in the case of soils presenting high acidity) by the application of bases relies on pH measurements.

The pH of mineral soils is normally determined using slurries of water and soil [1]. The use of $CaCl_2$ solution for determining the pH of soils was proposed by Schofield and Taylor [3], with the aim of minimizing interferences due to particles suspended in the soil solution and variable salt contents.

In 1990, the Soil Science Society of America (SSSA) and the Association of Official Agricultural Chemists (AOAC) decided to conduct collaborative studies in order to validate techniques applied to soils. Four potentiometric methods for soil pH measurement were considered, according to the characteristics of the soil: (a) pH measurement in a soil suspension obtained by stirring the sample with distilled or deionized water, applied to mineral soil samples containing less than 17%of organic carbon; (b) pH measurement in a soil suspension obtained by stirring the sample with 0.01 mol L^{-1} $CaCl_2$ solution, applied to mineral soils with variable salt content; (c) pH measurement in a soil paste obtained by moistening the sample with distilled or deionized water, applied to soils containing large amounts of soluble salts and sufficient exchangeable sodium; (d) pH measurement in an aqueous soil extract, applied to soils containing organic carbon at levels equal to or greater than 17% Based on the results of this study, methods for pH measurements of mineral, saline-sodic, and organic soils were adopted by AOAC International [4].

Although the methods recommended by AOAC are effective, they involve the use of potentiometric measurements, which require the preparation of a soil solution for each sample [5]. Moreover, the dependence of the sample preparation method on the characteristics of the soil

* Corresponding author. Tel.: + 55 16 33019616.
E-mail address: edilene@iq.unesp.br (E.C. Ferreira).

http://dx.doi.org/10.1016/j.sab.2015.06.002
0584-8547/© 2015 Elsevier B.V. All rights reserved.

requires previous soil characterization, which complicates the analysis of a heterogeneous set of soil samples.

The present work proposes a new and simple method for the determination of soil pH, based on laser-induced breakdown spectroscopy (LIBS). LIBS is an optical technique capable of performing direct multielement analysis, eliminating the need for the conventional preparation of sample solutions before analysis [6,7]. Moreover, LIBS has potential for use in analyses conducted in situ. LIBS measurements are based on recording light emissions from atomic and ionic species present in a sample, after their excitation in a transient plasma produced by a laser pulse. Typically, a LIBS spectrum provides qualitative information about the elemental composition of the sample, although the signal intensities for each wavelength can be used for quantitative determinations [7,8]. In this proposal, the LIBS emission lines of elements related to soil acidity were selected to fit a multivariate model for soil pH determination.

2. Experimental

A set of sixty soil samples with distinct textures was provided by the Agronomic Institute of Campinas (AIC, Campinas, Brazil). The samples were dried at 40 °C in an oven with air circulation and then passed through a sieve with 2 mm mesh openings.

The set of 60 samples was divided into two subsets: calibration and validation sets, containing 50 and 10 samples, respectively. The samples allocated to each group were randomly selected. No heuristics were used to balance the number of the samples in the calibration and validation sets, due to the relatively small number of samples.

As part of an AIC proficiency-testing program, several parameters (including pH) were determined for each soil sample by 89 Brazilian laboratories. The average pH values reported by AIC were used as reference values in the present work. The pH values of the 60 samples were from 4.0 to 6.3, with standard deviations ranging from 0.1 to 0.2 pH units.

For the LIBS analysis, the samples were submitted to cryogenic grinding in order to reduce their heterogeneity, using a SpexCertiprep Model 6750 cryogenic mill operated at liquid nitrogen temperature (− 196 °C). The grinding program consisted of two grinding steps of 2 min, 3 min for pre-cooling, and 2 min for cooling between the grinding steps. This procedure produced particles in the 60–120 μm size range. The ground samples were used to prepare pellets by applying 10-ton pressure on a portion (~500 mg) of sample during 3 min. The pellets were analyzed by LIBS, recording ten spectra for each sample. The spectra obtained for each sample were then averaged, without any preprocessing, to obtain a representative spectrum per sample.

The LIBS system comprised a Nd:YAG laser (Brilliant Quantel, Q-Switched) with a second harmonic generator (SHG), an xyz stage carrying the sample (Standa 011957), a spectrograph, and an intensified charge-coupled device (ICCD) detector. The characteristics of the laser were maximum laser pulse energy of 115 mJ (operating at 532 nm), 4.4 ns pulse duration, and 10 Hz repetition frequency. The plasma light was collected and transported to the spectrograph through a lens and an optical fiber. An external collimator was used as the collecting lens. The position of the fiber relative to the collecting lens was adjusted by means of a divergent beam from a diode laser (HE-OPI-0009, Andor) connected to the fiber, which was focused on the sample position by the collecting system. This arrangement ensured that the light emitted by the sample was focused on the fiber. An Echelle spectrograph (Andor Mechelle ME5000, focal length 195 mm, F/7, spectral range from 200 to 975 nm) was coupled to an ICCD detector (Andor iStar DH734, 1024 × 1024 pixels, 13.6 × 13.6 μ^2/pixel, 18 mm intensifier diameter). This system was calibrated using a mercury–argon lamp (Ocean Optics HG-1, 253–922 nm).

The LIBS experimental conditions established for acquisition of the spectra were 115 mJ laser pulse energy, two pulses per site, delay time of 400 ns, and integration time gate of 25 μs.

Wavelengths corresponding to the core lines of Al, Ca, H, and O, and wavelengths in the wings of these core lines, were selected as follows: 373.665 nm (wing of the Ca II line), 373.688 nm (Ca II line), 393.308 nm (wing of the Ca II line), 393.333 nm (Ca II line), 393.357 nm (wing of the Ca II line), 394.419 nm (Al I line), 396.103 nm (wing of the Al I line), 396.128 nm (wing of the Al I line), 396.153 nm (Al I line), 396.178 nm (wing of the Al I line), 396.799 nm (wing of the Ca II line), 396.824 nm (Ca II line), 655.461 nm (O II line), 655.502 nm (wing of the O II line), 655.542 (wing of the O II line), 655.582 (wing of the O II line), 655.622 nm (wing of the O II line), 655.662 nm (wing of the O II line), 656.065 nm (wing of the H I line), 656.105 nm (H I line), 656.145 nm (wing of the H I line), 656.306 nm (wing of the H I line), 656.346 nm (wing of the H I line), 656.387 nm (wing of the H I line), 656.427 nm (wing of the H I line), 656.467 nm (wing of the O II line), 656.507 nm (O II line), 656.991 (wing of the O II line), 657.031 nm (wing of the O II line), 657.071 nm (wing of the O II line), 657.112 nm (O II line), and 657.152 nm (wing of the O II line). Using the selected lines, a partial least squares (PLS) model for the prediction of soil pH was constructed using centralization of the data on the average, with five latent variables. The calibration model took account of at least nine sources of variability, considering only the centers of the selected lines. The Weka v. 3.5.7 system (Waikato Environment for Knowledge Analysis) was used to build and validate the calibration model [9].

3. Results and discussion

A heterogeneous set of soils (in terms of texture) was used in order to obtain a robust model for pH determination, independent of the sample matrix. The proposed model could therefore offer important advantages compared to the AOAC method, where different textural classes of soils require separate extraction procedures [4].

The influence of pH on processes occurring in the soil is complex. Some well-known processes in which the pH varies as a function of exchangeable cations were therefore used as criteria to select independent variables for the calibration model. Soil liming, a procedure employed to increase soil pH, is performed by adding limestone derived from calcareous sedimentary rock containing calcium carbonate at levels exceeding 30% [10]. The presence of calcium in the soil can therefore be directly correlated to the pH. At acid pH, exchangeable aluminum predominates, while with liming, Al^{+} is progressively precipitated and remains in the form of $Al(OH)_3$ in alkaline soil [11]. Considering these processes, wavelengths corresponding to the emission lines of Ca, Al, H, and O were selected. Additionally, with the aim of circumventing matrix effects and self-absorption, which could affect the cores of the selected emission lines, several wavelengths in the wings of the peaks were also selected. It is important to mention that although organic acids influence soil pH, the carbon line at 247.856 nm showed an unresolved iron interference (247.857 nm). Since the samples presented high iron contents, this carbon line could not be included. The spectral regions of the selected lines are shown in Fig. 1. The labeled peaks correspond to Ca II (373.688 nm) (Fig. 1a); Ca II (393.333 nm), Al I (394.419 nm), Al I (396.153 nm), and Ca II (396.824 nm) (Fig. 1b); and O II (655.461 nm), H I (656.105 nm), O II (656.507 nm), and O II (657.112 nm) (Fig. 1c).

An average spectrum was calculated from the ten replicates measured for each sample. The coefficients of variation observed for the selected lines ranged from 8% to 30%, depending on the sample composition and the wavelength used. Bousquet et al. [12] reported variability ranging from 10% to 25% in LIBS signals resulting from the ablation of a typical soil prepared as a pressed pellet. On this basis, the present data were considered acceptable for the construction of a multivariate calibration model.

To build the calibration model, the emission intensities at each selected wavelength for each calibration sample (independent variables) were organized in line vectors to obtain the X matrix (50 × 32), while pH values (dependent variables) corresponding to each calibration

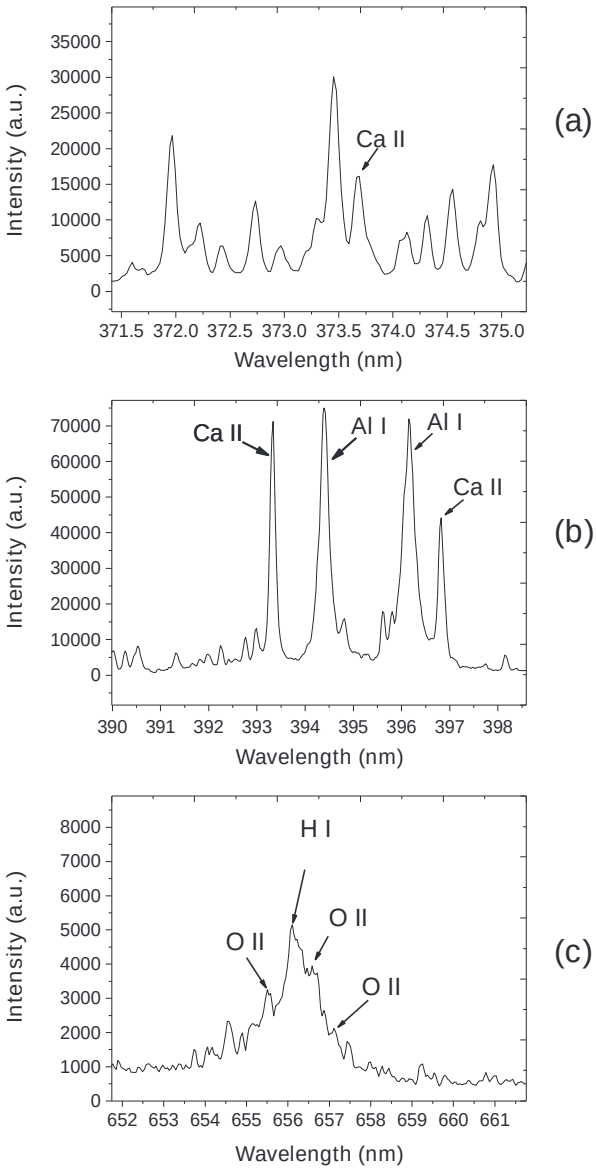


Fig. 1. Extracts of a typical LIBS spectrum of a soil sample, highlighting the cores of selected emission lines: (a) Ca II 373.688 nm, (b) Ca II 393.333 nm, Al I 394.419 nm, Al I 396.153 nm, Ca II 396.824 nm, (c) O II 655.461 nm, H I 656.105 nm, O II 656.507 nm, and O II 657.112 nm.

sample were organized in a column vector to obtain the Y matrix (50 × 1). From these matrices, a partial least squares (PLS) model was built and optimized with respect to the numbers of latent variables. The optimization results indicated that the use of five latent variables provided the best model fitting ($R = 0.8661$).

After obtaining the calibration model, it was applied for prediction of the pH of the 10 validation set samples. The results of the method validation are shown in Table 1. The values predicted by the proposed model showed a positive correlation with the reference pH values, with a root mean square error of prediction (RMSEP) of 0.4. The mean absolute error (MAE) was 0.3 pH units, which can be considered acceptable for this type of determination. Furthermore, the sample with pH 6.2 showed the largest absolute error of prediction ($AE = 1.3$), which acted to increase the MAE. It is important to mention that this same sample showed the largest relative standard deviation calculated from determinations using the reference method ($RSD = 3.2\%$ $n = 89$). These results suggest that the physical characteristics of this sample interfered with the pH measurements made using both methods.

Table 1
Reference and predicted pH values, and absolute errors of prediction, for ten samples of the validation set.

pH reference value	pH predicted value	Absolute error*
6.2	4.9	1.3
5.4	5.0	0.6
4.5	4.4	0.1
5.4	5.3	0.1
5.0	5.1	0.1
4.5	4.5	0.0
5.6	5.6	0.0
4.1	4.4	0.3
4.8	4.7	0.1
5.9	5.7	0.2

* Mean absolute error (MAE) = 0.3

The variances observed for the dependent variable (pH), of around 6%, were lower compared to those for the independent variables (wavelengths), which ranged from 8% to 30%. This indicates that despite the difficulties that high signal variability can cause for quantitative analysis of soil by LIBS, calibration models that use multiple variables (such as PLS) can minimize the influence of the variances as well as matrix and self-absorption effects.

These findings highlight the potential of LIBS for obtaining other important sample information, in addition to elemental composition, demonstrating that the technique can make a significant contribution to soil science.

4. Conclusions

A clean and simple method for the determination of soil pH by LIBS is proposed, using a PLS calibration model and taking into account variables corresponding to elements that influence soil pH. The pH values obtained by the LIBS and reference methods were positively correlated, with low MAE (0.3 pH units). The results show the potential of LIBS for evaluating soil acidity, with advantages over traditional potentiometric methods including low analytical cost, no chemical waste generation, and a single analytical procedure irrespective of the soil composition. Furthermore, the proposed method offers the possibility of determining pH, as well as nutrients and contaminants, in a single LIBS measurement.

Future studies should be carried out to obtain a better understanding of the effects of the selected variables and their contributions to the performance of the calibration model.

Acknowledgements

The authors thank the São Paulo State Research Foundation (FAPESP, grants 2006/61741-4 and 2014/26185-0), Fundación Carolina, the European Social Fund, the Government of Aragón, and the University of Zaragoza (proposal #E75).

References

[1] E.O. McLean, Soil pH and Lime Requirement, in: A.L. Page, R.H. Miller, D.R. Keeney (Eds.), Methods of Soil Analysis. Part 2. Chemical and Microbiological Properties, American Society of Agronomy, Soil Science Society of America, Madison 1982, pp. 199–224.
[2] J.B. Jones Jr., Plant Nutrition and Soil Fertility Manual, 2nd ed. CRC Press, Taylor & Francis Group, Boca Raton, 2012.
[3] R.K. Schofield, A.W. Taylor, The measurement of soil pH, Soil Sci. Soc. Am. Proc. 19 (1955) 164–167.
[4] Y.P. Kalra, Determination of pH of soils by different methods: collaborative study, J. AOAC Int. 78 (1995) 310–324.
[5] D.A. Skoog, D.M. West, F.J. Holler, Fundamentals of Analytical Chemistry, 6th ed. Saunders College Publishing, New York, 1992.
[6] A.W. Miziolek, V. Palleschi, I. Schechter, Laser Induced Breakdown Spectroscopy—Fundamentals and Applications, Cambridge University Press, Cambridge, 2012.

[7] D.W. Hahn, N. Omenetto, Laser-induced breakdown spectroscopy (LIBS). Part II: Review of instrumental and methodological approaches to material analysis and applications to different fields, Appl. Spectrosc. 66 (2012) 347–419.
[8] D.A. Cremers, L.J. Radziemski, Handbook of Laser-Induced Breakdown Spectroscopy, Wiley & Sons, Chichester, 2006.
[9] M. Hall, E. Frank, G. Holmes, B. Pfahringer, P. Reutemann, I.H. Witten, The WEKA data mining software: an update, SIGKDD Explor. 11 (2009) 10–17.
[10] S.L. Tisdale, W.L. Nelson, Soil Fertility and Fertilizers, 2nd ed. Macmillan, New York, 1966.
[11] N.T. Coleman, D. Craig, The spontaneous alteration of hydrogen clay, Soil Sci. 91 (1961) 14–18.
[12] B. Bousquet, G. Travaillé, A. Ismaël, L. Canioni, K. Michel-Le Pierrès, E. Brasseur, S. Roy, I. le Hecho, M. Larregieu, S. Tellier, M. Potin-Gautier, T. Boriachon, P. Wazen, A. Diard, S. Belbèze, Development of a mobile system based on laser-induced breakdown spectroscopy and dedicated to in situ analysis of polluted soils, Spectrochim. Acta Part B 63 (2008) 1085–1090.

Anexo 5

Geoderma 263 (2016) 195–202

Contents lists available at ScienceDirect

Geoderma

journal homepage: www.elsevier.com/locate/geoderma

Laser-induced breakdown spectroscopy to determine soil texture: A fast analytical technique

Paulino Ribeiro Villas-Boas [a,*], Renan Arnon Romano [a,b], Marco Aurélio de Menezes Franco [a,c], Edilene Cristina Ferreira [d], Ednaldo José Ferreira [a], Silvio Crestana [a], Débora Marcondes Bastos Pereira Milori [a]

[a] Embrapa Instrumentation, R. XV de Novembro, 1452, 13560–970 São Carlos, SP, Brazil
[b] Physics Institute of São Carlos, University of São Paulo, IFSC-USP, Av. Trabalhador Sancarlense, 400 Pq. Arnold Schimid, 13566–590 São Carlos, SP, Brazil
[c] Physics Department, São Carlos Federal University, P.O. Box 676, 13565–905 São Carlos, SP, Brazil
[d] São Paulo State University — UNESP, Analytical Chemistry Department, P.O. Box 355, 14801–970, R. Prof. Francisco Degni, 55, 14800–900 Araraquara, SP, Brazil

ARTICLE INFO

Article history:
Received 17 July 2015
Received in revised form 17 September 2015
Accepted 20 September 2015
Available online 1 October 2015

Keywords:
Soil texture
Soil particle size
LIBS
Spectroscopy
PLSR

ABSTRACT

The analysis of soil texture is crucial for the proper management of agricultural systems and for environmental studies. Soil texture is important as it affects erosion potential, water retention capacity, organic matter complexation, and the retention of nutrients, among others. It is usually determined by pipette or hydrometer methods, but analysis requires a preparation with chemical reagents, which can take hours and hence is unfeasible for large number of samples. Here we propose the use of laser-induced breakdown spectroscopy (LIBS) to estimate the proportions of sand, silt, and clay in 60 Brazilian soil samples of varying composition. Two calibration models were developed with the partial least square regression method: one considering the spectral region from 188 to 980 nm and the other, emission lines of the elements Si, Na, Fe, Ti, Ca, K, Al, Co, Mg, V, Ba, and Be. The Pearson correlation coefficients for the estimated values were 0.89 and 0.90 on average for the first and second models, respectively. The uncertainties were 6% on average for both models. These results demonstrate the use of LIBS for rapid scanning of the texture of soil samples with distinct composition. The procedure presented here can be extended to other chemical and physical soil properties, which makes LIBS a universal tool for rapid soil analysis without preparation with chemical reagents.

© 2015 Elsevier B.V. All rights reserved.

1. Introduction

The relative proportion of sand, silt, and clay – texture – is one of the most important physical properties of soils. It directly affects other critical properties, including susceptibility to erosion, drainage, water-holding capacity, organic matter content, and capacity for leaching nutrients and pollutants (Hassink et al., 1993). Soil texture is, therefore, one of the key components for assessing soil quality and the sustainability of agricultural management practices (Kettler et al., 2001).

In the field, agronomists can estimate soil texture by rubbing a soil sample between their fingers and thumb and feeling its physical characteristics. However, such a technique is of low accuracy and requires skill and experience (Brown, 2003). In the laboratory, sand can be easily separated from soil samples by sieving, and clay and silt can be accurately determined by two well-established conventional methods: pipette and hydrometer. The former is more accurate and is considered the standard method for texture determination. It is based on Stoke's law, which states that denser (i.e. larger) particles sink faster than lighter (i.e. smaller) particles. Therefore, after a predetermined time in water suspension clay particles can be separated from the settled silt. Despite its accuracy, the pipette method is time-consuming and laborious, depends on the operator and requires sample pretreatment to disperse soil aggregates (Gee and Bauder, 1986; Kettler et al., 2001).

Other methods for direct determination of soil particle sizes have been developed, including gamma-ray attenuation (Naime et al., 2001), X-ray attenuation, electroresistance particle counting, photometrical techniques, and laser diffractometry (e.g., McCave and Syvitski, 2007). Prior to analysis, however, all these methods also require a pre-processing step to disperse the aggregates, which usually takes a full day. Furthermore, these methods do not have proper correspondence with the pipette or hydrometer for determining the size of the smallest particles, clay and silt (Taubner et al., 2009). Soil texture can also be indirectly determined by visible or infrared reflectance spectroscopy (e.g., Chang et al., 2001; Madari et al., 2006; Rossel et al., 2006; Curcio et al., 2013). The reflectance spectroscopy does not require the sample pre-processing step and has a good correspondence with traditional methods, but its accuracy depends on the amount and diversity of samples used to build calibration models.

In this article, we propose a method for evaluating the relative proportions of sand, clay, and silt in soils without the need for preparing samples, hence reducing the overall time of analysis to a few minutes.

* Corresponding author.
E-mail address: paulino.villas-boas@embrapa.br (P.R. Villas-Boas).

http://dx.doi.org/10.1016/j.geoderma.2015.09.018
0016-7061/© 2015 Elsevier B.V. All rights reserved.

The method consists in using the soil elemental composition assessed by laser-induced breakdown spectroscopy (LIBS) (Miziolek et al., 2006) and building calibration models based on the correlation between emission lines and the relative proportions of sand, silt, and clay. We hypothesized that each relative proportion is mainly constituted by certain elements (e.g., silicon in sand), which are either absent or present in small amounts in the other proportions.

The LIBS is a multi-elemental spectroscopic technique based on emission of plasma induced by laser (Miziolek et al., 2006; Cremers and Radziemski, 2006; Singh and Thakur, 2007). Sample can be analyzed with minimal manipulation (i.e. without reagents) or even directly in situ (Theriault et al., 1998; Harmon et al., 2005; Corsi et al., 2006; Palanco et al., 2006). The LIBS analytic process starts by focusing a highly energetic pulse onto the sample. The laser energy density is so high ($\sim 10^9$ W cm^{-2}) that it can break molecular bonds, generating a small plasma plume — a gas of unbound atoms, ions, electrons, and photons. During laser interaction, the ablated material can reach a temperature of 100,000 K (Miziolek et al., 2006), whereby its emission is basically composed of continuum radiation. As the plasma cools, the continuum emission reduces, allowing the observation of atomic and ionic lines derived from the excited elements (Singh and Thakur, 2007), which is usually performed at ~10,000 K. The elemental composition of the samples can be determined, and with appropriate calibration models the elemental concentration can be obtained. In the case of soil analysis, the LIBS has been applied to evaluate nutrients (Hussain et al., 2007; Ferreira et al., 2011; Braga et al., 2010; Cremers et al., 2001; Ebinger et al., 2003), contaminants (Bousquet et al., 2007; Senesi et al., 2009), and carbon (Nicolodelli et al., 2014; Ebinger and Harris, 2010; Silva et al., 2008), as well as humification degree of soil organic matter (Ferreira et al., 2014), soil pH (Ferreira et al., 2015), and soil classification (Pontes et al., 2009). However, no applications of LIBS have been reported for the evaluation of any soil physical characteristics.

2. Materials and methods

2.1. Soil samples

A set of 60 samples, collected from farmlands all over Brazil and characterized by the Agronomic Institute of Campinas, São Paulo State, Brazil were used in the following analyses. The relative proportions of sand, silt, and clay were determined by the pipette method and were in the range of 4–92%, 2–35% and 6–66%, respectively. Prior to the texture analysis by the LIBS technique, the soil samples were sieved to remove roots and ground to reduce particle size heterogeneity by a cryogenic mill working with liquid nitrogen at a temperature of −196 °C. For the LIBS analysis, the ground samples were pressed into pellets with 10 tons of hand press.

2.2. Laser-induced breakdown spectroscopy (LIBS)

The LIBS spectra of the soil samples were acquired with a LIBS2500plus spectrometer (Ocean Optics, Dunedin, FL, USA), which utilized a Q-switched Nd:YAG laser at 1064 nm (Quantel, Bozeman, MT, USA) operating at 75 mJ maximum power energy, 8 ns pulse width, and 10 Hz frame rate. The laser pulse was focused on the sample inside an ablation chamber. After the plasma was formed, the emission of excited species was carried by an optical fiber bundle connected to seven spectrometers ranging from 188 to 980 nm, each one coupled with a 2048 element linear silicon CCD array whose resolution was ~0.1 nm (FWHM). The distance from the sample to the collecting optical fiber bundle was approximately 7 mm. All measurements were performed in air, and the LIBS system was set to 50 mJ per laser pulse with a 2.1 ms integration time and a fixed delay time of 2 μs. On each soil sample, 60 measurements were carried out, two accumulated shots each.

2.3. Spectral processing

The LIBS spectra of a sample may vary from one shot to another, since they are strongly affected by acquisition system and plasma instability. The former depends on optical and electronic systems and may impose offset and random noise on the spectra acquired. The latter is caused by several aspects related to radiation–matter interaction – also known as matrix effects – including the composition and aggregation state of the samples, surface roughness, homogeneity, and optical alignment. The plasma formation involves a combination of non-linear dynamics such as radiation–matter interaction, laser-ablation mechanisms, production of free electrons, radiation absorbed by the plasma, and reabsorption of the species (Tognoni et al., 2010). Also, because of the non-linear plasma formation, LIBS measurements follow a generalized distribution of extreme values (Michel and Chave, 2007), instead of a normal distribution. All these issues lead to a non-reproducible background continuum emission of the spectra, which makes quantitative elemental analysis difficult. To develop calibration models for elemental quantification with LIBS, these issues have to be eliminated or reduced. In this study, only offset, random noise, and background continuum emission were corrected.

The offset of each spectrum was corrected separately for each spectrometer by subtracting the minimum value found in each spectral region. To reduce the random noise, the spectra were smoothed with a Savitzky–Golay filter (Savitzky and Golay, 1964), whose parameters were selected according to the genetic optimization algorithm (Mebane and Sekhon, 2011).

The background continuum emission – the spectral baseline – was corrected by two methods. The first one was 4S Peak Filling (Liland, 2015), which was developed for similar spectra found in other spectroscopy techniques, such as NMR and Raman (Liland et al., 2010; Liland and Mevik, 2011). The method estimates the baseline by iteratively suppressing the spectrum with a moving window and is based on four operations: smoothing, subsampling, suppression, and stretching. The parameters of the 4S Peak Filling method were also selected according to the genetic optimization algorithm. The second method estimates a baseline for each peak independently through a linear fit of the points on the left and right sides. It depends on the fact that the baseline approaches a straight line for small spectral regions and considers only spectral points not belonging to peaks (Dawson et al., 1993).

Since finding the elements whose concentration was most correlated to the soil, textural proportions was also important for this study, the intensity of lines was approximated by the area of the fitted function to the experimental points. If the line of interest was interfered by other lines, a deconvolution method was applied, in which a distribution was fitted for each peak in the analyzed range. In this study, only Lorentzian distribution was considered for the peaks.

2.4. Calibration model

Since the sum of the relative proportions of sand, silt, and clay is 100%, it is not necessary to build a calibration model for all relative proportions. For instance, if a model is built to predict the relative proportion of sand and clay, the proportion of silt would be 100% minus the sum of the other two. However, the uncertainty of estimating the relative proportion of silt would be higher than if it was directly predicted by the model (assuming that the model is less accurate than the reference method). One way to improve the predictions using just two variables is to combine the relative proportions of sand, silt, and clay prior to building the calibration model. Thus, we defined two variables as follows:

$$\begin{aligned} e &= a - b - c \\ f &= b - c, \end{aligned} \tag{1}$$

where a, b and c are the relative proportions of sand, clay, and silt, respectively. Such a combination is similar to what is provided by

the pipette method, where sand is first separated from clay and silt by sieving, and then silt is separated from clay by sedimentation in an aqueous solution. After the model is built with variables *e* and *f*, the relative proportions of sand, clay, and silt can be obtained by the following expressions:

$$\begin{aligned} a &= (1+e)/2 \\ b &= (1+2f-e)/4 \\ c &= (1-2f-e)/4. \end{aligned} \quad (2)$$

A test (not shown) was performed to verify these assumptions, and the accuracy and precision of the model built with variables *e* and *f* were higher than those of the model built with *a*, *b*, and *c* or the model built with *a* and *b*, in which $c = 1 - a - b$. Therefore, the models were built with variables *e* and *f*.

Partial least square regression (PLSR) was the calibration model applied to correlate LIBS spectra with the variables *e* and *f*. PLSR is a multivariate linear statistical method, which finds the best combination of prediction variables to explain the variation in the response variable (e.g., Wold et al., 2001). To some extent, this method is similar to principal component analysis (PCA), which defines a new set of linearly independent variables ordered by maximum variance without relation to the response variables (e.g., Costa and Cesar, 2001). PLSR, on the other hand, determines a new set of variables whose variation is maximized to explain the response variables. This method is particularly useful when the number of prediction variables is higher than the number of observations, and the prediction variables are multicollinear (Tobias, 1995). The method is commonly used in chemometrics to quantify the concentration of elements in samples by considering their spectra. In this kind of application, PLSR is a suitable method since the number of spectral points is usually higher than the number of samples, and the transition lines are generally correlated among them. The model accuracy was evaluated by leave-one-out cross-validation, which consists in using all samples minus one to build the PLSR model and estimating the proportions of sand, clay, and silt with the remaining sample. The procedure is repeated until all samples are tested.

2.5. Data analysis

The overall data analysis involved several steps from spectral processing to the building of regression models, as schematized in Fig. 1. The analysis started by removing the offset and proceeded by dividing the 60 samples into two sets: one-quarter for spectral processing (optimization of spectral correction parameters and peak-finding) and the remainder for building the regression models. To be representative, the first set was chosen in such a way as to cover all types of textures ranging from clay to sandy soils uniformly distributed.

The second step in the data analysis was the spectral processing and peak-finding, represented by the left dotted block in Fig. 1. The spectral processing consisted in optimizing two methods: the Savitzky–Golay filter and 4S Peak Filling for random noise and baseline correction, respectively. Both methods were optimized with a genetic algorithm based on derivatives (Mebane and Sekhon, 2011), implemented in package rgenoud of the R programming environment (R Core Team, 2014). For each realization, random parameters were chosen according to the genetic algorithm for the methods to correct the spectra of the samples. Since each sample corresponded to 60 spectra, they were averaged after the corrections. The resulting spectra were then used to build a regression model for the variables *e* and *f* (Eq. (1)) with the PLSR model and tested with leave-one-out cross-validation. The result of each realization was $\overline{\rho}$: the average of correlation coefficients calculated between the estimated and measured soil textural proportions. The estimated proportions were obtained according to Eq. (2). The optimization procedure finished when the convergence criteria were met (no improvement after 10 generations) or the maximum number of generations (100) was reached (default values in package rgenoud). Each generation corresponded to 1000 combinations of parameters. The optimized input parameters were recorded for building the model A. The peak-finding was performed by linearly correlating each point of the corrected spectra with the soil textural proportions. Then, the peak-finding selected the peaks near to the points whose correlation was higher than a given threshold. Peaks close to many emission lines were discarded because they could not be properly separated from the others. The elements were identified by using the NIST database

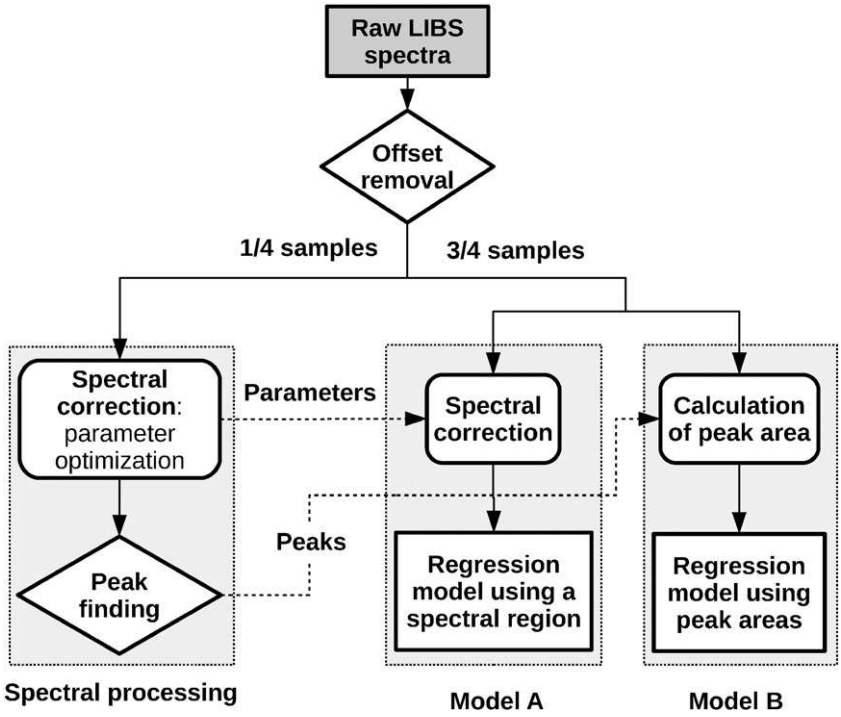


Fig. 1. Scheme used to process LIBS spectra and to create regression models for the estimation of the relative proportions of sand, clay, and silt in soils.

(Kramida et al., 2014). In this part of the analysis, the main idea was to find elements whose concentration varied according to the soil textural proportions. For instance, silicon concentration was expected to correlate positively with the relative proportion of sand in soil samples.

The third step in Fig. 1 was the process of building the regression models A and B: the first was based on the whole corrected spectra and the second on the peaks found in the previous step. Prior to building model A, the remaining spectra were corrected with the Savitzky–Golay filter and 4S Peak Filling method with the parameters optimized in the spectral processing part. Then, all spectra of each sample were averaged and used to build model A, which was tested by leave-one-out cross-validation, as in the spectral correction part.

Before the calculation of peak areas for the second model, a local baseline correction was used for each peak selected in the peak-finding step. Such a correction starts by choosing points in the left and right side of a peak, which only consist of random noise and without other peaks. Then, a linear function is fitted with the points chosen and used as a local baseline for the peak. The same procedure can be used for more than one peak in a small region provided that the points chosen for the correction are outside that region. This method is not suitable for large regions, since a straight line or a quadratic function may not be a good approximation for the baseline. This procedure was applied for all peaks identified in the peak-finding step, and the corresponding corrected regions were averaged for all spectra of each sample.

For each averaged spectrum, a Lorentzian distribution was then fitted for each peak in the spectral range selected. Model B was built using the area of the peaks as input variables for the PLSR method similarly to what was done for model A.

Since the PLSR model can use negative coefficients to correlate the spectral points with the variables *e* and *f*, the predicted textural proportions can also be negative, which has no physical meaning. In order to avoid such an inconsistency, all negative predictions were converted to zero, and the sum of predicted sand, silt, and clay proportions for each sample was normalized to 100%. After these corrections, the models were evaluated according to the Pearson correlation coefficient between the estimated and measured textural proportions and the root mean squared error (RMSE).

3. Results

The data were processed as in Fig. 1, starting with the offset removal and the sample division for the spectral correction and for building the models. The spectral correction consisted in optimizing the Savitzky–Golay filter to smooth the random noise and the 4S Peak Filling method to correct the baseline for each spectrometer region separately. The results of the optimization process were $\overline{\rho} = 0.83, 0.83, 0.82, 0.86, 0.87, 0.63,$ and 0.81 for spectrometers 1 to 7, respectively, and the parameters were recorded for building model A. Even though the baseline correction was optimized in relation to $\overline{\rho}$, a visual inspection was also performed to verify whether the baseline was physically meaningful, that is neither over-fitted nor above the spectrum (see example in Fig. 2(a)).

After the baseline correction, the peaks were found by using the linear correlation between the wavelength and the relative proportions of sand, silt, and clay, as in Fig. 2(b). Since most points were highly correlated with the textural proportions, we considered only those whose absolute correlation was higher than 0.80 with the proportions of sand, silt or clay. Also, to establish a model with a true physical-chemical meaning, regions of random noise, continuum background, and interfered lines were not considered, such as the regions 210.5–211.5 and 213.5–214.5 nm in Fig. 2(b). The Si I peak at 212.41 nm, on the other hand, was taken into account because of a correlation above 0.8 and higher than the neighborhood. The complete set of lines selected is shown in Table 1.

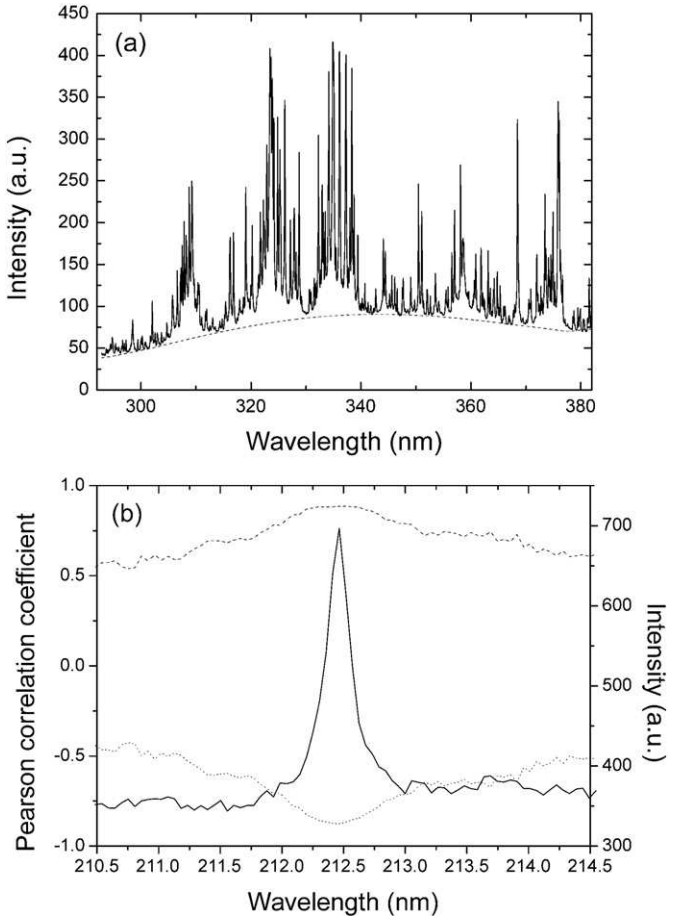


Fig. 2. (a) Example of a baseline estimated by 4S Peak Filling method (dashed line) in a LIBS spectrum (solid line). (b) Pearson correlation coefficient between the wavelength and the proportions of sand (dashed line) and clay (dot line). The solid line corresponds to a sample spectrum for the Si I peak at 212.41 nm.

The next step was the construction of the models, in which the PLSR method was used to correlate the textural proportions of the second set of samples with the spectral points of all spectrometer ranges and the areas of peaks of Table 1 for models A and B, respectively. For model A, the spectral baseline of all samples of the second set was corrected by using the Savitzky–Golay filter and 4S Peak Filling method

Table 1
Emission lines found in the peak-finding step and identified with NIST database (Kramida et al., 2014).

Wavelength (nm)			
Si I	**Fe I**	**Na I**	**Co II**
212.41	305.89	588.99	237.73
221.80	358.53	589.59	241.16
250.69	406.36	**Na II**	**Mg I**
251.61	432.57	288.42	285.21
288.16	438.35	520.85	**Mg II**
390.55	440.47	**Ca I**	279.55
Si II	528.36	610.27	279.49
412.08	532.41	612.22	280.27
413.09	532.80	**Ca II**	**V I**
634.56	544.69	866.21	412.35
636.99	**Fe II**	**K I**	**Ba I**
Ti I	233.27	766.49	553.54
394.86	235.53	769.89	**Ba II**
398.17	236.03	**Al I**	614.17
Ti II	238.86	308.21	**Be I**
306.62	242.41	394.40	235.08
454.96	244.45		

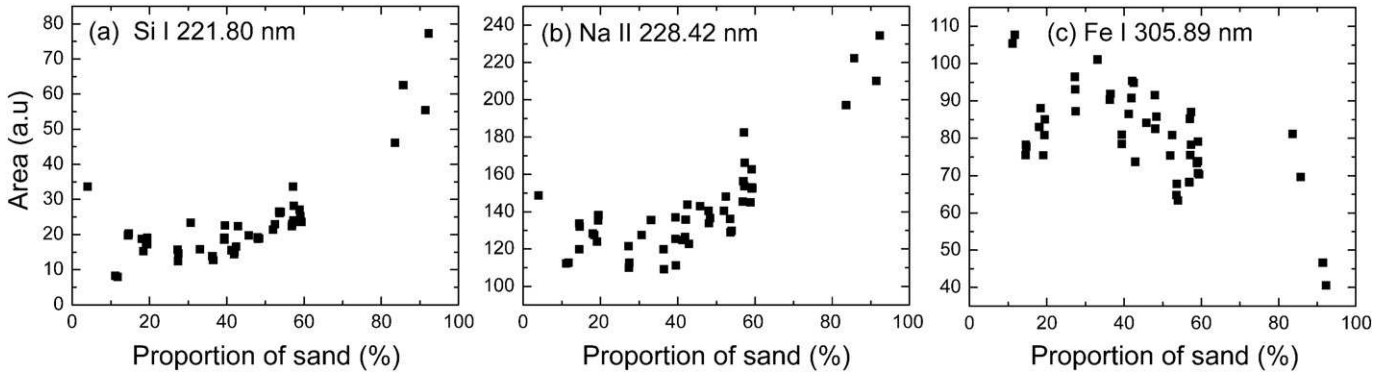


Fig. 3. Relation between the proportion of sand and the peak emission area of Si I at 221.80 nm (a), Na II at 228.42 nm (b), and Fe I 305.89 nm (c).

with the parameters determined in the optimization step of Fig. 1. Only then were the spectra of each sample averaged and used in the PLSR method.

For the second model, the areas of peaks in Table 1 were calculated for the spectra of all samples of the second set by fitting the Lorentz distribution after the local baseline correction, as described in Section 2.5. Before construction of the second model, the relation between the area of peaks and the textural proportions was analyzed to infer which elements were more abundant in each part. In particular, the concentration of Si and Na was positively correlated with the proportion of sand, in contrast to the concentration of Fe (Fig. 3).

The results of the leave-one-out cross-validation are shown in Fig. 4. The Pearson correlation coefficients for model A were 0.92, 0.85, and 0.90 with RMSE 8%, 4%, and 7% for sand (a), silt (b) and clay (c), respectively. On the other hand, the Pearson correlation coefficients for model B were 0.92, 0.86, and 0.91 with RMSE 8%, 4%, and 7% for sand (d), silt (e), and clay (f), respectively. Even though given in percentages, the uncertainties are absolute and not relative (i.e. the uncertainties represent

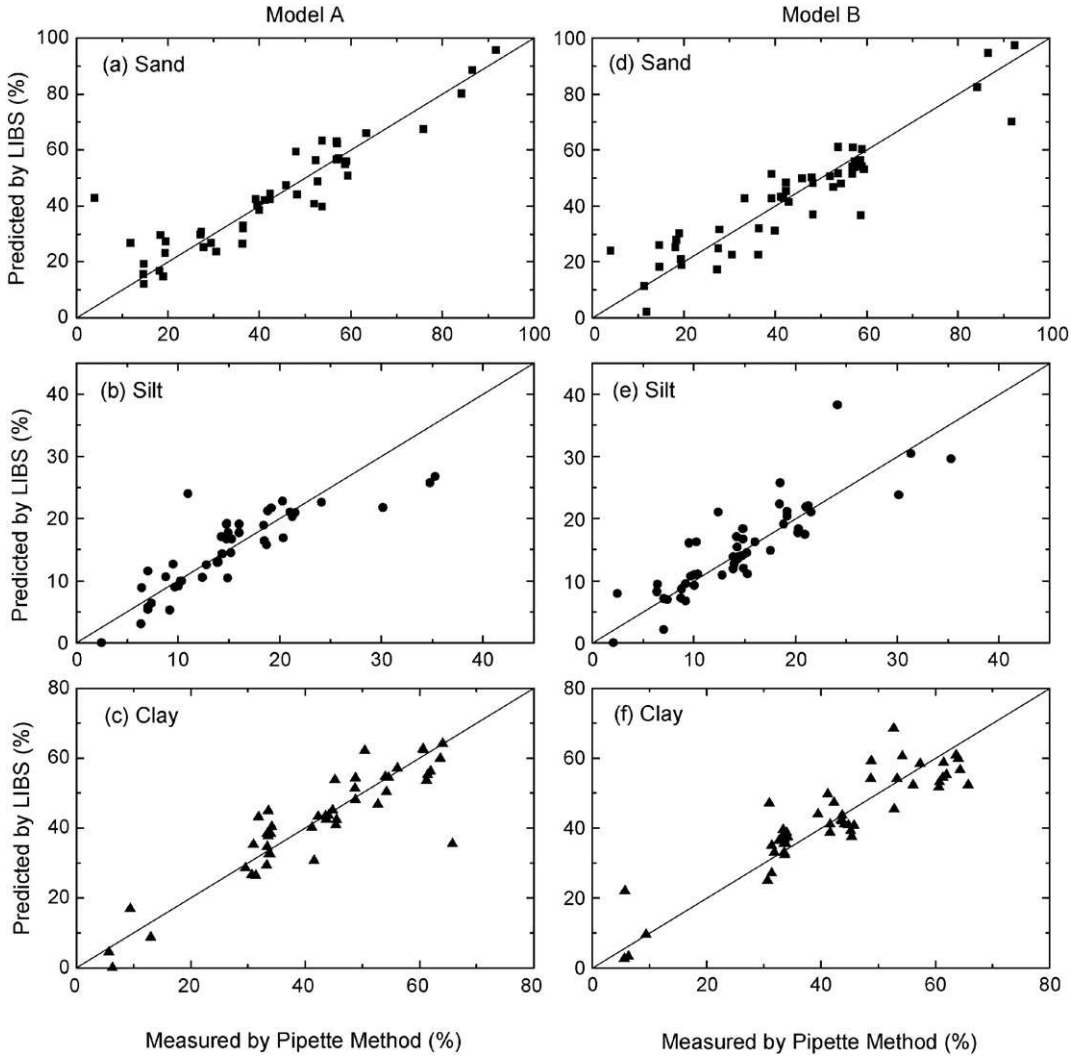


Fig. 4. Results of the leave-one-out cross-validation for models A and B and the relative proportions of sand, silt, and clay. The diagonal line represents the ideal calibration model.

percentage of sand, silt, or clay and are not relative to the textural proportions). Both models provided a strong correlation (higher than 0.85) with a RMSE below 8%. On average, the performance of model B was slightly better than that of model A: $\overline{\rho_B} = 0.90$ and $\overline{\rho_A} = 0.89$; $\overline{RMSE_B} = 6\%$ and $\overline{RMSE_A} = 6\%$.

The LIBS had a good agreement with the pipette method in terms of soil texture classification (Table 2). According to the soil texture triangle (Saxton et al., 1986), model B classified soil samples similarly to the pipette method, featuring 32 correct classifications. Of the misclassifications, 13 were classified into adjacent classes, whereas the other two were two and three classes distant.

4. Discussion

We found that LIBS can be used to estimate and classify soil texture based on the assumption of the chemical composition. Our results have shown that the relative textural proportions estimated by the calibration models were strongly correlated (higher than 0.85) with those measured by the pipette method. Such a correlation was achieved because of the relation between the relative textural proportions and the LIBS emission profile (both spectral range and peak areas) such as those in Fig. 2(b). Therefore, the elemental composition should differ between sand, silt, and clay particles. Similar conclusions were drawn for Martian soils, in which distinct compositions were found for coarse (N0.5 mm) and fine (b0.5 mm) particles (Cousin et al., 2015). In addition, Fig. 3 indicates that the proportion of sand is positively correlated with Si and Na peaks, but negatively with Fe peak. Similar observations for Si, Na, and Fe were also found in Martian soils (Cousin et al., 2015). Correlation of Si is not surprising since silica (SiO_2) is the most common constituent of sands; Na correlation may be related to the type of Brazilian rock from which sand is derived: probably feldspar, the composition of which includes Na. On the other hand, the negative correlation with Fe concentration may be because Fe oxides are mostly found in clay particles.

Models A and B provided a strong correlation coefficient with the proportions of sand, silt, and clay, but the latter performed better than the former. The slightly worse performance of model A may be explained by the fact that it includes all spectral points in the range from 188 to 980 nm, without excluding noise, baseline, and interfered peaks. In addition, it is more dependent on matrix effects than the second model, because fluctuations in the concentration of elements not included in Table 1 affect the calibration, in contrast to the second model.

Even though the spectral processing step did not completely remove the correlation with the background (Fig. 2(b)), it provided a means to

Table 2
Comparison of the percentages of sand, silt, and clay of the second sample set measured by the pipette method and estimated by LIBS and model B. The soil samples were classified according to Saxton et al. (1986) and considering only sand and clay percentages. The symbols * and † denote samples misclassified two and three classes distant, respectively.

	Reference values				Estimated by LIBS and model B			
Sample	Sand	Silt	Clay	Classification	Sand	Silt	Clay	Classification
1	27.3	18.4	54.3	Clay	17.2	22.3	60.4	Clay
2	39.9	18.9	41.2	Clay	31.2	19.1	49.7	Clay
3	57.2	9.2	33.6	Sandy clay loam	53.7	9.5	36.9	Sandy clay
4	27.8	16.0	56.2	Clay	31.5	16.2	52.3	Clay
5	92.3	2.1	5.6	Sand	97.4	0.0	2.6	Sand
6	36.5	14.8	48.7	Clay	32.0	14.0	54.0	Clay
7	59.4	6.4	34.2	Sandy clay loam	53.1	9.4	37.4	Sandy clay
8	57.1	9.2	33.7	Sandy clay loam	60.9	6.8	32.3	Sandy clay loam
9	48.2	9.5	42.3	Sandy clay	36.8	16.0	47.1	Clay
10	52.8	13.9	33.4	Sandy clay loam	46.7	13.8	39.5	Sandy clay
11	19.4	19.2	61.4	Clay	20.8	20.4	58.8	Clay
12	27.5	19.2	53.3	Clay	24.7	21.1	54.2	Clay
13	84.2	6.3	9.5	Loamy sand	82.4	8.2	9.4	Loamy sand
14	58.8	10.2	30.9	Sandy clay loam	36.8	16.2	47.1	Clay*
15	59.0	7.4	33.6	Sandy clay loam	60.2	6.9	33.0	Sandy clay loam
16	39.3	15.3	45.5	Clay	51.5	11.0	37.5	Sandy clay
17	52.0	14.4	33.6	Sandy clay loam	50.6	13.8	35.6	Sandy clay
18	48.3	10.1	41.6	Sandy clay	48.1	10.9	41.0	Sandy clay
19	19.0	20.3	60.7	Clay	30.1	18.4	51.6	Clay
20	36.3	14.8	48.8	Clay	22.5	18.3	59.2	Clay
21	4.0	30.2	65.8	Clay	23.9	23.8	52.3	Clay
22	14.7	20.9	64.4	Clay	26.0	17.4	56.5	Clay
23	18.4	20.2	61.3	Clay	27.9	17.7	54.4	Clay
24	33.3	13.9	52.8	Clay	42.7	11.9	45.5	Clay
25	18.2	21.0	60.7	Clay	25.1	21.8	53.1	Clay
26	41.2	15.2	43.6	Clay	43.2	14.4	42.3	Clay
27	56.9	12.4	30.7	Sandy clay loam	54.1	21.0	24.9	Sandy clay loam
28	86.6	7.1	6.4	Loamy sand	94.7	2.1	3.2	Sand
29	45.8	10.0	44.1	Sandy clay	49.7	9.2	41.0	Sandy clay
30	53.8	14.9	31.3	Sandy clay loam	61.0	12.0	27.0	Sandy clay loam
31	56.9	9.7	33.4	Sandy clay loam	51.5	10.7	37.8	Sandy clay
32	53.8	14.3	31.9	Sandy clay loam	51.6	15.4	33.0	Sandy clay loam
33	14.7	21.3	64.0	Clay	18.2	22.0	59.8	Clay
34	42.4	12.8	44.8	Clay	48.4	10.9	40.8	Sandy clay
35	48.1	10.4	41.6	Sandy clay	50.3	11.1	38.6	Sandy clay
36	42.4	14.0	43.7	Clay	45.2	12.7	42.0	Sandy clay
37	30.6	24.2	45.2	Clay	22.6	38.2	39.2	Clay loam
38	57.3	8.8	33.9	Sandy clay loam	56.0	8.6	35.4	Sandy clay
39	14.8	21.5	63.6	Clay	18.2	21.0	60.8	Clay
40	11.9	35.3	52.8	Clay	2.0	29.6	68.5	Clay
41	39.3	14.9	45.9	Clay	42.6	16.7	40.7	Clay
42	91.8	2.5	5.7	Sand	70.1	7.9	22.0	Sandy clay loam†
43	11.4	31.3	57.3	Clay	11.3	30.4	58.3	Clay
44	59.0	7.1	34.0	Sandy clay loam	54.1	7.1	38.8	Sandy clay
45	19.6	18.5	61.9	Clay	18.9	25.7	55.3	Clay

correct small LIBS spectral problems and to improve the estimation of soil texture. Also, the purpose of the peak-finding step was to find elements with strong correlation with the proportions of sand, silt, and clay. It was not an exhaustive search. Better algorithms to correct LIBS spectra and to find peaks are reserved for future works.

Despite the strong correlation with the reference technique, the uncertainties of the models (6%) were higher than those of the reference method (3%). Nonetheless, the purpose of this study was to show the possibility of estimating and classifying soil texture using LIBS and not to replace the reference technique. Even with such uncertainties, the LIBS can be useful in certain cases where time is crucial: for example, building a map of the soil texture for a large farm, an unfeasible task for the pipette method. Also, the precision of the reference method was low, providing uncertainties of 3%, 2%, and 3% for sand, clay, and silt, respectively. Precise values for textural soil proportions could have helped better identify the elements, which in turn could have reduced LIBS uncertainties.

Our results have shown that it is possible to estimate the proportions of sand, silt, and clay in terrain soils despite their complex composition. Our findings offer a new possibility to analyze not only chemical but also physical properties of soil samples. Therefore, LIBS is a powerful technique that can be used to estimate many soil properties in just a few minutes without chemical reagents.

5. Conclusions

We have shown that LIBS can be used to estimate the relative proportions of sand, silt, and clay in soil samples. We developed two models: one based on a range of 188 to 980 nm and the other based on emission lines of the elements Si, Na, Fe, Ti, Ca, K, Al, Co, Mg, V, Ba, and Be. We built the models with the PLSR method, taking into account the proportions of sand, silt, and clay of 60 Brazilian soil samples of varying composition. The results indicated that the models strongly correlated with the pipette method (Pearson correlation coefficient was higher than 0.85 for all textural proportions), meaning that LIBS can be used to estimate soil texture. Despite showing a higher uncertainty (6%) than that of the reference method (3%), the LIBS can be used for rapid scanning of the soil texture of large regions, which may be unfeasible by the pipette method. Since LIBS does not require sample preparation with chemical reagents, it is less error prone than the pipette method.

Our results could be improved with a more precise reference technique such as a gamma-ray attenuation analyzer, which may help identify other elements related to sand, silt, and clay content. Also, better algorithms to correct the spectra could help to find a higher number of peaks than that found in this work. Another way to improve our results would be to increase the number of samples by at least one order of magnitude (for instance 500 samples).

The procedure employed in this work can be extended to other soil chemical and physical properties. With models for several properties, LIBS can become a universal tool for soil analysis, including quantification of nutrients, organic matter, and contaminants, not only in the laboratory but also in situ.

Acknowledgments

The authors thank FAPESP (No. 06/61741-4) and EMBRAPA (No. 04.11.10.004.00.00) for the financial support of this study.

References

Bousquet, B., Sirven, J.B., Canioni, L., 2007. Towards quantitative laser-induced breakdown spectroscopy analysis of soil samples. Spectrochim. Acta B At. Spectrosc. 62, 1582–1589.

Braga, J.W.B., Trevizan, L.C., Nunes, L.C., Rufini, I.A., Santos D. Jr., Krug, F.J., 2010. Comparison of univariate and multivariate calibration for the determination of micronutrients in pellets of plant materials by laser induced breakdown spectrometry. Spectrochim. Acta B At. Spectrosc. 65, 66–74.

Brown, R.B., 2003. Soil Texture. Technical Report Fact Sheet SL-29. University of Florida. Soil and Water Science Department, Florida Cooperative Extensin Service, Institute of Food and Agricultural Sciences (http://edis.ifas.ufl.edu).

Chang, C.W., Laird, D.A., Mausbach, M.J., Hurburgh, C.R., 2001. Near-infrared reflectance spectroscopy—principal components regression analyses of soil properties. Soil Sci. Soc. Am. J. 65, 480–490.

Corsi, M., Cristoforetti, G., Hidalgo, M., Legnaioli, S., Palleschi, V., Salvetti, A., Tognoni, E., Vallebona, C., 2006. Double pulse, calibration-free laser-induced breakdown spectroscopy: a new technique for in situ standard-less analysis of polluted soils. Appl. Geochem. 21, 748–755.

Costa, L.F., Cesar Jr., R.M., 2001. Shape Analysis and Classification: Theory and Practice. CRC Press, Boca Raton, FL, USA.

Cousin, A., Meslin, P., Wiens, R., Rapin, W., Mangold, N., Fabre, C., Gasnault, O., Forni, O., Tokar, R., Ollila, A., Schröder, S., Lasue, J., Maurice, S., Sautter, V., Newsom, H., Vaniman, D., Mouélic, S.L., Dyar, D., Berger, G., Blaney, D., Nachon, M., Dromart, G., Lanza, N., Clark, B., Clegg, S., Goetz, W., Berger, J., Barraclough, B., Delapp, D., 2015. Compositions of coarse and fine particles in martian soils at gale: a window into the production of soils. Icarus 249, 22–42.

Cremers, D.A., Radziemski, L.J., 2006. Handbook of Laser-Induced Breakdown Spectroscopy. Wiley, Chichester, England.

Cremers, D.A., Ebinger, M.H., Breshears, D.D., Unkefer, P.J., Kammerdiener, S.A., Ferris, M.J., Catlett, K.M., Brown, J.R., 2001. Measuring total soil carbon with laser-induced breakdown spectroscopy (LIBS). J. Environ. Qual. 30, 2202–2206.

Curcio, D., Ciraolo, G., D'Asaro, F., Minacapilli, M., 2013. Prediction of soil texture distributions using vnir-swir reflectance spectroscopy. Procedia Environ. Sci. 19, 494–503.

Dawson, J.B., Snook, R.D., Price, W.J., 1993. Background and background correction in analytical atomic spectrometry. Part 1. Emission spectrometry. A tutorial review. J. Anal. At. Spectrom. 8, 517–537.

Ebinger, M.H., Harris, R.D., 2010. High resolution analysis of soil elements with laser-induced breakdown. US Patent 7,692,789.

Ebinger, M.H., Norfleet, M.L., Breshears, D.D., Cremers, D.A., Ferris, M.J., Unkefer, P.J., Lamb, M.S., Goddard, K.L., Meyer, C.W., 2003. Extending the applicability of laser-induced breakdown spectroscopy for total soil carbon measurement. Soil Sci. Soc. Am. J. 67, 1616–1619.

Ferreira, E.C., Ferreira, E.J., Villas-Boas, P.R., Senesi, G.S., Carvalho, C.M., Romano, R.A., Martin-Neto, L., Milori, D.M.B.P., 2014. Novel estimation of the humification degree of soil organic matter by laser-induced breakdown spectroscopy. Spectrochim. Acta B At. Spectrosc. 99, 76–81.

Ferreira, E.C., Milori, D.M.B.P., Ferreira, E.J., dos Santos, L.M., Martin-Neto, L., de Araújo Nogueira, A.R., 2011. Evaluation of laser induced breakdown spectroscopy for multielemental determination in soils under sewage sludge application. Talanta 85, 435–440.

Ferreira, E.C., Neto, J.A.G., Milori, D.M., Ferreira, E.J., Anzano, J.M., 2015. Laser-induced breakdown spectroscopy: extending its application to soil ph measurements. Spectrochim. Acta B At. Spectrosc. 110, 96–99.

Gee, G.W., Bauder, J.W., 1986. Particle-size analysis. In: Klute, A. (Ed.), Methods of Soil Analysis, Part 1, 2nd ed. American Society of Agronomy, Inc., Madison, WI, USA, pp. 383–411.

Harmon, R.S., De Lucia, F.C., Miziolek, A.W., McNesby, K.L., Walters, R.A., French, P.D., 2005. Laser-induced breakdown spectroscopy (LIBS) — an emerging field-portable sensor technology for real-time, in-situ geochemical and environmental analysis. Geochem. Explor. Environ. Anal. 5, 21–28.

Hassink, J., Bouwman, L., Zwart, K., Brussaard, L., 1993. Relationships between habitable pore space, soil biota and mineralization rates in grassland soils. Soil Biol. Biochem. 25, 47–55.

Hussain, T., Gondal, M.A., Yamani, Z.H., Baig, M.A., 2007. Measurement of nutrients in green house soil with laser induced breakdown spectroscopy. Environ. Monit. Assess. 124, 131–139.

Kettler, T.A., Doran, J.W., Gilbert, T.L., 2001. Simplified method for soil particle-size determination to accompany soil-quality analyses. Soil Sci. Soc. Am. J. 65, 849–852.

Kramida, A., Ralchenko, Y., Reader, J., NIST ASD Team, 2014. 2014. NIST Atomic Spectra Database (ver. 5.2)[Online]. National Institute of Standards and Technology, Gaithersburg, MD (Available at: http://physics.nist.gov/asd. Accessed: 2015–04–29).

Liland, K.H., 2015. 4S Peak Filling — baseline estimation by iterative mean suppression. MethodsX 2, 135–140.

Liland, K.H., Mevik, T.A.B.H., 2011. Optimal baseline correction for multivariate calibration using open-source software. Life Sci. Instrum. 3, 007.

Liland, K.H., Almøy, T., Mevik, B.H., 2010. Optimal choice of baseline correction for multivariate calibration of spectra. Appl. Spectrosc. 64, 1007–1016.

Madari, B.E., Reeves III, J.B., Machado, P.L.O.A., Guimarães, C.M., Torres, E., McCarty, G.W., 2006. Mid- and near-infrared spectroscopic assessment of soil compositional parameters and structural indices in two ferralsols. Geoderma 136, 245–259.

McCave, I.N., Syvitski, J.P.M., 2007. Principles and methods of geological particle size analysis. In: Syvitski, J.P.M. (Ed.), Principles, Methods, and Application of Particle Size Analysis. Cambridge University Press, New York, NY, USA, pp. 3–21.

Mebane Jr., W.R., Sekhon, J.S., 2011. Genetic optimization using derivatives: the rgenoud package for R. J. Stat. Softw. 42, 1–26.

Michel, A.P., Chave, A.D., 2007. Analysis of laser-induced breakdown spectroscopy spectra: the case for extreme value statistics. Spectrochim. Acta B At. Spectrosc. 62, 1370–1378.

Miziolek, A., Palleschi, V., Schechter, I., 2006. Laser-Induced Breakdown Spectroscopy (LIBS): Fundamentals and Applications. Cambridge University Press, New York, NY, USA.

Naime, J.M., Vaz, C.M.P., Macedo, A., 2001. Automated soil particle size analyzer based on gamma-ray attenuation. Comput. Electron. Agric. 31, 295–304.

Nicolodelli, G., Marangoni, B.S., Cabral, J.S., Villas-Boas, P.R., Senesi, G.S., dos Santos, C.H., Romano, R.A., Segnini, A., Lucas, Y., Montes, C.R., Milori, D.M.B.P., 2014. Quantification

of total carbon in soil using laser-induced breakdown spectroscopy: a method to correct interference lines. Appl. Opt. 53, 2170–2176.
Palanco, S., López-Moreno, C., Laserna, J.J., 2006. Design, construction and assessment of a field-deployable laser-induced breakdown spectrometer for remote elemental sensing. Spectrochim. Acta B At. Spectrosc. 61, 88–95.
Pontes, M., Cortez, J., Galvão, R., Pasquini, C., Araújo, M., Coelho, R., Chiba, M., De Abreu, M., Madari, B., 2009. Classification of Brazilian soils by using LIBS and variable selection in the wavelet domain. Anal. Chim. Acta 642, 12–18.
R Core Team, 2014. R: A Language and Environment for Statistical Computing. R Foundation for Statistical Computing, Vienna, Austria (URL: http://www.R-project.org).
Rossel, R.A.V., Walvoort, D.J.J., McBratney, A.B., Janik, L.J., Skjemstad, J.O., 2006. Visible, near infrared, mid infrared or combined diffuse reflectance spectroscopy for simultaneous assessment of various soil properties. Geoderma 131, 59–75.
Savitzky, A., Golay, M.J., 1964. Smoothing and differentiation of data by simplified least squares procedures. Anal. Chem. 36, 1627–1639.
Saxton, K., Rawls, W., Romberger, J., Papendick, R., 1986. Estimating generalized soil-water characteristics from texture. Soil Sci. Soc. Am. J. 50, 1031–1036.
Senesi, G., Dell'Aglio, M., Gaudiuso, R., De Giacomo, A., Zaccone, C., De Pascale, O., Miano, T., Capitelli, M., 2009. Heavy metal concentrations in soils as determined by laser-induced breakdown spectroscopy (LIBS), with special emphasis on chromium. Environ. Res. 109, 413–420.
Silva, R.M., Milori, D.M.B.P., Ferreira, E.C., Ferreira, E.J., Krug, F.J., Martin-Neto, L., 2008. Total carbon measurement in whole tropical soil sample. Spectrochim. Acta B At. Spectrosc. 63, 1221–1224.
Singh, J.P., Thakur, S.N., 2007. Laser-Induced Breakdown Spectroscopy. Elsevier Science, Amsterdam.
Taubner, H., Roth, B., Tippkötter, R., 2009. Determination of soil texture: comparison of the sedimentation method and the laser-diffraction analysis. J. Plant Nutr. Soil Sci. 172, 161–171.
Theriault, G.A., Bodensteiner, S., Lieberman, S.H., 1998. A real-time fiber-optic LIBS probe for the in situ delineation of metals in soils. Field Anal. Chem. Technol. 2, 117–125.
Tobias, R.D., 1995. An introduction to partial least squares regression. Proc. Ann. SAS Users Group Int. Conf., 20th, Orlando, FL, pp. 2–5.
Tognoni, E., Cristoforetti, G., Legnaioli, S., Palleschi, V., 2010. Calibration-free laser-induced breakdown spectroscopy: state of the art. Spectrochim. Acta B At. Spectrosc. 65, 1–14.
Wold, S., Sjöström, M., Eriksson, L., 2001. PLS-regression: a basic tool of chemometrics. Chemom. Intell. Lab. Syst. 58, 109–130.

Anexo 6

Spectrochimica Acta Part B 135 (2017) 29–33

Contents lists available at ScienceDirect

Spectrochimica Acta Part B

journal homepage: www.elsevier.com/locate/sab

Potential of Laser Induced Breakdown Spectroscopy for analyzing the quality of unroasted and ground coffee

Tiago Varão Silva [a], Silviane Zanni Hubinger [b], José Anchieta Gomes Neto [a], Débora Marcondes Bastos Pereira Milori [b], Ednaldo José Ferreira [b], Edilene Cristina Ferreira [a,*]

[a] São Paulo State University - UNESP, Analytical Chemistry Department, P.O. Box 355, 14801-970 Araraquara, SP, Brazil
[b] Embrapa Instrumentation, P.O. Box 741, 13560-970 São Carlos, SP, Brazil

ARTICLE INFO

Article history:
Received 13 September 2016
Received in revised form 23 June 2017
Accepted 25 June 2017
Available online 28 June 2017

Keywords:
Coffee global quality
BGS
Classes discrimination
NIRS
LIBS

ABSTRACT

Coffee is an important commodity and a very popular beverage around the world. Its economic value as well as beverage quality are strongly dependent of the quality of beans. The presence of defective beans in coffee blends has caused a negative impact on the beverage Global Quality (GQ) assessed by cupping tests. The main defective beans observed in the productive chain has been those *Blacks*, *Greens* and *Sours* (BGS). Chemical composition of BGS has a damaging impact on beverage GQ. That is why analytical tools are needed for monitoring and controlling the GQ in coffee agro-industry. Near Infrared Spectroscopy (NIRS) has been successfully applied for assessment of coffee quality. Another potential technique for direct, clean and fast measurement of coffee GQ is Laser Induced Breakdown Spectroscopy (LIBS). Elements and diatomic molecules commonly present in organic compounds (structure) can be assessed by using LIBS. In this article is reported an evaluation of LIBS for the main interferents of GQ (BGS defects). Results confirm the great potential of LIBS for discriminating good beans from those with BGS defects by using emission lines of C, CN, C_2 and N. Most importantly, some emission lines presented strong linear correlation ($r > 0.9$) with NIRS absorption bands assigned to proteins, lipids, sugar and carboxylic acids, suggesting LIBS potential to estimate these compounds in unroasted and ground coffee samples.
© 2016 Elsevier B.V. All rights reserved.

1. Introduction

For many years coffee has been one of the most consumed beverages in the world. The International Coffee Organization estimated a world consumption of coffee around 144.8 million of 60 kg bags in 2015 and the coffee exports in May 2016 in 9.32 million bags [1]. Due to this widespread consumption, the quality is no longer a simple differential to become an essential prerequisite [2,3].

The quality of coffee is related to its organoleptic properties which are result of several factors oscillating from planting to processing post-harvest [4]. One of the most important factors for expert tasters (and consumers) is related to bean variety. In general, a high quality coffee is essentially composed by flawless beans from Arabica specie [5], i.e., avoiding excessively blends. Blends of different species and defective beans are the cause of coffee quality depreciation [6].

Among several types of bean defects notable in the Brazilian processing agro-industry, three of them are the most frequent and can be categorized as: Black, Green and Sour (BGS). Black beans are commonly originated from over-ripened beans. Greens are immature fruits known by increasing beverage astringency. Sour beans have the cause of water scarcity during development of the fruits or by abnormal fermentation [7]. The presence of BGS defects has a direct impact on demeaning the final beverage quality. The more BGS defects, the less the final beverage quality.

In order to aggregate value and expand internal consumption, the Secretary of Agriculture of São Paulo/Brazil, through the normative resolution (called as: SAA-28) of June 1, 2007 [8] established a technical standard for Brazilian coffee quality certification, based on a score, called Global Quality (GQ), assessed by a panel of experts (experienced tasters), using a very similar methodology to that one recommended by Technical Standards Committee of the Specialty Coffee Association of America (SCAA) for standards for cupping coffee [9]. From GQ, coffees are classified as: Traditional (GQ score: 4.5 to 6.0) Superior (GQ score: 6.1 to 7.2) and Gourmet (score 7.3 to 10) [10]. Additionally, SAA-28 establishes the maximum contents of BGS defects for Gourmet (0%), Superior (up to 10%) and Traditional (up to 20%) classes [8]. The method for assessing GQ by a panel of experts is expensive, time consuming, demands drink preparation and is rather subjective [11]. Therefore, a simple, fast, low-cost and reliable analytical method is still an essential (important and desirable) tool for an efficient, highly standardized, competitive and modern coffee industry.

Aiming to verify coffee quality authenticity and prevent fraud, several analytical methods have been developed for monitoring and

* Corresponding author.
E-mail address: edilene@iq.unesp.br (E.C. Ferreira).

http://dx.doi.org/10.1016/j.sab.2017.06.015
0584-8547/© 2016 Elsevier B.V. All rights reserved.

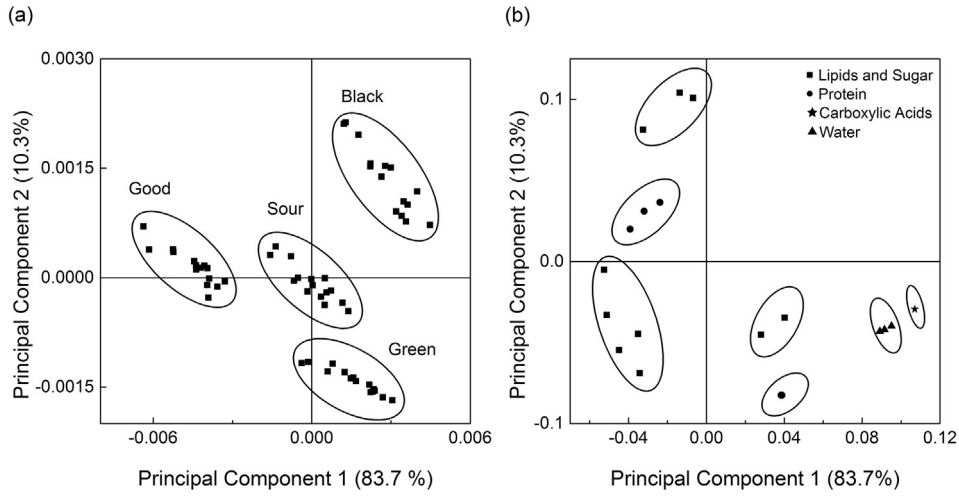


Fig. 1. Results of Principal Component Analysis (PC1xPC2) from NIRS derived spectral data: a) scores plot b) Wavenumbers contributions for discrimination among classes (see Table 2).

classifying the coffee beans [12,13]. Among the analytical techniques commonly applied to that purpose, Near Infrared Spectroscopy (NIRS) has been outstanding with good results [14–16]. The NIRS shows advantages over others dedicated to organic composition analysis (e.g. chromatography), since it performs direct, fast and low-cost analysis, dispensing complex procedures for samples (minimal pretreatment). Absorption bands in NIRS spectrum provide information about organic molecular compounds present in sample [17]. Thus, NIRS has an enormous potential for discriminating different coffee classes, since there exist organic composition differences among them [5].

On the other hand, a more complete chemical profile for different coffee beans (including BGS defects) can extend current knowledge to beyond the molecular comprehension, providing scientific novelty and making technological development viable for analyzing quality tasted in coffee cupping.

Different methods based on atomic absorption and emission spectroscopy have been used to determine concentrations of elements in

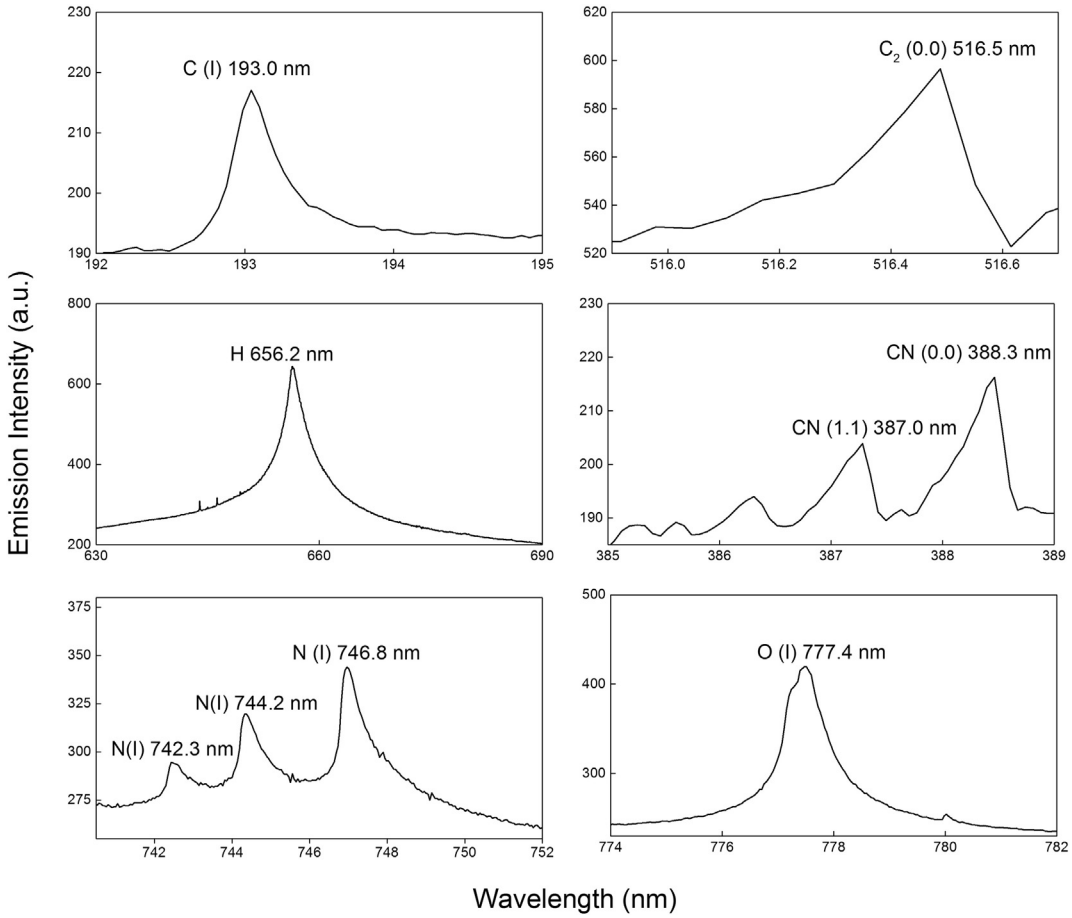


Fig. 2. Fragments of medium LIBS spectrum ($n = 40$) of good coffee sample in different spectral regions of the selected lines.

coffee samples [18]. In general, these techniques need an adequate sample preparation, some of them involving complicated procedures of acid decomposition in high temperatures. In this context, the technique Laser Induced Breakdown Spectroscopy (LIBS) stands out as an interesting alternative. LIBS is based on application of short energetic laser pulses, directly in sample surface. Laser pulse removes a reduced mass of sample, vaporizes it and produces a plasma. Breakdown of sample compounds and species excitation occurs as a result of laser pulse and the plasma action. The evaluation of the recorded light emission intensity, arising from the de-excitation processes, permits a qualitative and sometimes quantitative sample characterization [19]. As LIBS is directly performed on solid samples, a sample pretreatment is practically unnecessary. Although direct analysis may result in precision reduction, speed and lower cost per analysis make viable a high number of analyzes per sample, which improves representativeness [20,21].

LIBS potential has also been exploited for classification of organic compounds in biological materials [20], oils [22] and explosives [23]. These applications are possible because of emission lines of major elements present in organic compounds, such as C, H, N and O [22,23] as well as lines corresponding to emission bands of diatomic molecules, such as CN [24] and C_2 [23]. Additionally, LIBS has also been investigated for determination of other samples properties such as pH and soil texture with high correlation among properties and emission lines [25,26].

Ferreira et al. (2011) [27] applied LIBS for classification of roasted coffees according to their respective GQ classes (Gourmet, Superior, Traditional and Inferior). According to them, wavelengths in the region of the hydrogen emission line (close to 680 nm) were useful to build a high accurate ensemble of decision trees for classification of roasted and ground coffees (commercially available).

An increasing demand for coffee quality certification in the world market brings with it an emergent necessity of techniques endowed with features like those immanent in LIBS. Thus, the aim of this study was investigating elemental and molecular compositions by using LIBS (establishing LIBS-NIRS correlations) to thereby demonstrate its potential for distinguishing classes of coffee beans, especially among good beans and BGS defects, as previous discrimination task intrinsically (and strongly) linked to the GQ of the resultant coffee drink. Elemental and molecular emission lines were analyzed by observing the highest correlations to molecular bands of C—H, C═O and O—H assessed through NIRS spectrum.

2. Material and methods

Samples of coffee beans (Arabic specie from the same crop) classified by an expert as “good” (good quality/no defects), “black”, “green” and “sour” were provided by a Brazilian coffee cooperative of Minas Gerais state. All samples were submitted to a cryogenic grinding, using grinding cycle of 2.0 min, followed by 3.0 min of sample refreezing and other grinding cycle of 2.0 min.

2.1. Sample analysis

The NIRS instrument used for analysis was a near infrared spectrometer, model Spectrum 100 N (Perkin-Elmer Corp., Norwalk, CT) covering 4000–10,000 cm^{-1} range of wavenumbers with spectral resolution of 2 cm^{-1}. Masses around 2.0 g were placed in a glass cuvette, which was introduced over the sample holder of the spectrometer. For each of one of the five sample repetition per class, three measurements were carried. Each measurement corresponded to 32 averaged spectra.

For LIBS analysis, five pellets of each coffee class were prepared by applying 10 tons in 200 mg of ground samples. The pellets were placed in sample holder of a LIBS system. The mentioned equipment comprises seven spectrometers (model LIBS2500 from Ocean Optics, USA) with resolution around 0.1 nm (FWHM) for the spectral analysis ranging from 188 to 980 nm, a Q-switched Nd:YAG laser at 1064 nm, manufactured by Quantel (Big Sky Laser Ultra50), an ablation chamber, a lens for laser focalization (10 cm of focal distance) and an optical system to collect plasma emission and to conduct it the spectrometers made up of a lens and a fiber optic bundle. All measurements were acquired by setting a pulse energy of 50 mJ with 8 ns duration, resulting in an output laser fluency around 0.3 J cm^{-2} and an irradiance in focal point around 10^{12} W cm^{-2}. The delay time (relative to a Q-switch delay) used was 11 μs and the fixed system instrumental conditions of integration time 2.1 ms. Laser pulses were spread on both sides of each pellet. Forty spectra were obtained from each prepared pellet resulting in 200 spectra per class of samples, since five pellets of each class were analyzed.

2.2. Data processing

NIRS spectra show undesirable effects like light scattering, which can account negatively to the results interpretation. Then an adequate spectral treatment is important to minimize these effects [17]. First derivative was chosen for this proposal considering its simplicity [17,28]. Therefore each mean spectrum (average of 32 spectra) acquired by the instrument was differentiated. A Principal Component Analysis (PCA) was carried on considering derivative spectra. Pirouette® 4.5 (Infometrix) software was used for PCA and the data were mean centering. The spectral bands responsible for separating the coffee classes

Table 1
Coffee classes discrimination according to LIBS emission lines.

Emission line	Significant difference between classes (p-value < 0.05)	No significant difference between classes (p-value > 0.05)
C (I) 193.0 nm	Green – Good Black – Good Sour – Good	Green – Black Green – Sour Black – Sour
CN (1.1) 387.0 nm	Green – Good Black – Good Sour – Good	Green – Black Green – Sour Black – Sour
CN (0.0) 388.5 nm	Green – Good Black – Good Sour – Good Green – Sour Black – Sour Green – Black	
C_2 (0.0) 516.6 nm	Green – Good Black – Good Sour – Good Green – Sour Black – Sour	Green – Black
H 656.2 nm	Green – Good Black – Green	Green – Sour Black – Good Black – Sour Sour – Good
N (I) 742.3 nm	Green – Black Green – Good Black – Good Good - Sour	Green – Sour Black – Sour
N (I) 744.2 nm	Green – Black Green – Good Black – Good Good – Sour Green – Sour	Black – Sour
N (I) 746.8 nm	Green – Black Green – Good Black – Good Good – Sour Green – Sour	Black – Sour
O (I) 777.4 nm	Green – Black Green – Good Green – Sour Black – Sour	Black – Good Sour – Good

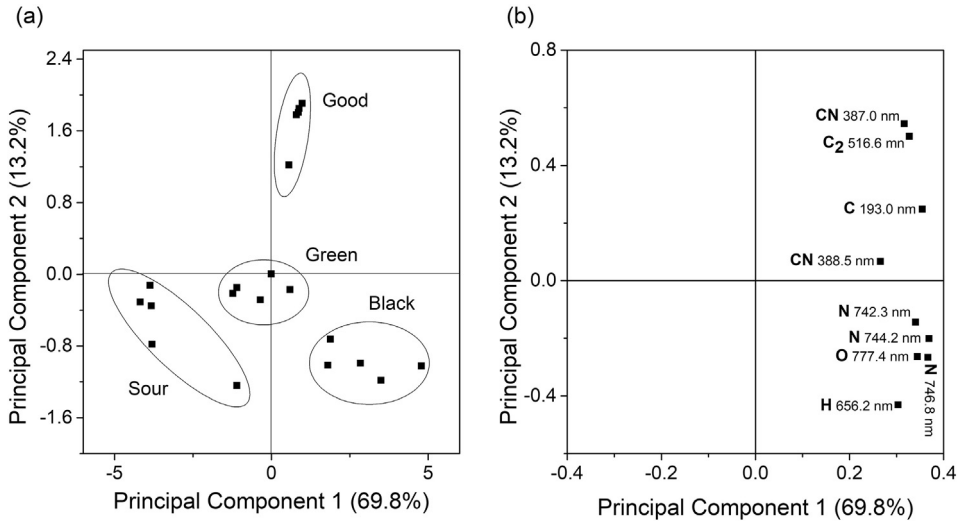


Fig. 3. Results of Principal Component Analysis (PC1xPC2) from LIBS derived spectral data: a) scores plot b) Species contributions for discrimination among classes (see Table 1).

were identified and associated with the compounds present in the samples.

In LIBS spectra, emission lines corresponding to species commonly present in organic molecules were selected: C (I) 193.0 nm, CN (0.0) 387.0 nm, CN (1.1) 388.5 nm, C_2 (0.0) 516.6 nm, H 656.2 nm, N (I) 742.3 nm, N (I) 744.2 nm, N (I) 746.8 nm and O (I) 777.4 nm. For all selected lines, Voigt functions were fitted and then integrated (area under the curve). An average spectrum corresponding to each coffee class was obtained (average of 200 spectra). Significant differences among means from coffee classes were assessed by using Analysis of Variance (ANOVA) with Tukey test (significance level equal to 0.05) for pairwise comparisons. Additionally a PCA was applied to the autoscaled data.

Afterwards, LIBS spectra were processed by first derivative only to get the same mathematical transformation applied to NIRS spectra, making possible a direct correlation (rate of change in LIBS vs. rate of change in NIRS). Derivative spectra from each coffee class for both analytical techniques were averaged, and then linear correlations between narrow ranges (peak interval) of emission lines (LIBS) and NIRS bands (C—H, C═O and O—H) were assessed exactly on inflection points (minimum value of the first derivative) of the interest regions.

3. Results and discussion

Discrimination of coffee classes from the NIRS results were clearly observed by PCA plot. The results of this analysis are shown in Fig. 1, where PC1 represents 83.7% and PC2 10.3% of total data variance. Ellipses were draw to guide the eyes for the clustering of the classes. In Fig. 1b can be observed contributions for PCs. There are strong indications that main absorption bands are contributing for a clear discrimination among classes, i.e., C—H at 4244–4350 cm^{-1} from lipids, sugars and proteins, C═O at about 5260 cm^{-1} from carboxylic acid and O—H at 5280–5286 cm^{-1} from water [2]. The Fig. 1b indicates that good beans, distinct by PC1, contain higher amounts of lipids, sugars and/or proteins. The green class, discriminated from the black and sour shows also proteins, lipids and sugars besides of the highest amounts of water and carboxylic acids. The sour class shows intermediate amounts of the mentioned compounds while black class shows lower amounts of these compounds. The color of black beans is result of a non enzimatic browning known as Maillard reactions, i.e. reactions between carbonyl groups of the sugars with the nucleophilic amino group of the amino acids [29]. As carboxylic acids and proteins are consumed in Maillard reaction these compounds were lower in black class.

Table 2
Linear correlation coefficient (in module) for differentiated minimum inflections of LIBS and NIRS signals.

Wavenumber attribution	NIRS wave number (cm-1)	LIBS wavelength (nm)								
		C (I) 193.0	CN (1.1) 387.2	CN (0.0) 388.5	C2 (0.0) 516.6	H 656.2	N (I) 742.3	N (I) 744.2	N (I) 746.8	O(I) 777.4
Protein	4244	0.894	0.821	0.815	0.663	0.948	0.935	0.922	0.898	0.872
	4246	0.958	0.908	0.902	0.766	0.881	0.885	0.852	0.830	0.779
	4248	0.990	0.962	0.956	0.839	0.799	0.818	0.768	0.748	0.675
Lipids, sugars and oils	4256	0.903	0.955	0.951	0.924	0.348	0.415	0.315	0.309	0.175
	4266	0.970	0.802	0.796	0.640	0.958	0.942	0.933	0.908	0.887
	4270	0.965	0.919	0.913	0.782	0.868	0.874	0.838	0.816	0.761
	4314	0.289	0.157	0.162	0.020	0.859	0.763	0.845	0.810	0.916
	4318	0.745	0.650	0.652	0.507	0.980	0.927	0.950	0.914	0.942
	4324	0.993	0.997	0.996	0.923	0.651	0.579	0.613	0.592	0.501
	4326	0.964	0.993	0.992	0.944	0.510	0.482	0.472	0.457	0.345
	4328	0.910	0.961	0.960	0.939	0.362	0.379	0.326	0.315	0.188
	4330	0.816	0.892	0.892	0.904	0.182	0.251	0.147	0.141	0.003
Protein	4348	0.803	0.711	0.704	0.538	0.986	0.915	0.965	0.939	0.940
	4350	0.800	0.707	0.701	0.536	0.986	0.907	0.965	0.938	0.940
Carboxil acids	5264	0.990	0.961	0.941	0.793	0.768	0.640	0.754	0.752	0.647
Water	5280	0.983	0.945	0.923	0.764	0.801	0.653	0.790	0.788	0.689
	5284	0.980	0.940	0.919	0.758	0.811	0.657	0.800	0.798	0.701
	5286	0.979	0.937	0.916	0.754	0.817	0.661	0.806	0.803	0.708

The above results suggest that proteins, lipids, sugar and carboxylic acids besides the water are important chemical compounds for discrimination of coffee classes and these compounds can be measured by NIRS to infer the coffee quality.

Whereas proteins, lipids, sugar, water and carboxylic acids are relevant for discrimination among coffee classes, emission lines of elements or diatomic species mostly present in the structures of these compounds were selected from LIBS spectra for evaluation. The selected lines in LIBS spectra can be observed in Fig. 2.

The coffee classes were compared considering medium areas of each selected emission lines. The significant differences (p-value < 0.05) among the classes in function of selected emission lines are shown in Table 1. For clarifying result visualizations a PCA was performed. Scores and loading plots are shown in Fig. 3. Except for the H 656.2 nm and O (I) 777.4 nm lines, the other lines are suitable to be used for discrimination of good beans. These results emphasize LIBS potential for detecting improper blends of BGS defects in Gourmet coffees (100% good beans). Furthermore, it is highlighted the potential of the lines of CN (0.0) 388.5 nm, C_2 (0.0) 516.6 nm, N (I) 744.2 nm and N(I) 746.8 nm for discrimination of the mostly studied classes.

A study was carried out to check the correlations between NIRS absorption bands and LIBS emission lines. All pairwise correlation (using linear correlation as a metric) were applied to values extracted from inflection points. The results of linear correlation (in module) are shown in Table 2.

Absorption bands corresponding to proteins, lipids, sugar and carboxylic acids and emission lines of C(I) 193.0 nm, CN (1.1) 387.0 nm, CN (0.0) 388.5 nm showed correlation coefficient higher than 0.9 suggesting the potential of these emission lines to estimate classes of compounds in coffee samples by using only LIBS technique. The triplet of nitrogen, N (I) 742.3 nm, 744.2 nm and 746.8 nm, have potential for a linear modeling capable of estimating protein contents as well as C_2 (0.0) 516.6 nm for lipids, since these lines showed high correlation with respective NIRS absorption bands ($r \geq 0.9$). It is highlighted that CN emission band at 388.5 nm provided the best class discriminations and it was strongly correlated to coffee proteins (Table 2), suggesting that CN monitored lines are predominantly from protein molecular fragmentations.

The LIBS and NIRS techniques show similar features in terms of analytical simplicity, direct and fast analysis and portability potential. On the other hand, results suggest that LIBS can be capable of performing some kind of analysis similarly to NIRS, besides its ability to analyze the elemental composition, which is not feasible by using NIRS.

4. Conclusion

The quality of coffee is strongly linked to blends with defective beans. Black, Green and Sour beans damage beverage quality. Thus, the development of tools for detection of coffee quality adulteration is very important for world coffee agro-industry. LIBS technique showed a high potential for discriminating good beans from BGS defects from unroasted ground coffee. Emission lines of elements and emission bands of diatomic molecules derived from organic compounds showed good discriminant power. The high correlations ($r > 0.9$) observed for N, CN, C and C_2 LIBS emissions and NIRS absorption bands of proteins, lipids, sugars and carboxylic acids also suggest the potential of LIBS for estimation of these compounds. Finally, more than a multielemental determination, LIBS has shown a capacity for aggregating information on molecular and organic aspects (a particular feature attributed to NIRS) related to quality of coffee beans, and consequently coffee beverage resultant from them. These findings confirm LIBS as a promising tool for analyzing food quality in many agro-industry branches.

Acknowledgement

Special thanks to Coffee Research Consortium (Brazilian Ministry of Agriculture and Embrapa, Grant # 04.13.02.003.00.0) for supporting research through MP4 project.

References

[1] ICO, International Coffee Organization. http://www.ico.org/, 2016 (accessed 26 July 2016).
[2] N. Yang, C. Liu, X. Liu, T.K. Degn, M. Munchow, I. Fisk, Determination of volatile marker compounds of common coffee roast defects, Food Chem. 211 (2016) 206–214.
[3] W.B. Sunarharum, D.J. Williams, H.E. Smyth, Complexity of coffee flavor: a compositional and sensory perspective, Food Res. Int. 62 (2014) 315–325.
[4] A.T. Toci, A. Farah, Volatile fingerprint of Brazilian defective coffee seeds: corroboration of potential marker compounds and identification of new low quality indicators, Food Chem. 153 (2014) 298–314.
[5] Yi-Fang Chu, Coffee: Emerging Health Effects and Disease Prevention, First Edition John Wiley & Sons, Blackwell Publishing Inc, Iowa, 2012.
[6] A. Farah, M.C. Monteiro, V. Calado, A.S. Franca, L.C. Trugo, Correlation between cup quality and chemical attributes of Brazilian coffee, Food Chem. 98 (2006) 373–380.
[7] A.T. Toci, A. Farah, Volatile compounds as potential defective coffee beans' markers, Food Chem. 108 (2008) 1133–1141.
[8] Codeagro, Resolução SAA - 28, de 01 de junho de, 2007 http://www.codeagro.agricultura.sp.gov.br/arquivos/selo/saa_28a191a62ed1008f350553a619ba36f7e7.pdf, 2016 (accessed 07.27.2016).
[9] F.M. Borém, F.C. Ribeiro, L.P. Figueiredo, G.S. Giomo, V.A. Fortunato, E.P. Isquierdo, Evaluation of the sensory and color quality of coffee beans stored in hermetic packaging, J. Stored Prod. Res. 52 (2013) 1–6.
[10] Specialty Coffee Association of America (SCAA), Cupping Specialty Coffee, 2016 http://www.scaa.org/PDF/resources/cupping-protocols.pdf, 2016 (accessed 07.27.2016).
[11] K. Tolessa, M. Rademaker, B. De Baets, P. Boeckx, Prediction of specialty coffee cup quality based on near infrared spectra of green coffee beans, Talanta 150 (2016) 367–374.
[12] M. Oliveira, S. Casal, S. Morais, C. Alves, F. Dias, S. Ramos, E. Mendes, C. Deleruе-Matos, M. Beatriz, P.P. Oliveira, Intra- and interspecific mineral composition variability of commercial instant coffees and coffee substitutes: contribution to mineral intake, Food Chem. 130 (2012) 702–709.
[13] R.M. Barbosa, B.L. Batista, R.M. Varrique, V.A. Coelho, A.D. Campiglia, F. Barbosa, The use of advanced chemometric techniques and trace element levels for controlling the authenticity of organic coffee, Food Res. Int. (2013).
[14] A.P. Craig, A.S. Franca, L.S. Oliveira, J. Irudayaraj, K. Ileleji, Fourier transform infrared spectroscopy and near infrared spectroscopy for the quantification of defects in roasted coffees, Talanta 134 (2015) 379–386.
[15] J.R. Santos, M.C. Sarraguça, A.O.S.S. Rangel, J.A. Lopes, Evaluation of green coffee beans quality using near infrared spectroscopy: a quantitative approach, Food Chem. 135 (2012) 1828–1835.
[16] E. Bertone, A. Venturello, A. Giraudo, G. Pellegrino, F. Geobaldo, Simultaneous determination by NIR spectroscopy of the roasting degree and Arabica/Robusta ratio in roasted and ground coffee, Food Control 59 (2016) 683–689.
[17] C. Pasquini, Near infrared spectroscopy: fundamentals, practical aspects and analytical applications, J. Braz. Chem. Soc. 14 (2003) 198–219.
[18] P. Pohl, E. Stelmach, M. Welna, A. Szymczycha-Madeja, Determination of the elemental composition of coffee using instrumental methods, Food Anal. Methods 6 (2013) 598–613.
[19] D. Cremers, L.J. Radziemski, Handbook of Laser-Induced Breakdown Spectroscopy, John Wiley & Sons, Chichester, 2006.
[20] S.J. Rehse, H. Salimnia, A.W. Miziolek, Laser-induced breakdown spectroscopy (LIBS): an overview of recent progress and future potential for biomedical applications, J. Med. Eng. Technol. 36 (2012).
[21] A.W. Miziolek, V. Palleschi, I. Schechter, LIBS Fundamentals and Applications, Cambridge, 2006.
[22] Y.G. MbesseKongbonga, H. Ghalila, M.B. Onana, Z. Ben Lakhdar, Classification of vegetable oils based on their concentration of saturated fatty acids using laser induced breakdown spectroscopy (LIBS), Food Chem. 147 (2014) 327–331.
[23] P. Lucena, A. Doña, L.M. Tobaria, J.J. Laserna, New challenges and insights in the detection and spectral identification of organic explosives by laser induced breakdown spectroscopy, Spectrochim. Acta B 66 (2011) 12–20.
[24] Á. Fernández-Bravo, T. Delgado, P. Lucena, J.J. Laserna, Vibrational emission analysis of the CN molecules in laser-induced breakdown spectroscopy of organic compounds, Spectrochim. Acta B At. Spectrosc. 89 (2013) 77–83.
[25] E.C. Ferreira, J.A. Gomes Neto, D.M.B.P. Milori, E.J. Ferreira, J.M.A. Lacarte, Laser-induced breakdown spectroscopy: extending its application to soil pH measurements, Spectrochim. Acta B At. Spectrosc. 110 (2015) 96–99.
[26] P.R. Villas-Boas, R.A. Romano, M.A. de Menezes Franco, E.C. Ferreira, E.J. Ferreira, S. Crestana, D.M.B.P. Milori, Laser-induced breakdown spectroscopy to determine soil texture: a fast analytical technique, Geoderma 263 (2016) 195–202.
[27] E.J. Ferreira, E.C. Ferreira, A.C.B. Delbem, D.M.B.P. Milori, Ensemble of predictors and laser induced breakdown spectroscopy for certifying coffee, Electron. Lett. 47 (2011) 967–969.
[28] D. Burns, E. Ciurczak, Handbook of Near-Infrared Analysis Second Edition, Revised and Expanded Edited, Marcel Dekker, New York, 2007.
[29] A. Farah, C.M. Donangelo, Phenolic compounds in coffee, Braz. J. Plant Physiol. 18 (2006) 23–36.

Anexo 7

Microchemical Journal 134 (2017) 370–373

Contents lists available at ScienceDirect

Microchemical Journal

journal homepage: www.elsevier.com/locate/microc

Calcium determination in biochar-based fertilizers by laser-induced breakdown spectroscopy using sodium as internal standard

Carla Pereira de Morais [a], Ariane Isis Barros [a], Dário Santos Júnior [b], Clóvis Augusto Ribeiro [a], Marisa Spirandeli Crespi [a], Giorgio Saverio Senesi [c], José Anchieta Gomes Neto [a], Edilene Cristina Ferreira [a,*]

[a] São Paulo State University - UNESP, Analytical Chemistry Department, P.O. Box 355, 14801-970 Araraquara, SP, Brazil
[b] Federal University of São Paulo, UNIFESP, Chemistry Department, Rua São Nicolau, n° 210 - Centro - CEP: 09913-030, Diadema, SP, Brazil
[c] CNR, NANOTEC - PlasMI Lab, Via Amendola 122/D, 70126 Bari, Italy

ARTICLE INFO

Article history:
Received 19 April 2017
Received in revised form 5 July 2017
Accepted 5 July 2017
Available online 6 July 2017

Keywords:
Biochar-based fertilizers
Calcium
Libs
Internal standardization

ABSTRACT

Biochar has gained agricultural importance as a soil amendment because of its important agricultural properties such as water retention, plant nutrient supplier, promoter of microorganism growth, sequestration action of atmospheric CO_2, etc. Further, it is a low cost material being produced by recycling. Due to its active sites, biochar can adsorb nutrients so acting as a soil fertilizer. Thus the rapid assessment of nutrients in these materials is essential to ensure quality control for agricultural purposes. This work aimed to develop a simple analytical method based on Laser-Induced Breakdown Spectroscopy (LIBS) to determine Ca in biochar-based fertilizers. In particular, biochar samples enriched with Ca were prepared from peanut shells, residues of eucalyptus and banana fibers. The calibration standards were prepared by matrix matching using a biochar from eucalyptus residues. Different spectral preprocessing were evaluated to enhance the precision and accuracy of the method. However, the matrix effects demanded the use of internal standardization as the appropriate methodology to obtain the best accuracy. A linear correlation coefficient of 0.989 and a linear work range of 1.51–11.23% Ca were obtained using the proposed method, which yielded limits of detection and quantification of 0.45% e 1.51%, respectively. Calcium contents determined by LIBS in biochar-based fertilizers were in good agreement (paired *t*-test at 95% confidence level) with those determined by using High-Resolution Continuous Source Atomic Absorption Spectrometry (HR-CS FAAS) as the reference technique. Thus, the importance of internal standardization was demonstrated to be successful for the quantitative analysis of Ca in complex matrices like biochar-based fertilizers.
© 2017 Elsevier B.V. All rights reserved.

1. Introduction

The use of biochar in agriculture to improve soil quality is a millenarian practice used by indigenous tribes of the central Amazonian basin, which resulted in a kind of soil known as indian dark earth [1]. The high fertility of Amazon Indians soils has been attracted the interest of soil scientists due to the intrinsic low fertility of tropical Amazonian soils are originally low fertility [2].

Currently this practice is known as pyrolytic conversion of agricultural waste into biochar, which is considered a soil enhancer due to its capacity to hold carbon, to assist water and nutrients retention and increase soil biodiversity [3,4]. The interest in biochar is growing up, driven by two major global issues, i.e. climate change and need for a more sustainable soil management [1]. In this context, Dias et al. [5] have recently proposed the use of biochar as potential fertilizer, possibly working by releasing nutrients in a controlled manner. In face of the perspective of biochar use for agricultural purposes, the International Biochar Initiative (IBI), started in 2006 during the World Soil Science Congress (WSSC), has highlighted the importance of the analytical characterization and producer's certification of biochar used as soil amendment [6].

The consolidated analytical techniques commonly used for elemental determinations require the dissolution of the solid sample, which involves the use of strong oxidants and high temperatures [7,8]. However, biochar consists of a recalcitrant material that is hardly soluble under normal conditions of wet decomposition, thus requiring more drastic conditions, such as high pressures or decomposition in dry conditions using fluxing agents [9]. As consequence, the use of the aforementioned conditions increases the possibility of systematic errors besides producing large volumes of chemical residues [10].

Laser-Induced Breakdown Spectroscopy (LIBS) is an analytical technique able to perform direct simultaneous multielemental analysis of solid samples by applying a highly energetic laser pulse on the sample surface, so promoting the sample breakdown, plasma generation and species excitation in a single step [11,12]. Then, the characteristic

* Corresponding author.
E-mail address: edilene@iq.unesp.br (E.C. Ferreira).

http://dx.doi.org/10.1016/j.microc.2017.07.005
0026-265X/© 2017 Elsevier B.V. All rights reserved.

wavelengths of the radiation emitted by de-excitation of the species in the plasma are recorded simultaneously, so yielding a sample emission spectrum that provides a qualitative overview of sample composition. The quantitative information is then extracted from the emission signal magnitudes, which are related to standard concentrations through a suitable calibration model [11,13–15]. Linear calibration models are more adequate, considering the emission intensities of excited elements are directly proportional to their concentration [16]. In particular, due to the common fluctuations observed in LIBS measurements associated to both, instrumentation and sample heterogeneity, various strategies are experimented for the calibration of LIBS methods, which include various different spectral preprocessing and multivariate (linear and non-linear) calibration models [17–20]. Among these, internal standardization, which consists in normalizing the analyte signal by the signal of an internal standard (IS), is a well known methodology used to minimize fluctuations in spectroscopic techniques including LIBS [21–24]. To perform internal standardization, the IS concentration must be known and nearly constant [25,26]. However, in some cases it is difficult to select an adequate IS in LIBS analysis because the IS may be subject to temporal processes different from those experienced by the analyte in the plasma. The use as IS of an element naturally present in the samples analyzed may also be inappropriate as the IS concentration may change from sample to sample, thus not fitting the IS requirements [22,23,27].

In this work, different spectral preprocessing and internal standardization methods were evaluated to find out the best methodology that can allow minimizing fluctuations in LIBS measurements, so enabling the adequate LIBS analysis of Ca in biochar-based fertilizers.

2. Materials and methods

2.1. Eucalyptus biochar production

The original eucalyptus biochar was produced by using leaves and branches of eucalyptus. The materials were mixed and crushed using a knife mill from Tecnal (Willey TE 340, Piracicaba, Brazil). Then 2.0 g of this powdered biomass were transferred to a porcelain crucible capped with aluminum paper to keep the atmosphere rare in oxygen, heated in a muffle oven from EDG (EDGCON 5P, São Carlos, Brazil) from room temperature to 260 °C at a heating rate of 10 °C min^{-1}, and finally maintained at 260 °C for 60 min. After cooling to room temperature, the biochar was stored in an amber flask inside a desiccator to be used in standards calibration for matrix matching.

2.2. Fertilizer samples production

Fertilizer samples were produced from leaves and branches of eucalyptus, banana fibers and peanut shells. In particular, 3.0 g of each biomass were placed in Erlenmeyer flasks containing 100 mL of 1.80 g L^{-1} Ca^{2+} water solution prepared from CaO (Alfa Aesar), and then shaken at 25 °C for 24 h in a incubator with orbital agitation at 150 rpm. After filtration, the biomasses were dried at 40 °C for 24 h. Then 3.0 g of each dried biomass were submitted to the same procedure and heating program described above to produce the eucalyptus biochar. Each fertilizer was prepared in triplicate.

An aliquot of 200 mg of each fertilizer so produced was mixed with 80 mg of cellulose (type 101 Sigmacell) for sample compaction, homogenized in an agate mortar, and finally converted into pellets by applying a pressure of 10 tons in a hydraulic press from Specac (GS15011, Swedesboro, USA).

2.3. LIBS analysis

The LIBS instrument used was a homemade system equipped with a Q-switched Nd:YAG laser from Quantel (Big Sky Ultra 50, Bozeman, USA) emitting at 1064 nm and operating at a maximum power energy of 50 mJ and a repetition rate of up to 20 Hz, with a pulse duration of 20 ns, and a laser spot diameter of about 0.5 mm. The detection device used was the spectrometer from Ocean Optics (HR2000+, Dunedin,USA) that is composed of four spectrometers with optical resolution of 0.1–0.2 nm (FWHM) which measure the range between 199 and 631 nm at a fixed integration time of 1 μs. Individual samples were placed in an electronically controlled sampling chamber with movement in the x-y directions and equipped with a video camera for monitoring the process. The Q-Switched delay time selected for spectra acquisition was 2.0 μs. The system was controlled by the OOLIBS software (Ocean Optics). Sixty LIBS spectra were acquired from each standard and sample pellet. The average spectra of individual studied biomasses plus cellulose are shown in the Supplementary Material (Fig. S1).

The application of a univariate linear calibration model was evaluated by the Least-Squares Regression method for the Ca atomic emission line at 612.22 nm. This low relative intensity emission line (13%) was selected to avoid the self-absorption effects that were observed for more sensitive lines. The intensity of the peak, the peak area fitted by the Lorentz and Voigt functions and the maximum variation ratio of the first derived spectrum were evaluated in spectral preprocessing.

The calibration standards were prepared by matrix matching by mixing 156 mg of eucalyptus biochar, 80 mg of cellulose, CaO at different amounts to produce Ca standards with the following concentrations: 0, 1.02, 2.55, 5.10, 8.17 and 11.23% (*w*/w), and maize starch in different amounts up to 280 mg. All components were homogenized using an agate mortar and pistil, and then compacted in pellets using a pressure of 10 tons. For calibration purposes internal standardization was also evaluated by using as IS the Na atomic line at 588.99 nm to normalize the Ca atomic line after spectrum derivation.

2.4. Thermal and atomic absorption spectrometry analyses

Thermal analysis was performed on the original eucalyptus biochar, the eucalyptus fertilizer sample and a calibration standard by simultaneous TGA-DTA using a TA Instruments apparatus (SDT 2960, New Castle, USA). Samples were heated from room temperature up to 800 °C at a heating rate of 30 °C min^{-1} under compressed air atmosphere and a flow rate of 100 mL min^{-1}.

In order to check the accuracy of the LIBS method, the Ca contents in fertilizer samples were determined by High Resolution Continuous Source Flame Atomic Absorption Spectrometry (HR-CS FAAS) from AnalytikJena (ContrAA 300 spectrometer, Jena, Germany). The instrumental conditions used for analysis were: flame of nitrous oxide and acetylene at a flowing rate of 210 and 80 L min^{-1}, respectively, burner (50 mm) at a height of 6 mm, and aspiration rate of 5 mL min^{-1}. The Ca line monitored was at 239.8559 nm (secondary line, with 1.1% of sensitivity).

The HR-CS FAAS analysis was conducted on sample digests prepared as follows. Fertilizers samples were mineralized in triplicate in a close-vessels microwave-assisted acid-digestion system. Specifically, 100 mg of each sample were accurately weighed and transferred to a microwave flask, to which 3.0 mL of 70% (*v*/v) nitric acid solution, 2.0 mL of deionized water and 1.0 mL of H_2O_2 30% (*v*/v) were added. The mixtures were heated in a microwave oven from Anton Paar (Multiwave, Graz, Austria) using an optimized program involving power/ramp time/hold time of 900 W/15 min/30 min, respectively. After digesting and cooling, the resulting digests were transferred to 25 mL volumetric flasks, and the volume completed with de-ionized water. The accuracy of the reference method was evaluated using the certified reference material Pine Needles (NIST - 1575a).

3. Results and discussions

Calibration models were calculated for the direct correlation between Ca concentration and parameters extracted from the LIBS emission signal of Ca I 612.22 nm in calibration standards. To this purpose,

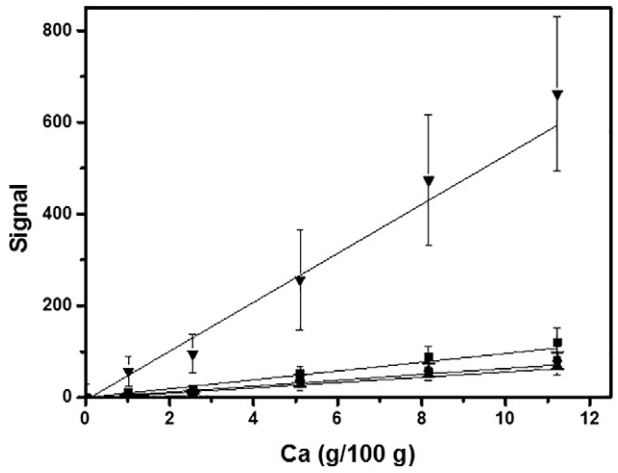


Fig. 1. Evaluated calibration curves for Ca determination based on: peak intensity (■), peak area fitted by Lorentz function (●), peak area fitted by Voigt function (▲) and maximum variation rate of derived signal (▼).

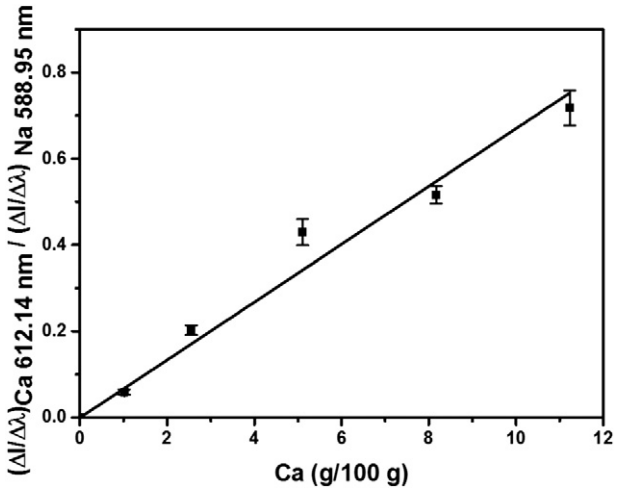


Fig. 3. Calibration curve for Ca determination by LIBS using Na as internal standard.

LIBS spectra were preprocessed in different ways, aiming to minimize common fluctuations in measurements and obtain a suitable calibration model. The four evaluated models considered (Fig. 1), based on the spectral information of peak intensity, peak area fitted by Lorentz function, peak area fitted by Voigt function and maximum variation rate of derived signal, showed correlation coefficients of 0.974, 0.963, 0.952 and 0.971, respectively. Additionally, the amount of Ca (g/100 g) predicted by these models were 1.20 ± 0.35%, 1.20 ± 0.08%, 1.68 ± 0.20%, 1.29 ± 0.11%, respectively. These results indicated that well fitted analytical curves with similar prediction capabilities were obtained. Further, the application of peak areas or spectrum differentiation caused a considerable reduction of the relative standard deviation that dropped from 29% obtained by the peak intensity method to an average of 9%. However, the prediction accuracy was not acceptable because the Ca concentration determined in the sample by the reference method was 5.38 ± 0.27%. These results suggested that, although fluctuations were minimized by spectral preprocessing, the matrix effect persisted causing an underestimation of the Ca content in the sample.

To evaluate the occurrence of matrix effects, thermal analysis was performed on the original biochar, the biochar-based fertilizer and a calibration standard (Fig. 2). The DTA curves show that the sum of the events is exothermic, and the TG and DTG curves indicate that the three events imply a weight loss. The first event can be ascribed to sample dehydration, the second one to evaporation of volatile compounds, and the third to the decomposition of $CaCO_3$ in CaO (s) and CO_2 (g) [28]. The analysis of the third event, in which Ca is involved, shows that: for the original biochar (Fig. 2a) the event started at 572.80 °C and was completed at 770.97 °C with 1.43% of weight loss; for the fertilizer (Fig. 2b) the event started at 597.57 °C and finished at 771.86 °C with 8.20% of weight loss; and for the calibration standard (Fig. 2c) the event started at 559.01 °C and finished at 773.82 °C with 5.83% of

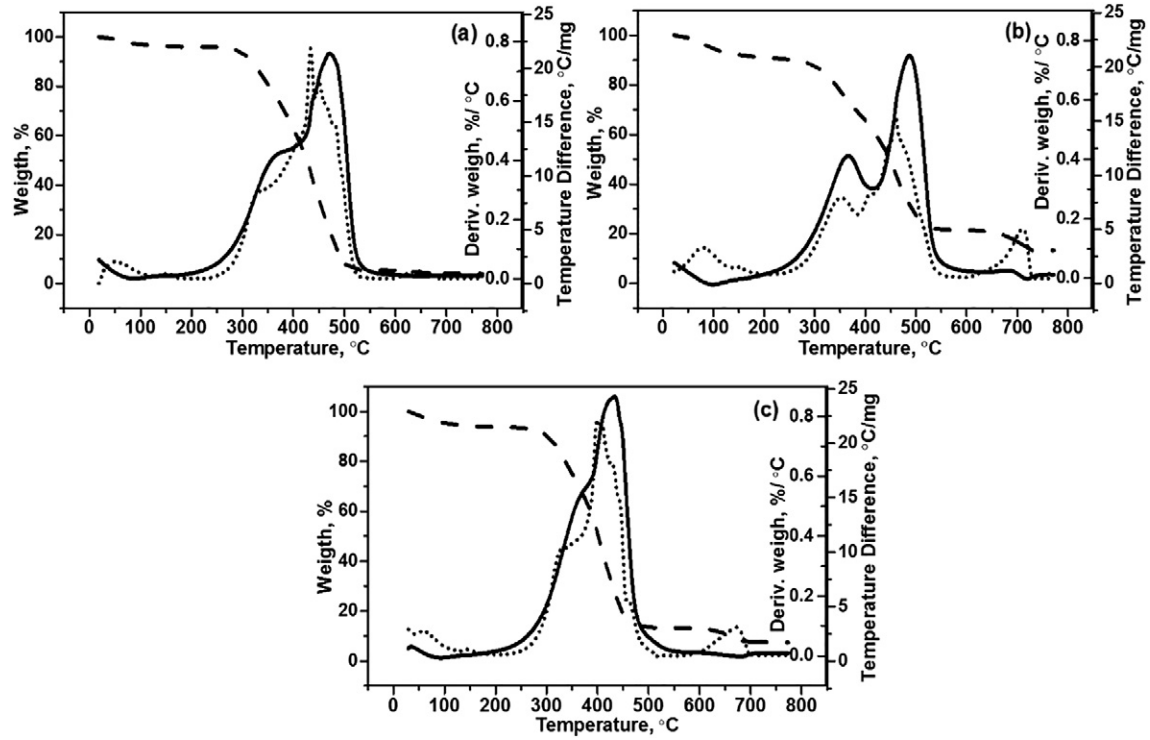


Fig. 2. TG (- - -), DTG (· · · ·) e a DTA (—) curves of (a) eucalyptus biochar, (b) eucalyptus fertilizer biochar, and (c) calibration standard containing 5.19 Ca%.

weight loss. These results would suggest that the fertilizer and the calibration standard are more similar compared to the original biochar, thus suggesting that Ca incorporation changes the original biochar properties. Thus, the use of matrix matching for Ca determination seems to be a good choice.

Despite the similarity between the standard and fertilizer sample, the different weight loss measured suggests that Ca was incorporated in a different way in the two materials. The original biochar possesses many active sites available for Ca incorporation by simple physical mixing [29], whereas incorporation would occur differently during the pyrolysis of Ca-added biochar. The different way in which elements are bound to the matrix probably causes the standard and the samples to experience differentiated breakdown and excitation processes during LIBS analysis.

In the attempt to minimize the differences between the sample and the calibration standard, the internal standardization method was also applied. The LIBS spectrum of the original eucalyptus biochar shows an unresolved line in the range of 585 to 595 nm that corresponds to a doublet of Na atomic lines (588.99 and 589.59 nm). Considering that Na is from the biochar and this matrix is similarly diluted in samples and standards, a similar Na concentration is expected in both materials. Thus, Na was used as IS for Ca determination.

To minimize fluctuations the spectrum derivation method was used in spectral preprocessing. A well fitted linear correlation ($R = 0.989$) was obtained by plotting the ratio of the maximum variation rate of Ca I 612.22 nm to the maximum variation rate of Na I 588.99 nm as a function of the Ca % in the calibration standard (Fig. 3). This calibration model was applied for Ca concentration predictions by LIBS in the biochar-based fertilizers. The biochar fertilizers of eucalyptus, peanut shells and banana fiber showed Ca% of 5.89 ± 0.70, 3.69 ± 0.56 and 8.71 ± 1.13, respectively. These values are in good agreement (paired *t*-test at a 95% confidence level) with reference values, 5.38 ± 0.27, 3.71 ± 0.22, 9.17 ± 0.13, respectively. Further, the LIBS method featured a linear work range of 1.51–11.23%Ca, and limits of detection and quantification of 0.45% and 1.51% respectively, as calculated according to Currie [30].

4. Conclusions

The application of the LIBS technique to the determination of Ca in biochars-based fertilizers showed the need of a preliminary spectral processing in order to minimize the common fluctuations occurring in LIBS measurements, which usually decrease their precision. Due to the occurrence of matrix effects, as proven by thermal analysis, the prediction accuracy of the method could not be achieved by applying common spectral preprocessing methods, but using the internal standardization method based on Na naturally present in the samples, which permitted the proper correction of the Ca signal.

The LIBS method developed appeared to respond to the IBI demands as it shows promising analytical features, i.e. it is fast, does not require drastic preparation conditions and is environmentally friend because it does not generate chemical residues of analysis. Further, LIBS can be adapted to other types of coals of difficult decomposition.

Supplementary data to this article can be found online at http://dx.doi.org/10.1016/j.microc.2017.07.005.

Acknowledgements

The authors thank the Fundação de Amparo à Pesquisa do Estado de São Paulo (FAPESP) for financial support of this work (Grant # 2015/24757-9), the Coordenação de Aperfeiçoamento Pessoal de Nível Superior (CAPES) for providing a fellowship to C.P.M, and the Conselho Nacional de Desenvolvimento Científico e Tecnológico for a fellowship to A.I·B and a research grant to J.A.G.N and D.S.J.

References

[1] K.Y. Chan, L. van Zwieten, I. Meszaros, A. Downie, S. Joseph, Agronomic values of greenwaste biochar as a soil amendment, Aust. J. Soil Res. 45 (2007) 629–634.
[2] B. Glaser, L. Haumaier, G. Guggenberger, W. Zech, The "Terra Preta" phenomenon: a model for sustainable agriculture in the humid tropics, Naturwissenschaften 88 (2001) 37–41.
[3] C.J. Atkinson, J.D. Fitzgerald, N.A. Hipps, Potential mechanisms for achieving agricultural benefits from biochar application to temperate soils: a review, Plant Soil 337 (2010) 1–18.
[4] Y. Fang, B. Singh, B.P. Singh, E. Krull, Biochar carbon stability in four contrasting soils, Eur. J. Soil Sci. 65 (2014) 60–71.
[5] D.S. Dias, M.S. Crespi, L.D.M. Torquato, M. Kobelnik, C.A. Ribeiro, Torrefied banana tree fiber pellets having embedded urea for agricultural use, J. Therm. Anal. Calorim. (2017) 1–8.
[6] International Biochar Initiative (IBI), http://www.biochar-international.org 2017 (accessed 04.18.17).
[7] H.M. Kingston, S.J. Haswell, Microwave-Enhanced Chemistry: Fundamentals, Sample Preparation, and Applications, first ed. American Chemical Society, Washington, DC, 1997.
[8] US Environmental Protection Agency (EPA), Microwave-assisted acid digestion of siliceous and organically based matrices, method 3052, Office of Solid Waste and Emergency Response, U.S. Government Printing Office, Washington, D.C, 1996.
[9] G. Corazza, A.S. Henn, M.F. Mesko, F.A. Duarte, E.M.M. Flores, P.A. Mello, Microwave-induced combustion of coal for further sulfur determination by inductively coupled plasma optical emission spectrometry or ion chromatography, J. Braz. Chem. Soc. 27 (2016) 1569–1576.
[10] P.T. Anastas, Green chemistry and the role of analytical methodology development, Crit. Rev. Anal. Chem. 29 (1999) 167–175.
[11] A.W. Miziolek, V. Palleschi, I. Schechter, Laser-Induced Breakdown Spectroscopy (LIBS): Fundamentals and Applications, Cambridge University Press, New York, 2006.
[12] D.W. Hahn, N. Omenetto, Laser-induced breakdown spectroscopy (LIBS), part I: review of basic diagnostics and plasmaparticle interactions: still-challenging issues within the analytical plasma community, Appl. Spectrosc. 64 (2010) 335A–366A.
[13] A.P.M. Michel, Review: applications of single-shot laser-induced breakdown spectroscopy, Spectrochim, Acta Part B 65 (2010) 185–191.
[14] L. Radziemski, D. Cremers, A brief history of laser-induced breakdown spectroscopy: from the concept of atoms to LIBS 2012, Spectrochim. Acta B 87 (2013) 3–10.
[15] P. Pořízka, A. Demidov, J. Kaiser, J. Keivanian, I. Gornushkin, U. Panne, J. Riedel, Laser-induced breakdown spectroscopy for in situ qualitative and quantitative analysis of mineral ores, Spectrochim. Acta B 101 (2014) 155–163.
[16] D.A. Skoog, F.J. Holler, S.R. Crouch, Principles of Instrumental Analysis, sixth ed. Brooks/Cole, Boston, 2006.
[17] E.C. Ferreira, D.M.B.P. Milori, E.J. Ferreira, R.M. Da Silva, L. Martin-Neto, Artificial neural network for Cu quantitative determination in soil using a portable laser induced breakdown spectroscopy system, Spectrochim. Acta B 63 (2008) 1216–1220.
[18] D. Santos, L.C. Nunes, G.G.A. De Carvalho, M.D.S. Gomes, P.F. de Souza, F.D.O. Leme, L.G.C. dos Santos, F.J. Krug, Laser-induced breakdown spectroscopy for analysis of plant materials: a review, Spectrochim. Acta B 71-72 (2012) 3–13.
[19] D.A. Cremers, L.J. Radziemski, Handbook of Laser-Induced Breakdown Spectroscopy, John Wiley & Sons, West Sussex, 2013.
[20] J. El Haddad, L. Canioni, B. Bousquet, Good practices in LIBS analysis: review and advices, Spectrochim. Acta B 101 (2014) 171–182.
[21] K.G. Fernandes, M. de Moraes, J.A. Gomes Neto, J.A. Nóbrega, P.V. Oliveira, Padronização interna em espectrometria de absorção atômica, Quim Nova 26 (2003) 249–252.
[22] S. Yao, J. Xu, K. Bai, J. Lu, Improved measurement performance of inorganic elements in coal by laser-induced breakdown spectroscopy coupled with internal standardization, Plasma Sci. Technol. 17 (2015) 938–943.
[23] H.K. Sanghapi, K.K. Ayyalasomayajula, F.Y. Yueh, J.P. Singh, D.L. McIntyre, J.C. Jain, J. Nakano, Analysis of slags using laser-induced breakdown spectroscopy, Spectrochim. Acta B 115 (2016) 40–45.
[24] H. Shirvani-Mahdavi, P. Shafiee, Quantitative analysis of soil calcium by laser-induced breakdown spectroscopy using addition and addition-internal standardizations, Meas. Sci. Technol. 27 (2016).
[25] W. Gerlach, E. Schweitezer, Foundations and Methods of Chemical Analysis by Emission Spectrometry, Adam Hilger, London, 1929.
[26] M.A. Bechlin, E.C. Ferreira, J.A. Gomes Neto, J.C. Ramos, D.L.G. Borges, Contributions on the use of bismuth as internal standard for lead determinations using ICP-based techniques, J. Braz. Chem. Soc. 26 (2015) 1879–1886.
[27] L. Sheng, T. Zhang, K. Wang, H. Tang, H. Li, Quantitative analysis of Fe content in iron ore via external calibration in conjunction with internal standardization method coupled with LIBS, Chem. Res. Chin. Univ. 31 (2014) 107–111.
[28] R.L. Frost, M.C. Hales, W.N. Martens, Thermogravimetric analysis of selected group (II) carbonateminerals - implication for the geosequestration of greenhouse gases, J. Therm. Anal. Calorim. 95 (2009) 999–1005.
[29] J. Lehmann, S. Joseph, Biochar for Environmental Management: Science and Technology, first ed. Earthscan, Sterling, 2009.
[30] L.A. Currie, Nomenclature in evaluation of analytical methods including detection and quantification capabilities (IUPAC Recommendations 1995), Anal. Chim. Acta 391 (1999) 105–126.

Anexo 8

Talanta 188 (2018) 199–202

Contents lists available at ScienceDirect

Talanta

journal homepage: www.elsevier.com/locate/talanta

Laser-induced breakdown spectroscopy determination of K in biochar-based fertilizers in the presence of easily ionizable element

Carla Pereira de Morais[a], Ariane Isis Barros[a], Marcos André Bechlin[a], Tiago Varão Silva[a], Dário Santos Júnior[b], Giorgio Saverio Senesi[c], Marisa Spirandeli Crespi[a], Clóvis Augusto Ribeiro[a], José Anchieta Gomes Neto[a], Edilene Cristina Ferreira[a,*]

[a] São Paulo State University - UNESP, Analytical Chemistry Department, P.O. Box 355, 14801-970 Araraquara, SP, Brazil
[b] Federal University of São Paulo, UNIFESP, Chemistry Department, Rua São Nicolau, no 210 - Centro, CEP: 09913-030 Diadema, SP, Brazil
[c] CNR-Istituto di Nanotecnologia (NANOTEC) - PLasMI Lab, Via Amendola 122/D, 70126 Bari, Italy

ARTICLE INFO

Keywords:
LIBS
Detection improvement
Easily ionizable elements
K
Biochar-based fertilizers

ABSTRACT

Laser-induced breakdown spectroscopy is an optical emission technique quite suitable for the analysis of recalcitrant materials as it eliminates complex procedures of sample preparation. However, for some simple LIBS instrumentation the detection limits are still higher compared to those of consolidated spectroscopic techniques. The aim of the present work was to develop a method for the determination of K in new biochar-based fertilizer samples using a simple single pulse LIBS arrangement. Due to the low K detectability, which made impossible to obtain calibration curves, an exploratory qualitative study was performed aiming to evaluate the influence of the addition of easily ionizable elements (EIE) on the sensitivity. To this aim different salts containing EIE (K, Li and Na) and other cations (Cu and Mg) have been evaluated. Results obtained showed that salts containing EIE cations increased the spectral emission signals of some elements in samples previously submitted to charring. In particular, the strategy of using Li^+ was applied to the determination of K in biochar-based fertilizers. The addition of Li^+ allowed to develop an analytical method for K determination featuring a linear dynamic range from 0.8% to 21.56% K, and limits of detection and quantification of 0.2% and 0.8%, respectively.

1. Introduction

Laser-induced breakdown spectroscopy (LIBS) is a modern spectroanalytical technique that allows direct analysis of solid, liquid or gaseous samples [1–3]. LIBS uses laser pulses to ablate a small fraction of sample that generates a plasma where the species present are excited and emit characteristic radiations that are recorded, thus allowing the qualitative and quantitative elemental analysis of the sample [2,4].

Although this technique shows a number of attractive analytical features, depending on the instrumentation used it presents low sensitivity in comparison with classical spectrometric techniques, such as flame atomic absorption spectrometry (FAAS) and inductively coupled plasma optical emission spectrometry (ICP OES) [5]. However, some strategies have been developed [6–9] to improve the detectability of LIBS, which include the use of a spark for sample pre-ablation [10,11], spatial confinement of laser-induced plasma [12–14], use of a micro torch [15] and use of two (double-pulse) or more lasers pulses for plasma species excitation [16–20]. Some authors attribute the observed increase in sensitivity to the increment of temperature and electronic density of the plasma, an higher sample mass ablation and plasma reheating [21–27].

Besides instrumental strategies, some chemical strategies, such as nanoparticle-enhanced (NE) LIBS, have also been evaluated to improve sensitivity. This method consists in the deposition of Au and Ag nanoparticles on the sample surface, which improves sample ablation due to the laser irradiance amplification caused by the low thermal conductivity of nanoparticles [28,29]. However, despite the various strategies mentioned above, the improvement of LIBS sensitivity when employing simple and low-cost instrumentation is still an analytical challenge.

Among several other applications, LIBS has been shown to be a promising analytical tool for biochar elemental analysis [30]. However, low emission signal intensities were obtained due to the matrix complexity (high C content) of these materials, which rendered difficult the excitation of the species of interest. In particular, the sensitivity reduction was possibly ascribed to the weakly ionized plasmas where collisional processes predominated over the radiant processes [31].

Due to the increasing interest in the use of biochars as agricultural

* Corresponding author.
E-mail address: edilene@iq.unesp.br (E.C. Ferreira).

https://doi.org/10.1016/j.talanta.2018.05.089
Received 7 April 2018; Received in revised form 23 May 2018; Accepted 24 May 2018
Available online 25 May 2018
0039-9140/ © 2018 Elsevier B.V. All rights reserved.

fertilizers [32–34], the analysis of plant nutrients like K in these materials is very relevant. In this perspective, the objective of this work is to evaluate qualitatively the detection improvement of a simple, single pulse LIBS instrumental arrangement achieved by the addition of various easily ionizable element (EIE) cations, and to apply this strategy to the measurement of K in biochar-based fertilizers.

2. Materials and methods

2.1. Reagents and substrates

To evaluate the influence of different cations on LIBS sensitivity, the following salts were used: $CuSO_4$ (Synth, Brazil), KCl (Mallinckrodt, England), Li_2CO_3 (Vetec, Brazil), $MgSO_4$ (Synth, Brazil), NaCl (Mallinckrodt, England). The effects of salt addition on elements detectability in different matrices was evaluated for the following samples: eucalyptus biochar (produced by charring branches and leaves of eucalyptus trees); banana fiber biochar (produced by charring of pseudo stems of banana trees); rice husk biochar (produced by the charring rice husks); roasted and unroasted coffee; and orange leaves. Cellulose type 101 (Sigmacell, USA) was used as pellet binding agent.

In particular, the biochar samples were prepared according to the following procedure: the substrate materials were dried, crushed and grounded. Approximately 2.0 g of each material were accurately weighed and placed in a porcelain crucible that was closed to maintain the inside atmosphere at a low oxygen content. The crucibles were placed in a muffle oven (EDGCON 5P, Brazil) and the heating program was performed, i.e. a heating rate of 10 °C min^{-1} was applied up to the temperature of 260 °C, at which the sample was maintained for 60 min. Then the temperature was lowered to 60 °C and the crucibles were removed. The biochar samples produced were stored in polypropylene flasks. The orange leave and unroasted coffee samples were only dried, if required, crushed, grounded and stored for further studies.

2.2. Sample preparation and experiments

Four experiments were conducted in this work: (i) the effect of different salts on LIBS signal intensities of eucalyptus biochar was evaluated on mixtures of 160 mg of eucalyptus biochar, 80 mg of cellulose and 40 mg of each salt; (ii) the effect of Li^+ on the signal intensities of all samples indicated above was evaluated in mixtures of 160 mg of each sample, 80 mg of cellulose and 40 mg of Li_2CO_3; (iii) the optimal amount of Li^+ to be used to maximize signal intensities of eucalyptus biochar was evaluated on mixtures of 160 mg of eucalyptus biochar and 80 mg of cellulose added with Li_2CO_3 to obtain increasing Li^+ concentrations, i.e. 0%; 0.17%; 0.67%; 1.33%; 2.04% and 2.72% and corn starch to reach a final mass of 280 mg; and (iv) to evaluate the effect of addition of Li_2CO_3 on K determination in biochar-based fertilizer samples were prepared by mixing 177 mg of biochar (eucalyptus, banana fiber and peanut shells), 80 mg of cellulose and 28 mg of Li_2CO_3, whereas the calibration standard pellets were prepared by mixing 60 mg of eucalyptus biochar, 80 mg of cellulose and 28 mg of Li_2CO_3 added with variable masses of KCl to obtain K concentrations of 0.0%; 5.7%; 8.3%; 12.9%; 16.5% and 21.6% (m/m)) and corn starch to reach a final mass of 285 mg.

2.3. Instrumentation and analytical procedure

The LIBS system used was equipped with a Q-switched Nd:YAG laser emitting at 1064 nm (Quantel, Big Sky Laser, Ultra 50) and operating at 50 mJ maximum power energy with a repetition rate up to 20 Hz, a pulse duration of 20 ns and a laser spot diameter of 0.5 mm. The detection device consisted of 4 pieces of HR2000 + spectrometers (Ocean Optics, USA) that provided an optical resolution of 0.1 nm (FWHM) on a wavelength range of 199–631 nm with an integration time of 1 μs. Each sample was placed in a sampling chamber controlled by a joystick with movement in the x-y directions and equipped with a video camera for monitoring in real time the laser pulse-sample interaction. The Q-Switched delay time selected for spectra acquisition was 0.5 μs. The system was controlled by the OOLIBS software (Ocean Optics, USA).

All experiments were carried in triplicate and each sample mixture was pelletized by applying a pressure of 10 tons. For each sample sixty emission spectra were acquired by shooting 30 laser pulses on each pellet side. Each spectrum was submitted to baseline correction by deducting from the spectral region an average of intensities calculated in a window containing pure noise. Finally, an average spectrum for each pellet was calculated.

To check the accuracy of LIBS results in K determination, a contrAA 300 (Analytik Jena, Germany) high-resolution continuum source flame atomic absorption spectrometer (HR-CS FAAS) equipped with a xenon short-arc lamp operating in the “hot-spot” mode as a continuum radiation source was used. The flame was produced by mixing high-purity acetylene (99.7%) (Air Liquid, SP, Brazil) and compressed air at flow rates of 594 and 80 L h^{-1}, respectively, and the sample aspiration rate was of 5.0 mL min^{-1}. An amount of 100 mg of each sample (five replicates) was digested for 65 min at a temperature not exceeding 220 °C in 3,00 mL of HNO_3 70% (v/v), 2,00 mL of deionized water and 1,00 mL of H_2O_2 30% (v/v) in quartz flasks using a microwave oven (Multiwave, Anton Paar, Graz, Austria).

3. Results and discussion

3.1. Qualitative evaluation of salt addition on LIBS detectability

The original eucalyptus biochar sample yielded a simple LIBS spectrum with few, very weak emission lines that showed no apparent significant spectral variation when $CuSO_4$ and $MgSO_4$ were added, whereas the addition of KCl, Li_2CO_3 and NaCl yielded a variable increase of some emission line intensities (Fig. 1). In particular, the low intensity of Ca I emission lines at 428.30, 428.94, 430.25 and 431.86 nm increased with EIE cations addition.

As the LIBS plasma is considered a low ionized plasma with a free

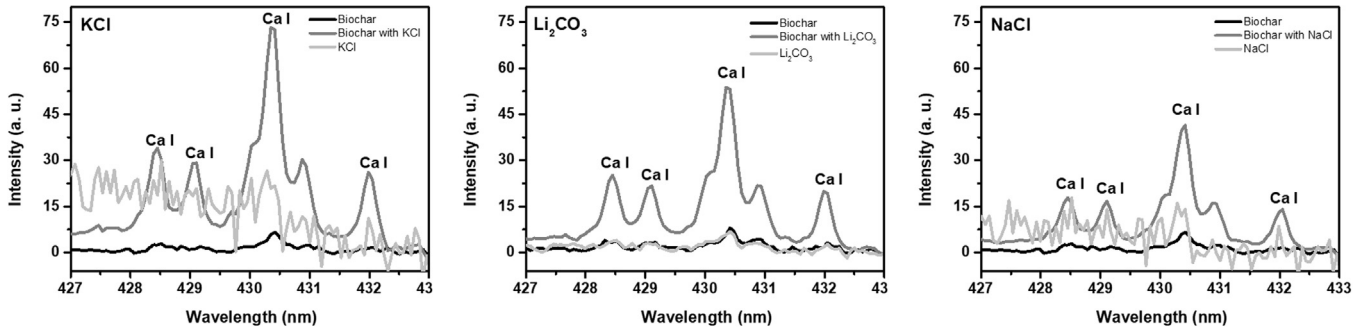


Fig. 1. Average LIBS spectra ($n = 60$) of the salt and the eucalyptus biochar sample without and with salt addition.

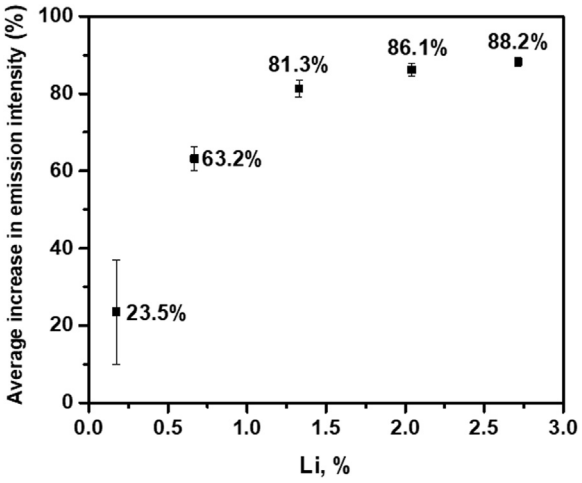


Fig. 2. Average increase of emission line intensities of the eucalyptus biochar sample as a function of Li% addition.

electron amount lower than 10% of the other species present [31], the addition of salts of EIE cations would produce an increment of plasma electron density, thus increasing the collisional probability and plasma temperature, and making more efficient the excitation processes.

Although the largest increase of signal intensities was obtained by KCl, the K^+ added would obviously affect the K analysis in biochar-based fertilizers that are also rich in Na but not in Li. Thus, Li_2CO_3, was selected for the next experiments. The effect of Li^+ addition on LIBS sensitivity was evaluated in the other samples, i.e. banana fiber biochar, rice husk biochar, roasted and unroasted coffee and orange leaves. Results showed no significant effect of Li^+ addition on LIBS signals sensitivity for unroasted coffee and orange leaves, whereas an apparent increase was observed for all biochars and roasted coffee samples. Previous thermal analysis results [30] have shown that in mixtures of eucalyptus biochar and Ca^{2+}, the thermal decomposition of $CaCO_3$ occurred at temperatures higher than those measured for the eucalyptus biochar itself, which suggested the occurrence of incorporation of Ca by the biochar, so changing its thermal properties. These results suggested that the increase of emission signals in burned samples could be explained by salt cation incorporation to biochar, which yielded the simultaneous breakdown processes for both the analyte and Li^+.

After having verified the positive effect of Li^+, its optimal concentration to be used was evaluated for eucalyptus biochar. The emission line intensities appeared to increase with increasing the amount of Li^+ added. The plot of the percentage of the average increase of emission line intensities as a function of Li^+ addition showed that no further increase was measured at Li^+ concentrations higher than 1,85% (Fig. 2). Thus, the concentration of 1.85% of Li^+ was used in the further experiment.

3.2. Determination of potassium

In attempting to use LIBS to measure the K content in commercial fertilizers, Yao et al. [35] found that the K (I) 404.41 nm emission line intensity was not linearly correlated to the analyte concentration, which was possibly due to the matrix effects caused by the large amount of other elements present in the samples. In an attempt to solve this problem the authors used a multivariate LIBS calibration approach. The same lack of correlation was observed in this work for the determination of K in biochar-based fertilizers, i.e. no significant differences of K emission lines were observed for calibration standards with different concentrations of the analyte. Thus, Li^+ at the optimal concentration of 1,85% was added to the calibration standards and fertilizer samples in the form of Li_2CO_3, which allowed to obtain satisfactory differences of K signals in the spectra of calibration standards containing different K concentration.

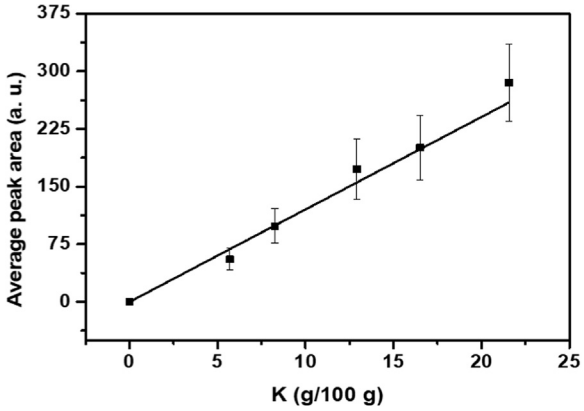


Fig. 3. Average peak area of the K I line at 404.64 nm as a function of K % in biochar-based fertilizers.

The calibration model so constructed (Fig. 3) showed the existence of a strong linear correlation (R = 0.993) between K concentration and the average peak area of the K (I) line at 404.64 nm as fitted by the Lorentzian function in the calibration standards. The calibration model was then applied to measure the concentration of K in eucalyptus, peanut shells and banana fiber biochar fertilizers, which yielded K% of 0.82 ± 0.02, 1.82 ± 0.12 and 8.23 ± 0.11, respectively. These values were in good agreement (paired *t*-test at a 95% confidence level) with the reference values of 0.81 ± 0.01, 1.79 ± 0.13, 8.29 ± 0.18, respectively, obtained by HR-CS FAAS. Further, the LIBS method featured a linear dynamic range of 0.8–21.56% K, and limits of detection and quantification of 0.2% and 0,8% respectively.

4. Conclusion

Materials, such as biochar-based fertilizers, which are able to incorporate EIE cations showed an improvement of analyte detectability when using a simple single pulse LIBS instrument. This effect was feasibly due to the salt cations contribution to the plasma electronic density, which was apparently indispensable for K determination in biochar-based fertilizers. The method developed incorporated all the advantages of the LIBS technique, including simple sample preparation consisting only in mixing Li_2CO_3 and cellulose with the sample. Differently, any other analytical technique would require the application of drastic conditions for solubilization of such recalcitrant samples.

Acknowledgments

The authors thank the Fundação de Amparo à Pesquisa do Estado de São Paulo (FAPESP) for financial support of this work (Grant # 2015/24757-9), the Coordenação de Aperfeiçoamento Pessoal de Nível Superior (CAPES) (Grant # 1490630) CNPQ (Grants # 302414/2017–7, 311085/2014–8) for providing a fellowship to C.P.M, and the Conselho Nacional de Desenvolvimento Científico e Tecnológico for a research grant to J.A.G.N and D.S.J.

References

[1] C. Pasquini, J. Corttez, L.M.C. Silva, F.B. Gonzaga, Laser-induced breakdown spectroscopy, J. Braz. Chem. Soc. 18 (2007) 463–512.
[2] A.W. Miziolek, V. Palleschi, I. Schechter, Laser Induced Breakdown Spectroscopy (LIBS): Fundamentals and Applications, first ed., Cambridge University Press, New York, 2006.
[3] L. St-Onge, R. Sing, S. Béchard, M. Sabsabi, Carbon emissions following 1.064 μm laser ablation of graphite and organic samples in ambient air, Appl. Phys. A Mater. Sci. Process. 69 (1999) S913–S916.
[4] D. Santos Jr., L.V.G. Tarelho, F.J. Krug, D.M.B.P. Milor, L. Martin Neto, N.D. Vieira Jr., Espectrometria de emissão óptica com plasma induzido por laser (LIBS)-Fundamentos, aplicações e perspectivas, Rev. Anal. 24 (2006) 72–81.

[5] D.L.G. Borges, A.J. Curtius, B. Welz, U. Heitmann, Fundamentos da espectrometria de absorção atômica de alta resolução com fonte contínua, Rev. Anal. 1 (2005) 58–67.
[6] Z.Z. Wang, Y. Deguchi, M. Kuwahara, J.J. Yan, J.P. Liu, Enhancement of laser-induced breakdown spectroscopy (LIBS) detection limit using a low-pressure and short-pulse laser-induced plasma process, Appl. Spectrosc. 67 (2013) 1242–1251.
[7] P.A. Benedetti, G. Cristoforetti, S. Legnaioli, V. Palleschi, L. Pardini, A. Salvetti, E. Tognoni, Effect of laser pulse energies in laser induced breakdown spectroscopy in double-pulse configuration, Spectrochim. Acta B 60 (2005) 1392–1401.
[8] D.N. Stratis, K.L. Eland, S.M. Angel, Effect of pulse delay time on a pre-ablation dual-pulse LIBS plasma, Appl. Spectrosc. 55 (2001) 1297–1303.
[9] V.N. Rai, F.Y. Yueh, J.P. Singh, Theoretical model for double pulse laser-induced breakdown spectroscopy, Appl. Opt. 47 (2008) G30–G37.
[10] S.C. Choi, M.K. Oh, Y. Lee, S. Namb, D.K. Ko, J. Lee, Dynamic effects of a pre-ablation spark in the orthogonal dual-pulse laser induced breakdown spectroscopy, Spectrochim. Acta B 64 (2009) 427–435.
[11] O.A. Nassef, H.E. Elsayed-Ali, Spark discharge assisted laser induced breakdown spectroscopy, Spectrochim. Acta B 60 (2005) 1564–1572.
[12] A.M. Popov, F. Colao, R. Fantoni, Spatial confinement of laser-induced plasma to enhance LIBS sensitivity for trace elements determination in soils, J. Anal. At. Spectrom. 25 (2010) 837–848.
[13] D.S. Meng, N.J. Zhao, M.J. Ma, Y. Wang, L. Hu, Y. Yu, L. Fang, W.Q. Liu, Heavy metal detection in soils by laser induced breakdown spectroscopy using hemi-spherical spatial confinement, Plasma Sci. Technol. 17 (2015) 632–637.
[14] S.J. Choi, K. Lee, J.J. Yoh, The laser-induced plasma persistence time extension in low pressures using the ablated mass confinement method, Spectrochim. Acta B 97 (2014) 113–117.
[15] L. Liu, X. Huang, S. Li, Y. Lu, K. Chen, Y.F. Lu, Optical emission enhancement in laser-induced breakdown spectroscopy using micro-torches, Spie Dig. Libr. 9736 (2016) (97361S–97361S-7).
[16] E. Tognoni, G. Cristoforetti, Basic mechanisms of signal enhancement in ns double-pulse laser-induced breakdown spectroscopy in a gas environment, J. Anal. At. Spectrom. 29 (2014) 1318–1338.
[17] G.S. Senesi, I. Carrara, G. Nicolodelli, D.M.B.P. Milori, O. De Pascale, Laser cleaning and laser-induced breakdown spectroscopy applied in removing and characterizing black crusts from limestones of Castello Svevo, Bari, Italy: a case study, Microchem. J. 124 (2016) 296–305.
[18] G. Cristoforetti, S. Legnaioli, V. Palleschi, A. Salvetti, E. Tognoni, Characterization of a collinear double pulse laser-induced plasma at several ambient gas pressures by spectrally- and time-resolved imaging, Appl. Phys. B Lasers Opt. 80 (2005) 559–568.
[19] F. Colao, V. Lazic, R. Fantoni, S. Pershin, A comparison of single and double pulse laser-induced breakdown spectroscopy of aluminum samples, Spectrochim. Acta B 57 (2002) 1167–1179.
[20] V.S. Burakov, N.V. Tarasenko, M.I. Nedelko, V.A. Kononov, N.N. Vasilev, S.N. Isakov, Analysis of lead and sulfur in environmental samples by double pulse laser induced breakdown spectroscopy, Spectrochim. Acta B 64 (2009) 141–146.
[21] S. Beldjilali, W.L. Yip, J. Hermann, T. Baba-Hamed, A. Belasri, Investigation of plasmas produced by laser ablation using single and double pulses for food analysis demonstrated by probing potato skins, Anal. Bioanal. Chem. 400 (2011) 2173–2183.
[22] J. Scaffidi, S.M. Angel, D.A. Cremers, Emission enhancement mechanisms in dual-pulse LIBS, Anal. Chem. 1 (2006) 25–32.
[23] P.K. Diwakar, S.S. Harilal, J.R. Freeman, A. Hassanein, Role of laser pre-pulse wavelength and inter-pulse delay on signal enhancement in collinear double-pulse laser-induced breakdown spectroscopy, Spectrochim. Acta B 87 (2013) 65–73.
[24] G. Nicolodelli, G.S. Senesi, I.L.O. Perazzoli, B.S. Marangoni, V.M. Benites, D.M.B.P. Milori, Double pulse laser induced breakdown spectroscopy: a potential tool for the analysis of contaminants and macro/micronutrients in organic mineral fertilizers, Sci. Total Environ. 565 (2016) 1116–1123.
[25] M. Corsi, G. Cristoforetti, M. Hidalgo, S. Legnaioli, V. Palleschi, A. Salvetti, E. Tognoni, C. Vallebona, Double pulse, calibration-free laser-induced breakdown spectroscopy: a new technique for in situ standard-less analysis of polluted soils, Appl. Geochem. 21 (2006) 748–755.
[26] G.S. Senesi, M. Dell'Aglio, R. Gaudiuso, A. De Giacomo, C. Zaccone, O. De Pascale, T.M. Miano, M. Capitelli, Heavy metal concentrations in soils as determined by laser-induced breakdown spectroscopy (LIBS), with special emphasis on chromium, Environ. Res. 109 (2009) 413–420.
[27] G. Nicolodelli, G.S. Senesi, R.A. Romano, I.L.O. Perazzoli, D.M.B.P. Milori, Signal enhancement in collinear double-pulse laser-induced breakdown spectroscopy applied to different soils, Spectrochim. Acta B 111 (2016) 23–29.
[28] A. De Giacomo, R. Gaudiuso, C. Koral, M. Dell'Aglio, O. De Pascale, Nanoparticle enhanced laser induced breakdown spectroscopy: effect of nanoparticles deposited on sample surface on laser ablation and plasma emission, Spectrochim. Acta B 98 (2014) 19–27.
[29] A. De Giacomo, M. Dell'Aglio, R. Gaudiuso, C. Koral, G. Valenza, Perspective on the use of nanoparticles to improve the LIBS analytical performances: nanoparticle enhanced laser induced breakdown spectroscopy (NELIBS), J. Anal. At. Spectrom. 31 (2016) 1566–1573.
[30] C.P. Morais, A.I. Barros, D. Santos Jr., C.A. Ribeiro, M.S. Crespi, G.S. Senesi, J.A. Gomes Neto, E.C. Ferreira, Calcium determination in biochar-based fertilizers by laser-induced breakdown spectroscopy using sodium as internal standard, Microchem. J. 134 (2017) 370–373.
[31] D.A. Cremers, L.J. Radziemski, Handbook of Laser-Induced Breakdown Spectroscopy, first ed., John Wiley & Sons, England, 2013.
[32] D.S. Dias, M.S. Crespi, L.D.M. Torquato, M. Kobelnik, C.A. Ribeiro, Torrefied banana tree fiber pellets having embedded urea for agricultural use, Therm. Anal. Calorim. 131 (2018) 705–712.
[33] E.H. Novotny, M.H.B. Hayes, B.E. Madari, T.J. Bonagamba, E.R. Azevedo, A.A. Souza, G. Song, C.M. Nogueira, A.S. Mangrich, Lessons from the Terra Preta de Índios of the Amazon region for the utilisation of charcoal for soil amendment, J. Braz. Chem. Soc. 20 (2009) 1003–1010.
[34] J. Lehmann, J. Gaunt, M. Rondon, Bio-char sequestration in terrestrial ecosystems – a review, Mitig. Adapt. Strat. Global 11 (2006) 403–427.
[35] S. Yao, J. Lu, J. Li, K. Chen, J. Li, M. Dong, Multi-elemental analysis of fertilizer using laser-induced breakdown spectroscopy coupled with partial least squares regression, J. Anal. At. Spectrom. 25 (2010) 1733–1738.

Anexo 9

Microchemical Journal 139 (2018) 322–326

Contents lists available at ScienceDirect

Microchemical Journal

journal homepage: www.elsevier.com/locate/microc

Determinations of phosphorus in fertilizers by spark discharge-assisted laser-induced breakdown spectroscopy

Alan Lima Vieira [a], Tiago Varão Silva [a], Felipe Schiavon Inocêncio de Sousa [b], Giorgio Saverio Senesi [c], Dário Santos Júnior [d], Edilene Cristina Ferreira [a], José Anchieta Gomes Neto [a,*]

[a] São Paulo State University - UNESP, Analytical Chemistry Department, P.O. Box 355, 14801-970 Araraquara, SP, Brazil
[b] University of São Paulo – USP, Department of Electrical and Computer Engineering, 13566-590 São Carlos, SP, Brazil
[c] CNR-Istituto di Nanotecnologia (NANOTEC) – PLasMI Lab, Via Amendola 122/D, 70126 Bari, Italy
[d] Federal University of São Paulo - UNIFESP, Exact and Earth Sciences Department, 09913-030 Diadema, SP, Brazil

ARTICLE INFO

Article history:
Received 27 December 2017
Received in revised form 5 March 2018
Accepted 5 March 2018
Available online 7 March 2018

Keywords:
Spark discharge
LIBS
Fertilizer analysis
Phosphorus determination

ABSTRACT

A spark discharge system was coupled to laser-induced breakdown spectroscopy (SD-LIBS) to improve sensitivity in the determination of P in fertilizers. A LIBS system consisting of a Q-switched Nd:YAG laser operating at 1064 nm and emitting pulses at 50 mJ with a fluence of 70 J cm^{-2} at the focal point was used. Results of preliminary experiments suggested that the most appropriate wavelength to measure P was the P (I) line at 214.9 nm, which did not show interferences by Fe, Cu and Zn. The electrical discharge was provided by a homemade high-voltage electronic circuit consisting of two cylindrical tungsten electrodes at the optimized output voltage of 4.5 kV, with tips arranged at the optimal distances of 4 mm between them and 2 mm above the sample surface. To minimize the expected matrix effects calibration standards of P_2O_5 in the range of 4.8 and 33.3% were prepared by mixing various amounts of a phosphate rock reference material (SRM-120c) with a mixture of $CaCO_3$, $CaSO_4$, $(NH_2)_2CO$ and KCl at a 1:1:1:1 mass ratio. The calibration curves obtained at a 4.5 kV SD-LIBS output voltage showed correlation coefficients ≥0.993, RSD ≤8% and LOQ 5.3% (m/m) P_2O_5. Data obtained by analyzing commercial samples by the proposed system were in good agreement, at 95% confidence level, with those obtained by using high-resolution continuum-source flame atomic absorption spectroscopy.

© 2018 Elsevier B.V. All rights reserved.

1. Introduction

Phosphorus (P) plays an important role in several plant processes such as energy generation, photosynthesis, several enzymatic and redox reactions, carbohydrate metabolism and nitrogen fixation [1,2]. Being native soil P supplies generally poor [3], fertilizers derived from phosphate rocks are largely used in agriculture. About 40 billion tons of phosphate fertilizers were consumed in the world in the year 2000, and about 60 billion tons are expected to be used in 2040 [1,2,4]. Thus, the development of simple, modern, rapid and rugged methods for P determination in fertilizers is relevant in the context of the increasing food demand by a growing global population and decreasing non-renewable resources of phosphate rocks.

In the last years, laser-induced breakdown spectroscopy (LIBS) has been employed for P determination in phosphate ores [5,6] mineral fertilizers [7,8] and organic mineral fertilizers [9,10]. Although the low resolution of simple LIBS systems has limited initially their applications, various methods have been suggested to laser-induced breakdown spectroscopy signal enhancement [11] such as dual-pulse LIBS [9,12,13], multi-pulse LIBS [14,15], spatial [16] or magnetic [17] confinement, spark discharge [18–31]. A detailed discussion on fundamentals on each enhancement method described above can be found in the review of Y. Li et al. [11]. Among other strategies to enhance sensitivity are the use of CCD detector and high fluence [8], intensified CCD detector [5,6], resonance LIBS [29], laser-induced fluorescence LIBS [32]. However, most of these approaches require additional laser devices and/or optical arrangements that often increase the system complexity and costs.

Regarding SD, it is a simple and low-cost method to overcome the low energies of lasers by reheating the plasma so increasing emission intensities [11]. In the last decade many efforts have been conducted to increase the performances of spark-assisted LIBS analysis. These include the development of fast discharge circuits [25,29], optimization of the temperature and electronic density of reheated plasma [30] and of the voltage and capacitance of the spark discharge [27], and use of electric pulses for molecular and isotopic analysis [31]. In particular, spark-assisted LIBS has been used for analysis of soil [18,19,23,25–27,30], silicon [24,29], Al [22,31], Cu [22], gypsum [21],

* Corresponding author.
E-mail address: anchieta@iq.unesp.br (J.A.G. Neto).

https://doi.org/10.1016/j.microc.2018.03.011
0026-265X/© 2018 Elsevier B.V. All rights reserved.

metallurgical slag [21], lime, rock, CaF_2, CaO [31]. But the determination of P in fertilizers is scarce in the current literature.

Thus, the aim of this work was to test the best performance conditions of a homemade spark discharge system to be associated to a low energy LIBS system for the determination of P in commercial fertilizers.

2. Materials and methods

2.1. Instrumentation

A LIBS system consisting of a Q-switched Nd:YAG laser (Quantel, Big Sky Ultra 50, Bozeman, USA) emitting at 1064 nm and operating at a maximum power energy of 50 mJ with a pulse duration of 20 ns, a laser spot diameter of about 300 μm and an ablation laser fluence of ~70 J cm^{-2} was used in this work. The plasma emission was collected at an angle of 45° with respect to the laser beam by using an optical fiber bundle, and then addressed to four spectrometers Ocean Optics (HR2000+, Dunedin, USA) featuring an optical resolution of 0.1 nm (full width at half maximum) and a spectral range from 200 to 630 nm. The integration time and the Q-Switched delay used for spectra acquisition were 1 ms and 1 μs, respectively.

Individual samples were placed in an automatic sample holder able to move in the 'x-y' directions under the control of the analyst. The sampling chamber included an inner video camera able to monitor the entire process. Experiments were performed in air and ambient pressure. Thirty spectra were acquired at different positions of each calibration standard and sample. After spectral baseline correction performed by a Whittaker filter on MATLAB® (R2010a) and PLS Toolbox, a software Microsoft Excel® (2016) was used for data (peak intensities) treatment.

The spark discharge was obtained using two cylindrical pure tungsten electrodes (100 × 2.6 mm) with tips arranged at a distance of 4 mm between them and 2 mm above the sample surface (Fig. 1). The laser beam was focused on the sample surface in the middle of the two electrode tips. The homemade high-voltage electronic circuit consisted of simple components, i.e. a primary circuit of the transformer, a secondary circuit and a voltage divider. The first circuit consisted of an on/off switch, a signal lamp indicator, overcurrent protection and a potentiometer allowing the operator to adjust the desired voltage output from the source to the transformer. The voltage ratio of the transformer was approximately 1:1.35, which increased the 60 Hz and 127 V of the source to a maximum of approximately 171 V. The sinusoidal output voltage of the transformer was then multiplied and rectified by a Walton-Cockroft circuit consisting of twenty-eight 1 μF/250 V capacitors and 1N4007 diodes, which converted the 171 V/60 Hz sinusoidal signal to a DC signal of 4500 V. As the high currents due to the high voltage might interfere in the circuit, a 1 Ohm-resistance was connected to the high voltage terminal, which was, in turn, connected to a resistive voltage divider that allowed to lower the DC voltage signal by a factor of 100 to yield a value that could be measured safely and easily by a multimeter.

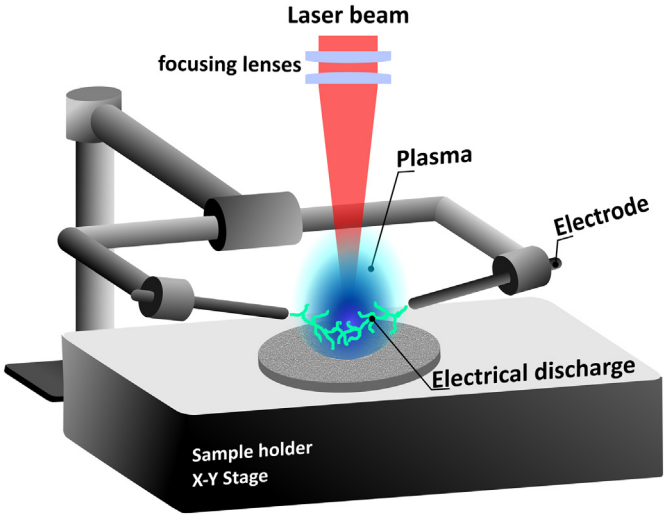


Fig. 1. Scheme of the experimental set up of the SD-LIBS system employed for P determination.

As the comparative technique, an Analytik Jena ContrAA 300 high-resolution continuum source flame atomic absorption spectrometer (Jena, Germany) equipped with a xenon short-arc lamp XBO 301 (GLE, Berlin, Germany) operating at the nominal power of 300 W and in the hot-spot mode as the continuum radiation source was used. The instrument was equipped with a compact, high-resolution double-Echelle grating monochromator featuring a spectral band width <2 pm per pixel in the far ultraviolet range, and a charge-coupled device (CCD) array detector. All measurements (n = 3) were done according to instrumental conditions published elsewhere [33].

2.2. Reagents, samples and procedures

High-purity water (resistivity 18.2 ΩM·cm) obtained from a Millipore Rios 5® reverse osmosis and a Millipore Milli-Q™ Academic® deionizer system (Bedford, USA) and Merck Suprapur® nitric and hydrochloric acids (Darmstadt, Germany) were used to prepare all solutions.

Matrix-matched solid standards containing 4.8, 11.9, 22.9, 27.8 and 33.34% (m/m) P_2O_5 were prepared by mixing proper amounts of the SRM-120c phosphate rock reference material (National Institute of Standard and Technology, Gaithersburg, USA) and a combined reagent containing $(NH_2)_2CO$ (Merck), $CaCO_3$ (Synth, Diadema, Brazil), $CaSO_4$ (Merck, Darmstadt, Germany) and KCl (Mallinckrodt, Xalostoc, Mexico) (mass ratio of 1:1:1:1). The combined reagent was employed as the blank.

Six phosphate fertilizer samples containing phosphorus in the 6–17% (m/m) P_2O_5 range (values declared on the label of samples, Table 1) were acquired from local market in Araraquara-SP, Brazil. Samples, solid standards and blank were ground manually in an agate mortar, homogenized and dried at 105 °C (up to a constant weight). A portion of about 300 mg was compacted using the Solab SL - 10/15 hydraulic press (Piracicaba, Brazil) by applying a pressure of 7.5 t cm^{-2} for 3 min to obtain disc-shaped pellets of approximately 13-mm diameter for further analysis.

For comparison results, all samples were also analyzed (n = 3) by HR-CS FAAS. Samples were pretreated by using a microwave-assisted acid-digestion system. Masses of 200 mg of samples and the SRM-120c were accurately weighted and transferred to microwave flasks followed by 2.25 mL of 65% (m/m) HNO_3, 0.75 mL of 32% (m/m) HCl, 1 mL of 30% (v/v) H_2O_2 (Merck, Darmstadt, Germany) and 2 mL of deionized water. The closed-vessels were inserted into the cavity of the Multiwave Anton Paar microwave oven (Graz, Austria) and the heating program was run: 15 min from 0 at 1000 W and 10 min at 1000 W

Table 1
Results (mean ± SD) (n = 3) for P determination in the SRM standard and fertilizer samples (% m/m P_2O_5) by SD-LIBS and HR-CS-FAAS.

Sample	ED-LIBS[a]			HR-CS FAAS[b]		
04-14-08[c]	15.0	±	1.0	14.6	±	0.4
09-06-09[c]	6.8	±	0.6	6.5	±	0.2
08-12-10[c]	10.8	±	0.3	11.1	±	0.4
08-09-09[c]	9.7	±	0.6	9.2	±	0.1
00-17-00[c]	16.4	±	0.7	17.2	±	0.4
00-17-00[c]	16.6	±	0.3	17.3	±	0.5
SRM-120c[d]	33.0	±	2.0	33.6	±	0.4

[a] LOQ = 5.3%.
[b] LOQ = 4.1%.
[c] N, P, K%.
[d] Certified value: 33.34 ± 0.06%.

followed by 20 min of cooling. After digesting and cooling, the resulting digests were transferred to polypropylene flasks, and the volume was made up to 30 mL with deionized water.

All solutions were stored in high-density polypropylene bottles (Nalgene, Rochester, NY, USA). Plastic bottles and glassware materials were cleaned by soaking in 10% (v/v) HNO_3 at least 24 h, and then rinsed abundantly in deionized water before use.

3. Results and discussion

The first experiments aimed to identify the most appropriate LIBS emission line of P to be used for analysis. The SD-LIBS spectra measured at a 4.5 kV output on the sample 04-14-08 showed a number of P (I) lines at 213.6, 214.9 and 215.4, 253.4 and 253.6 nm, which were much more intense than those of the corresponding LIBS spectra (an example of sample spectra is shown in Fig. 2). Further, some emission lines of Fe (II) at 253.4, 253.9 and 254.2 nm [34] were present due to Fe naturally present in the samples. To confirm the presence of Fe lines, the SD-LIBS spectrum of the San Joaquin Soil Standard SRM 2709a (certified values: 3.36 ± 0.07% Fe; 0.0688% P) was measured and compared to that of sample 04-14-08 (Fig. 3). Intense Fe emissions at 253.4, 253.7, 253.9 and 254.2 nm were present in the standard, whereas no Fe lines were observed in the 213–216 nm interval (Fig. 3). These results suggested that P (I) lines at 253.4 and 253.6 nm should be avoided for P determination in fertilizers when using a 0.1 nm resolution spectrometer.

Further, the concentrations of Fe previously determined by HR-CS FAAS in all samples examined fell in the range from 0.14 to 1.08% (m/m), i.e. they were about 2–3 times lower than that in the SRM 2709a standard. This result confirmed that a negligible Fe interference would be expected on P (I) lines located in the 213–216 nm spectral range. However, the P (I) line at 213.6 nm might overlap with the Cu (I) line at 213.5 nm and Zn (I) line at 213.9 nm. As Cu and Zn might be present at low concentration in some phosphate fertilizer formulations [35], the P (I) line at 213.6 nm might be interfered by these elements, thus this line should also be excluded from the P analysis. In conclusion, although both P (I) lines at 215.4 nm and 214.9 nm presented suitable selectivity, the latter was chosen for further experiments due to its higher (about 3.4) relative sensitivity.

The possible effect of the components of the tungsten electrodes used to obtain the spark was evaluated by comparing the SD-LIBS spectrum of sample 04-14-08 to that of the blank (Fig. 2). Apparently, the emissions from these components were close to the background, which confirmed the suitability of these electrodes to be used even at the maximum voltage applied (4.5 kV).

The influence of SD voltage on the P (I) emission intensity at 214.9 nm was tested by varying it in the range 0–4.5 kV at a fixed

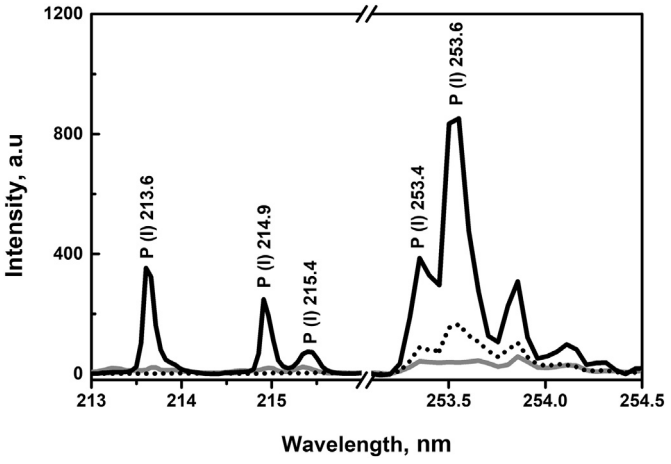


Fig. 2. LIBS (▪▪▪) and SD-LIBS (—) spectra of the sample 04-14-08 and SD-LIBS (▬) spectrum of the blank. SD-LIBS spectra were obtained at a 4.5 kV output.

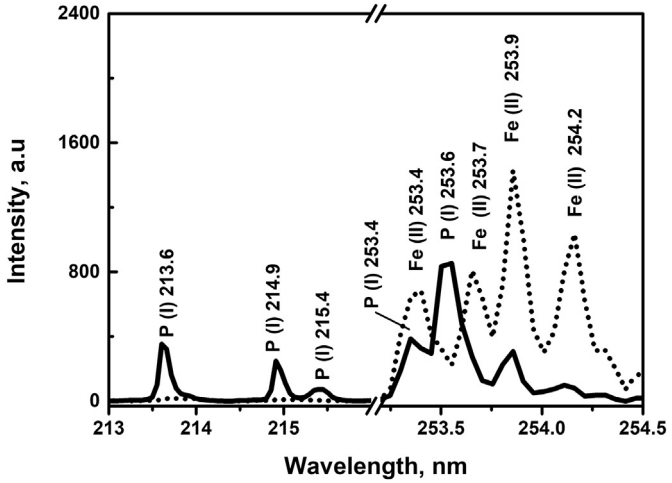


Fig. 3. SD-LIBS spectra obtained at a 4.5 kV output of sample 04-14-08 (—) and SRM 2709a standard (▪▪▪).

distance of 4 mm between electrode tips. The emission intensity increased linearly with increasing the voltage up to 4.5 kV (Fig. 4), with a typical RSD ≤7%, which could be ascribed to the increase of plasma temperature caused by the reheating electric pulse [11,23,27,29]. Thus, the voltage of 4.5 kV was chosen to analyze the samples.

The effect of the distance between electrode tips on the performance of the SD circuit was evaluated by measuring the intensity of the P (I) line at 214.9 nm at distances of 2, 3, 4, 5 and 6 mm (Fig. 5). The emission intensity appeared to increase up to a tip distance of 4 mm and then decrease. At the shortest distances, the ionic species produced in the plasma favored the flowing of a fast current through the circuit, which caused the electrical arc produced to enter only partially into the bulk plasma, so that the plasma reheating contribution was low. At distances greater than 4 mm more collisions were favored in the electron path between electrodes, which reduced the energy of electrons so that they were less efficient in exciting/ionizing the species present in the plasma. These findings were in agreement with the Paschen law, which states that the breakdown voltage at a certain distance between electrode tips is a function of the product of the gas pressure and the distance [36]. Thus, all further experiments were performed at a distance of 4 mm between electrode tips.

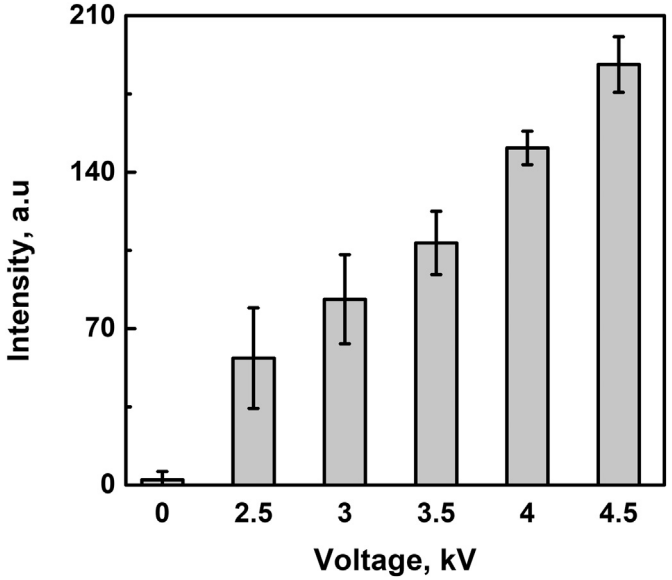


Fig. 4. Emission intensity of P (I) at line 214.9 nm as a function of output applied voltage.

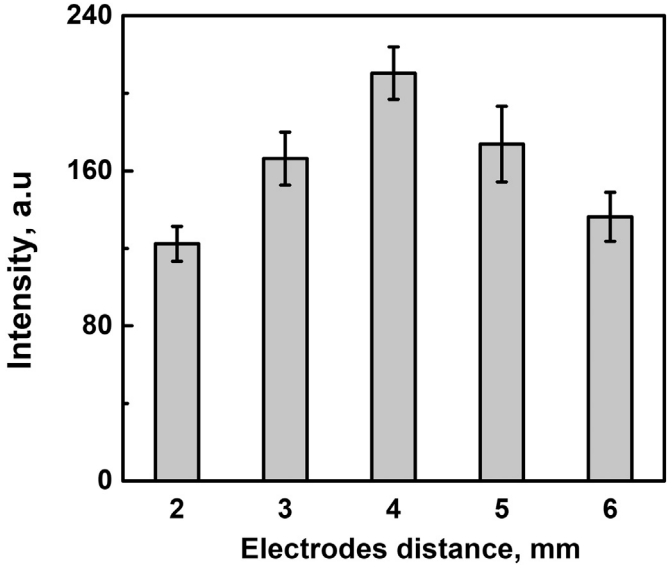


Fig. 5. Emission intensity of the P (I) line at 214.9 nm as a function of the electrode tips distance at a 4.5 kV output.

After the optimization of SD operational parameters, calibration curves were firstly constructed by using $NaHPO_4$ as solid standard. Although this standard provided satisfactory linear correlation coefficients, the accuracy was poor, i.e. the P content measured by SD-LIBS in some samples was almost twice than that measured by HR-CS-FAAS, probably because the matrix-effects influenced markedly the interaction laser-samples and processes of plasma formation [5,37]. Thus, considering that most commercial phosphate fertilizers contain phosphate rocks, $NaHPO_4$ was replaced by the phosphate rock standard SRM-120c to yield solid standards containing the same percentage of P_2O_5 as indicated above in Section 2.2.

The calibration curves constructed using the SAM-120c standard featured correlation coefficients higher than 0.993 between the P (I) emission at 214.9 nm and the P_2O_5 concentration in % (m/m) measured by HR-CS-FAAS. The RSD values were ≤8% and the limit of quantification (LOQ) calculated by the 10σ/Slope, where σ is the standard deviation of 10 measurements of the blank, was 5.3% (m/m) P_2O_5, which is equivalent to 2.3% (m/m) P. Although the LOQ value obtained by SD-LIBS can be considered fully acceptable for P measurement in commercial fertilizers [6,35], that LOQ can be improved by using the procedure of summation of spectra to increase sensibility. In particular, by employing ten cumulative spectra on each site of the sample surface, the LOQ was reduced to 3% (m/m) P_2O_5. In particular, due to limitations of the low energy LIBS system employed in this work, the data processing associated to the spectral sum was performed using an external software (Microsoft office excel 2016). However, this procedure was not required to analyze the samples used in this work.

The level contents of P in fertilizer samples analyzed by the proposed SD-LIBS method were in agreement at 95% confidence with those obtained by HR-CS FAAS comparative technique (Table 1). For further accuracy evaluation, the phosphate rock standard SRM-120c was also analyzed by SD-LIBS, and the P concentration measured was in agreement (at 95% confidence) with the certified value of the SRM (Table 1).

4. Conclusions

In conclusion, the SD-assisted LIBS system showed to be an efficient tool to increase the sensitivity of P measurement in phosphate fertilizers. The coupling SD-LIBS did not require any synchronization tool between the laser pulse and the electrical discharge, i.e. the latter was the result of charged conducting species in the laser-induced plasma. Further, the SD circuit represents a simple, easily operated and low-cost acquisition and maintenance system that can be coupled to any LIBS apparatus showing promising for further applications to other analytes and matrices.

Acknowledgments

The authors are grateful to the Fundação de Amparo à Pesquisa do Estado de São Paulo (FAPESP) (Grant# 2004/14212-0) for supporting financially this work, and to the Conselho Nacional de Desenvolvimento Científico e Tecnológico (Grant# 2015/24757-9) (CNPq) for fellowship granted to A.L.V. (Grant# 141977/2016-7) and research ship granted to J.A.G.N. (Grant# 303255/2013-7) and D.S.J. (Grant# 311085/2014-8). The authors are also grateful to R.A.C.A. of the Department of Electrical and Computer Engineering of the Engineering School of São Carlos - USP, for providing the materials and instruments used for the design of the high voltage circuit.

References

[1] S. Suh, S. Yee, Phosphorus use-efficiency of agriculture and food system in the US, Chemosphere 84 (2011) 806–813.
[2] C.P. Vance, Symbiotic nitrogen fixation and phosphorus acquisition. Plant nutrition in a world of declining renewable resources, Plant Physiol. 127 (2001) 390–397.
[3] K. Ashley, D. Cordell, D. Mavinic, A brief history of phosphorus: from the philosopher's stone to nutrient recovery and reuse, Chemosphere 84 (2011) 737–746.
[4] C.P. Vance, C. Uhde-Stone, D.L. Allan, Phosphorus acquisition and use: critical adaptations by plants for securing a nonrenewable resource, New Phytol. 157 (2003) 423–447.
[5] S. Rosenwasser, G. Asimellis, B. Bromley, R. Hazlett, J. Martin, T. Pearce, A. Zigler, Development of a method for automated quantitative analysis of ores using LIBS, Spectrochim. Acta B 56 (2001) 707–714.
[6] G. Asimellis, A. Giannoudakos, M. Kompitsas, Phosphate ore beneficiation via determination of phosphorus-to-silica ratios by Laser Induced Breakdown Spectroscopy, Spectrochim. Acta B 61 (2006) 1253–1259.
[7] S. Yao, J. Lu, J. Li, K. Chen, J. Li, M. Dong, Multi-elemental analysis of fertilizer using laser-induced breakdown spectroscopy coupled with partial least squares regression, J. Anal. At. Spectrom. 25 (2010) 1733–1738.
[8] B.S. Marangoni, K.S.G. Silva, G. Nicolodelli, G.S. Senesi, J.S. Cabral, P.R. Villas-Boas, C.S. Silva, P.C. Teixeira, A.R.A. Nogueira, V.M. Benites, D.M.B.P. Milori, Phosphorus quantification in fertilizers using laser induced breakdown spectroscopy (LIBS): a methodology of analysis to correct physical matrix effects, Anal. Methods 8 (2015) 78–82.
[9] G. Nicolodelli, G.S. Senesi, I.L. de Oliveira Perazzoli, B.S. Marangoni, V. De Melo Benites, D.M.B.P. Milori, Double pulse laser induced breakdown spectroscopy: A potential tool for the analysis of contaminants and macro/micronutrients in organic mineral fertilizers, Sci. Total Environ. 565 (2016) 1116–1123.
[10] G.S. Senesi, R.A. Romano, B.S. Marangoni, G. Nicolodelli, P.R. Villas-Boas, V.M. Benites, D.M.B.P. Milori, Laser-induced breakdown spectroscopy associated with multivariate analysis applied to discriminate fertilizers of different nature, J. Appl. Spectrosc. 84 (2017) 923–928.
[11] Y. Li, D. Tian, Y. Ding, G. Yang, K. Liu, C. Wang, X. Han, A review of laser-induced breakdown spectroscopy signal enhancement, Appl. Spectrosc. Rev. 53 (2018) 1–35.
[12] K.H. Kurniawan, M.O. Tija, K. Kagawa, Review of laser-induced plasma, its mechanism, and application to quantitative analysis of hydrogen and deuterium, Appl. Spectrosc. Rev. 49 (2014) 323–434.
[13] G. Nicolodelli, G.S. Senesi, A.C. Ranulfi, B.S. Marangoni, A. Watanabe, V.M. Benites, P.P.A. de Oliveira, P. Villas-Boas, D.M.B.P. Milori, Double-pulse laser induced breakdown spectroscopy in orthogonal beam geometry to enhance line emission intensity from agricultural samples, Microchem. J. 133 (2017) 272–278.
[14] N. Jedlinszki, G. Galbács, An evaluation of the analytical performance of collinear multi-pulse laser induced breakdown spectroscopy, Microchem. J. 97 (2011) 255–263.
[15] A. De Giacomo, M. Dell'Aglio, D. Bruno, R. Gaudiuso, O. De Pascale, Experimental and theoretical comparison of single-pulse and double-pulse laser induced breakdown spectroscopy on metallic samples, Spectrochim. Acta B 63 (2008) 805–816.
[16] A.M. Popov, F. Colao, R. Fantoni, Enhancement of LIBS signal by spatially confining the laser-induced plasma, J. Anal. At. Spectrom. 24 (2009) 602–604.
[17] L. Cheng, G. Xun, L. Qi, C. Song, Spectral enhancement of laser-induced breakdown spectroscopy in external magnetic field, Plasma Sci. Technol. 17 (2015) 919–922.
[18] K.X. Li, W.D. Zhou, Q.M. Shen, Z.J. Ren, B.J. Peng, Laser ablation assisted spark induced breakdown spectroscopy on soil samples, J. Anal. At. Spectrom. 25 (2010) 1475–1481.
[19] M.V. Belkov, V.S. Burakov, A. De Giacomo, V.V. Kiris, S.N. Raikov, N.V. Tarasenko, Comparison of two laser-induced breakdown spectroscopy techniques for total carbon measurement in soils, Spectrochim. Acta B 64 (2009) 899–904.
[20] H. Sobral, A. Robledo-Martinez, Signal enhancement in laser-induced breakdown spectroscopy using fast square-pulse discharges, Spectrochim. Acta B 124 (2016) 67–73.
[21] S. Eschlböck-Fuchs, P.J. Kolmhofer, M.A. Bodea, J.G. Hechenberger, N. Huber, R. Rössler, J.D. Pedarnig, Boosting persistence time of laser-induced plasma by electric arc discharge for optical emission spectroscopy, Spectrochim. Acta B 109 (2015) 31–38.

[22] O.A. Nassef, H.E. Elsayed-Ali, Spark discharge assisted laser induced breakdown spectroscopy, Spectrochim. Acta B 60 (2005) 1564–1572.
[23] L.I. Kexue, W. Zhou, Q. Shen, J. Shao, H. Qian, Signal enhancement of lead and arsenic in soil using laser ablation combined with fast electric discharge, Spectrochim. Acta B 65 (2010) 420–424.
[24] W. Zhou, K. Li, Q. Shen, Q. Chen, J. Long, Optical emission enhancement using laser ablation combined with fast pulse discharge, Opt. Express 18 (2010) 2573–2578.
[25] W. Zhou, K. Li, X. Li, H. Qian, J. Shao, X. Fang, P. Xie, W. Liu, Development of a nanosecond discharge-enhanced laser plasma spectroscopy, Opt. Lett. 36 (2011) 2961–2963.
[26] X. Li, W. Zhou, K. Li, H. Qian, Z. Ren, Laser ablation fast pulse discharge plasma spectroscopy analysis of Pb, Mg and Sn in soil, Opt. Commun. 285 (2011) 54–58.
[27] W. Zhou, K. Li, H. Qian, Z. Ren, Y. Yu, Effect of voltage and capacitance in nanosecond pulse discharge enhanced laser-induced breakdown spectroscopy, Appl. Opt. 51 (2012) 42–48.
[28] D. Wu, L. Sun, P. Liu, R. Hai, H. Ding, Enhancement of laser-induced breakdown spectroscopic signals in a liquid jet with glow discharge, Appl. Spectrosc. 72 (2018) 225–233.
[29] W. Zhou, X. Su, H. Qian, K. Li, X. Li, Y. Yu, Z. Ren, Discharge character and optical emission in a laser ablation nanosecond discharge enhanced silicon plasma, J. Anal. At. Spectrom. 28 (2013) 702–710.
[30] X.F. Li, W.D. Zhou, Z.F. Cui, Temperature and electron density of soil plasma generated by LA-FPDPS, Front. Phys. 7 (2012) 721–727.
[31] A.A. Bol'shakov, X. Mao, R.E. Russo, Spectral emission enhancement by an electric pulse for LIBS and LAMIS, J. Anal. At. Spectrom. 32 (2017) 657–670.
[32] S. Laville, C. Goueguel, H. Loudyi, F. Vidal, M. Chaker, M. Sabsabi, Laser-induced fluorescence detection of lead atoms in a laser-induced plasma: an experimental analytical optimization study, Spectrochim. Acta B 64 (2009) 347–353.
[33] M.A. Bechlin, F.M. Fortunato, R.M. Da Silva, E.C. Ferreira, J.A. Gomes Neto, A simple and fast method for assessment of the nitrogen-phosphorus-potassium rating of fertilizers using high-resolution continuum source atomic and molecular absorption spectrometry, Spectrochim. Acta B 101 (2014) 240–244.
[34] [26] NIST Atomic Spectra Database, https://physics.nist.gov/PhysRefData/ASD/lines_form.html (accessed 2 March 2018).
[35] P.E. Trani, A.L. Trani, Fertilizantes: cálculo de fórmulas comerciais, Instituto Agronômico, Campinas, 2011 (29 pp., Série Tecnologia APTA. Boletim Técnico IAC, 208).
[36] A.P. Henry, College Physics, New York, 13th ed., 1947.
[37] D.A. Cremers, L.J. Radziemski, Handbook of Laser-Induced Breakdown Spectroscopy, 2nd ed. John Wiley & Sons, Tucson, 2013.

Anexo 10

Food Chemistry 278 (2019) 223–227

Contents lists available at ScienceDirect

Food Chemistry

journal homepage: www.elsevier.com/locate/foodchem

Analytical Methods

Prediction of black, immature and sour defective beans in coffee blends by using Laser-Induced Breakdown Spectroscopy

Tiago Varão Silva[a], Débora Marcondes Bastos Pereira Milori[b], José Anchieta Gomes Neto[a], Ednaldo José Ferreira[b], Edilene Cristina Ferreira[a,*]

[a] São Paulo State University – UNESP, Chemistry Institute of Araraquara, Analytical Chemistry Department. P.O. Box 355, 14801-970 Araraquara, SP, Brazil
[b] Embrapa Instrumentation, P.O. Box 741, 13560-970 São Carlos, SP, Brazil

ARTICLE INFO

Keywords:
Coffee quality
Defective beans
BIS
LIBS

ABSTRACT

One of the most important factors that interfere negatively in coffee global quality has been blends with defective beans, especially those called Black, Immature and Sour (BIS). The methods based on visual-manual estimation of defective beans have shown their inefficiency in coffee value chain for large-scale analysis. The lack of fast, accurate and robust analytical methods for BIS determination is still a research gap. Laser-Induced Breakdown Spectroscopy (LIBS) is a fast, low-cost and residue-free technique capable of performing multielemental determination and investigating organic composition of samples. In the present work, LIBS together with spectral processing and variable selection were evaluated to fit linear regression models for predicting BIS in blends. Models showed high capacity of prediction with RMSEP smaller than 3.8% and R^2 higher than 80%. Most importantly, measurements are guided by chemical responses, which make LIBS-based methods less susceptible to the visual indistinguishability that occurs in manual inspections.

1. Introduction

Coffee is an important agricultural commodity and its global quality is fundamental for coffee agribusiness (International Coffee Organization, 2016). The global quality of coffee can be damaged by insertion of defective beans (Toci, Farah, Pezza, & Pezza, 2016). Black, Immature and Sour (BIS) are the main defective coffee beans present in post-harvest processes and they can negatively impact on the beverage quality. Immature are beans harvested prematurely. Sour are healthy or immature beans under abnormal fermentation processes. Black beans have as main cause a late harvesting (Evangelista et al., 2014; Toci & Farah, 2008).

In Brazilian coffee production, it is estimated that from 15% to 20% consists of BIS beans (Mendonça, Franca, Oliveira, & Nunes, 2008). According to the Brazilian normative resolution (SAA-28), high-quality coffees (also called *Gourmet*) must not contain BIS for blends of *C. arabica* varieties, since they cause intense, sour and astringent flavors (Clarke & Macrae, 1987). For other commercialized coffee beans (classified as *Superior* and *Traditional* according to SAA-28), BIS are allowed up to 20% (Ferreira, Pereira, Delbem, Oliveira, & Mattoso, 2011; Secretaria de Agricultura e Abastecimento, 2007). For exportation purposes, the International Coffee Organization (2002) recommends up to 86 defects/300 g for Arabica varieties.

Currently, visual-manual processes for quantifying BIS practiced for Brazilian coffee organizations (agro-industries, cooperatives, producers, exporters, etc.) have been negatively impacted by subjective factors, visual fatigue, time-consuming for separation of defects, lack of experts, incapacity for inspecting a large amount of samples during the harvesting periods, among others. The challenge has attracted researchers for solving related problems by applying analytical instruments. Several methods and techniques have been developed for discriminating defects using, for instance, gas chromatography–mass spectrometry (Agresti, Franca, Oliveira, & Augusti, 2008), electrospray ionization mass spectrometry (Mendonça et al., 2008) and diffuse reflectance infrared Fourier transform spectroscopy (Craig, Franca, & Oliveira, 2012). However, quantitative estimations of BIS were only addressed by Santos, Sarraguça, Rangel, and Lopes, (2012) by applying Near Infrared Spectroscopy (NIRS).

Laser-Induced Breakdown Spectroscopy (LIBS) is a multielement analytical technique that uses a pulsed laser to ablate a small portion of a sample, promoting breakdown of chemical bonds, vaporization and plasma. In plasma, highly excited species of the sample composition decay emitting radiation at specific frequencies (Miziolek, Palleschi, & Schechter, 2006). Frequencies are captured, separated in spectrometers

* Corresponding author.
E-mail address: edilene.c.ferreira@unesp.br (E.C. Ferreira).

https://doi.org/10.1016/j.foodchem.2018.11.062
Received 15 August 2018; Received in revised form 9 November 2018; Accepted 11 November 2018
Available online 12 November 2018
0308-8146/ © 2018 Elsevier Ltd. All rights reserved.

and their intensities are then measured to build a spectrum (signal intensities *vs* wavelength). A LIBS spectrum may be the sample signature and/or a powerful information source for determining its chemical constituents (Pasquini, Corttez, Silva, & Gonzaga, 2007). In addition, LIBS is capable of performing fast analysis with minimal requirements in terms of sample preparation (Cremers & Radziemski, 2006).

The exploration of LIBS data for different materials has shown its potential goes beyond elemental determinations. LIBS has successfully been applied to discriminate of lymphomas (Chen, Li, Yang, Yu, & Liu, 2018), detection of calcific aortic valve disease (Davari, Masjedi, Ferdous, & Mukherjee, 2018), bacterium detection and identification (Baudelet et al., 2006), detection of explosive molecules (Shaik, Epuru, Syed, Byram, & Soma, 2018), detection of fraud in food (Alfarraj, Sanghapi, Bhatt, Yueh, & Singh, 2018; Cama-Moncunill et al., 2017; Sezer et al., 2018; Temiz, Sezer, Berkkan, Tamer, & Boyaci, 2018), determination of pH and degree of humification of soils (Ferreira et al., 2014; Ferreira, Gomes Neto, Milori, Ferreira, & Anzano, 2015), application in the field of the cultural heritage (Gaona et al., 2013), classification of rocks (Li et al., 2018), studies of nanocarbon materials chemical composition (Lebedev et al., 2013) search of organic matter on Mars (Dequaire et al., 2017) among others.

Few researches are focused on application of LIBS for analyzing parameters intrinsically related to coffee quality (Alresawum, 2016; Anggraeni, Nasution, & Suyanto, 2016; Ferreira et al., 2011; Sezer, Apaydin, Bilge, & Boyaci, 2018; Silva et al., 2017; Zhang, Shen, Liu, & He, 2017). Additionally, the literature is scarce on the use of LIBS for BIS determination. Thus, the novelty presented here comes from the investigation of the LIBS and its spectral responses for some coffee compounds together with a linear regression modeling aiming to solve a current problem in coffee value chain.

2. Material and methods

2.1. Samples and standards preparation

Samples of defective and non-defective beans of Coffee *Arabica* L. were obtained from a Brazilian's cooperative located at Minas Gerais State (Brazil), which receives beans from several producers in different geographic regions of the country. The non-defective, black, immature and sour beans were electronically separated (color sorting machine) and subsequently checked by experts.

Aiming to perform a suitable statistical sampling, all samples from each defective class were quartered and one subsample was taken. The remaining portions were mixed again and the quartering and sampling procedures were repeated to obtain five new subsamples. Thereafter each subsample was submitted to a cryogenic grinding using a Spex 6800 cryogenic mill (USA) set with the following grinding program: 2.0 min. for pre-freezing; 3.0 min. for grinding and 2.0 min for freezing between the two milling steps. The grounded samples were reserved for calibration and validation.

For calibration and validation sets, BIS were gradually mixed to the non-defective beans in different ratios (w/w). In calibration standards, BIS contents were 0, 3, 6, 9, 12, 15, 18, 21, 24, 27, 30 and 100% (g/100 g) – the concentrations for each individual defect were 0, 1, 2, 3, 4, 5, 6, 7 8, 9, 10 and 100% – where the minimum concentration (0%) means a sample with only non-defective beans and the maximum concentration (100%) is just one of the three defects (B or I or S from BIS beans). Adding the maximum concentration aims avoiding that predictions from a linear model fitted to a specific defect could be driven by input variables chemically linked to other defects blended in the same sample. For validation samples, the concentrations of BIS were 7.8, 9.9, 13.8, 15.9, 21.9, 25.8 and 27.9% – the concentration of each individual defect was 2.6, 3.3, 4.6, 5.3, 7.3, 8.6 and 9.3%. Calibration and validation samples were prepared in five replicates, taking masses before quartering. The samples were then homogenized and made into pellets by applying 10 tons using a mechanical press (Solab SL – 10/15, Piracicaba, Brazil).

2.2. LIBS instrumentation

A commercial LIBS system LIBS2500 (Ocean Optics, USA) was used. The system comprises a Q-switched laser Nd:YAG emitting pulses at 1064 nm (Quantel BigSky Laser Ultra50), lens for laser focalization (focal distance of 10 cm), an ablation chamber, a mobile sample holder with adjustment on the *x* and *y* axes, an optical system made up of lens and optical fiber bundle to collect plasma emission and drive it to the spectrometers. The seven spectrometers cover a spectral range from 188 to 950 nm with resolution of 0.1 nm (FWHM). All measurements were performed setting the laser pulse energy to around 50 mJ with 8 ns pulse duration and laser spot diameter about 300 μm, resulting in a fluency around 70 J cm^{-2}. The delay time (relative to a Q-switch delay) was set to 11 μs and the integration time to 2.1 ms.

Twenty laser pulses were randomly fired at different positions on both pellet surfaces, resulting in 40 spectra per sample.

2.3. Data processing

The performance of LIBS is intrinsically dependent on signal variations that might result from laser instability, reflectivity of the sample surface and nonlinear processes that come from laser-sample interaction (so-called matrix effects) which cause signal variations, pulse to pulse (Cremers & Radziemski, 2006). For several cases, besides accumulating pulse responses, an adequate spectral preprocessing is also necessary. According to Syvilay et al. (2015) and Bilge et al. (2016), a spectral preprocessing based on Standard Normal Variate (SNV) and first derivative allows minimizing matrix effects and correcting baselines. Thus, each spectrum acquired from a coffee sample was preprocessed by SNV followed by the first derivative. An average of the preprocessed spectra (40 laser pulses/pellet) was assessed for representing each pellet. An average of five pellets was assessed for a statistical inference of the mean spectral behavior.

Based on prior knowledge (Silva et al., 2017), sixteen variables were manually preselected (a prefiltering procedure), which comprise both inflection points for eight peaks (emission lines) after first derivative. The preselected emission lines were: C (I) 193.0 nm; CN (1.1) 387.0 nm; CN (0.0) 388.5 nm; C_2 (0.0) 516.6 nm; N (I) 742.3 nm; N (I) 744.2 nm; N (I) 746.8 nm and O (I) 777.4 nm. The heuristic behind the procedure was based on intrinsic correlations of these emission lines with organic compounds with potential for discriminating BIS from non-defective beans. In addition, a discriminating test was performed for identifying the power for distinguishing (a variable by itself) among all classes. The statistical test was the analysis of variance (ANOVA) together with Tukey test (*p-value* < 0.05) for pairwise comparisons (Silva et al., 2017).

From the preselected variable set, three new selection procedures were accomplished aiming to select subsets of variables optimized for defect prediction models. For each defective class, only variables capable of discriminating that defect with respect to two other classes (at least two statistically significant differences) were selected for fitting its respective regression model.

For estimations of BIS concentrations, three multiple linear regression (MLR) models were fitted. Their performances were evaluated through the root mean squared error on calibration set (RMSEC), root mean squared error on validation set (RMSEV) and coefficient of determination (R^2) (Bilge et al., 2016; Gemperline, 2006).

The weka free software, version 3.6.12 was used for all experiments (Frank, Hall, M. A., Witten, & I. A., 2016).

3. Results and discussion

In Fig. 1a is shown forty LIBS spectra obtained from a pellet of black defective beans. The SNV (Fig. 1b) promoted an autoscaling

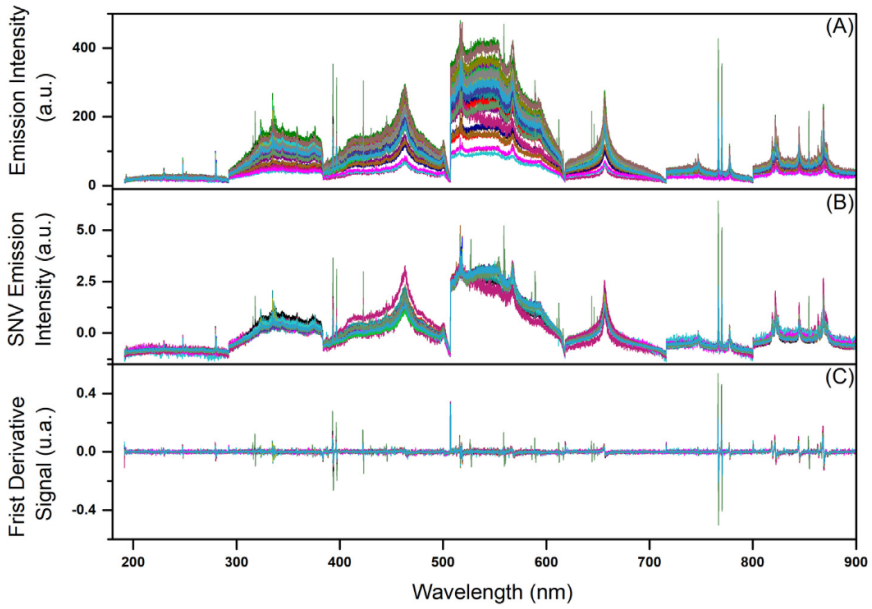


Fig. 1. LIBS spectra ($n = 40$) of black beans: (A) raw data, (B) data preprocessed by SNV, (C) data preprocessed by SNV plus first derivative.

transformation focused on a standardized variance which is capable of minimizing baseline and pathlength effects. The SNV followed by first derivative (Fig. 1c) minimized spectral fluctuations and noise levels. Thus, the SNV followed by first derivative was the spectral treatment adopted.

The selected emission lines for description of each defective class, i.e. BIS, were respectively: B) CN (388.5 nm) and N atomic lines (742.3, 744.2 and 746.8 nm); I) O atomic line (777.4 nm) and N atomic lines (744.2 and 746.8 nm); S) C_2 (516.6 nm) and N atomic lines (744.2 and 746.8 nm). The derivative signals from these lines were picked for fitting calibration models. In Table 1 is shown all statistics obtained for calibration and validation sets, including the relative error for predictions (REP), limit of detection (LOD) and limit of quantification (LOQ), calculated according to Sezer et al. (2018).

The models fitted for black and sour (Fig. 2a and c) showed the smallest RMSEPs (1.7 and 2.5%, respectively), also the smallest limits of quantification (4.8 and 4.3% respectively). The model fitted to predict the immature defect (Fig. 2b) showed a lower performance compared to the others, with RMSEP of 3.8% and limit of quantification of 7.4%, making it impossible to determine four (2.6, 3.3, 4.6, 5.3%) among seven prepared samples. However, the high R^2 values ($R^2 > 0.85$) and low RMSEC and RMSEP corroborate the suitability of the proposed methods for BIS prediction.

It is noteworthy that N emission lines contribute for discriminating any defect from non-defective beans. According to Mazzafera (1999), N content is strongly correlated to coffee proteins and their concentrations are different in BIS and non-defective beans. Thus, the contribution of N lines to the class discriminations might be due to different amounts of proteins in each evaluated class.

Silva et al. (2017) observed that CN emission signal in LIBS spectrum presents a strong correlation with absorption bands in NIRS spectrum corresponding to proteins, carbohydrates and lipids. In addition, C_2 also shows correlation with lipids. These observations suggest that lipids appear to exert relevant effect for distinction of sour beans. On the other hand, lipids, protein and/or carbohydrates are important compounds for discriminating black beans from the other classes. These findings corroborate results obtained by Oliveira, Franca, Mendonça, and Barros-Júnior, (2006), which show that lipids are in lower content in sour beans (9.2% w/w) compared to other classes (9.6%, 10%, 11% for immature, black and non-defective beans, respectively).

The CN emission, selected for black defective beans, is also highly correlated to carbohydrate compounds (Silva et al., 2017). Sucrose, a disaccharide of carbohydrate, is the main free sugar in green coffees and its levels increase with coffee maturation and decrease during fermentation processes (Franca & Oliveira, 2008). Thus, CN appears to be related to the low contents of sucrose in black beans as a consequence of the fermentation, and otherwise higher sugar contents are in non-defective beans.

The slight access to the complex coffee organic chemical composition through LIBS together with an appropriate data treatment approach made viable the development of models for accurately predicting concentrations of B, I and S in blends with non-defective beans. The same strategy can also be investigated for BIS directly in roasted and ground coffee, since some compounds correlated to emission lines in LIBS spectrum do not change significantly due to a bland roasting (Franca & Oliveira, 2008).

4. Conclusion

LIBS emission lines of N, O, CN and C_2 showed high power for discriminating defective classes and also for assuring a good performances of BIS predicting models. The approach based on LIBS, spectral processing, variable selection procedures and linear models resulted in

Table 1
Statistics for calibration and validation in BIS prediction.

Defective beans	Selected Variables (nm)	RMSEC (%)	RMSEP (%)	REP (%)	LOD (%)	LOQ (%)	R^2
Black (B)	CN (0.0) 388.5/N I 742.3/N I 744.2/N I 746.8	0.7	1.7	4.4	1.6	4.8	0.801
Immature (I)	N I 744.2/N I 746.8/O I 777.4	2.2	3.8	9.3	2.4	7.4	0.902
Sour (S)	C_2 (0.0) 516.6/N I 744.2/N I 746.8	1.7	2.5	7.2	1.4	4.3	0.804

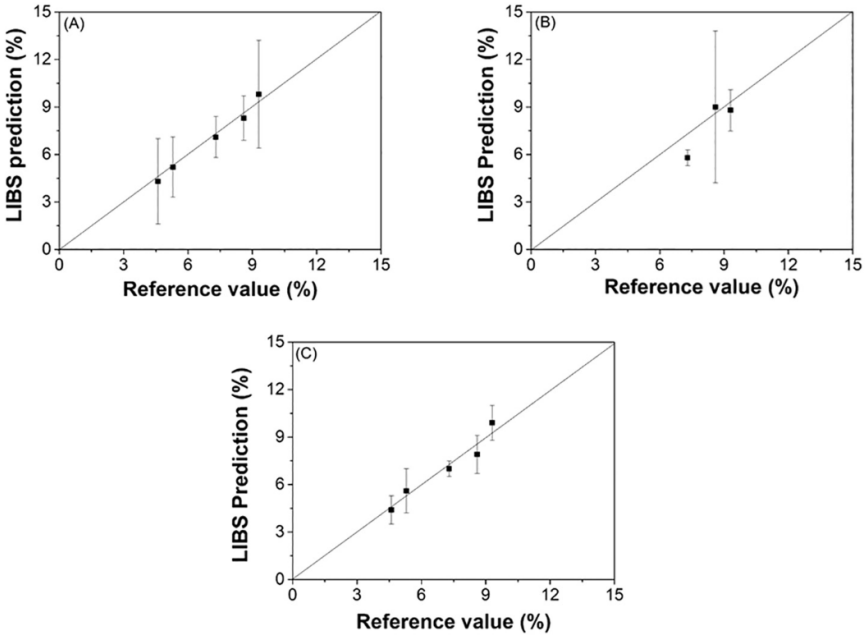


Fig. 2. Plots of BIS prediction for validation samples of concentrations above the LOQs of the developed methods: (A) Black, (B) Immature and (C) Sour beans. The bars refer to mean standard deviation of five predictions.

three analytical methods capable of predicting BIS with root mean squared error on validation smaller than 3.8%. From the perspective of large-scale analysis, the proposal may bring innovation to control quality stages of the coffee value chain (before roasting), especially because of its simplicity, fastness, precision, low cost per analysis and no chemical residues resulting. In addition, the same scientific workflow may be applied to roasted and ground coffee analysis.

Acknowledgements

Special thanks to Coffee Research Consortium (Brazilian Ministry of Agriculture and Embrapa, Grant # 04.13.02.003.00.0) for supporting research through MP4 project, Coordenação de Aperfeiçoamento de Pessoal de Nível Superior (CAPES) for fellowship granted to T.V.S. and Conselho Nacional de Desenvolvimento Científico e Tecnológico (CNPq) for research ship granted to J.A.G.N.

Conflicts of interest

The authors declare no conflict of interest.

References

Agresti, P. D. C. M., Franca, A. S., Oliveira, L. S., & Augusti, R. (2008). Discrimination between defective and non-defective Brazilian coffee beans by their volatile profile. *Food Chemistry, 106*(2), 787–796.

Alfarraj, B. A., Sanghapi, H. K., Bhatt, C. R., Yueh, F. Y., & Singh, J. P. (2018). Qualitative analysis of dairy and powder milk using Laser-Induced Breakdown Spectroscopy (LIBS). *Applied Spectroscopy, 72*(1), 89–101.

Alresawum, Y. (2016). *Laser Induced Breakdown Spectroscopy (LIBS) coupled with multivariate chemometric method for characterization and quality control of Ethiopian coffee and herbal medicines.* Addis Ababa University.

Anggraeni, K., Nasution, A., & Suyanto, H. (2016). *Recognition of spectral identifier from green coffee beans of arabica and robusta varieties using laser-induced breakdown spectroscopy. Second International Seminar on Photonics, Optics, and Its Applications (ISPhOA 2016).* International Society for Optics and Photonics 1015019–1015016.

Baudelet, M., Guyon, L., Yu, J., Wolf, J. P., Amodeo, T., Fŕjafon, E., & Laloi, P. (2006). Spectral signature of native CN bonds for bacterium detection and identification using femtosecond laser-induced breakdown spectroscopy. *Applied Physics Letters, 88*(6), 10–14.

Bilge, G., Sezer, B., Efe, K., Berberoglu, H., Topcu, A., & Hakki, I. (2016). Determination of whey adulteration in milk powder by using laser induced breakdown spectroscopy. *Food Chemistry, 212*, 183–188.

Cama-Moncunill, R., Casado-Gavalda, M. P., Cama-Moncunill, X., Markiewicz-Keszycka, M., Dixit, Y., Cullen, P. J., & Sullivan, C. (2017). Quantification of trace metals in infant formula premixes using laser-induced breakdown spectroscopy. *Spectrochimica Acta – Part B Atomic Spectroscopy, 135*, 6–14.

Chen, X., Li, X., Yang, S., Yu, X., & Liu, A. (2018). Discrimination of lymphoma using laser-induced breakdown spectroscopy conducted on whole blood samples. *Biomedical Optics Express, 9*(3), 1057–1069.

Clarke, R. J., & Macrae, R. (1987). In R. J. Clarke, & R. Macrae (Eds.). *Coffee, Volume 2: Technology*(1st ed.). London and New York: Elsevier Science Publishers Ltd.

Craig, A. P., Franca, A. S., & Oliveira, L. S. (2012). Discrimination between defective and non-defective roasted coffees by diffuse reflectance infrared Fourier transform spectroscopy. *LWT – Food Science and Technology, 47*(2), 505–511.

Cremers, D., & Radziemski, L. J. (2006). *Handbook of Laser-Induced Breakdown Spectroscopy* (1st ed.). West Sussex: John Wiley & Sons Ltd.

Davari, S. A., Masjedi, S., Ferdous, Z., & Mukherjee, D. (2018). In-vitro analysis of early calcification in aortic valvular interstitial cells using Laser-Induced Breakdown Spectroscopy (LIBS). *Journal of Biophotonics, 11*(1), 1–11.

Dequaire, T., Meslin, P. Y., Beck, P., Jaber, M., Cousin, A., Rapin, W., & Coll, P. (2017). Analysis of carbon and nitrogen signatures with laser-induced breakdown spectroscopy; the quest for organics under Mars-like conditions. *Spectrochimica Acta – Part B Atomic Spectroscopy, 131*, 8–17.

Evangelista, S. R., Silva, C. F., Miguel, M. G. P. D. C., Cordeiro, C. D. S., Pinheiro, A. C. M., Duarte, W. F., & Schwan, R. F. (2014). Improvement of coffee beverage quality by using selected yeasts strains during the fermentation in dry process. *Food Research International, 64*, 183–195.

Ferreira, E. C., Ferreira, E. J., Villas-Boas, P. R., Senesi, G. S., Carvalho, C. M., Romano, R. A., & Milori, D. M. B. P. (2014). Novel estimation of the humification degree of soil organic matter by laser-induced breakdown spectroscopy. *Spectrochimica Acta – Part B Atomic Spectroscopy, 99*, 76–81.

Ferreira, E. C., Gomes Neto, J. A., Milori, D. M. B. P., Ferreira, E. J., & Anzano, J. M. (2015). Laser-induced breakdown spectroscopy: Extending its application to soil pH measurements. *Spectrochimica Acta – Part B Atomic Spectroscopy, 110*, 96–99.

Ferreira, E. D., Pereira, R. C. T., Delbem, A. C. B., Oliveira, O. N., Jr, & Mattoso, L. H. C. (2011). Random subspace method for analysing coffee with electronic tongue. *Electronics Letters, 43*(21), 1138–1140.

Franca, A. S., & Oliveira, L. S. (2008). Chemistry of defective coffee beans. ISBN: 978-1-60456-303-0 In Ernst N. Koeffer (Ed.). *Food chemistry research developments* (pp. 105–138). Nova Science Publishers, Inc.

Frank, E., Hall, M. A., & Witten, I. A. (2016). The WEKA Workbench. Online Appendix for "Data Mining: Practical Machine Learning Tools and Techniques.".

Gaona, I., Lucena, P., Moros, J., Fortes, F. J., Guirado, S., Serrano, J., & Laserna, J. J. (2013). Evaluating the use of standoff LIBS in architectural heritage: Surveying the Cathedral of Málaga. *Journal of Analytical Atomic Spectrometry, 28*(6), 810–820.

Gemperline, P. (2006). *Practical guide to chemometrics* (2nd ed.). New York: Taylor & Francis.

International coffee organization. (2002). Available July 4, 2018, from http://www.ico.org/show_document.asp?id=133.

International coffee organization. (2016). Available March 20, 2016, from http://www.

ico.org/pt/trade_statisticsp.asp?section=Estatistica.
Lebedev, V. F., Rabchinskii, M. K., Kozlyakov, M., Stepanov, D., Shvidchenko, A., Nikonorov, N. V., & Vul, A. (2013). Laser-Induced Breakdown Spectroscopy: An advanced method for analysis of nanocarbon materials chemical composition. *Journal of Analytical Atomic Spectrometry, 28*, 177–216.
Li, W. T., Zhu, Y. N., Li, X., Hao, Z. Q., Guo, L. B., Li, X. Y., ... Lu, Y. F. (2018). In situ classification of rocks using stand-off laser-induced breakdown spectroscopy with a compact spectrometer. *Journal of Analytical Atomic Spectrometry, 33*(3), 461–467.
Mazzafera, P. (1999). Chemical composition of defective coffee beans. *Food Chemistry, 64*(4), 547–554.
Mendonça, J. C. F., Franca, A. S., Oliveira, L. S., & Nunes, M. (2008). Chemical characterisation of non-defective and defective green arabica and robusta coffees by electrospray ionization-mass spectrometry (ESI-MS). *Food Chemistry, 111*(2), 490–497.
Miziolek, A. W., Palleschi, V., & Schechter, I. (2006). *LIBS fundamentals and applications* (1st ed.). New York: Cambridge University Press.
Oliveira, L. S., Franca, A. S., Mendonça, J. C. F., & Barros-Júnior, M. C. (2006). Proximate composition and fatty acids profile of green and roasted defective coffee beans. *LWT – Food Science and Technology, 39*(3), 235–239.
Pasquini, C., Corttez, J., Silva, L. M. C., & Gonzaga, F. B. (2007). Laser-induced breakdown spectroscopy. *Journal of Brazilian Chemical Society, 18*(3), 463–512.
Santos, J. R., Sarraguça, M. C., Rangel, A. O. S. S., & Lopes, J. A. (2012). Evaluation of green coffee beans quality using near infrared spectroscopy: A quantitative approach. *Food Chemistry, 135*(3), 1828–1835.
Secretaria de Agricultura e Abastecimento. (2007). Resolução SAA – 28, de 1 de junho de 2007, Define Norma Técnica para fixação de identidade e qualidade de café torrado em grão e café torrado moído. Available March 20, 2016, from http://www.codeagro.agricultura.sp.gov.br/arquivos/selo/saa_28a191a62ed1008f350553a619ba36f7e7.pdf.
Sezer, B., Apaydin, H., Bilge, G., & Boyaci, I. H. (2018). Coffee arabica adulteration: Detection of wheat, corn and chickpea. *Food Chemistry, 264*, 142–148.
Sezer, B., Durna, S., Bilge, G., Berkkan, A., Yetisemiyen, A., & Boyaci, I. H. (2018). Identification of milk fraud using laser-induced breakdown spectroscopy (LIBS). *International Dairy Journal, 81*, 1–7.
Shaik, A. K., Epuru, N. R., Syed, H., Byram, C., & Soma, V. R. (2018). Femtosecond laser induced breakdown spectroscopy based standoff detection of explosives and discrimination using principal component analysis. *Optics Express, 26*(7), 53–59.
Silva, T. V., Hubinger, S. Z., Neto, J. A. G., Milori, D. M. B. P., Ferreira, E. J., & Ferreira, E. C. (2017). Potential of Laser Induced Breakdown Spectroscopy for analyzing the quality of unroasted and ground coffee. *Spectrochimica Acta Part B: Atomic Spectroscopy, 135*, 29–33.
Syvilay, D., Wilkie-Chancellier, N., Trichereau, B., Texier, A., Martinez, L., Serfaty, S., & Detalle, V. (2015). Evaluation of the standard normal variate method for Laser-Induced Breakdown Spectroscopy data treatment applied to the discrimination of painting layers. *Spectrochimica Acta – Part B Atomic Spectroscopy, 114*, 38–45.
Temiz, H. T., Sezer, B., Berkkan, A., Tamer, U., & Boyaci, I. H. (2018). Assessment of laser induced breakdown spectroscopy as a tool for analysis of butter adulteration. *Journal of Food Composition and Analysis, 67*(December 2017), 48–54.
Toci, A. T., & Farah, A. (2008). Volatile compounds as potential defective coffee beans' markers. *Food Chemistry, 108*(3), 1133–1141.
Toci, A. T., Farah, A., Pezza, H. R., & Pezza, L. (2016). Coffee Adulteration: More than two decades of research. *Critical Reviews in Analytical Chemistry, 46*(2), 83–92.
Zhang, C., Shen, T., Liu, F., & He, Y. (2017). Identification of coffee varieties using Laser-Induced Breakdown Spectroscopy and chemometrics. *Sensors, 18*(1), 95–108.

Anexo 11

Food Chemistry 297 (2019) 124960

Contents lists available at ScienceDirect

Food Chemistry

journal homepage: www.elsevier.com/locate/foodchem

Brown rice authenticity evaluation by spark discharge-laser-induced breakdown spectroscopy

Michael Pérez-Rodríguez[a,*], Pamela Maia Dirchwolf[b], Tiago Varão Silva[c], Roxana Noelia Villafañe[a], José Anchieta Gomes Neto[c], Roberto Gerardo Pellerano[a], Edilene Cristina Ferreira[c]

[a] Institute of Basic and Applied Chemistry of the Northeast of Argentina (IQUIBA-NEA), National Scientific and Technical Research Council (CONICET), Faculty of Exact and Natural Science and Surveying, National University of the Northeast – UNNE, Av. Libertad 5470, 3400 Corrientes, Argentina
[b] Faculty of Agricultural Sciences, UNNE, Sgto. Cabral 2131, 3400 Corrientes, Argentina
[c] São Paulo State University – UNESP, Chemistry Institute of Araraquara, R. Prof. Francisco Degni 55, 14800-900 Araraquara, SP, Brazil

ARTICLE INFO

Keywords:
Food authenticity
PDO
Brown rice
SD-LIBS
Pattern recognition

ABSTRACT

Rice is the most consumed food worldwide, therefore its designation of origin (PDO) is very useful. Laser-induced breakdown spectroscopy (LIBS) is an interesting analytical technique for PDO certification, since it provides fast multielemental analysis requiring minimal sample treatment. In this work LIBS spectral data from rice analysis were evaluated for PDO certification of Argentine brown rice. Samples from two PDOs were analyzed by LIBS coupled to spark discharge. The selection of spectral data was accomplished by extreme gradient boosting (XGBoost), an algorithm currently used in machine learning, but rarely applied in chemical issues. Emission lines of C, Ca, Fe, Mg and Na were selected, and the best performance of classification were obtained using k-nearest neighbor (k-NN) algorithm. The developed method provided 84% of accuracy, 100% of sensitivity and 78% of specificity in classification of test samples. Furthermore, it is simple, clean and can be easily applied for rice certification.

1. Introduction

Rice is an important staple food around the world. The cereal is rich in vitamins, fibers and essential minerals, making it a high nutritional value food. The nutritional properties, and therefore the quality of rice is related to its geographical origin. Thus, it is highlighted the need for controlled labeling to protect the authenticity of rice (Ariyama, Shinozaki, & Kawasaki, 2012; Promchan, Günther, Siripinyanond, & Shiowatana, 2016). Many countries have adopted for different food a controlled labeling based on protected designation of origin (PDO). The PDO information is a guarantee of the quality, tradition, and authenticity, and therefore food safety. In addition, PDO is also used as a brand strategy influencing the customer final decision (Dias & Mendes, 2018).

Worldwide several studies have been carried out aiming to determine the geographic origin of agricultural products (Becerra-herrera et al., 2018; Canizo, Escudero, Pérez, Pellerano, & Wuilloud, 2018; Magdas, Feher, Dehelean, & Cristea, 2018; Monahan, Schmidt, & Moloney, 2018; Moncayo, Rosales, Izquierdo-hornillos, Anzano, & Caceres, 2016; She et al., 2019). Particularly for rice, the combination of pattern recognition algorithms with multielemental techniques has been predominantly applied. To this purpose the most commonly used analytical techniques are inductively coupled plasma optical emission spectrometry (ICP OES) (Chung, Kim, Lee, & Kim, 2015) and inductively coupled plasma mass spectrometry (ICP-MS) (Ariyama et al., 2012; Cheajesadagul, Arnaudguilhem, Shiowatana, Siripinyanond, & Szpunar, 2013; Maione, Batista, Campiglia, Barbosa, & Barbosa, 2016). Although these techniques require a complex sample pre-treatment, they provide access to the sample elemental composition supplying a kind of fingerprint of the samples, which is useful for the food authentication.

Laser-induced breakdown spectroscopy (LIBS) is also a multielemental technique able to supply a fingerprint of sample composition. The advantage of LIBS over the aforementioned techniques is that LIBS is able to perform direct analysis, demanding minimum or no sample preparation and no generation of waste after analysis (Cremers & Radziemski, 2006; Miziolek, Palleschi, & Schechter, 2006). LIBS data assisted by chemometric methods have been successfully applied in different troubleshoot of classification, including classification based in

* Corresponding author.
E-mail address: michaelpr1984@gmail.com (M. Pérez-Rodríguez).

https://doi.org/10.1016/j.foodchem.2019.124960
Received 29 March 2019; Received in revised form 17 May 2019; Accepted 7 June 2019
Available online 08 June 2019
0308-8146/ © 2019 Elsevier Ltd. All rights reserved.

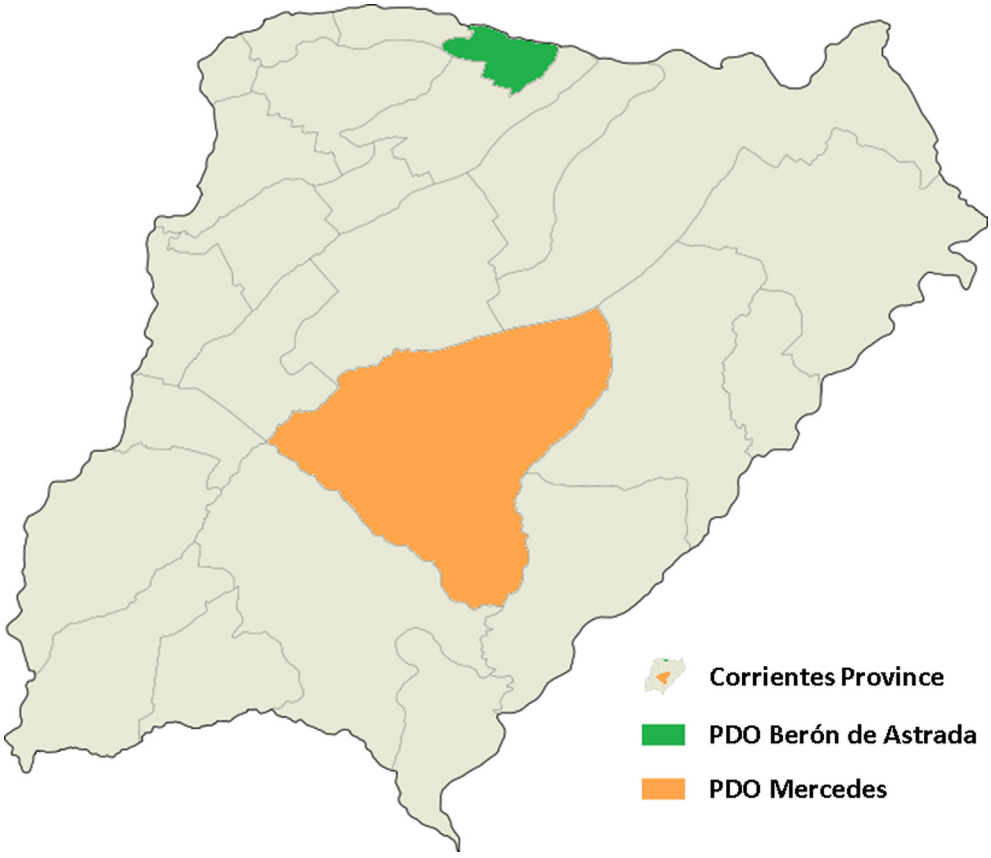


Fig. 1. Geographical regions selected for PDO rice sampling in Corrientes Province, Argentina.

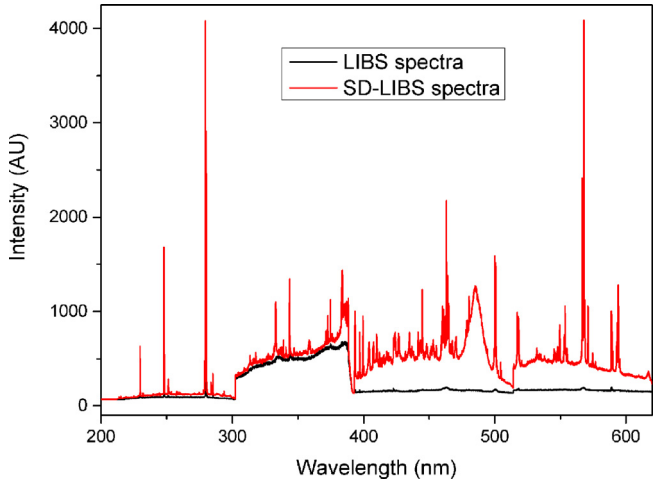


Fig. 2. LIBS (A) and SD-LIBS (B) spectra obtained from a brown rice sample.

PDO of different food samples (Bassbasi, Luca, Ioele, Oussama, & Ragno, 2014; Kumar et al., 2011; Moncayo, Manzoor, & Caceres, 2015; Moncayo et al., 2016; Zhang, Xia, Tang, Yang, & Li, 2016; Zhang, Shen, Liu, & He, 2018). Recently, Yang and collaborators have evaluated LIBS data processed by several chemometric algorithms to study the Chinese rice sample classification (Yang, Zhou et al., 2018; Yang, Zhu et al., 2018). In these studies, the number of inputted parameters for mathematical modeling was larger than the available samples. According to Hastie and collaborators (Hastie, Tibshirani, & Friedman, 2008), statistical models that contain more variables than can be justified by the data are prone to overfit, low capacity of generalization and weighting of spurious variables. Therefore, a suitable method for features selection is crucial, specially for spectra containing a large number of variables, like that provided by LIBS.

The extreme gradient boosting (XGBoost) is an algorithm also known as gradient boosted trees (GBT). Besides being an excellent classifier, it can be used to optimize and select features. Feature selection accomplished by XGboost is based on the action of boosting, where a weak learner can be modified to become better. In gradient boosting, weak learners are decision trees with a single split, called decision stumps. The great advantage of this method is that the importance of the variables for the classification models can be retrieved from the decision trees construction. In addition, the feature importance is estimated from trained predictive models and these tasks can be automatized. The variable importance means how useful it was to the model construction. The higher times the variable is used, the more important it is (Brownlee, 2017; Hastie et al., 2008). XGBoost is currently used by machine learning enthusiasts (Mustapha & Saeed, 2016; Torlay, Perrone-Bertolotti, Thomas, & Baciu, 2017; Zheng, Yuan, & Chen, 2017; Wang, Liu, & Deng, 2018), but very rarely used in chemical issues. In the best of our knowledge it has never been used to select variables from LIBS spectral data.

Considering the above, the aim of the present work was to develop a new method to determine PDO of Argentinean brown rice using LIBS as analytical technique and XGBoost for the spectral features selection to be used in the classification model fitting.

2. Material and methods

2.1. Rice samples

Brown rice of the species *Oryza sativa* L., coming from the northeastern of Argentine, was evaluated. A total of 66 samples were collected from rice fields located in two main producing regions of

Table 1
Performance evaluation measurements (Feature importance and F-Score metric) for variables selection by using XGBoost algorithm and identification of the selected spectral lines.

Variable	Importance	F-score	Maximum	Minimum	Spectral line	Element
1	0.215	61	X		335.3	Fe I
2	0.125	36		X	229.7	Fe I
3	0.112	34	X		247.8	C I/Fe II
4	0.075	22		X	588.9	Na I
5	0.070	21		X	409.8	Ca I
6	0.068	20		X	464.3	Fe I
7	0.060	18		X	374.8	Fe I
8	0.037	11		X	280.2	Mg II
9	0.035	10	X		463.1	Mg II
10	0.017	9	X		229.7	Fe I

Note: (I) indicates atomic spectral lines and (II) indicates ionic spectral lines.

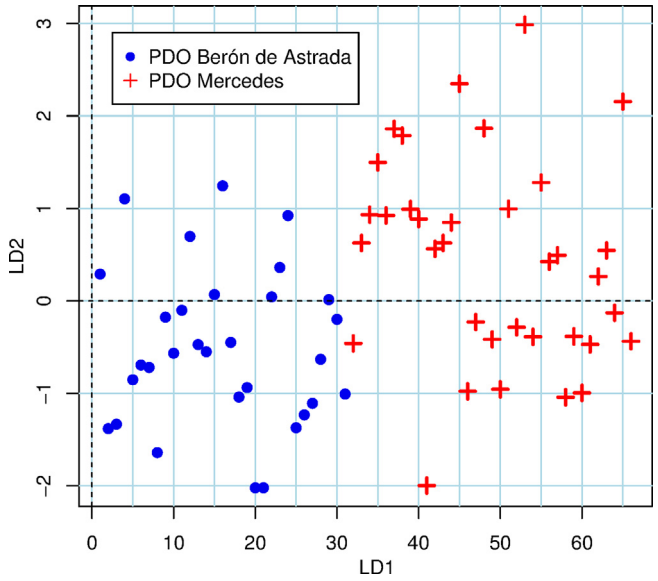


Fig. 3. Scatter plot of the first two discriminant functions obtained from LDA model to discriminate brown rice based on their PDO.

Table 2
Results of the classification metrics calculated for different evaluated models.

Algorithms	Parameters[a]	Accuracy (%)	Sensitivity (%)	Specificity (%)
LDA	–	53	70	33
k-NN	k = 7	84	100	78
SVM	C = 0.8; ε = 0.075	74	90	44
RF	nt = 500; mtry = 1	57	70	44

[a] k: number of k neighbors; nt: number of trees; mtry: number of variables tried at each split; C: penalty factor; ε: ε -insensitive loss function.

Corrientes province: thirty-five samples came from PDO Mercedes (29° 12′ S, 58° 05′ W) and thirty-one samples came from PDO Berón de Astrada (27° 33′ S, 57° 32′ W). All samples coming from the harvest of 2017. In Fig. 1 are shown the geographical locations of the producing regions with protected designation of origin.

The collected rice samples were peeled and were singly ground using a cryogenic mill from Spex 6750 (Metuchen, NJ, USA). The set grinding program consisted of 2.0 min for pre-freezing, 2.0 min for grinding and 3.0 min for freezing between the two milling steps. Around 250 mg of each homogenized sample were made into pellets by applying 10 tons using a mechanical press (Solab SL – 10/15, Piracicaba, Brazil). Two pellets were prepared for each of the 66 samples.

2.2. LIBS experimental setup and measurements

The LIBS system used for pellets analysis comprises a Q-switched laser Nd:YAG (Quantel, Big Sky Ultra 50, Bozeman, USA) emitting pulses at 1064 nm, lens for laser focalization (focal distance of 10 cm), an ablation chamber, a mobile sample holder with adjustment on the x and y axes, an optical system made up of lens and optical fiber bundle to collect plasma emission and drive it to the spectrometers. The plasma emission was collected by means of an optical fiber bundle and conducted to four spectrometers, Ocean Optics (HR2000 + , Dunedin, USA). The spectrometers optical resolution was 0.1 nm FWHM (full width at half maximum) and the spectral range measured for this instrument is 200 to 630 nm. All measurements were performed using laser pulse energy around 50 mJ, with 20 ns pulse duration. The interaction laser-sample provides a spot diameter around 300 μm, resulting in an irradiance in the focal point around 0.35 TW cm^{-2}. The delay time (relative to a Q-switch delay) was set to 1 μs and the integration time is instrumentally fixed at 1 ms.

Aiming to improve the sensitivity of measured spectrum, a system able to promote a spark discharge (SD) on the plasma, previously described by Vieira et al. (2018), was used coupled to the LIBS system above described. The discharge output was set to 4.5 kV and SD-LIBS spectra were acquired by applying 40 laser pulses spread on the surface of each pellet.

2.3. Data processing

Aiming to minimize undesirable fluctuation effects in LIBS spectra, due to laser pulses fluctuation and different laser-sample interaction, which occurs at each pulse (Miziolek et al., 2006), the spectra were individually transformed by the first derivative. Each prepared pellet was represented by an average of derived spectra (n = 40). Further an average of two pellets spectra was assessed for statistical inference of sampling behavior. For features selection step, the derived spectral data were autoscaled, to equalize the ranges of variability in prediction results.

Thereafter, XGBoost, available in the XGBoost Python package, was applied to select descriptors from the entire spectral range. The descriptors corresponded to the maximum and/or minimum variation ratio of derived spectra. For XGBoost algorithm application, the data matrix was randomly divided into two subsets, which consisted of a training set (70% of the samples) and a test set (the remaining 30%). The hyperparameters needing optimization included the number of trees (nt) and the learning rate (lr). These parameters were calculated during the training step by ten-fold cross-validation. Then, the method performance was measured from the feature importance and F-Score metric values. A detailed description regarding the calculation of the F-Score statistic can be found from Maione et al. (2016).

After features selection, the samples spectra were again divided in sets of calibration (training) and validation (testing). For calibration set

Table 3
Analytical methods evaluating the geographical authenticity of rice samples.

Reference	Analytical technique[a]	Chemometric technique[b]	Classification criteria[c]	Rice geographical origin
Ariyama et al. (2012)	HR-ICP-MS	LDA–SIMCA–k-NN	ACC: 97.0%	Japan, United States, China and Thailand
Promchan et al. (2016)	LA-ICP-MS	LDA	ACC: 91.1%	Thailand
Chung et al. (2015)	ICP OES	PLS–DA	–	Korea, China and Philippines
Maione et al. (2016)	ICP-MS	RF	ACC: 93.8%	Brazil
Cheajesadagul et al. (2013)	HR-ICP-MS	DA	OCI: 90.3–100%	Asia, Europe and Thailand
Chung et al. (2018)	IRMS and ICP-MS	OPLS–DA	Q^2Y: 0.834–0.963	Cambodia, China, Japan, Korea, Philippines and Thailand
Kukusamude and Kongsri (2018)	INAA and EA-IRMS	LDA	ACC: 95.5%	Thailand
Gonzálvez, Armenta, and Guardia (2011)	ICP OES	LDA	ACC: 91.3%	Brazil, India, Japan and Spain
Li et al. (2012)	ICP-MS and ICP OES	DFA and FIA	–	China
Qian et al. (2019)	HR-ICP-MS	DA	OCI: 89.6–96.6%	China
Teye, Amuah, McGrath, and Elliott (2019)	NIR	k-NN	ACC: 90.6%	Ghana, Thailand and Vietnam
Hwang, Kang, Lee, and Chung (2012)	Raman	LDA	DE: 1.61–9.97%	China and Korea
Zhu et al. (2018)	Raman	SIMCA	RR: 95.4%	China
Li et al. (2018)	XRF Raman	KMC–	ACC: 60–85.7%	China
Proposed method	SD-LIBS	XGBoost and k-NN	ACC: 84.0%	Argentina

[a] EA-IRMS: elemental analyzer isotope ratio mass spectrometry; HR-ICP-MS: high-resolution inductively coupled plasma mass spectrometry; ICP OES: inductively coupled plasma optical emission spectrometry; INAA: instrumental neutron activation analysis; LA-ICP-MS: laser ablation inductively coupled plasma mass spectrometry; NIR: near infrared spectrometry; Raman: Raman spectroscopy; SD-LIBS: spark discharge-laser-induced breakdown spectroscopy; XRF: X-ray fluorescence.
[b] DA: discriminant analysis; DFA: discriminant function analysis; FIA: Fibonacci index analysis; HC: hierarchical clustering; k-NN: k-nearest neighbors; KMC: k-means clustering; LDA: linear discriminant analysis; OPLS–DA: orthogonal projection to latent structure-discriminant analysis; PLS–DA: partial least-squares discriminant analysis; RF: random forest; SIMCA: soft independent modeling of class analogy; SVM: and support vector machine; XGBoost: extreme gradient boosting.
[c] ACC: Accuracy rate; DE: discrimination error; OCI: overall correct identification; Q^2Y: proportion of variance in the data predicted by a model; RR rejection rate (number of identified non-similar samples divided by the total number of unknown samples (non – class)).

25 spectra from PDO Mercedes plus 22 from PDO Berón de Astrada were randomly selected while for validation it was selected 10 from PDO Mercedes plus 9 from PDO Berón de Astrada. The division into subgroups was performed in a stratified manner, so that the proportion of each class in the original matrix was kept in the new subgroups. In addition, the samples included in each set were randomly changed for each reproduced model. This sampling scheme guaranteed the random sampling consistency.

Algorithms based on pattern recognition were evaluated to fit a suitable PDO classifier. The following supervised classification algorithms were evaluated: linear discriminant analysis (LDA), support vector machine (SVM), k-nearest neighbors (k-NN), and random forest (RF). The different classification models were validated by ten-fold cross-validation. An unknown group of samples belonging to known classes were used to assess the performance of the fitted models. All calculations for classification modeling were made using R-project software version 3.3.3 (R Core Team, 2017). The performance of the classification models were compared using the metrics of overall accuracy (all correct predictions divided by the total number of examined cases), sensitivity (correct positive predictions divided by the number of positive cases), and specificity (correct negative predictions divided by the number of negative cases) (Lantz, 2015).

3. Results and discussion

An initial assessment of the LIBS performance in rice analysis indicated low sensitivity of the available LIBS system. Aiming to improve the sensitivity of measurements a SD device previously proposed (Vieira et al., 2018), was coupled to the LIBS system. The coupling has reached its goal as can be seen in Fig. 2, therefore it was set as instrumental analytical condition.

After data acquisition spectral preprocessing was performed to minimize characteristic fluctuations of LIBS spectra that could affect the performance of the classification models. The first derivative transformation was applied to each individual spectrum because this preprocessing method has been demonstrated effectiveness and simplicity of application (Silva et al., 2017).

Considering many inputted variables can hinders the successful performance of the classification models (Hastie et al., 2008), the XGBoost algorithm was evaluated for spectral feature selection. The results obtained by applying the XGBoost algorithm in the set of training samples are shown in Table 1. The best performance for this feature selection was reached when the hyperparameters nt = 100 and lr = 0.1 were used. In this particular case, since the learning rate value was less than 1.0, the modeling have the effect of making the corrections for each tree added of the model (Brownlee, 2017). As can be observed in Table 1, ten variables obtained from maximum and minimum values from derived spectra were selected. According to the database of the National Institute of Standards and Technology (NIST, 2018), the selected variables corresponded to the emission lines of C, Fe, Ca, Na and Mg. These findings corroborate those observed by Maione et al. and Promchan et al. wherein Ca, Fe, Mg, and Na were also important elements for classification of Brazilian (Maione et al., 2016) and Thai (Promchan et al., 2016) rice, according to geographic origin. Moreover, the F-Score shows that Fe is the most important element to distinguish the evaluated classes with 59.5% of total importance, followed by C (plus Fe) with 14%, Na, 9.1% and Ca and Mg, both showing 8.7% of total importance.

Thereafter, the selected data were used to fit four different classifiers (LDA, RF, SVM and k-NN). In Fig. 3 are shown the patterns distribution of brown rice samples according to their PDO defined by the first two discriminant functions of LDA fitted model. A notably discrimination between the two studied groups can be observed in the whole set of samples with PDO Mercedes showing positive and negative scores on LD2 and PDO Berón de Astrada showing the majority of negative scores with a few positive scores on LD2. Nevertheless, the prediction accuracy in the testing set was 53%, indicating the PDO brown rice samples were not successfully classified.

Therefore, k-NN, SVM and RF non-linear algorithms were also evaluated. In Table 2 are shown the classification metrics calculated for each fitted model, including LDA linear algorithm.

The better classification metrics were obtained for k-NN, SVM and RF. These findings suggest non-linear models fit better the behavior of C, Fe, Ca, Na and Mg in the two PDO evaluated. The highest accuracy in prediction of test samples were given by SVM (74%) with radial basis kernel function using hyperparameters C = 0.8 and ε = 0.075 and k-NN (84%) with an optimized neighbor's number of seven. The best model for differentiating brown rice samples according to their PDO

was k-NN. This model also showed the highest sensitivity (100%) and specificity (78%), compared to the other methods studied.

A comparison of the performance of the proposed method, with methods previously described for the rice geographical authenticity is given in Table 3.

Each method uses as variables specific properties provided by the different employed analytical techniques. All classification methods are multivariate, suggesting more than one feature is frequently required to perform geographical classification of rice. For the several evaluated methods, analytical performance in terms of accuracy ranged from 60 to 97%, indicating the suitability of the proposed method. Compared to the methods using multielement techniques (e.g. ICP OES and ICP MS) the SD-LIBS is faster and more environmentally friendly, since it dispenses complexes sample pretreatments and the use of any chemical reagent.

4. Conclusions

Spectral fingerprints of brown rice obtained by SD-LIBS were investigated to discriminate samples according to their PDO. XGBoost algorithm were used for the first time to select relevant features from LIBS spectra. The analysis of F-Scores of the variables suggested that Fe were the most important element to discriminate the studied PDOs. The other elements presented the following order of importance: C > Na > Ca = Mg. The evaluated algorithms for classification suggested the amounts of selected elements changes in a non-linear fashion for the evaluated PDOs. Moreover, a non-linear classifier based on k-NN showed the best classification performance, achieving 84% of accuracy in prediction of test samples. The developed method is simple, fast and reliable approach, demands minimal sample preparation and does not produce waste after analysis. Its application can help to identify rice mislabeling protecting market rice brands and preventing consumers and producers from financial damage.

Declaration of Competing Interest

The authors have no conflicts of interest to declare.

Acknowledgements

The authors would like to thank National Scientific and Technical Research Council (LH: 172645 CONICET) for granting a postdoctoral scholarship to M. Pérez-Rodríguez and the Conselho Nacional de Desenvolvimento Tecnológico (CNPq) for the research grant to E.C.F. (308200/2018-7).

References

Ariyama, K., Shinozaki, M., & Kawasaki, A. (2012). Determination of the geographic origin of rice by chemometrics with strontium and lead isotope ratios and multi-element concentrations. *Journal of Agricultural and Food Chemistry, 60*, 1628–1634.

Bassbasi, M., De Luca, M., Ioele, G., Oussama, A., & Ragno, G. (2014). Prediction of the geographical origin of butters by partial least square discriminant analysis (PLS-DA) applied to infrared spectroscopy (FTIR) data. *Journal of Food Composition and Analysis, 33*, 210–215.

Becerra-herrera, M., Vélez-martín, A., Ramos-merchante, A., Richter, P., Beltrán, R., & Sayago, A. (2018). Characterization and evaluation of phenolic pro fi les and color as potential discriminating features among Spanish extra virgin olive oils with protected designation of origin. *Food Chemistry, 241*, 328–337.

Brownlee, J. (2017). XGBoost with Paython.

Canizo, B. V., Escudero, L. B., Pérez, M. B., Pellerano, R. G., & Wuilloud, R. G. (2018). Intra-regional classi fi cation of grape seeds produced in Mendoza province (Argentina) by multi-elemental analysis and chemometrics tools. *Food Chemistry, 242*, 272–278.

Cheajesadagul, P., Arnaudguilhem, C., Shiowatana, J., Siripinyanond, A., & Szpunar, J. (2013). Discrimination of geographical origin of rice based on multi-element fingerprinting by high resolution inductively coupled plasma mass spectrometry. *Food Chemistry, 141*, 3504–3509.

Chung, I., Kim, J., Lee, J., & Kim, S. (2015). Discrimination of geographical origin of rice (Oryza sativa L.) by multielement analysis using inductively coupled plasma atomic emission spectroscopy and multivariate analysis. *Journal of Cereal Science, 65*, 252–259.

Chung, I., Kim, J., Lee, K., Park, S., Lee, J., Son, N., ... Kim, S. (2018). Geographic authentication of Asian rice (Oryza sativa L.) using multielemental and stable isotopic data combined with multivariate analysis. *Food Chemistry, 240*, 840–849.

Cremers, D., & Radziemski, L. J. (2006). *Handbook of laser-induced breakdown spectroscopy* (2nd Ed.). Chichester: John Wiley & Sons.

Dias, C., & Mendes, L. (2018). Protected designation of origin (PDO), protected geographical indication (PGI) and traditional speciality guaranteed (TSG): a bibliometric analysis. *Food Research International, 103*, 492–508.

Gonzálvez, A., Armenta, S., & Guardia, M. (2011). Geographical traceability of "Arròs de Valencia" rice grain based on mineral element composition. *Food Chemistry, 126*, 1254–1260.

Hastie, T., Tibshirani, R., & Friedman, J. (2008). *The elements of statistical learning: Data mining, inference, and prediction* (2nd Ed.). Springer: Stanford University.

Hwang, J., Kang, S., Lee, K., & Chung, H. (2012). Enhanced Raman spectroscopic discrimination of the geographical origins of rice samples via transmission spectral collection through packed grains. *Talanta, 101*, 488–494.

Kukusamude, C., & Kongsri, S. (2018). Elemental and isotopic profiling of Thai jasmine rice (Khao Dawk Mali 105) for discrimination of geographical origins in Thung Kula Rong Hai area, Thailand. *Food Control, 91*, 357–364.

Kumar, A., Sreedhar, S., Barman, I., Chari, N., Rao, S. V., Kiran, P. P., ... Kumar, G. M. (2011). Laser-induced breakdown spectroscopy-based investigation and classification of pharmaceutical tablets using multivariate chemometric analysis. *Talanta, 87*, 53–59.

Lantz, B. (2015). *Machine learning with R* (Second Ed.). Birmingham: Packt Publishing Ltd.

Li, G., Nunes, L., Wang, Y., Williams, P. N., Zheng, M., Zhang, Q., & Zhu, Y. (2012). Profiling the ionome of rice and its use indiscriminating geographical origins at the regional scale, China. *Journal of Environmental Sciences, 25*, 144–154.

Li, F., Wang, J., Xu, L., Wang, S., Zhou, M., Yin, J., & Lu, A. (2018). Rapid screening of cadmium in rice and identification of geographical origins by spectral method. *International Journal of Environmental Research and Public Health, 15*, 312–324.

Magdas, D. A., Feher, I., Dehelean, A., & Cristea, G. (2018). Isotopic and elemental markers for geographical origin and organically grown carrots discrimination. *Food Chemistry, 26*, 231–239.

Maione, C., Batista, B. L., Campiglia, A. D., Barbosa, F., & Barbosa, R. M. (2016). Classification of geographic origin of rice by data mining and inductively coupled plasma mass spectrometry. *Computers and Electronics in Agriculture, 121*, 101–107.

Miziolek, A. W., Palleschi, V., & Schechter, I. (2006). *Laser-induced breakdown spectroscopy (LIBS) – Fundamentals and Applications* (1st Ed.). New York – USA: Cambridge University Press.

Monahan, F. J., Schmidt, O., & Moloney, A. P. (2018). Meat provenance: Authentication of geographical origin and dietary background of meat. *Meat Science, 144*, 2–14.

Moncayo, S., Manzoor, S., & Caceres, J. O. (2015). Chemometrics and Intelligent Laboratory Systems Evaluation of supervised chemometric methods for sample classi fi cation by Laser Induced Breakdown Spectroscopy. *Chemometrics and Intelligent Laboratory Systems, 146*, 354–364.

Moncayo, S., Rosales, J. D., Izquierdo-hornillos, R., Anzano, J., & Caceres, J. O. (2016). Talanta Classi fi cation of red wine based on its protected designation of origin (PDO) using Laser-induced Breakdown Spectroscopy (LIBS). *Talanta, 158*, 185–191.

Mustapha, I. B., & Saeed, F. (2016). Bioactive molecule prediction using extreme gradient boosting. *Molecules, 21*, 983–994.

NIST Atomic Spectra Database (2018). https://physics.nist.gov/PhysRefData/ASD/lines_form.html.

Promchan, J., Günther, D., Siripinyanond, A., & Shiowatana, J. (2016). Elemental imaging and classifying rice grains by using laser ablation inductively coupled plasma mass spectrometry and linear discriminant analysis. *Journal of Cereal Science, 71*, 198–203.

Qian, L., Zuo, F., Liu, H., Zhang, C., Chi, X., & Zhang, D. (2019). Determination of geographical origin of Wuchang rice with the geographical indicator by multielement analysis. *Journal of Food Quality*.

R Core Team (2017). *R: A language and environment for statistical computing.* R Foundation for Statistical Computing Accessed from https://www.r-project.org/.

She, S., Chen, L., Song, H., Lin, G., Li, Y., & Zhou, J. (2019). Discrimination of geographical origins of Chinese acacia honey using complex $^{13}C/^{12}C$ oligosaccharides and polyphenols. *Food Chemistry, 272*, 580–585.

Silva, T. V., Hubinger, S. Z., Neto, J. A. G., Milori, D. M. B. P., Ferreira, E. J., & Ferreira, E. C. (2017). Potential of Laser Induced Breakdown Spectroscopy for analyzing the quality of unroasted and ground coffee. *Spectrochimica Acta Part B, 135*, 29–33.

Teye, E., Amuah, C. L. Y., McGrath, T., & Elliott, C. (2019). Innovative and rapid analysis for rice authenticity using hand-held NIR spectrometry and chemometrics. *Spectrochimica Acta Part A, 217*, 147–154.

Torlay, L., Perrone-Bertolotti, M., Thomas, E., & Baciu, M. (2017). Machine learning–XGBoost analysis of language networks to classify patients with epilepsy. *Brain Informatics, 4*, 159–169.

Vieira, A. L., Silva, T. V., Sousa, F. S. I., Senesi, G. S., Santos, D., Ferreira, E. C., & Neto, J. A. G. (2018). Determinations of phosphorus in fertilizers by spark discharge-assisted laser-induced breakdown spectroscopy. *Microchemical Journal, 139*, 322–326.

Wang, H., Liu, C., & Deng, L. (2018). Enhanced prediction of hot spots at protein-protein interfaces using extreme gradient boosting. *Scientific Reports, 8*, 14285–14298.

Yang, P., Zhou, R., Zhang, W., Tang, S., Hao, Z., Li, X., ... Zeng, X. (2018). Laser-induced breakdown spectroscopy assisted chemometric methods for rice geographic origin classification. *Applied Optics, 57*, 8297–8302.

Yang, P., Zhu, Y., Yang, X., Li, J., Tang, S., Hao, Z., ... Lu, Y. (2018). Evaluation of sample preparation methods for rice geographic origin classification using laser-induced breakdown spectroscopy. *Journal of Cereal Science, 80*, 111–1188.

Zhang, C., Shen, T., Liu, F., & He, Y. (2018). Identification of coffee varieties using laser-

induced breakdown spectroscopy and chemometrics. *Sensors, 18*, 95–107.
Zhang, T., Xia, D., Tang, H., Yang, X., & Li, H. (2016). Chemometrics and intelligent laboratory systems classification of steel samples by laser-induced breakdown spectroscopy and random forest. *Chemometrics and Intelligent Laboratory Systems, 157*, 196–201.
Zheng, H., Yuan, J., & Chen, L. (2017). Short-term load forecasting using EMD-LSTM neural networks with an XGBoost algorithm for feature importance evaluation. *Energies, 10*, 1168–1188.
Zhu, L., Sun, J., Wu, G., Wang, Y., Zhang, H., Wang, L., ... Qi, X. (2018). Identification of rice varieties and determination of their geographical origin in China using Raman spectroscopy. *Journal of Cereal Science, 82*, 175–182.

Anexo 12

Food Chemistry 331 (2020) 127051

Contents lists available at ScienceDirect

Food Chemistry

journal homepage: www.elsevier.com/locate/foodchem

Fast spark discharge-laser-induced breakdown spectroscopy method for rice botanic origin determination

Michael Pérez-Rodríguez[a,b,*], Pamela Maia Dirchwolf[c], Tiago Varão Silva[b], Alan Lima Vieira[b], José Anchieta Gomes Neto[b], Roberto Gerardo Pellerano[a], Edilene Cristina Ferreira[b]

[a] Institute of Basic and Applied Chemistry of the Northeast of Argentina (IQUIBA-NEA), National Scientific and Technical Research Council (CONICET), Faculty of Exact and Natural Science and Surveying National University of the Northeast – UNNE, Av. Libertad 5470, 3400 Corrientes, Argentina
[b] Chemistry Institute of Araraquara, São Paulo State University – UNESP, R. Prof. Francisco Degni 55, 14800-900 Araraquara, SP, Brazil
[c] Faculty of Agricultural Sciences, UNNE, Sgto. Cabral, 1213, 3400 Corrientes, Argentina

ARTICLE INFO

Keywords:
Rice
Botanical origin
SD-LIBS
Support vector machine

ABSTRACT

A simple, fast, and efficient spark discharge-laser-induced breakdown spectroscopy (SD-LIBS) method was developed for determining rice botanic origin using predictive modeling based on support vector machine (SVM). Seventy-two samples from four rice varieties (Guri, Irga 424, Puitá, and Taim) were analyzed by SD-LIBS. Spectral lines of C, Ca, Fe, Mg, N and Na were selected as input variables for prediction model fitting. The SVM algorithm parameters were optimized using a central composite design (CCD) to find the better classification performance. The optimum model for discriminating rice samples according to their botanical variety was obtained using $C = 5.25$ and $\gamma = 0.119$. This model achieved 96.4% of correct predictions in test samples and showed sensitivities and specificities per class within the range of 92–100%. The developed method is robust and eco-friendly for rice botanic identification since its prediction results are consistent and reproducible and its application does not generate chemical waste.

1. Introduction

Quality and safety of food crops are essential for protecting the consumers. Rice is one of the most worldwide consumed cereals since it is an important source of carbohydrates, proteins, vitamins and minerals and its production cost is relatively low (Gupta, 2015; Promchan, Günther, Siripinyanond, & Shiowatana, 2016; Zhu et al., 2018). The quality of rice mainly depends on its harvest, seed type, processing, geographical origin, and botanical variety. Nowadays the high demand for quality products has resulted in a large number of rice genotypes. According to the requirements of international trade, the variety labeling must be controlled for protecting the authenticity of rice (Gupta, 2015; Luo et al., 2019). In this context, the identification of botanical origin of the rice grains is crucial for research related to this crop.Rice authenticity analysis is a challenging due to the similarity in grain composition and chemical properties. A huge number of proposals employing different analytical techniques have been carried for this purpose. Rice varieties harvested from several countries have been accurately differentiated by hyperspectral imaging (Wang et al., 2015), Raman spectroscopy (Zhu et al., 2018), genomic DNA extraction (Becerra, Paredes, Gutiérrez, & Rojo, 2015; Brondani, Borba, Rangel, & Brondani, 2006; Chuang, Lur, Hwu, & Chang, 2011), chemical tests (Tiwari, Rastogi, Chandrakar, Sarawgi, & Verulkar, 2013), and digital image analysis based on color and morphological features (Gupta, 2015; Zhao-yan, Fang, Yi-bin, & Xiu-qin, 2005). The above methods related to chemical analysis require the use of reagents and generate chemical residues after analysis, increasing the cost per analysis. In addition, chemical methods involve extensive sample handling, increasing the analysis time and the risk of introducing errors. In contrast, methods using Raman spectroscopy and images (digital or hyperspectral) are fast and clean methods, however they are unable to generate results correlated to mineral chemical composition of samples. According to previous studies the genotype significantly affects the mineral content in rice (Itani, Tamaki, Arai, & Horino, 2002; Meng, Wei, & Yang, 2005). Therefore, there is still a lack of a fast and clean method, capable of providing an accurate classification of rice genotypes based on their mineral composition.

Laser-induced breakdown spectroscopy (LIBS) is an emission spectroscopy technique able to perform multielemental analysis. A LIBS measure is accomplished from a laser pulse, which promotes a

* Corresponding author at: Institute of Basic and Applied Chemistry of the Northeast of Argentina (IQUIBA-NEA), National Scientific and Technical Research Council (CONICET), Faculty of Exact and Natural Science and Surveying National University of the Northeast – UNNE, Av. Libertad 5470, 3400 Corrientes, Argentina.
E-mail address: michaelpr1984@gmail.com (M. Pérez-Rodríguez).

https://doi.org/10.1016/j.foodchem.2020.127051
Received 18 December 2019; Received in revised form 9 May 2020; Accepted 11 May 2020
Available online 15 June 2020
0308-8146/ © 2020 Elsevier Ltd. All rights reserved.

microsampling, vaporization of sampled portion, breakdown and ionization of sample compounds. From ionization processes a plasma with temperatures reaching 10,000 K is produced. The plasma temperature causes atomization/ionization and excitation of sample elements. Upon returning to the lower energy state, excited species emit electromagnetic radiation at characteristics wavelengths allowing the identification of the specie. Additionally, the intensities of radiation can be correlated to the concentration of the species in the sample (Miziolek, Palleschi, & Schechter, 2006). Some LIBS system can show low analytical sensitivity, but this inconvenience has been overcome by coupling devices for signal enhancement (Bol'shakov, Mao, & Russo, 2017; Li et al., 2018; Sobral & Robledo-martinez, 2016), like spark discharge (SD) (Vieira et al., 2018; Pérez-rodríguez et al., 2019).

Due to its analytical advantages such as providing quick analyzes, dispensing or requiring minimal sample pretreatment and not using chemical supplies for analysis, the LIBS technique has been extensively applied for qualitative and quantitative analysis in various fields of the science including industrial (Noll, Fricke-Begemann, Connemann, Meinhardt, & Sturm, 2018; Sun et al., 2018), agricultural (Andrade & Pereira-filho, 2016; Sezer, Bilge, Sanal, Koksel, & Boyaci, 2017), biomedical (Busser, Moncayo, Coll, Sancey, & Motto-ros, 2018; Rehse, Salimnia, & Miziolek, 2012) and environmental researches (Butler, Cairns, Cook, Davidson, & Mertz-kraus, 2018; Zorov, Popov, Zaytsev, & Labutin, 2015). More recently it has gained special attention for cereal monitoring and control (Peng, He, Jiang, et al., 2019; Peng, He, Zhao, et al., 2019; Yang, Zhu et al., 2018).

The multielemental LIBS spectrum contains a large volume of sample information and the extraction of important spectral characteristics for the analytical purpose, as well as the simultaneous use of these characteristics with their respective weights, depends on the development of multivariate methods. In this context, chemometrics has effectively contributed to the development of LIBS methods. Some methods have been reported for rice analysis. Luo et al. (2019) adopted LIBS combined with multilayer perceptron neural network (MLP) for rapid identification of rice species. Other authors employed LIBS for successfully classification of rice samples according to its geographic origin by using principal component analysis (PCA) coupled to support vector machine (SVM) (Yang, Zhou, et al., 2018; Yang, Zhu et al., 2018) and extreme gradient boosting (XGBoost) together with k-nearest neighbor (k-NN) (Pérez-rodríguez et al., 2019). These methods suggest the LIBS potential for rice classification issue. However, the great challenge of each application is to extract the relevant information from the LIBS spectra according to the intended purpose and the choice of appropriate algorithm to process such information and generate the classification model.

Considering the above, the present work focuses on the development of a SD-LIBS-based method for rapid determination of rice botanic origin using SVM. Aiming to build an optimal classifier, a central composite design (CCD) was used to successfully fit the algorithm performance parameters.

2. Material and methods

2.1. LIBS instrumentation

A LIBS system coupled to a spark discharge (SD) device for sensitivity improvement, previously described by Vieira et al. (2018), was used in this work. The LIBS system consisted of a Q-switched laser Nd:YAG (Quantel, Big Sky Ultra 50, USA) emitting pulses at 1064 nm and operating at its maximum power energy (50 mJ) with a pulse duration of 20 ns, ablation laser fluence of ~ 70 J cm^{-2} and spot diameter about 300 μm. The plasma emission was collected at an angle of 45° in relation to the laser beam by using an optical fiber bundle and conducted to four spectrometers, Ocean Optics (LIBS HR2000+, USA). The spectrometers provided an optical resolution of 0.1 nm FWHM (full width at half maximum) and cover the spectral range from 200 to 600 nm. The Q-switched delay was set to 1 μs and the fix spectrometer integration time was 1 ms. The OOLIBS software (Ocean Optics, USA) was used to control the instrument and data acquisition.

Each sample were placed in sampling chamber which included a sample holder controlled by a joystick able to move the sample in the "x-y" directions and a video camera for monitoring the laser pulses on sample. All spectra were acquired by setting an output voltage of 4.5 kV.

2.2. Rice samples

Rice samples from four genotypes of Oryza Sativa L. species were obtained from different agricultural cooperatives of Corrientes province (Argentina). The samples were randomly selected by the cooperatives and, a set containing fifteen samples from Guri genotype, twenty-two from Irga 424, twenty from Puitá and fifteen from Taim was constituted. All 72 samples acquired come from the 2017 harvest.

2.3. Sample preparation and analysis

Considering the concentration of minerals differs in the different fractions of the grain (Lu, Tian, Liao, Zhang, Yang, Labavitch, & Chen, 2013) and aiming to measure the total content of minerals with adequate precision, the rice samples were individually homogenized by cryogenic grinding using a cryogenic mill from Spex 6750 (Metuchen, NJ, USA). Grinding program consisted of: 2.0 min for pre-freezing, 2.0 min for grinding and 3.0 min for freezing between the two milling steps. A mechanical press (Solab SL – 10/15, Piracicaba, Brazil) was used to prepare two pellets of each sample. The pellets with 12 mm in diameter and 2 mm thick were prepared by applying 10 tons of pressure to about 250 mg of powdered samples. The pellets were analyzed by LIBS spreading twenty laser pulses on each side of the pellet in different locations, moving the sampler in the x-y directions for each pulse. Thereby forty spectra were obtained from each prepared pellet resulting in 80 spectra per rice sample.

2.4. Multivariate data analysis

The LIBS spectra were preprocessed for base line correction and peak area integration. These tasks were carried using the Microsoft Excel® (2016). Support vector machine (SVM) classifiers, which are based on constructing a separating maximal margin hyperplane through the training data mapping into a higher dimension space, were evaluated for rice botanical origin prediction. SVM was chosen because it is able to solve nonlinear classification problems establishing linear boundaries among samples groups by using the kernel trick. Kernel function is used to transform the input data into required dimensions, in a more efficient way and with little computational cost (Lantz, 2015).

The SVM parameters were optimized by multivariate analysis using a central composite design (CCD). The parameters needing optimization included the insensitive loss function (γ) and the penalty factor (C). γ controls the amplitude of the kernel function and its choice determines the dimensionality of the feature space; while C controls the trade-off between prediction error minimization on training data and margin maximization (Bona et al., 2017). The modeling from these parameters was evaluated by ten-fold cross-validation. The classification performance of the models obtained was evaluated considering the overall accuracy, which is calculated as the ratio between all correct predictions and total number of examined cases. The maximum accuracy value was considered as the selection criterion. Design matrix and corresponding optimization graph were constructed using Minitab 16 software.

For fitting the classifier from optimized SVM parameters, the samples spectra were again randomly split up into two subsets, a calibration set which corresponded to 75% of the total samples (n = 54), and a validation set containing the remaining 25% (n = 18). In order to keep

the proportion of rice varieties in the new subgroups matching to original matrix, the split up into subgroups was performed in a stratified manner.

The metrics calculated per class included specificity (correct negative predictions divided by the number of negative cases) and sensitivity (correct positive predictions divided by the number of positive cases) (Lantz, 2015). In addition, the Kappa statistic was also calculated. Kappa value is a coefficient of agreement commonly used either for evaluating intra-classifier or inter-classifier reliability, and its measurement takes on greater significance for unbalanced datasets. The calculation of this statistic was detailed by Mchugh (2012). Chemometric data processing was made using R-project software version 3.3.3 (R Core Team, 2017) with caret and chemometric-with-R packages.

3. Results and discussion

The analysis of LIBS spectra from rice samples showed the most of the valuable and high-intensity spectral lines were in following spectral ranges: 247.8 to 343.7, 399.6 to 480.4 and 549.5 to 594.1 nm. After data acquisition, the integrated LIBS spectra were projected on computing platform of R-project software. The software identified collinear variables and peaks with identical areas in the sample groups, which could affect the classification performance. Therefore, the original spectral data was reduced by selecting valuable and high-intensity emission lines as descriptors for the chemometric analysis. The spectral lines assigned to the elements C, Ca, Fe, Mg, N and Na were selected as the input variables for rice varieties predictive modeling. The assignments of these lines were made using the database of the National Institute of Standards and Technology (NIST, 2019). Fig. 1 shows an average spectrum of a rice sample where the selected variables were highlighted. The potential of C, Ca, Fe, Mg, N and Na elements to discriminate rice samples has already been reported by other authors (Luo et al., 2019; Maione, Batista, Campiglia, Barbosa, & Barbosa, 2016; Pérez-rodríguez et al., 2019; Promchan et al., 2016; Yang, Zhou, et al., 2018; Yang, Zhu et al., 2018).

The parameters affecting the SVM classification performance were optimized by multivariate analysis using a CCD (Mason, Gunst, & Hess, 2003). The best conditions for predictive modeling have been established considering the penalty factor (C), and insensitive loss function (γ). The effects of these parameters on the overall accuracy were studied using five levels ($-\sqrt{2}$, –1, 0, +1, and $\sqrt{2}$) to model a second order polynomial. The levels of a CCD are $\sqrt{2}$ coded units distant from the central level (coded as zero level), so all the points lie on a circumference with radius $\sqrt{2}$. The maximum (+1) and minimum (–1) levels for each parameter were defined on the basis of the run tests previously performed, and the values of the levels corresponding to $-\sqrt{2}$, 0, and $\sqrt{2}$ were calculated. Table 1 shows the design matrix with coded and uncoded studied levels of C and γ factors, and the thirteen experiments randomly performed in order to obtain the combination leading to greater accuracy. In addition, Kernel trick was evaluated in order to enable the input data transformation in a linearly separable higher-dimensional feature space (Moncayo, Manzoor, & Caceres, 2015). For this proposal, several functions based on linear, polynomial, gaussian, sigmoid and radial basis function (RBF) kernel, were carried out to test the classification. The use of the latter allowed obtaining the best prediction results in the training samples probably due to its ability to handle multivariate data, and therefore the RBF kernel was set for all the optimization runs.

Table 1
Matrix obtained from the central composite design.

Experiment	Levels of coded factors[a]		Levels of uncoded factors[a]	
	C (AU)	γ (AU)	C (AU)	γ (AU)
1	–1	–1	0.50	0.010
2	$-\sqrt{2}$	0	0.45	0.055
3	$+\sqrt{2}$	0	11.97	0.055
4	0	0	5.25	0.055
5	0	0	5.25	0.055
6	0	$+\sqrt{2}$	5.25	0.119
7	+1	+1	10.00	0.100
8	0	0	5.25	0.055
9	+1	–1	10.00	0.010
10	–1	+1	0.50	0.100
11	0	$-\sqrt{2}$	5.25	0.009
12	0	0	5.25	0.055
13	0	0	5.25	0.055

[a] C: penalty factor; γ: insensitive loss function.

The resulting two-dimensional graph of contour curves is shown in Fig. 2. The dark green region represents the maximum overall accuracy and indicates the levels of the parameters to which the prediction in test samples was most successful.

The multiple regression analysis resulted in the following equation:

$$A = 0.2448 + 0.06790 \times C + 5.190 \times \gamma - -0.003450 \times C^2 - -18.54 \times \gamma^2 + 0.07300 \times C \times \gamma$$

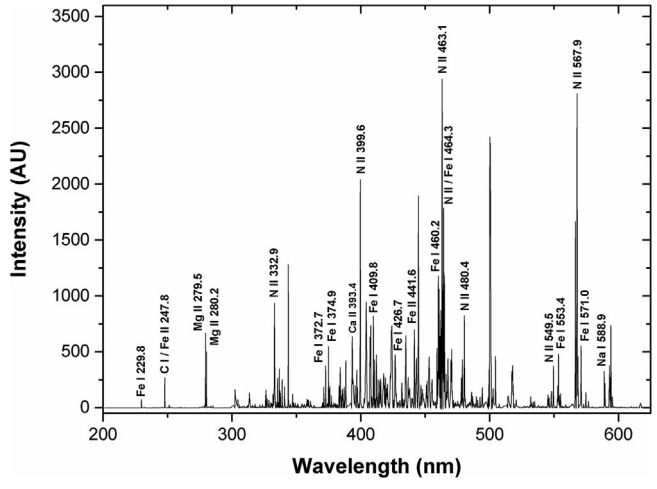


Fig. 1. Average spectra of different rice varieties showing the selected emission lines and corresponding elements used as input variables for sample classification.

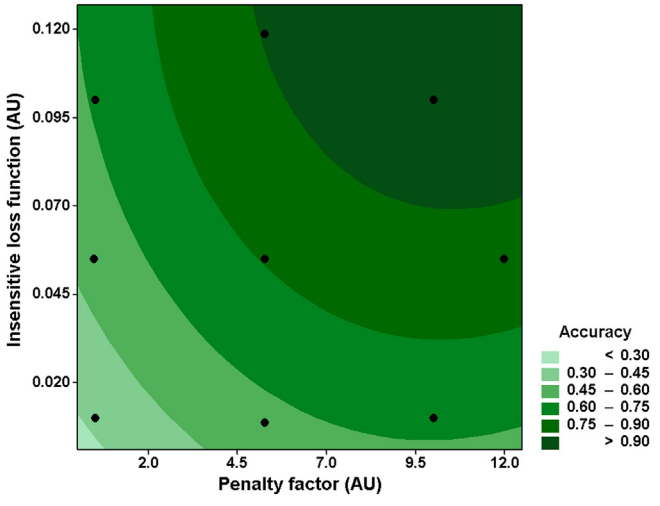


Fig. 2. Central composite design contour curves obtained for the influence of the penalty factor and insensitive loss function parameters on prediction accuracy.

Table 2
Classification metrics obtained from optimized parameters of SVM.

Variety	Number of samples		Sensitivity(%)	Specificity(%)	Balanced accuracy(%)
	Training	Test			
Guri	11	4	100	100	100
Irga 424	16	6	100	95	97.4
Puitá	15	5	93	100	96.7
Taim	12	3	92	100	95.8
Optimized parameters[a]			C = 5.25; γ = 0.119		
Overall accuracy (%)			96.4		
Kappa value			0.952		

[a] C: penalty factor; γ: insensitive loss function.

Where, A is the response factor corresponding to the overall accuracy, C is the penalty factor, and γ is the insensitive loss function. The adjusted regression coefficient was 93.9%, indicating that the quadratic regression model obtained was able to explain the relationship between the prediction results and the effects of the parameters studied.

Based on the analysis of Fig. 2, it was possible to identify the most suitable region for predicting the rice varieties. The ranges of studied parameters showing the best success rates were 5.25 to 10.0 for penalty factor and 0.055 to 0.119 for insensitive loss function. The optimal classifier was obtained when the parameters $C = 5.25$ and $\gamma = 0.119$ were used, achieving the highest overall accuracy of 96.4%. These optimized values were therefore selected to classify the rice samples according to their botanical variety.

After the optimization of the classifier parameters, it was again trained and validated. Table 2 shows the metrics calculated per class for the best fitted model. The balanced accuracies in prediction of test samples were 100% for Guri, 97.4% for Irga 424, 96.7% for Puitá and 95.8% for Taim samples; and the sensitivities and specificities were in the ranges 92–100% and 95–100%, respectively. Furthermore, this model also showed a kappa value of 0.952 being within the data reliability range of 82–100%, which indicates an almost perfect agreement between the predicted classes and the real classes.

The optimized SVM parameters by two-dimensional response surface analysis allowed improving classification algorithm performance in terms of higher modeling speed, stability and accuracy. Additionally, it favored the computing environment to develop a mathematical model with greater consistency and reproducibility in the prediction results.

4. Conclusions

A new method based on SD-LIBS was developed to authenticate rice samples according to their botanical origin using an optimized SVM model. The predictors for classification were related to C, Ca, Fe, Mg, N and Na elements. A CCD was used to optimize SVM performance. The optimal classifier was built using parameters $C = 5.25$ and $\gamma = 0.119$, which achieved an overall accuracy of 96.4% in test samples. This is the first work describing the chemometric optimization of a SVM model from LIBS profiling to solve rice classification issues. The ability and flexibility of this algorithm for building a generalized rice genotype predictive model have been demonstrated in this work.

The developed method is simpler, faster, and more efficient, compared to other methodologies previously described. Its application could contribute to reduce the number of runs to be undertaken to find a tuned classifier and improving quality of prediction results, and modeling time and computing handling were therefore substantially decreased. Furthermore, the analytical approach addressed here is environmentally safe because it no resulting chemical residues.

CRediT authorship contribution statement

Michael Pérez-Rodríguez: Formal analysis, Writing - original draft, Writing - review & editing. **Pamela Maia Dirchwolf:** Formal analysis. **Tiago Varão Silva:** Formal analysis. **Alan Lima Vieira:** Formal analysis. **José Anchieta Gomes Neto:** Formal analysis, Writing - review & editing. **Roberto Gerardo Pellerano:** Formal analysis, Writing - review & editing. **Edilene Cristina Ferreira:** Formal analysis, Writing - original draft, Writing - review & editing.

Declaration of Competing Interest

The authors declare that they have no known competing financial interests or personal relationships that could have appeared to influence the work reported in this paper.

Acknowledgements

The authors are sincerely grateful to National Scientific and Technical Research Council (CONICET) for the postdoctoral scholarship granted to M. Pérez-Rodríguez (LH: 172645) and to Conselho Nacional de Desenvolvimento Tecnológico (CNPq) for the research grant to E.C.F. (308200/2018-7).

References

Andrade, D. F., & Pereira-filho, E. R. (2016). Direct determination of contaminants, major and minor nutrients in solid fertilizers using Laser-Induced Breakdown Spectroscopy (LIBS). *Journal of Agricultural and Food Chemistry, 64*, 7890–7898.

Becerra, V., Paredes, M., Gutiérrez, E., & Rojo, C. (2015). Genetic diversity, identification, and certification of Chilean rice varieties using molecular markers. *Chilean Journal of Agricultural Research, 75*, 267–274.

Bol'shakov, A. A., Mao, X., & Russo, R. E. (2017). Spectral emission enhancement by an electric pulse for LIBS and LAMIS. Journal of Analytical Atomic Spectrometry, 32, 657–670.

Bona, E., Marquetti, I., Link, J. V., Makimori, G. Y. F., Arca, V. da C., Lemes, A. L. G., Ferreira, J. M. G., Scholz, M. B. dos S., Valderrama, P., & Poppi, R. J. (2017). Support vector machines in tandem with infrared spectroscopy for geographical classification of green arabica coffee. LWT - Food Science and Technology Journal, 76, 330–336.

Brondani, C., Borba, T. C. O., Rangel, P. H. N., & Brondani, R. P. V. (2006). Determination of genetic variability of traditional varieties of Brazilian rice using microsatellite markers. *Genetics and Molecular Biology, 29*(4), 676–684.

Busser, B., Moncayo, S., Coll, J., Sancey, L., & Motto-ros, V. (2018). Elemental imaging using laser-induced breakdown spectroscopy: A new and promising approach for biological and medical applications. *Coordination Chemistry Reviews, 358*, 70–79.

Butler, O. T., Cairns, W. R. L., Cook, J. M., Davidson, C. M., & Mertz-kraus, R. (2018). Atomic spectrometry update – a review of advances in environmental analysis. *Journal of Analytical Atomic Spectrometry, 33*, 8–56.

Chuang, H., Lur, H., Hwu, K., & Chang, M. (2011). Authentication of domestic Taiwan rice varieties based on fingerprinting analysis of microsatellite DNA markers. *Botanical Studies, 52*, 393–405.

Gupta, J. (2015). Identification and Classification of Rice varieties using Mahalanobis Distance by Computer Vision. *International Journal of Scientific and Research Publications, 5*, 1–6.

Itani, T., Tamaki, M., Arai, E., & Horino, T. (2002). Distribution of amylose, nitrogen, and minerals in rice kernels with various characters. *Journal of Agricultural and Food Chemistry, 50*, 5326–5332.

Lantz, B. (2015). Machinelearning with R (Second Ed.). Birmingham: Packt Publishing Ltd.

Li, Y., Tian, D., Ding, Y., Yang, G., Liu, K., Wang, C., & Han, X. (2018). A review of laser-induced breakdown spectroscopy signal enhancement. *Applied Spectroscopy Reviews, 53*(1), 1–35.

Lu, L., Tian, S., Liao, H., Zhang, J., Yang, X., Labavitch, J. M., & Chen, W. (2013). Analysis of metal element distributions in rice (Oryza sativa L.) seeds and relocation during germination based on X-Ray fluorescence imaging of Zn, Fe, K, Ca, and Mn. PLoS One, 8, e57360.

Luo, Z., Zhang, L., Chen, T., Liu, M., Chen, J., Zhou, H., & Yao, M. (2019). Rapid identification of rice species by laser-induced breakdown spectroscopy combined with pattern recognition. *Applied Optics, 58*, 1631–1638.

Maione, C., Batista, B. L., Campiglia, A. D., Barbosa, F., & Barbosa, R. M. (2016). Classification of geographic origin of rice by data mining and inductively coupled plasma mass spectrometry. *Computers and Electronics in Agriculture Journal, 121*, 101–107.

Mason, R. L., Gunst, R. F., & Hess, J. L. (2003). Statistical design and analysis of experiments. 2nd ed. Hoboken, New Jersey: Wiley.

Mchugh, M. L. (2012). Interrater reliability: The kappa statistic. *Biochemia Medica, 22*, 276–282.

Meng, F., Wei, Y., & Yang, X. (2005). Iron content and bioavailability in rice. *Journal of Trace Elements in Medicine and Biology, 18*, 333–338.

Miziolek, A. W., Palleschi, V., & Schechter, I. (2006). Laser-induced breakdown spectroscopy (LIBS) – Fundamentals and Applications (1st Ed.). New York – USA:

Cambridge University Press.
Moncayo, S., Manzoor, S., & Caceres, J. O. (2015). Chemometrics and Intelligent Laboratory Systems Evaluation of supervised chemometric methods for sample classi fi cation by Laser Induced Breakdown Spectroscopy. *Chemometrics and Intelligent Laboratory Systems, 146*, 354–364.
NIST Atomic Spectra (2019). Accessed from https://physics.nist.gov/PhysRefData/ASD/lines _form.html. *Database*.
Noll, R., Fricke-Begemann, C., Connemann, S., Meinhardt, C., & Sturm, V. (2018). LIBS analyses for industrial applications – an overview of developments from 2014 to 2018. *Journal of Analytical Atomic Spectrometry, 33*, 945–956.
Peng, J., He, Y., Jiang, J., Zhao, Z., Zhou, F., & Liu, F. (2019). High-accuracy and fast determination of chromium content in rice leaves based on collinear dual-pulse laser-induced breakdown spectroscopy and chemometric methods. *Food Chemistry, 295*, 327–333.
Peng, J., He, Y., Zhao, Z., Jiang, J., Zhou, F., & Liu, F. (2019). Fast visualization of distribution of chromium in rice leaves by re-heating dual-pulse laser-induced breakdown spectroscopy and chemometric methods. *Environmental Pollution, 252*, 1125–1132.
Pérez-rodríguez, M., Dirchwolf, P. M., Silva, T. V., Villafañe, R. N., Neto, J. A. G., Pellerano, R. G., & Ferreira, E. C. (2019). Brown rice authenticity evaluation by spark discharge-laser-induced breakdown spectroscopy. *Food Chemistry, 297*, 124960.
Promchan, J., Günther, D., Siripinyanond, A., & Shiowatana, J. (2016). Elemental imaging and classifying rice grains by using laser ablation inductively coupled plasma mass spectrometry and linear discriminant analysis. *Journal of Cereal Science, 71*, 198–203.
R Core Team (2017). R: A language and environment for statistical computing. R Foundation for Statistical Computing. Accessed from https://www.r-project.org/.
Rehse, S. J., Salimnia, H., & Miziolek, A. W. (2012). Laser-induced breakdown spectroscopy (LIBS): An overview of recent progress and future potential for biomedical applications. *Journal of Medical Engineering & Technology, 36*, 77–89.
Sezer, B., Bilge, G., Sanal, T., Koksel, H., & Boyaci, I. H. (2017). A novel method for ash analysis in wheat milling fractions by using laser-induced breakdown spectroscopy. *Journal of Cereal Science, 78*, 33–38.
Sobral, H., & Robledo-martinez, A. (2016). Signal enhancement in laser-induced breakdown spectroscopy using fast square-pulse discharges. *Spectrochimica Acta Part B: Atomic Spectroscopy, 124*, 67–73.
Sun, L., Yu, H., Cong, Z., Lu, H., Cao, B., Zeng, P., ... Li, Y. (2018). Applications of laser-induced breakdown spectroscopy in the aluminum electrolysis industry. *Spectrochimica Acta Part B: Atomic Spectroscopy, 142*, 29–36.
Tiwari, J. K., Rastogi, N. K., Chandrakar, P. K., Sarawgi, A. K., & Verulkar, S. B. (2013). Identification of rice varieties through chemical tests. *Seed Research, 41*, 83–90.
Vieira, A. L., Silva, T. V., de Sousa, F. S. I., Senesi, G. S., Santos, D., Ferreira, E. C., & Neto, J. A. G. (2018). Determinations of phosphorus in fertilizers by spark discharge-assisted laser-induced breakdown spectroscopy. *Microchemical Journal, 139*, 322–326.
Wang, L., Liu, D., Pu, H., Sun, D., Gao, W., & Xiong, Z. (2015). Use of Hyperspectral Imaging to Discriminate the Variety and Quality of Rice. *Food Analytical Methods, 8*, 515–523.
Yang, P., Zhou, R., Zhang, W., Tang, S., Hao, Z., Li, X., ... Zeng, X. (2018). Laser-induced breakdown spectroscopy assisted chemometric methods for rice geographic origin classification. *Applied Optics, 57*, 8297–8302.
Yang, P., Zhu, Y., Yang, X., Li, J., Tang, S., Hao, Z., ... Lu, Y. (2018). Evaluation of sample preparation methods for rice geographic origin classification using laser-induced breakdown spectroscopy. *Journal of Cereal Science, 80*, 111–118.
Zhao-yan, L., Fang, C., Yi-bin, Y., & Xiu-qin, R. (2005). Identification of rice seed varieties using neural network. *Journal of Zhejiang University SCIENCE, 6B*, 1095–1100.
Zhu, L., Sun, J., Wu, G., Wang, Y., Zhang, H., & Wang, L. (2018). Identification of rice varieties and determination of their geographical origin in China using Raman spectroscopy. *Journal of Cereal Science, 82*, 175–182.
Zorov, N. B., Popov, A. M., Zaytsev, S. M., & Labutin, T. A. (2015). Qualitative and quantitative analysis of environmental samples by laser-induced breakdown spectrometry. *Russian Chemical Reviews, 84*, 1021–1050.

Anexo 13

ANALYTICAL LETTERS
2021, VOL. 54, NO. 12, 2009–2021
https://doi.org/10.1080/00032719.2020.1833021

Taylor & Francis
Taylor & Francis Group

PLASMA SPECTROSCOPY

Check for updates

Dry Ashing for Signal Enhancement in Laser-Induced Breakdown Spectroscopy (LIBS)

Maisa Cristina Lázaro[a], Carla Pereira de Morais[a], Tiago Varão Silva[a], Giorgio Saverio Senesi[b], Dário Santos Júnior[c], José Anchieta Gomes Neto[a], and Edilene Cristina Ferreira[a]

[a]Department of Analytical, Physical-Chemical and Inorganic Chemistry, São Paulo State University - UNESP, Araraquara, SP, Brazil; [b]Istituto per la Scienza e Tecnologia dei Plasmi (ISTP) Sede di Bari, CNR, Bari, Italy; [c]Exact and Earth Sciences Department, Federal University of São Paulo - UNIFESP, Diadema, SP, Brazil

ABSTRACT

Limited sensitivities of some laser-induced breakdown spectroscopy (LIBS) instruments may impair some applications. Although this drawback can be minimized by instrumental improvements, the complexity of operations and cost increases. In this work the principle of conventional dry ashing for sample preparation was evaluated as a simple and low-cost alternative to improve the sensitivity of LIBS analysis. Botanical, agronomic and industrial samples were analyzed. Samples were dry heated and their LIBS emission signals were evaluated. The results suggest the dry heating caused structural changes in samples providing greater availability of the analyte, which resulted in the enhancement of the signals. As proof of concept, the strategy was applied for Sr determination in plant leaves. Two Sr emission lines, enhanced after sample dry ashing were used. The developed methods showed similar performance featuring a good linear range (10 to 70 μg g^{-1}) with coefficient of correlations higher than 0.99. Additionally, the accurate determination of Sr in apple and peach leaves standard materials was achieved.

ARTICLE HISTORY
Received 11 June 2020
Accepted 2 October 2020

KEYWORDS
Dry ashing; dry heating; laser-induced breakdown spectroscopy (LIBS); sensitivity

Introduction

Laser-induced breakdown spectroscopy (LIBS) is an efficient optical emission technique allowing fast, low cost, direct, and clean multi-element analysis; thus, LIBS is a very attractive technique for many types of samples (Senesi et al. 2019; Nicolodelli et al. 2019; Bhatt, Angeyo, and Dehayem-Kamadjeu 2018; Lazic, Filella, and Turner 2018; Morais et al. 2017; Senesi 2014). Due to the microsampling (typically ng to μg), homogenization by milling is the most common pretreatment of solid samples performed to ensure representativeness (Miziolek, Palleschi, and Schechter 2006; Santos et al. 2012). However, this treatment is minimal compared to those required by traditional analytical techniques, which usually involve, besides homogenization, sample decomposition by oxidant reagents at high temperature and pressure.

CONTACT Edilene Cristina Ferreira edilene.c.ferreira@unesp.br Department of Analytical, Physical-Chemical and Inorganic Chemistry, São Paulo State University - UNESP, P.O. Box 355, 14801-970 Araraquara, SP, Brazil.

© 2020 Taylor & Francis Group, LLC

Despite the attractive analytical characteristics, LIBS shows low sensitivity compared to well establish analytical techniques, which make some applications unfeasible. According to Jantzi et al. (2016), although direct analysis is one of the most important advantages of LIBS, this may be the biggest factor that prevents it from becoming a mature analytical technique like laser ablation – inductively coupled plasma – mass spectrometry (LA-ICP-MS), inductively coupled plasma – optical emission spectrometry (ICP–OES), and X-ray fluorescence (XRF). For this reason, several strategies have been developed to improve the LIBS sensitivity by improving the emission processes in the plasma. The mentioned strategies include resonance-enhanced (RE)-LIBS (Goueguel et al. 2010), dual-pulse (DP)-LIBS (Khalil and Labib 2018; Ahmed and Baig 2009), LIBS assisted by laser-induced fluorescence (LIF) (Gao et al. 2018), microwave-assisted (MA)-LIBS (Viljanen et al. 2018), spark discharge-assisted (SD)-LIBS (Vieira et al. 2018), electric field-assisted LIBS (Jabbar et al. 2019) and ionization enhancement (Ahmed, Umar, and Baig 2019). Although the mentioned strategies have advantages, they demand complex instrumental configurations and sometimes high implementation costs. A lower-cost method proposed to improve LIBS sensitivity in metal analysis is nanoparticle enhanced (NE)-LIBS which consists in depositing silver nanoparticles on the sample surface before LIBS analysis that allow to obtain increases in emission signals of 1 to 2 orders of magnitude (De Giacomo et al. 2013; Dell'Aglio, Alrifai, and De Giacomo 2018). Even so, this methodology involves the use of expensive reagents to generate nanoparticles.

Solid sample breakdown is crucial to make the sample constituents, i.e., atoms, ions and molecules, available in the vapor phase and trigger the ionization processes. The free electrons produced in these processes are accelerated by the electric field generated by the laser pulse and can ionize neutral species by collisions. The increase of ionization results in an avalanche of electrons as well as plasma expansion (Singh and Thakur 2007). The breakdown threshold is usually defined to be the minimum laser irradiance (radiant power per area) needed to produce the plasma. Thus, at certain irradiance values, higher sample breakdown effectiveness would reduce the portion of energy needed for breakdown, so that the surplus power is available to increase the vaporized mass and plasma temperature, both of which contribute to increase the sensitivity of LIBS measurements. On these bases, a simplification of the sample matrix would be very favorable to improve the LIBS sensitivity.

Dry ashing is a traditional sample pretreatment used to oxidize organic matter by atmospheric oxygen and yield inorganic residues consisting of metal oxides and other involatile species, such as sulfates, phosphates and silicates, which are then solubilized in an acidic medium for further analysis (Krug 2016). Thus, the species that remain after sample treatment are structurally simpler as most of the matrix has been destroyed. Recently, a method based on the combination of sample pyrolysis and chemometric tools has been developed, which has improved the LIBS signal intensity of cadmium in lettuce leaves due to sample ashing (Chen et al. 2019).

Therefore, the aim of this study was to apply the dry ash principle for sample decomposition (here called dry heating, for samples which are not converted to ash) and evaluate its effect on LIBS emission signals from different types of samples, i.e., plant leaves, soil, and carbon steel alloy. A further objective was to develop a quantitative method using enhanced emission lines recorded in the LIBS spectrum of ashed samples.

Experimental

Samples

The citrus leaves were collected from a Brazilian orange cultivar from São Paulo State and cleaned in the laboratory with deionized water. The leaves were then lyophilized for 25 h using a L101 Liotop lyophilizer and then ground using a cryogenic mill (Spex 6750, Metuchen, NJ, USA). The grinding program consisted of 2.0 min pre-freezing, 3.0 min grinding, and 2.0 min freezing between the two milling steps.

The soil sample was a Brazilian soil of textural composition 270, 88 and 642 g kg^{-1} of clay, silt and sand, respectively, provided by a laboratory from Minas Gerais State, Brazil.

The steel sample consisted of a carbon steel alloy, i.e., the reference material IPT 14 A from the Institute of Technological Research, which is commercialized as filings.

Heating pretreatment and preparation of samples for LIBS analysis

The heating pretreatment of samples was performed in porcelain crucibles placed in a muffle furnace EDG, model EDG3P-S. To evaluate the main factors influencing organic matter decomposition, aliquots of 500 mg of dried and powdered citrus leaves were subjected to experiments outlined by a factorial design 2^3, so that a total of eight experiments were conducted in triplicate. The factors evaluated at two levels were temperature, heating rate, and heating time. The minimum and maximum levels evaluated for the heating time were 5 and 20 min, for heating rate 10 and 30 °C min^{-1}, and for temperature 100 °C and 600 °C. The maximum level of temperature was fixed at about the value usually necessary for organic matter decomposition (Krug 2016). The samples resulting from heating were cooled at room temperature and weighed to estimate the mass loss, which was restored by adding maize starch to each sample, in order to avoid the evaluation of preconcentration effects caused by the different applied heating procedure. Aiming to improve the precision, the mixture was homogenized in an agate mortar by a pestle for approximately 10 min. Next, aliquots of 200 mg were submitted to a 10-ton pressure for 30 s in a hydraulic press (GS15011, Specac, Swedesboro, NJ, USA), to obtain pellets of 13-mm diameter.

The dry heating of the soil was conducted in triplicate on 200 mg of sample by evaluating the same factors and following the same factorial design as described for citrus leaves. In particular, the minimum and maximum levels evaluated for the heating time were 5 and 20 min, for heating rate 10 and 30 °C min^{-1}, and for temperature 600 and 1000 °C (maximum work temperature). Higher temperatures were applied to the soil sample considering the lower quantity of organic matter and the greater recalcitrance of this type of sample. Similarly to citrus leaves, after heating, the samples were cooled at room temperature, weighed and treated with maize starch to restore the mass loss and a further 80 mg of cellulose (Sigma Aldrich, sigmacell type 101) as a binding agent to obtain a better compaction of the pellets that were prepared using the same procedure described above for leaves.

The heating pretreatment of the carbon steel alloy sample was performed on three replicates of 200 mg of sample at 1000 °C (maximum working temperature) with a

heating rate of 30 °C min^{-1} and a heating time of 20 min. After heating, the crucibles were removed from the muffle and cooled to room temperature. For this type of sample, no mass loss was observed; thus, after cooling, the samples were pelletized using the conditions previously described. For comparative purposes, three portions of 200 mg of steel alloy not subjected to the heating treatment were also converted into pellets.

LIBS instrumentation and measurements

The LIBS system consisted of a 1064 nm Q-switched Nd:YAG laser (Quantel, Big Sky Ultra 50, Bozeman, USA) operated at 50 mJ (maximum power energy) with pulse duration lower than 8 ns and repetition rate of up to 20 Hz, an optical fiber bundle, and four spectrometers Ocean Optics (HR 2000+, Dunedin, USA) featuring an optical resolution approximately 0.1 nm (full width at half maximum) and a spectral range from 200 nm to 630 nm. The delay time used for the analysis of plant leaves, soil and alloy were 2.5, 1 and 2 μs, respectively, and the gate delay was 1 ms (fixed time on the instrument). A micro-computer and an Ocean Optics LIBS software were used to control the laser pulse triggering, delay time, integration time, and spectral acquisition.

The LIBS spectra of plant leaves were acquired by impinging two laser pulses on 20 sites spread on each pellet surface, recording a total of 40 spectra. For the soil and steel alloy samples, 20 laser pulses were spread on each side of the pellets. The sum of all signal intensities measured in the LIBS spectrum (total emission intensities, TEI) was considered to be the response of each experiment. The software Statgraphics Centurion 18 (18.1.12 – 64 bits evaluation version) was used to analyze the effects of the studied factors on the responses.

Quantitative Sr determination in citrus leaves

As proof-of-concept of the potential of the dry ashing in LIBS analysis, two methods were developed for the quantitative determination of Sr in leaf samples by using calibration standards of tomato leaves (SRM 1573a) containing 85 μg g^{-1}. To avoid matrix effects and characterize matrix matching, tomato leaves were used after submitting them to the heating pretreatment in the same optimized conditions used for citrus leaves, as heating may significantly change the sample matrix. For this purpose, 600 mg of tomato leaves were heated in the muffle oven and the mass loss was restored by adding cellulose to keep constant and known the Sr concentration in the material. The SRM added with cellulose to obtain Sr concentrations of 10, 20, 30, 50, 60 and 70 μg g^{-1} with a final mass of 200 mg was homogenized for 10 min in agate mortar using a pestle. Analytical blank (pure cellulose) and samples were pelletized in triplicates.

LIBS spectra were acquired by firing two laser pulses on 20 different sites of each sample surface obtaining a representative mean spectrum for each sample. The intensity of the emission line of Sr II at 407.8 nm and Sr I at 460.7 nm were set for quantitative analysis. The methods were validated using the NIST standard reference material of apple leaves (SRM 1515) and peach leaves (SRM 1547), which contain 25 ± 2 μg g^{-1} and 53 ± 5 μg g^{-1} of Sr, respectively. Then the methods were applied for Sr determination in citrus leaves. Both SRMs and citrus leaf samples were submitted to the heating

pretreatment, cellulose addition for restoring mass losses, homogenization and LIBS analysis in similar conditions.

As the calibration models based on the linear correlation between area or peak intensity and Sr concentrations in the standards were unsatisfactory to predict Sr concentrations in apple and peach leaves SRMs, another strategy, i.e., a spectral processing based on Sr signal normalization, was attempted to overcome the matrix effects. In particular, to minimize the spectral signal fluctuations, the emission lines of Sr were normalized by the signal of the molecular emission of diatomic CN (0,0) at 388.4 nm, which was found to be free from spectral interference. This approach was based on the following considerations: (i) the greater intensities of CN emission in the LIBS plasma under air conditions is formed by recombinant processes, i.e., C in the sample and N in the surrounding atmosphere; (ii) C in the samples originates from cellulose, as the original organic matter has been destroyed during heating; and (iii) the quantity of CN formed under these conditions is approximately constant in samples and standards.

Results and discussion

Effect of ashing pretreatment on citrus leaves

The averaged total emission intensities (TEIs) obtained for the experiments performed to evaluate dry heating parameters (Table 1) were statistically analyzed. The results showed that significant positive standardized effects, at 95% confidence level, were observed for temperature and heating time. Additionally, significant effects were also observed to the following parameter interactions: temperature with heating time and heating rate with heating time (Figure 1).

Although the higher total emission intensities were obtained at the higher level of the temperature and heating time, the presence of significant interaction effects suggested that the main effects should be interpreted by considering the variables together. As shown in Table 1, the highest average TEI value was obtained using the higher heating time, heating rate and temperature simultaneously (experiment 8). Thus, these variables were fixed at 20 min, 30 °C min^{-1} and 600 °C, respectively.

Under fixed conditions, sample ashes were obtained. According to the initial hypothesis, the ashes containing the analytes in simplified forms (phosphates, sulfates and silicates) caused a general increase in the analytical signals obtained by LIBS, representing

Table 1. Total emission intensity from factorial design (2^3) to evaluate the influence of thermal pretreatment upon citrus leaves.

Experiment	Temperature (°C)	Heating rate (°C min^{-1})	Heating time (min)	Total emission intensity as mean ± standard deviation
1	100	10	5	$(3.93 \pm 0.27) \times 10^4$
2	600	10	5	$(3.02 \pm 0.40) \times 10^5$
3	100	30	5	$(3.95 \pm 0.28) \times 10^4$
4	600	30	5	$(1.85 \pm 0.59) \times 10^5$
5	100	10	20	$(3.79 \pm 0.09) \times 10^4$
6	600	10	20	$(2.79 \pm 0.41) \times 10^5$
7	100	30	20	$(4.02 \pm 0.32) \times 10^4$
8	600	30	20	$(3.77 \pm 0.24) \times 10^5$
Without heat	–	–	–	$(1.17 \pm 0.21) \times 10^4$

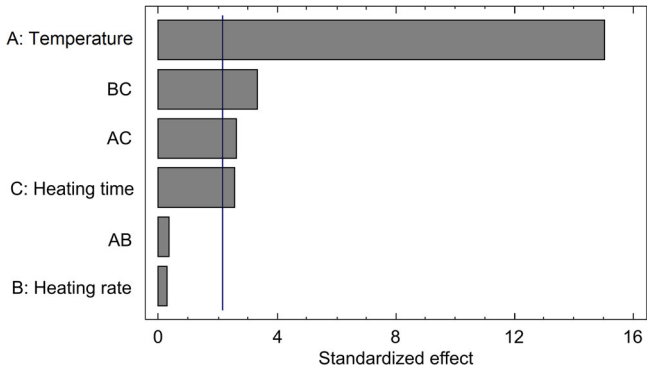


Figure 1. Standardized Pareto chart for the total emission intensities after the dry ashing of citrus leaves.

an increase of 3123% in the total emission intensity. To exemplify the signals enhancement obtained for this class of sample, spectra of citrus leaves either submitted or not to the optimized ashing pretreatment, recorded in the region of the Ca (I) emission line at 612.1 nm and of the Sr (II) emission line at 407.8 nm are shown in the Figures 2a and 2b, respectively. An increase of approximately 47 times was observed for the Ca I line, whereas the Sr (II) line appeared only after the sample dry ashing. The dry ashing pretreatment appeared very efficient to improve the sensitivity of LIBS measurements in this class of samples. The results suggest that the greater availability of analytes in the pretreated samples made available a surplus of energy that contributed to obtaining plasma more concentrated in the excited species.

Effect of heating pretreatment on soil

The statistical analysis of LIBS experimental measurements achieved for soil (Table 2) showed that at 95% confidence level, a significant and positive effect was obtained only for the heating time (Figure 3), which indicated that the highest TEI was obtained after 20 min heating at a temperature of 1000 °C and heating rate of 10 °C min^{-1} (experiment 6, Table 2). Under these conditions, the soil sample showed a general LIBS signals enhancement with an increase of 75% in the TEI.

To exemplify the signal enhancements for soil, a Na line and a Ti line were selected. The intensity of the Na (I) emission line at 589.5 nm was four times larger and that of the Ti (I) line at 464.0 nm 1.8 times larger in dry heated samples, as shown in Figures 4a and 4b, respectively. These results suggested that, although soil contains low levels of organic matter, the LIBS analytical sensitivity was increased by dry ashing. The higher temperature required for the soil pretreatment compared to that required by leaf sample may be due to phase changes of crystalline structures resulting in the release of the analytes. Probably due to the smaller content of easily destructible matter and experimental limited maximum temperature (1000 °C) for phase changes, this type of sample showed lower signal enhancements compared to leaves.

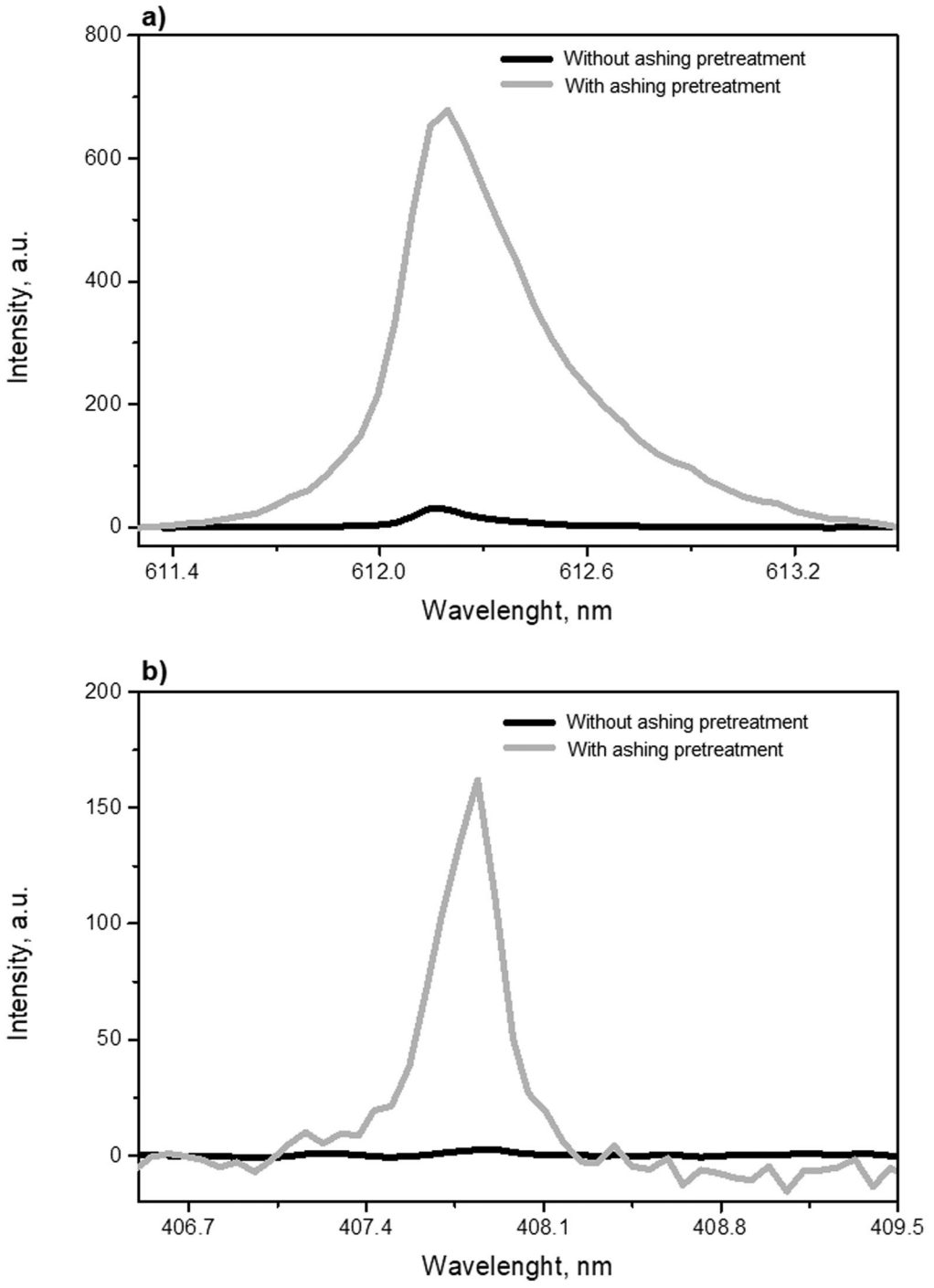


Figure 2. Averaged LIBS spectra (n = 3) of citrus leaf samples with and without dry ashing: (a) Ca (I) at 612.1 nm and (b) Sr (II) at 407.8 nm.

Table 2. Total emission intensity from the factorial design (2^3) to evaluate thermal pretreatment of the soil sample.

Experiment	Temperature (°C)	Heating rate (°C min^{-1})	Heating time (min)	Total emission intensity as mean ± standard deviation
1	600	10	5	$(3.15 \pm 0.28) \times 10^5$
2	1000	10	5	$(3.74 \pm 0.18) \times 10^5$
3	600	30	5	$(3.32 \pm 0.30) \times 10^5$
4	1000	30	5	$(3.91 \pm 0.33) \times 10^5$
5	600	10	20	$(3.41 \pm 0.44) \times 10^5$
6	1000	10	20	$(4.05 \pm 0.25) \times 10^5$
7	600	30	20	$(3.52 \pm 0.29) \times 10^5$
8	1000	30	20	$(3.87 \pm 0.29) \times 10^5$
Without heat	–	–	–	$(2.21 \pm 0.24) \times 10^5$

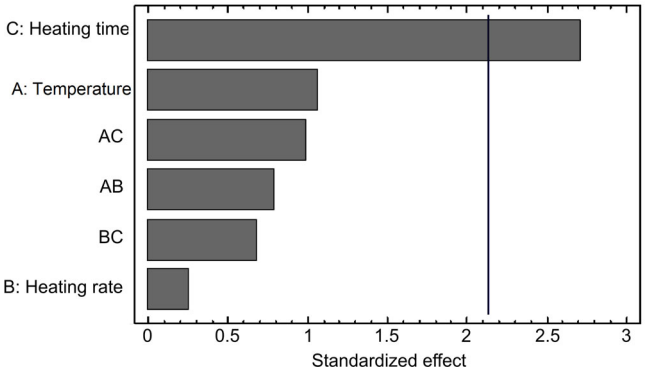


Figure 3. Standardized Pareto chart for total emission intensities after the soil dry heating.

Effect of heating pretreatment on the carbon steel alloy

General LIBS signal enhancements were also observed after steel alloy dry heating, which showed an increase of 33% in the total emission intensities. As an example of the signal enhancement in this sample, the atomic line of Fe at 489.22 nm was considered. The peak intensity of this line for the sample heated to 1000 °C was approximately 2.7 times higher than measured for the unheated sample (Figure 5). These results suggest that the sample matrix changed by heating to a form apparently easier to be broken down with a better release of analytes during the LIBS processes.

In evaluating lower resistance alloys and lower temperatures, Darbani et al. (2014) concluded that signals enhancement was due to an increase in the ablation ratio. Additionally, according to Connor, Urban, and Kaufmann (2008), the transformation of iron alloys involves molecular structural modifications that depend on the composition and occurs at a specific temperature. As carbon steel in the ferrite phase, i.e., a solution of approximately 0.4% of solid carbon in α-iron, is heated to 1000 °C, the phase changes to austenite, i.e., a solid carbon solution in γ-iron (Dosset and Boyer 2006). Furthermore, variation in the cooling rate of the heated material may also influence its properties. In particular, when the heating process yields a phase transformation to austenite, a slow cooling rate tends to return iron to its original structure, i.e., α-iron, whereas a rapid and non-isothermal cooling process may lead to a non-equilibrium

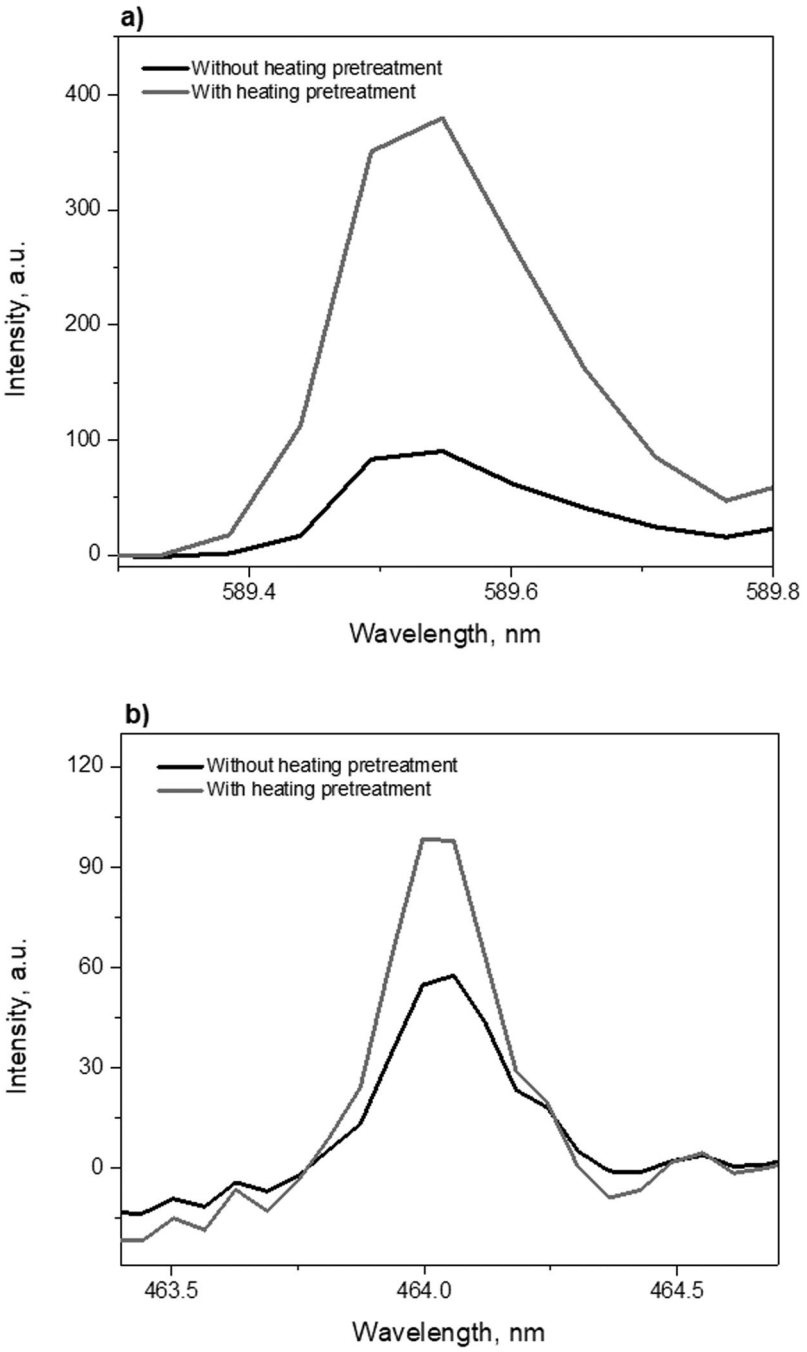


Figure 4. Averaged LIBS spectra (n = 3) of the soil sample with and without dry heating: (a) Na (I) at 589.5 nm and (b) Ti (I) at 464.0 nm.

metastable phase, such as martensite, which features a lower ductility and greater brittleness (Connor, Urban, and Kaufmann 2008). In this work, cooling was performed in an uncontrolled way yielding a sample of apparent greater fragility which is suggested

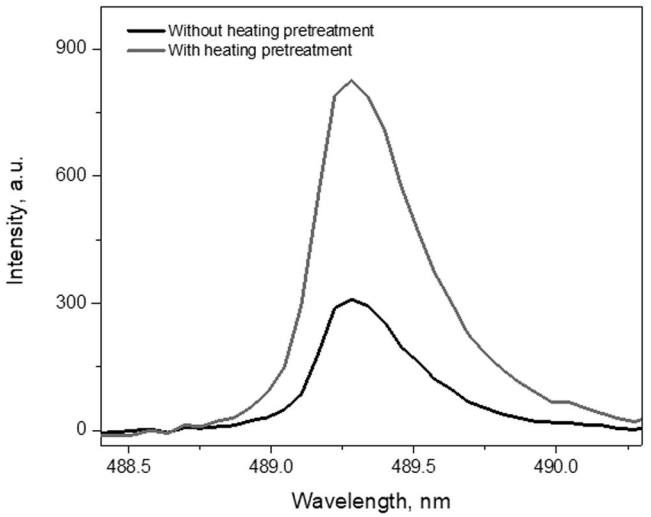


Figure 5. Averaged LIBS spectra (n = 3) of the iron-carbon alloy with and without dry heating in the spectral region of the Fe atomic line at 489.2 nm.

to be martensite. Thus, the structural simplification of the sample achieved by dry heating and the consequent increase in ablation ratio would support the improvement of sensitivity observed in the alloy sample.

The magnitude of the signal enhancements in this case was the lowest of the three samples evaluated. However, soil and alloy showed more similar enhancements compared to the leaf samples. These results confirmed the hypothesis that materials that depend on phase transitions to release the analyte were limited by the working temperatures.

Quantitative Sr determination in citrus leaves

The quantitative determination of Sr in citrus leaves was chosen for proof-of-concept measurements. For this aim, two Sr lines were chosen: (i) Sr II 407.8 nm that appeared only in the spectrum of ashed sample and (ii) Sr I 460.7 nm whose original intensity was increased 39 times after sample dry ashing. The use of a LIBS system with a higher energy laser and/or an iCCD detector would provide good signals for these lines, without the sample ashing. Although by applying this sample pretreatment, the intensities will also be increased allowing the determination of very low Sr concentrations.

The calibration curves obtained for dry ashed tomato leaves SRM using the intensities of the mentioned emission lines normalized by the intensity of the CN signal are shown in Figure 6. The curves are very similar with a slightly better analytical performance for that fitted using intensities of Sr II at 407.8 nm. Both curves showed a correlation coefficient greater than 0.99 and a linear range from 0.00 to 70.0 μg g^{-1}. The sensitivity (slope) for the Sr II and Sr I lines were, 0.07982 and 0.05465 g μg $^{-1}$, respectively. The limits of detection (LOD) were 3.00 μg g^{-1} and 4.00 μg g^{-1} and the limits of quantification (LOQ) 10 and 14 μg g^{-1}. Using laser ablation – inductively coupled plasma – mass spectrometry (LA-ICP-MS) for Sr determination in plant leaves SRMs, Cizdziel, Bu, and

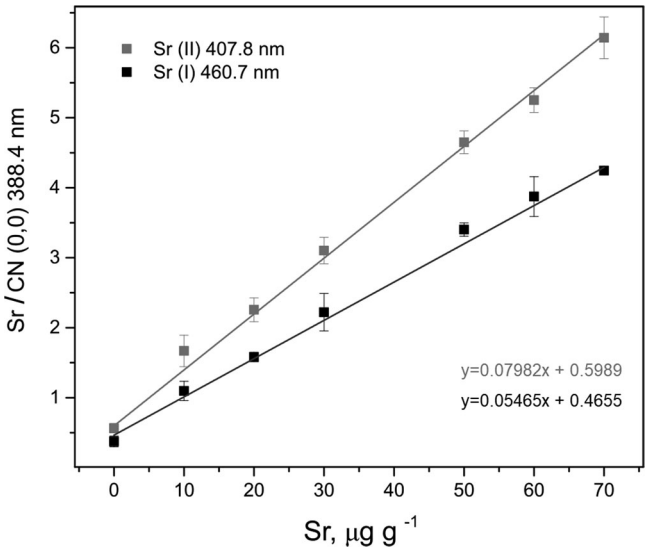


Figure 6. Calibration curves for the ratio of emission signals of Sr/CN as a function of the Sr concentration in tomato leaves.

Nowinski (2012) obtained a limit of detection of 2.3 μg g^{-1}, which is very close to the values achieved by LIBS. Therefore, sample dry ashing allows LIBS performance to be comparable to a well-established technique with high sensitivity.

To validate the proposed methods, Sr was determined in apple and peach leaf SRMs. Using the Sr II line, the Sr concentrations measured in apple and peach leaves were $21.1 \pm 2.6\,\mu g\ g^{-1}$ and $53.9 \pm 8.6\,\mu g\ g^{-1}$, respectively. Using Sr I, the values were $24.8 \pm 4.0\,\mu g\ g^{-1}$ and $55.7 \pm 4.1\,\mu g\ g^{-1}$. Thus, the use of either line provided results which were in good agreement with the certified values at 95% confidence level.

For the citrus leaf sample, Sr concentrations determined using Sr I and Sr II were $55.9 \pm 4.5\,\mu g\ g^{-1}$ and $61.1 \pm 4.0\,\mu g\ g^{-1}$, respectively, which were statistically consistent at 95% confidence level. These results showed that the sensitivity enhancement achieved by the dry ashing of the sample confirmed LIBS to be an accurate and precise analytical technique for determining Sr in the plant leaves.

Conclusions

The results of this work showed that heating pretreatment can induce changes in the sample which renders the analytes more available to the processes occurring during LIBS analysis and thereby provides a marked increase of sensitivity and improving LIBS qualitative and quantitative outcomes. However, the enhancement of the signals depended intrinsically on the nature of the sample. Greater signal enhancements were observed for samples rich in organic matter, such as plant leaves, which are easily destroyed by increased temperature. Samples with more recalcitrant structures needed higher temperatures to structural changes able to yield a higher analyte release for LIBS analysis. The application of dry ashing to the quantitative determination of Sr in plant leaves yielded limits of detection similar to those obtained by LA-ICP-MS even using a simple LIBS instrument. Thus, whether dry ashing pretreatment is applied to samples to

be analyzed by a more sophisticated LIBS system, trace analysis could be performed. The dry heating method is simple and does not require the use of any chemical reagent and therefore maintains one of the primary advantages of LIBS, i.e., no chemical residue generation.

Funding

This research received financial support from Conselho Nacional de Desenvolvimento Científico e Tecnológico (CNPq) through a scholarship to M.C.L. and through research grants to E.C.F. (Grant # 308200/2018-7) and J.A.G.N. (Grant #302414/2017-7).

References

Ahmed, R., and M. A. Baig. 2009. A comparative study of single and double pulse laser induced breakdown spectroscopy. *Journal of Applied Physics* 106 (3):033307. doi:10.1063/1.3190516.

Ahmed, R., Z. A. Umar, and M. A. Baig. 2019. Emission intensity enhancement by re-ionization of Nd:YAG laser-produced plasma using a nitrogen laser. *Laser Physics* 29 (5):055701. doi:10.1088/1555-6611/ab05d0.

Bhatt, B., K. H. Angeyo, and A. Dehayem-Kamadjeu. 2018. LIBS development methodology for forensic nuclear materials analysis. *Analytical Methods* 10 (7):791–8. doi:10.1039/C7AY02520C.

Chen, Z., T. Shen, J. Yao, W. Wang, F. Liu, X. Li, and Y. He. 2019. Signal enhancement of cadmium in lettuce using laser-induced breakdown spectroscopy combined with pyrolysis process. *Molecules* 24 (13):2517. doi:10.3390/molecules24132517.

Cizdziel, J., K. Bu, and P. Nowinski. 2012. Determination of elements in situ in green leaves by laser ablation ICP-MS using pressed reference materials for calibration. *Analytical Methods* 4 (2):564–9. doi:10.1039/C1AY05577A.

Connor, R. J., M. J. Urban, and E. J. Kaufmann. 2008. Proposed revisions to FHWA manual. In: Margaret B. Hagood Andrea Briere (Eds.), *Heat-straightening repair of damaged steel bridge girders: Fatigue and fracture performance*, 108–29. Washington, DC: The National Academies Press. doi:10.17226/23087.

Darbani, S. M. R., M. Ghezelbash, A. E. Majd, M. Soltanolkotabi, and H. Saghafifar. 2014. Temperature effect on the optical emission intensity in laser induced breakdown spectroscopy of super alloys. *Journal of the European Optical Society: Rapid Publications* 9:14058. doi:10.2971/jeos.2014.14058.

De Giacomo, A., R. Gaudiuso, C. Koral, M. Dell'Aglio, and O. De Pascale. 2013. Nanoparticle-enhanced laser-induced breakdown spectroscopy of metallic samples. *Analytical Chemistry* 85 (21):10180–7. doi:10.1021/ac4016165.

Dell'Aglio, M., R. Alrifai, and A. De Giacomo. 2018. Nanoparticle Enhanced Laser Induced Breakdown Spectroscopy (NELIBS), a first review. *Spectrochimica Acta Part B: Atomic Spectroscopy* 148:105–12. doi:10.1016/j.sab.2018.06.008.

Dosset, J. L., and H. E. Boyer. 2006. *Practical heat treating*. 2nd ed. Ohio: ASM International. doi:10.31399/asm.tb.pht2.9781627082624.

Gao, P., P. Yang, R. Zhou, S. Ma, W. Zhang, Z. Hao, S. Tang, X. Li, and X. Zeng. 2018. Determination of antimony in soil using laser-induced breakdown spectroscopy assisted with laser-induced fluorescence. *Applied Optics* 57 (30):8942–6. doi:10.1364/ao.57.008942.

Goueguel, C., S. Laville, F. Vidal, M. Sabsabi, and M. Chaker. 2010. Investigation of resonance-enhanced laser-induced breakdown spectroscopy for analysis of aluminium alloys. *Journal of Analytical Atomic Spectrometry* 25 (5):635–44. doi:10.1039/b927013b.

Jabbar, A., M. Akhtar, S. Mehmood, N. Ahmed, Z. A. Umar, R. Ahmed, and M. A. Baig. 2019. On the detection of heavy elements in the *Euphorbia indica* plant using laser-induced

breakdown spectroscopy and laser ablation time of flight mass spectrometry. *Journal of Analytical Atomic Spectrometry* 34 (5):954–62. doi:10.1039/C9JA00053D.

Jantzi, S. C., V. Motto-Ros, F. Trichard, Y. Markushin, N. Melikechi, and A. De Giacomo. 2016. Sample treatment and preparation for laser-induced breakdown spectroscopy. *Spectrochimica Acta Part B: Atomic Spectroscopy* 115:52–63. doi:10.1016/j.sab.2015.11.002.

Khalil, A. A. I., and O. A. Labib. 2018. Detection of micro-toxic elements in commercial coffee brands using optimized dual-pulsed laser-induced spectral analysis spectrometry. *Applied Optics* 57 (23):6729–41. doi:10.1364/AO.57.006729.

Krug, F. J. 2016. *Métodos de preparo de amostras para análise elementar [Our environment: Sample preparation methods for elementary analysis]*, ed. F. J. Krug and F. R. P. Rocha. São Paulo: EditSBQ - Sociedade Brasileira de Química. Decomposição de materiais orgânicos por combustão. pp.387–472.

Lazic, V., M. Filella, and A. Turner. 2018. Determination of antimony concentrations in widely used plastic objects by laser induced breakdown spectroscopy (LIBS). *Journal of Analytical Atomic Spectrometry* 33 (11):1917–24. doi:10.1039/C8JA00181B.

Miziolek, A. W., V. Palleschi, and I. Schechter. 2006. Laser-Induced Breakdown Spectroscopy (LIBS): Fundamentals and Applications. Cambridge, UK: Cambridge University Press.

Morais, C. P. D., A. I. Barros, D. Santos Júnior, C. A. Ribeiro, M. S. Crespi, G. S. Senesi, J. A. Gomes Neto, and E. C. Ferreira. 2017. Calcium determination in biochar-based fertilizers by laser-induced breakdown spectroscopy using sodium as internal standard. *Microchemical Journal* 134:370–3. doi:10.1016/j.microc.2017.07.005.

Nicolodelli, G., J. Cabral, C. R. Menegatti, B. Marangoni, and G. S. Senesi. 2019. Recent advances and future trends in LIBS applications to agricultural materials and their food derivatives: An overview of developments in thel decade (2010–2019). *TrAC Trends in Analytical Chemistry* 115:70–82. doi:10.1016/j.trac.2019.03.032.

Santos, D., L. C. Nunes, G. G. A. De Carvalho, M. D. S. Gomes, P. F. de Souza, F. D. O. Leme, L. G. C. dos Santos, and F. J. Krug. 2012. Laser-induced breakdown spectroscopy for analysis of plant materials: A review. *Spectrochimica Acta Part B: Atomic Spectroscopy* 71–72:3–13. doi:10.1016/j.sab.2012.05.005.

Senesi, G. S. 2014. Laser-Induced Breakdown Spectroscopy (LIBS) applied to terrestrial and extra-terrestrial analogue geomaterials with emphasis to minerals and rocks. Earth-Science Reviews 139:231–67. doi:10.1016/j.earscirev.2014.09.008.

Senesi, G. S., J. Cabral, C. R. Menegatti, B. Marangoni, and G. Nicolodelli. 2019. Recent advances and future trends in LIBS applications to agricultural materials and their food derivatives: An overview of developments in thel decade (2010–2019). Part II. Crop plants and their food derivatives. *TrAC Trends in Analytical Chemistry* 118:453–69. doi:10.1016/j.trac.2019.05.052.

Singh, J. P., and S. N. Thakur. 2007. *Laser-induced breakdown spectroscopy*. Amsterdam: Elsevier.

Vieira, A. L., T. V. Silva, F. S. I. de Sousa, G. S. Senesi, D. S. Júnior, E. C. Ferreira, and J. A. G. Neto. 2018. Determinations of phosphorus in fertilizers by spark discharge-assisted laser-induced breakdown spectroscopy. *Microchemical Journal* 139:322–6. doi:10.1016/j.microc.2018.03.011.

Viljanen, J., H. Zhao, Z. Zhang, J. Toivonen, and Z. T. Alwahabi. 2018. Real-time release of Na, K and Ca during thermal conversion of biomass using quantitative microwave-assisted laser-induced breakdown spectroscopy. *Spectrochimica Acta Part B: Atomic Spectroscopy* 149:76–83. doi:10.1016/j.sab.2018.07.022.

Anexo 14

Food Chemistry 311 (2020) 125886

Contents lists available at ScienceDirect

Food Chemistry

journal homepage: www.elsevier.com/locate/foodchem

Detection and quantification of adulterants in honey by LIBS

Maurílio Gustavo Nespeca[a,*], Alan Lima Vieira[a], Dário Santos Júnior[b], José Anchieta Gomes Neto[a], Edilene Cristina Ferreira[a]

[a] Analytical Chemistry Department, Institute of Chemistry, São Paulo State University – UNESP, Prof. Francisco Degni 55, 14800-060 Araraquara, SP, Brazil
[b] Department of Chemistry, Federal University of São Paulo – UNIFESP, R. São Nicolau 210, 09913-030 Diadema, SP, Brazil

ARTICLE INFO

Keywords:
Laser-induced breakdown spectroscopy
Honey
Adulteration
Spark discharge
Variable selection
Multivariate filters
Multivariate analysis

ABSTRACT

The present work proposes methods for detection and quantification of honey adulterants using laser-induced breakdown spectroscopy (LIBS). The sample set consisted of 6 pure honey from different botanical sources, 2 sweetener syrups and 228 fortified samples. The spectra acquired using a spark discharge coupled to the LIBS system were used for the development of the PLS-DA (classification) and PLS (calibration) models. Several data preprocessing and variable selection methods were evaluated to obtain the best fit. The detection of adulterants was performed with 100% of accuracy. The quantification of adulterants was possible through a PLS model with the variables selected by iPLS. The PLS model was validated with external samples and presented good accuracy, selectivity, sensitivity, and linearity. The proposed methods highlighted the potential of the LIBS technique for honey authenticity certification, providing fast, simple, and clean determinations since no sample pretreatment was required.

1. Introduction

Worldwide, natural honey is a product of great added value, and its distribution by the main world producers have been growing annually (Amiry, Esmaiili, & Alizadeh, 2017; Workman, 2018). In the last five years, countries such as Ukraine, Brazil, and New Zealand have shown a significant increase in exportation due to the greater acceptance of honey quality by the European and North American markets (Guimarães, 2018; Workman, 2018).

Since honey is a value-added food, this product is susceptible to adulteration by the addition of high fructose corn syrup (HFCS), sugar cane syrup, among other lower cost products, for illicit benefits (Pilizota & Tiban, 2009). The honey adulteration affects not only the consumers who seek a product of nutritional and therapeutic value but also makes the market disloyal to the producers of high-quality honey. Hence, the monitoring of honey composition is crucial to keep its quality and a fair competitive market. On the other hand, verification of honey authenticity is a difficult task due to its complex composition. Honey may contain more than 180 substances, mostly sugars (33.3–43.0%(w/w) of fructose, 25.2–35.3%(w/w) of glucose, 0–2%(w/w) sucrose, and other more complex sugars) and water. At lower amounts, there are minerals (K, Mg, Ca, Na, Fe, Zn, among others), vitamins, proteins, free amino acids, enzymes, and phenolic compounds in its composition (Biluca, Braghini, Gonzaga, Costa, & Fett, 2016; Kek, Chin, Tan, Yusof, & Chua, 2017). According to Codex Alimentarius (2001), the adulteration of honey with sugar cane or corn syrups is verified by stable carbon isotope ratio analysis or by the sugar profile determined by HPLC. However, these methods include costly instruments, complex techniques, sample preparation, and time-consuming analysis (Das et al., 2017; Wang, Kliks, Jun, Jackson, & Li, 2010).

In the last two decades, several alternative methods for the identification and quantification of adulterants (sweetener syrups) have been successfully developed using different spectroscopic techniques, such as Fourier transform mid-infrared (FT-IR) (Gallardo-Velázquez, Osorio-Revilla, de Loa, & Rivera-Espinoza, 2009; Ruoff et al., 2006), near infrared (NIR) (Bázár et al., 2016), visible and near infrared (vis-NIR) (Ferreiro-González et al., 2018), Raman (Chakraborty et al., 2012; Oroian, Ropciuc, & Paduret, 2018), Hyperspectral Imagining (Shafiee et al., 2016), and proton nuclear magnetic resonance (^{1}H NMR) (Spiteri et al., 2015). The developed methods have been consistent with traditional methods, but they are much faster and perform analysis without waste generation.

Despite the increasing of fast and clean methods for honey analysis, there is no report in the literature about the use of laser-induced breakdown spectroscopy (LIBS) for the detection of honey adulteration. Recently, Se, Ghoshal, and Wahab (2019) published the first study on honey analysis using LIBS, which demonstrated the potential of the technique for Ca, Mg and Na determination (Se et al., 2019). Unlike the

* Corresponding author.
E-mail address: maurilio.nespeca@unesp.br (M.G. Nespeca).

https://doi.org/10.1016/j.foodchem.2019.125886
Received 22 April 2019; Received in revised form 9 August 2019; Accepted 9 November 2019
Available online 14 November 2019
0308-8146/ © 2019 Elsevier Ltd. All rights reserved.

analytical techniques mentioned above, LIBS can simultaneously determine several elements, including those from organic and inorganic molecules (El Haddad, Canioni, & Bousquet, 2014). The LIBS application for detecting adulterants in honey is attractive since the analysis is fast, low-cost, waste-free, and does not require sample preparation. Although LIBS presents numerous applications, it is still little explored in food analysis (Alfarraj, Sanghapi, Bhatt, Yueh, & Singh, 2018; Bilge, Velioglu, Sezer, Eseller, & Boyaci, 2016; Silva, Torres Filho, & Resende, 2018), especially for viscous products like honey. Since the chemical profile of sweetener syrups differs from the honey in several aspects, such as mineral content, sugars, protein, enzymes, etc. (Abdel-Aal, Ziena, & Youssef, 1993; Pilando & Wrolstad, 1992), the presence of adulterants should influence the honey spectral profile. Moreover, many studies have demonstrated the potential of LIBS for determination of physicochemical parameters or class discrimination through the correlation with the fingerprint profile of samples (Biluca et al., 2016; Schenk & Almirall, 2010).

The application of spectroscopic techniques to obtain information about the honey depends on the chemometric tools due to the multivariate nature of the spectral data. Among the multivariate regression methods, the partial least squares (PLS) was used in several studies of quantification of honey adulterants by spectroscopic techniques (Bázár et al., 2016; Das et al., 2017; Ferreiro-González et al., 2018; Gallardo-Velázquez et al., 2009; Oroian et al., 2018). The coefficients of determination (R^2) above 90% obtained by the methods demonstrated the linear relationship between the adulterant content and the analytical signal in different spectroscopic techniques. Supervised methods, such as soft independent modelling of class analogies (SIMCA) (Gallardo-Velázquez et al., 2009), linear discriminant analysis (LDA) (Ferreiro-González et al., 2018; Paradkar, Irudayaraj, & Sakhamuri, 2002), partial least square linear discriminant analysis (PLS-LDA) (Oroian et al., 2018), canonical variate analysis (CVA) (Paradkar et al., 2002) and artificial neural networks (ANN) (Shafiee et al., 2016), have also been evaluated for the detection of adulterants in honey through spectral data. These studies are indicatives of the increasing consolidation of spectroscopic techniques associated with multivariate methods in the analysis of honey adulteration.

In view of the susceptibility of honey to fraud and the potential of the LIBS technique associated with chemometric methods to extract honey compositional information, the present work aimed at the detection and quantification of adulterants in honey samples using LIBS analysis associated with multivariate methods.

2. Material and methods

2.1. Samples

Six samples of honey from three different botanical origins (2 *Eucalyptus* spp., 2 *Citrus sinensis*, and 2 multifloral samples) were obtained from two producers located in Araraquara, São Paulo State, Brazil (21°47′41″ S, 48°10′36″ W). According to the Köppen-Geiger classification, the regional climate is tropical wet and dry (Aw) and the honeys were produced by bees of the *Apis mellifera* species. The honeys were collected in 2018, and the floral source was provided by the producer.

The adulterants chosen were high fructose corn syrup (HFCS) and sugar cane syrup (molasses) due to their greater availability in Brazilian market. Two commercial syrup samples were purchased on the local market in Araraquara city. The HFCS and sugar cane syrup samples were produced, respectively, in São Bernardo do Campo and Campos de Jordão, Brazil. The honey samples were fortified with the sweetener syrups in the range of 5–95%(w/w) with an increment of 5%(w/w) to access the relationship between analytical parameters and concentration levels (Ferreiro-González et al., 2018). Thus, the sample set consisted of 6 pure honeys, 2 sweetener syrups, and 228 adulterated honeys, totaling in 236 samples.

2.2. LIBS analysis

The spectra were acquired using a LIBS system designed for solid analysis, equipped with a 1064 nm Q-switched Nd:YAG laser (Quantel, Big Sky Ultra 50, Bozeman, USA) operated at 50 mJ maximum power energy with pulse duration less than 8 ns, an optical fiber bundle, four spectrometers Ocean Optics (HR2000+, Dunedin, USA), featuring an optical resolution of 0.1 nm (full width at half maximum), and a spectral range from 200 nm to 630 nm. The integration time and the Q-Switched delay used for spectra acquisition were 1 ms and 2.5 μs, respectively.

The sample was placed in a polyethylene flask with a maximum capacity of 1 mL. The flask was placed in the sample holder of LIBS system, which can be moved in the x-y directions. The volume of sample in the flask was set to keep the sample surface in the focal point of the waist of the laser beam (lens to sample distance equal to 12 cm). An inner video camera was installed in the sampling chamber to monitor the analyses. The experiments were performed in air and ambient pressure, and a spark discharge system was coupled to the LIBS system aiming to re-heating plasma and increase emission lines detectability. The spark discharge was obtained using two cylindrical pure tungsten electrodes (100 mm × 2.6 mm), positioned 4 mm of distance between them and 2 mm above the sample surface, and the DC voltage signal was 4600 V. More details on the electric discharge system can be found in (Vieira et al., 2018).

2.3. Chemometrics analysis

2.3.1. Preliminary analysis

Prior to the development of prediction models, the best number of replicates was verified to obtain the best fit. For this purpose, 20 replicates were obtained from 18 samples prepared with the *Eucalyptus* honey sample and HFCS in the concentration range of 0–100%(w/w). The best replicate number was evaluated through three PLS models developed with the average spectra of 6 replicates, 12 replicates, and 20 replicates. Since a small number of samples was used in the preliminary evaluation, the models were compared by the root-mean-square error of cross-validation (RMSECV). The data were preprocessed using multiplicative scatter correction (MSC) for normalization and then mean centered (Eum et al., 2018). All chemometric analyses were performed using the MATLAB 2013a (Mathworks) software associated with the PLS toolbox 7.3.1. (Eigenvector Research Inc.).

2.3.2. Classification models

The detection of adulterants in honey by LIBS analysis was evaluated using classification models developed by the Partial Least Squares Discriminant Analysis (PLS-DA) method. The PLS-DA is a supervised and probabilistic pattern recognition method based on the PLS algorithm, but coded classes are used as dependent vector (**y**) (Brereton & Lloyd, 2014). The PLS method maximizes the relationship between the scores and the **y** through latent variables (LV), which represent the best directions to discriminate the classes. Thus, the LV number should be determined through the values of RMSEC, RMSECV, and RMSEP to provide the best fit and avoid model overfitting. More details on the PLS-DA method can be found in (Brereton & Lloyd, 2014).

The full sample set was not used in the classification models due to the discrepancy between the number of pure and adulterated honey samples. So, the sample set consisted of 6 honeys samples (unadulterated class) plus 36 fortified samples (adulterated class). For each honey, the samples were fortified with each syrup at three concentration levels, 25%(w/w), 50%(w/w), and 75%(w/w). Then, the sample set was divided into 28 calibration samples and 14 validation samples.

Three models were developed according to the classes of samples. For the “A” model, the samples were separated into three classes: (i) pure honey; (ii) honey adulterated with HFCS; and (iii) honey adulterated with sugar cane syrup. The “B” model was developed with two

classes: (i) pure honey; and (ii) adulterated honey. And the "C" model: (i) honey adulterated with HFCS; and (ii) honey adulterated with sugar cane syrup. The performance of the models was evaluated by the percentage of correct classifications for the calibration, cross-validation (venetian blind) and external validation sets. The main atomic/ionic emission lines used in the chemometric models were assigned according to the NIST LIBS database (Kramida, Olsen, & Ralchenko, 2019).

2.3.3. Calibration model

The model for quantification of adulterants in honey was developed by the Partial Least Squares (PLS) regression method. The PLS is the multivariate regression method most used to deal with linear chemical problems (Douglas, Nawar, Alamar, Mouazen, & Coulon, 2018). Since the relationship between the spectral data (matrix **X**) and the property of interest is optimized through the latent variables, the high collinearity and the noise of the matrix **X** can be attenuated, and the analytical information extracted by the PLS.

Two-thirds of the 236 samples were used for model calibration and one-third for external validation. The cross-validation was performed by the venetian blind mode with 10 splits to determine the best number of latent variables and to evaluate the fit of the model.

The presence of outliers was visually verified through the spectral profile at first. Then, the verification was performed using the *y* studentized residual versus leverage plot from the PLS model developed with mean-centered and normalized data by the MSC. Samples with residue values above the 95% confidence limits and high leverages were excluded from the sample set.

2.3.4. Preprocessing

The first step to develop the prediction models was the definition of the most suitable preprocessing for the spectral data. Eighteen preprocessing were evaluated individually and combined: mean centering, autoscaling, Poisson scaling, Pareto scaling, Savitzky-Golay smoothing, baseline correction by weighted least squares polynomial, baseline correction by Whittaker filter, detrend, Savitzky-Golay first and second derivatives, row normalization by the area, standard normal variate (SNV), multiplicative scatter correction (MSC), extended multiplicative scatter correction (EMSC), orthogonal signal correction (OSC), generalized least squares weighting (GLSW), external parameter orthogonalization (EPO), and extended mixture model (EMM) filters.

The purpose of the OSC, GLSW, EPO, and EMM filters is to remove or attenuate the *x* variables that are not correlated with the property of interest, i.e. variations in the matrix **X** that are orthogonal to the vector **y** are not explanatory and therefore may be removed or attenuated (Eigenvector Research, 2013). As a result of the application of these multivariate filters, the complexity of the model is reduced and fewer latent variables are required to obtain a high explained variance. The performance of the preprocessing was evaluated by RMSEC, RMSECV, RMSEP, captured variance, and correlation coefficients values.

2.3.5. Variable selection

LIBS data usually present high covariance due to the ability of the technique to measure multiple emission lines of the same element or species – besides, each peak is generated by several *x* variables. Thus, the selection of variables may reduce the covariance and complexity of the model. In addition, the selection of more explanatory variables provides a better chemical understanding of the multivariate system (Xiaobo, Jiewen, Povey, Holmes, & Hanpin, 2010). The removal of noisy regions such as the extreme regions of each spectrometer and *x* variables without analytical information can also increase the explained variance and improve model fit (Xiaobo et al., 2010). Three variable selection strategies were used in this study:

(i) Manual selection using different approaches: (a) exclusion of variables with low selectivity ratio for **y** (Rajalahti et al., 2009); (b) exclusion of variables below the threshold defined by the variable importance projection (VIP) (El Haddad et al., 2014); and (c) exclusion of the noisy regions between the spectrometers (198.2–200.0 nm; 301.3–302.3 nm; 392.0–393.0; 513.8–514.2 nm; and 620.0–624.0 nm).

(ii) Selection by interval partial least squares (iPLS) algorithm. The application of the iPLS was evaluated in the forward mode (FiPLS), in which intervals of 50 spectral variables were inserted in the modeling until finding the lowest RMSECV; and in backward mode (BiPLS), where intervals were excluded until the model with the lowest RMSECV was defined (Xiaobo et al., 2010). In addition, the consecutive use of backward and forward modes (BiPLS + FiPLS) was also evaluated.

(iii) Selection by genetic algorithm (GA). The selection was performed using a population of 256 PLS models, windows size of one variable, start with 30% of the variables, 200 generations, mutation rate of 0.5%, and double cross-over. The application of two and three consecutive times of the algorithm was also evaluated (Nespeca, Rodrigues, Santana, Maintinguer, & de Oliveira, 2017). Details on the variable selection methods can be found in the review by Xiaobo et al. (2010).

2.3.6. Validation

The developed models were validated through cross-validation (venetian blind mode) and external validation samples (one-third of the full sample set). The predictive capacity of the classification models was evaluated through the percentage of true positives (TP) for the calibration, cross-validation, and external validation sets. The calibration model was validated through analytical parameters that represent accuracy, precision, linearity, bias, selectivity, and sensitivity. The selectivity, analytical sensitivity (γ), inverse of the analytical sensitivity (γ^{-1}), signal-to-noise ratio (S/N), limit of detection (LOD) and quantification (LOQ) were determined according to the concept of net analyte signal (NAS) (Ferré & Faber, 2003). The calculations involving in the NAS concept for the PLS method can be found in the work by Ferré and Faber (2003).

3. Results

3.1. Preliminary analysis

The best number of replicates was evaluated prior to the development of the prediction models. Although a larger number of replicates usually provide better models, the models developed with average spectra of 6, 12 and 20 replicates resulted in RMSECV equal to 9.9%(w/w), 11.5%(w/w) e 17.5%(w/w), respectively. The increase in prediction errors with increasing numbers of replicates was due to the introduction of systematic errors caused by changing the position of the sample relative to the laser and the collecting lens. According to rheological studies of different Brazilian honeys (Silva et al., 2018), the honey begins to present Newtonian behavior above 20 °C, i.e., its pseudoplastic characteristic corroborates the formation of a convex meniscus in the sampler. Consequently, the distance between the sample and the LIBS devices (laser, collector lens, and electrodes) was lower in the center of the sampler, resulting in saturated peaks in the spectra. Therefore, prediction models were developed using average spectra obtained from 6 replicates per sample, and the spectra were acquired at the extremities of the sampler, where is the focal point of the laser beam.

3.2. Classification models

The detection of adulterants in honey by LIBS analysis was evaluated through three PLS-DA models. Among the evaluated preprocessing, the 2nd derivative followed by the MSC and mean centering provided more correct classifications for the three models developed with the full spectral range. After the preprocessing was defined, the

Table 1
Results of classification models.

Model	A-I	A-II	B-I	B-II	C-I	C-II
Classes	Unadulterated/ Corn syrup addition/Sugar cane syrup addition		Unadulterated/ Adulterated		Corn syrup addition/Sugar cane syrup addition	
Variable selection	None	FiPLS	None	FiPLS	None	FiPLS
#variables *x*	7857	350	7857	150	7857	100
#LVs	9	8	8	6	4	6
Correct classifications						
Calibration	100%	100%	100%	100%	100%	100%
Cross-validation	61%	92%	44%	75%	100%	96%
Validation	95%	79%	96%	100%	93%	100%

variables were selected by the FiPLS algorithm and the performance of the models was evaluated through the percentage of true positives.

The number of variables *00D7*, latent variables and correct classifications of each model are shown in Table 1. The models developed with the full spectral range and after FiPLS application were symbolized by the Roman numerals "I" and "II", respectively. The A models, which aimed at the detection of honey adulteration and the type of adulterant, did not obtain 100% of correct classifications for the validation set. In addition, the variable selection reduced the number of true positives in external validation, despite increasing in cross-validation. On the other hand, the B-II and C-II models provided 100% accuracy for validation samples after variable selection. The separation of the classes in models B-II and C-II can be visualized through the scores plots with the first three latent variables in Figure SM1. The grouping of the samples did not show any tendency regarding the adulterant concentration level. This fact can be justified by the honey samples from different botanical origins and different types of adulterants used for modeling, which makes the model more robust for its application. Therefore, the detection of honey adulteration could be performed through the B-II model and the type of adulterant could be identified through the C-II model.

Since the addition of sweetener syrups results in the dilution of intrinsic honey compounds such as proteins, enzymes, lipids, minerals, etc., the change in composition reflects on the intensity of the peaks in LIBS spectra. This fact suggests the predictive capacity of the models was due to the difference between the minerals content in honeys before and after dilution with the sweetener syrups. Although honey is a complex matrix, few minerals are present in high concentrations, among them are K, Mg, Ca, Na, and Fe (Biluca et al., 2016; Kek et al., 2017; Souza et al., 2016). While sweetener syrups have much lower amounts of minerals. The major minerals in sugar cane syrup are Na, Mg, Ca, Fe, K and Cu (Pilando & Wrolstad, 1992), and in HFCS are Ca, K and Na (Abdel-Aal et al., 1993; Pilando & Wrolstad, 1992). Given the difference in the mineral content, the B-II model discriminated the classes through the intensities of species present in honey. The FiPLS algorithm selected three intervals of 50 variables (351.98–354.27 nm, 356.63–358.89 nm, and 383.43–385.55 nm). The variables that presented the highest regression coefficients (*b*) corresponded to the profile of ionic emission lines of Fe (352.22 nm, 352.64 nm, 352.88 nm, 353.38 nm, 353.67 nm, 357.19 nm, 357.57 nm, 384.52 nm, and 385.42 nm) (Kramida et al., 2019). The intensity of these peaks was reduced due to the honey dilution by the addition of adulterants, providing the separation of the classes by the PLS-DA model, after variable selection.

The identification of the adulterant type by the C-II model was mainly related to the emission lines of Ca and Fe in the selected intervals (251.57–254.05 nm and 394.82–398.21 nm) (Kramida et al., 2019). The emission lines at 394.86 nm (Ca I), 396.91 nm (Ca II), 397.38 nm (Ca I), and 398.2 nm (Ca I) presented positive values in the regression vector for the samples adulterated with HFCS. While the emission lines at 251.75 nm (Fe I), 252.15 nm (Fe I), 253.43 nm (Fe II) and 395.58 nm (Fe I) were related to samples adulterated with sugar cane syrup. Therefore, the discrimination of the type of adulterant present in honey was possible due to the higher Ca content in HFCS and the higher Fe content in sugar cane syrup.

3.3. Calibration model

The PLS model for adulterant quantification was developed using 158 calibration samples and validated with 78 external validation samples. Each sample was represented by the average spectrum of six replicates. Firstly, the presence of outliers was visually verified through the spectra profiles. Two spectra of the calibration set (samples 181 and 191) showed an anomalous profile in the spectral range between 200 nm and 392 nm (Figure SM2, Supplementary Material). Therefore, they were excluded from the sample set. No outlier was visually identified in the validation set.

After the visual verification, anomalous samples were identified by the studentized residual versus leverage plot. The PLS model, preprocessed with MSC and mean centering, presented two outliers in the calibration set (samples 1 and 58) and two in the validation set (samples 162 and 220) due to the high *y* residual value (Figure SM3, Supplementary Material). The outliers were confirmed by PLS models developed with other preprocessing, such as 1st derivative and baseline correction by weighted least squares. Finally, the sample set consisted of 154 calibration and 76 validation samples.

The next step was to set the most appropriate preprocessing for the regression model. The choice was based on the RMSECV (venetian blind with 10 splits), RMSEP, correlation coefficients (r), $bias_{val}$, and explained variance in **X** and **y** blocks. The results for all tested preprocessing are shown in Tables SM1 and SM2 (Supplementary Material).

The use of first derivative (15 variables per window) followed by orthogonal signal correction (two components, one interaction, and 99.9% of tolerance) and mean centering provided the lowest errors and the highest correlation coefficient in external validation. Through this preprocessing, the model with only 5 LVs explained 80.3% and 96.2% of the variance in the matrix **X** and in the vector **y**, respectively. The results of cross-validation were RMSECV = 13.1%(w/w) and r_{CV} = 0.8898, and of external validation were RMSEP = 11.7%(w/w) and r_{val} = 0.9067.

After the best preprocessing was defined, different approaches to variable selection were evaluated (Table 2). Although the manual approaches have reduced the bias in validation, prediction errors have become larger, so the prediction model has become less accurate. According to the selectivity rate for y plot (Figure SM4), all spectra range was important in the correlation between the matrix **X** with the vector y. The exclusion of the least correlated variables (below 10% of selectivity) reduced the correlation coefficients, so the robustness of the calibration model was impaired for the prediction of external samples. The same strategy using the VIP plot also led to a lower predictive capacity for the PLS model. The exclusion of variables from the extreme regions of the spectrometers did not influence the RMSEP value but increased the RMSECV and reduced $bias_{val}$. Therefore, none of the manual approaches provided a better fit to the PLS model.

Unlike manual approaches, variable selection algorithms systematically search for ranges or variables that generate a model with lower prediction errors. The FiPLS algorithm included 15 intervals of 50 variables and resulted in higher RMSEC and RMSECV values but lower RMSEP. Despite the reduction in model fit, the selected variables made the model more robust for external samples. The BiPLS algorithm reduced the errors of calibration, cross-validation, and external validation by excluding 105 intervals of 50 variables. The variables selected by the BiPLS algorithm are shown in Fig. 1. Moreover, the closeness of the RMSECV and RMSEP values shows the greater robustness of the prediction model after use of BiPLS. According to the regression

Table 2
Evaluation of different variable selection approaches.

Method	Preprocessing	#variables	LVs	RMSEC	RMSECV	RMSEP	bias $_{val}$	r $_{CV}$	r $_{val}$
Full spectra	1ªder + OSC	7857	5	5.5	13.1	11.7	−1.0	0.8899	0.9067
Selectivity ratio for Y	1ªder + OSC	1908	4	4.2	13.1	13.7	−0.4	0.8886	0.8734
VIP	1ªder + OSC	1745	5	5.5	13.2	12.5	−0.5	0.8895	0.8947
Exclusion of noisy regions	1ªder + OSC	7563	5	7.1	13.3	11.7	−0.8	0.8840	0.9052
FiPLS	1ªder + OSC	750	4	7.2	14.7	10.9	−3.0	0.8646	0.9231
BiPLS	1ªder + OSC	2607	6	2.7	11.1	10.4	−1.4	0.9205	0.9294
BiPLS + FiPLS	1ªder + OSC	850	4	5.9	13.1	12.4	−1.3	0.8887	0.9003
GA1	OSC	2108	5	3.0	14.4	11.7	−2.0	0.8689	0.9082
GA2	GLSW	446	4	5.9	15.0	11.0	−2.4	0.8565	0.9187
GA3	OSC	101	5	9.3	13.3	10.7	−0.3	0.8837	0.9199

*Unit for RMSEC, RMSECV, RMSEP and bias is %(w/w).

coefficients and the loadings, the emission lines that most contributed to the modeling were 247.8 nm (C I and Fe I), 279.6 nm (Mg II), and 393.4 nm (Ca II). The application of FiPLS utilizing the variables selected by BiPLS (BiPLS + FiPLS) made the prediction model less fitted than using full spectra.

The variable selection by GA reduced RMSEP values but increased RMSEC and RMSECV. Three consecutive runs of oGA (GA3) significantly reduced the value of bias, therefore, the prediction errors became more random. The variables selected by GA3 presented relative low intensity and were related to the electronic transitions: Fe I (248.3 nm, 407.8 nm, 413.3 nm, 422.6 nm, and 609.7 nm), Fe II (234.3 nm, 237.5 nm and 617.5 nm), O II (445.1 nm), Mg I (518.4 nm), K I (485.6 nm), and CN I (387.1 nm).

The variable selection by BiPLS and GA3 methods optimized the predictive capacity of the model by excluding less informative and noisy regions (BiPLS) or by selecting better predictor variables (GA3). However, both methods did not significantly reduce RMSEP values. This fact evidences the importance of all spectral range for correlation with adulterant content in honey. In other words, the correlation did not occur due to differences in specific signals but through changes in the fingerprint of honey samples with the addition of adulterant.

On the other hand, the application of the most adequate preprocessing associated to the BiPLS significantly reduced the RMSEP in comparison to the model generated with full spectral range and mean centered data. The significance of the optimization was verified through an F test, where F is equal to $RMSEP_1^2/RMSEP_2^2$ and $RMSEP_1$ is the highest value (Rocha et al., 2012). Since the calculated F was equal to 1.71 and the critical F is 1.46 (95% confidence level and 76 degrees of freedom), the proposed strategy significantly optimized the fit of the model. Thus, a deeper validation of the BiPLS model was carried out through other figures of merit. The validation results of the calibration model are shown in Table 3.

According to the results, the model showed good accuracy with $r > 0.92$, ARE = 37.2%, RPD = 2.7 (RPD critical = 2.0 (Nocita, Stevens, Noon, & Van Wesemael, 2013)), RMSECV = 11.1%(w/w), and RMSEP = 10.4%(w/w). The relationship between the adulterant concentration and relative error in the validation set (Fig. 2a) showed that the prediction error is less than 100% for concentration above 18%(w/w) and less than 40% above 30%(w/w). The linearity was verified through the measured values *vs.* predicted values plot and the residues plot (Fig. 3). The model was linear across the entire concentration range and the residuals were random, although the lowest concentration validation samples showed a higher positive bias. The model presented a negative bias of −1.4%(w/w), which was not significant according to the *t*-test (t_{bias} = 1.43; $t_{critical}$ = 1.67).

Regarding the selectivity, 13.4% of the instrumental signal was related to the analyte signal (Table 3). The model was sensitive with signal up to 72 times greater than noise and analytical sensitivity (γ) equal to 23.9%(w/w)$^{-1}$, that is, the model was able to distinguish differences in concentration of 0.04%(w/w). The values of LOD and LOQ were equal to 0.1%(w/w) and %(w/w), respectively.

Although the model presented good accuracy, linearity, selectivity, and sensitivity, the precision was low. In the validation set, the prediction of replicates resulted in a mean relative standard deviation (RSD_{mean}) of 53.8%. The high RSD_{mean} value was a consequence of the low precision for adulterant concentration below 20%(w/w). The

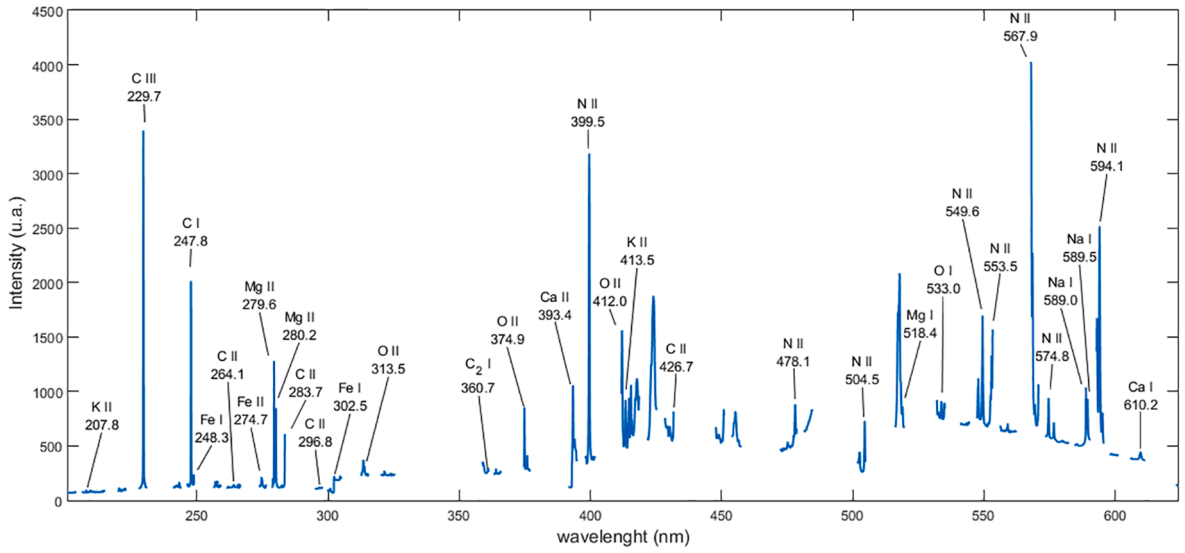


Fig. 1. Selected variables by iPLS in backward mode (BiPLS).

Table 3
Figures of merit of the BiPLS model for adulterant quantification.

Set	Parameter	Value	Set	Parameter	Value
Calibration	RMSEC	2.7%(w/w)	Validation	RMSEP	10.4%(w/w)
	RMSECV	11.1%(w/w)		r val	0.9294
	r cal	0.9955		ARE	37.2%
	r CV	0.9205		RPD[a]	2.7
	ARE	4.6%		Bias	−1.4%(w/w)
	RPD	2.5		t_{bias}[b]	1.43
	Selectivity	13.4%		RSD_{mean}	53.8%
	S/R max.	72		$RSD_{mean} > 20$[c]	39.6%
	Analytical sensitivity (γ)	23.9%(w/w)$^{-1}$			
	γ^{-1}	0.04%(w/w)			
	LOD	0.1%(w/w)			
	LOQ	0.4%(w/w)			

[a]$RPD_{critical} = 2.0$.
[b]$t_{critical} = 1.67$ (76 degrees of freedom; 95% level of confidence).
[c]Mean RSD of samples with concentration above 20%(w/w).

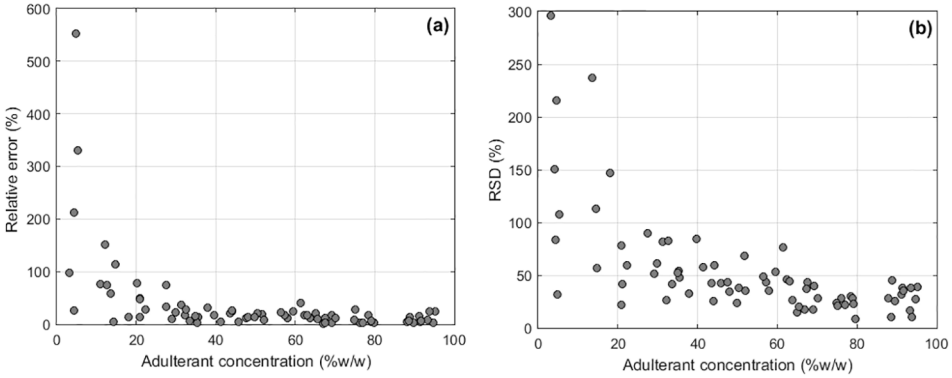


Fig. 2. (a) Relationship between the adulterant concentration and relative error in the validation set. (b) Relationship between adulterant concentration and RSD for the validation set.

relationship between the adulterant concentration and the RSD can be seen in Fig. 2b. The mean value of RSD for samples with a concentration above 20%(w/w) was 39.6%. The low precision can be justified by the variability in plasma formation. Plasma can be influenced by several factors such as heterogeneity of the sample, variations in the electric voltage of the electrodes responsible for the spark discharge, and position of the sample in relation to the LIBS devices (Miziolek, Palleschi, & Schechter, 2006). In addition, the convex meniscus formed by the honey in the sampler allowed a small number of replicates to obtain averaged spectrum, decreasing precision. Therefore, future studies can be performed to evaluate sample pretreatment or optimization of instrumental parameters, such as laser pulse time and number of pulses, to improve the precision of the LIBS method.

4. Conclusion

The present study demonstrated the potential of LIBS for the identification and quantification of adulterants in honey. The discrimination of pure and adulterated honeys was possible through a PLS-DA model with the variables selected by iPLS in forward mode (FiPLS). The emission lines of the atomic Fe presented higher regression coefficients for class discrimination. After adulteration detection, the type of adulterant (HFCS or sugar cane syrup) could be identified by a second PLS-DA model. The main variables related to the class separation were attributed to electronic transitions of Ca and Fe. Both pattern recognition models obtained 100% correct classifications for the calibration and external validation sets.

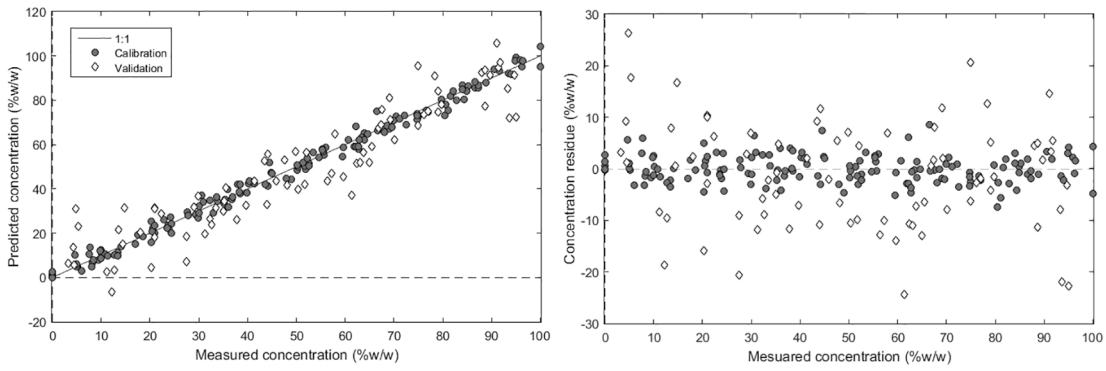


Fig. 3. Fit plot (left) and y residual (right).

Adulterants quantification by PLS model with adequate preprocessing (1st derivative plus orthogonal signal correction, and mean centering) and variables selected by backward iPLS (BiPLS) allowed significant reduction of RMSEP. The calibration model showed good accuracy, linearity, sensitivity, and selectivity with good precision for samples containing adulterants above 20%(w/w).

The association of LIBS and chemometric methods was effective and simple for the identification and quantification of adulterants (syrups) in honey. The proposed method provides a fast (3 min per sample) and simple way to verify the honey authenticity using small amounts of honey (1 mL) and without generating waste for the environment. Furthermore, the demonstrated potential of LIBS can be extended for analysis of other food of high density, such as condensed milk, mayonnaise, ketchup, among others.

Declaration of Competing Interest

The authors declare that they have no known competing financial interests or personal relationships that could have appeared to influence the work reported in this paper.

Acknowledgements

This research received financial support from Coordenação de Aperfeiçoamento de Pessoal de Nível Superior (CAPES) through scholarship to M.G.N., and Conselho Nacional de Desenvolvimento Científico e Tecnológico (CNPq) through scholarship to A.L.V (Grant # 141977/2016-7) and research grant to E.C.F (Grant # 308200/2018-7).

Appendix A. Supplementary data

Supplementary data to this article can be found online at https://doi.org/10.1016/j.foodchem.2019.125886.

References

Guimarães, E. (2018). Mel brasileiro se destaca nos mercados europeu e norte-americano. Retrieved October 8, 2018, from https://www.em.com.br/app/noticia/agropecuario/2018/01/22/interna_agropecuario,932500/mel-brasileiro-se-destaca-nos-mercados-europeu-e-norte-americano.shtml.

Abdel-Aal, E. S. M., Ziena, H. M., & Youssef, M. M. (1993). Adulteration of honey with high-fructose corn syrup: Detection by different methods. *Food Chemistry, 48*(2), 209–212. https://doi.org/10.1016/0308-8146(93)90061-J.

Alfarraj, B. A., Sanghapi, H. K., Bhatt, C. R., Yueh, F. Y., & Singh, J. P. (2018). Qualitative analysis of dairy and powder milk using laser-induced breakdown spectroscopy (LIBS). *Applied Spectroscopy*. https://doi.org/10.1177/0003702817733264.

Codex Alimentarius. (2001). CODEX standard for honey: CODEX STAN 12-1981 (Vol. 7).

Amiry, S., Esmaiili, M., & Alizadeh, M. (2017). Classification of adulterated honeys by multivariate analysis. *Food Chemistry, 224*, 390–397. https://doi.org/10.1016/j.foodchem.2016.12.025.

Bázár, G., Romvári, R., Szabó, A., Somogyi, T., Éles, V., & Tsenkova, R. (2016). NIR detection of honey adulteration reveals differences in water spectral pattern. *Food Chemistry, 194*, 873–880. https://doi.org/10.1016/j.foodchem.2015.08.092.

Bilge, G., Velioglu, H. M., Sezer, B., Eseller, K. E., & Boyaci, I. H. (2016). Identification of meat species by using laser-induced breakdown spectroscopy. *Meat Science, 119*, 118–122. https://doi.org/10.1016/j.meatsci.2016.04.035.

Biluca, F. C., Braghini, F., Gonzaga, L. V., Costa, A. C. O., & Fett, R. (2016). Physicochemical profiles, minerals and bioactive compounds of stingless bee honey (Meliponinae). *Journal of Food Composition and Analysis, 50*, 61–69. https://doi.org/10.1016/j.jfca.2016.05.007.

Brereton, R. G., & Lloyd, G. R. (2014). Partial least squares discriminant analysis: Taking the magic away. *Journal of Chemometrics, 28*(4), 213–225. https://doi.org/10.1002/cem.2609.

Chakraborty, S., Weindorf, D. C., Zhu, Y., Li, B., Morgan, C. L. S., Ge, Y., & Galbraith, J. (2012). Spectral reflectance variability from soil physicochemical properties in oil contaminated soils. *Geoderma, 177–178*, 80–89. https://doi.org/10.1016/j.geoderma.2012.01.018.

Silva, V. M. da, Torres Filho, R. de A., & Resende, J. V. de. (2018). Rheological properties of selected Brazilian honeys as a function of temperature and soluble solid concentration. International Journal of Food Properties, 20(3), S2481–S2494. 10.1080/10942912.2017.1370599.

Das, C., Chakraborty, S., Acharya, K., Bera, N. K., Chattopadhyay, D., Karmakar, A., & Chattopadhyay, S. (2017). FT-MIR supported Electrical Impedance Spectroscopy based study of sugar adulterated honeys from different floral origin. *Talanta, 171*(May), 327–334. https://doi.org/10.1016/j.talanta.2017.05.016.

Douglas, R. K., Nawar, S., Alamar, M. C., Mouazen, A. M., & Coulon, F. (2018). Rapid prediction of total petroleum hydrocarbons concentration in contaminated soil using vis-NIR spectroscopy and regression techniques. *Science of the Total Environment, 616–617*, 147–155. https://doi.org/10.1016/j.scitotenv.2017.10.323.

Eigenvector Research. (2013). Advanced Preprocessing: Multivariate Filtering. Retrieved from http://wiki.eigenvector.com/index.php?title=Advanced_Preprocessing:_Multivariate_Filtering.

El Haddad, J., Canioni, L., & Bousquet, B. (2014). Good practices in LIBS analysis: Review and advices. *Spectrochimica Acta – Part B Atomic Spectroscopy, 101*, 171–182. https://doi.org/10.1016/j.sab.2014.08.039.

Eum, C., Jang, D., Kim, J., Choi, S., Cha, K., & Chung, H. (2018). Improving the accuracy of spectroscopic identification of geographical origins of agricultural samples through cooperative combination of near-infrared and laser-induced breakdown spectroscopy. *Spectrochimica Acta Part B: Atomic Spectroscopy, 149*(March), 281–287. https://doi.org/10.1016/j.sab.2018.09.004.

Ferré, J., & Faber, N. M. (2003). Net analyte signal calculation for multivariate calibration. *Chemometrics and Intelligent Laboratory Systems, 69*(1–2), 123–136. https://doi.org/10.1016/S0169-7439(03)00118-7.

Ferreiro-González, M., Espada-Bellido, E., Guillén-Cueto, L., Palma, M., Barroso, C. G., & Barbero, G. F. (2018). Rapid quantification of honey adulteration by visible-near infrared spectroscopy combined with chemometrics. *Talanta, 188*(May), 288–292. https://doi.org/10.1016/j.talanta.2018.05.095.

Gallardo-Velázquez, T., Osorio-Revilla, G., de Loa, M. Z., & Rivera-Espinoza, Y. (2009). Application of FTIR-HATR spectroscopy and multivariate analysis to the quantification of adulterants in Mexican honeys. *Food Research International, 42*(3), 313–318. https://doi.org/10.1016/j.foodres.2008.11.010.

Kek, S. P., Chin, N. L., Tan, S. W., Yusof, Y. A., & Chua, L. S. (2017). Classification of honey from its bee origin via chemical profiles and mineral content. *Food Analytical Methods, 10*(1), 19–30. https://doi.org/10.1007/s12161-016-0544-0.

Kramida, A., Olsen, K., & Ralchenko, Y. (2019). NIST LIBS Database. Retrieved from https://physics.nist.gov/PhysRefData/ASD/LIBS/libs-form.html.

Miziolek, A. W., Palleschi, V., & Schechter, I. (2006). Laser-Induced Breakdown Spectroscopy (LIBS) (A. W. Miziolek, V. Palleschi, & I. Schechter, Eds.). Cambridge: Cambridge University Press. doi:10.1017/CBO9780511541261.

Nespeca, M. G., Rodrigues, C. V., Santana, K. O., Maintinguer, S. I., & de Oliveira, J. E. (2017). Determination of alcohols and volatile organic acids in anaerobic bioreactors for H2 production by near infrared spectroscopy. *International Journal of Hydrogen Energy*. https://doi.org/10.1016/j.ijhydene.2017.07.044.

Nocita, M., Stevens, A., Noon, C., & Van Wesemael, B. (2013). Prediction of soil organic carbon for different levels of soil moisture using Vis-NIR spectroscopy. *Geoderma, 199*, 37–42. https://doi.org/10.1016/j.geoderma.2012.07.020.

Oroian, M., Ropciuc, S., & Paduret, S. (2018). Honey adulteration detection using raman spectroscopy. *Food Analytical Methods, 11*(4), 959–968. https://doi.org/10.1007/s12161-017-1072-2.

Paradkar, M. M., Irudayaraj, J., & Sakhamuri, S. (2002). Discrimination and classification of beet and cane sugars and their inverts in maple syrup by FT-Raman. *Applied Engineering in Agriculture, 18*(3), 379–383. https://doi.org/10.1016/S0308-8146(01)00292-8.

Pilando, L. S., & Wrolstad, R. E. (1992). Compositional profiles of fruit juice concentrates and sweeteners. *Food Chemistry, 44*(1), 19–27. https://doi.org/10.1016/0308-8146(92)90252-W.

Pilizota, B. V., & Tiban, N. N. (2009). Advances in Honey Adulteration Detection (September), 1–6.

Rajalahti, T., Arneberg, R., Berven, F. S., Myhr, K. M., Ulvik, R. J., & Kvalheim, O. M. (2009). Biomarker discovery in mass spectral profiles by means of selectivity ratio plot. *Chemometrics and Intelligent Laboratory Systems, 95*(1), 35–48. https://doi.org/10.1016/j.chemolab.2008.08.004.

Rocha, W. F. C., Vaz, B. G., Sarmanho, G. F., Leal, L. H. C., Nogueira, R., Silva, V. F., & Borges, C. N. (2012). Chemometric techniques applied for classification and quantification of binary biodiesel/diesel blends. *Analytical Letters, 45*(16), 2398–2411. https://doi.org/10.1080/00032719.2012.686135.

Ruoff, K., Iglesias, M. T., Luginbühl, W., Bosset, J. O., Bogdanov, S., & Amadò, R. (2006). Quantitative analysis of physical and chemical measurands in honey by mid-infrared spectrometry. *European Food Research and Technology, 223*(1), 22–29. https://doi.org/10.1007/s00217-005-0085-z.

Schenk, E. R., & Almirall, J. R. (2010). Elemental analysis of cotton by laser-induced breakdown spectroscopy. *Applied Optics, 49*(13), C153. https://doi.org/10.1364/ao.49.00c153.

Se, K. W., Ghoshal, S. K., & Wahab, R. A. (2019). Laser-induced breakdown spectroscopy unified partial least squares regression: An easy and speedy strategy for predicting Ca, Mg and Na content in honey. *Measurement: Journal of the International Measurement Confederation, 136*, 1–10. https://doi.org/10.1016/j.measurement.2018.12.052.

Shafiee, S., Polder, G., Minaei, S., Moghadam-Charkari, N., van Ruth, S., & Kuś, P. M. (2016). Detection of honey adulteration using hyperspectral imaging. *IFAC-PapersOnLine, 49*(16), 311–314. https://doi.org/10.1016/j.ifacol.2016.10.057.

Souza, E. A., Zaluski, R., Veiga, N., Orsi, R. O., Souza, E. A., Zaluski, R., … Orsi, R. O. (2016). Effects of seasonal variations and collection methods on the mineral composition of propolis from Apis mellifera Linnaeus Beehives. *Brazilian Journal of Biology, 76*(2), 396–401. https://doi.org/10.1590/1519-6984.16714.

Spiteri, M., Jamin, E., Thomas, F., Rebours, A., Lees, M., Rogers, K. M., & Rutledge, D. N. (2015). Fast and global authenticity screening of honey using ^{1}H-NMR profiling. *Food Chemistry, 189*, 60–66. https://doi.org/10.1016/j.foodchem.2014.11.099.

Vieira, A. L., Silva, T. V., de Sousa, F. S. I., Senesi, G. S., Júnior, D. S., Ferreira, E. C., &

Neto, J. A. G. (2018). Determinations of phosphorus in fertilizers by spark discharge-assisted laser-induced breakdown spectroscopy. *Microchemical Journal, 139*, 322–326. https://doi.org/10.1016/j.microc.2018.03.011.

Wang, J., Kliks, M. M., Jun, S., Jackson, M., & Li, Q. X. (2010). Rapid analysis of glucose, fructose, sucrose, and maltose in honeys from different geographic regions using fourier transform infrared spectroscopy and multivariate analysis. *Journal of Food Science, 75*(2), 208–214. https://doi.org/10.1111/j.1750-3841.2009.01504.x.

Workman, D. (2018). Natural Honey Exports by Country. Retrieved October 11, 2018, from http://www.worldstopexports.com/natural-honey-exporters/.

Xiaobo, Z., Jiewen, Z., Povey, M. J. W., Holmes, M., & Hanpin, M. (2010). Variables selection methods in near-infrared spectroscopy. *Analytica Chimica Acta, 667*(1–2), 14–32. https://doi.org/10.1016/j.aca.2010.03.048.

Anexo 15

Microchemical Journal 157 (2020) 105107

Contents lists available at ScienceDirect

Microchemical Journal

journal homepage: www.elsevier.com/locate/microc

CN diatomic emission for N determination by LIBS

Samia R. Dib[a], Maurílio G. Nespeca[a], Dário Santos Junior[b], Clovis A. Ribeiro[a], Marisa S. Crespi[a], José Anchieta Gomes Neto[a], Edilene C. Ferreira[a,*]

[a] Department of Analytical Chemistry, São Paulo State University – UNESP, 14800-060 Araraquara, SP, Brazil
[b] Department of Chemistry, Federal University of São Paulo – UNIFESP, 09913-030 Diadema, SP, Brazil

ARTICLE INFO

Keywords:
LIBS
Nitrogen
CN diatomic emission
Biochar-based fertilizers

ABSTRACT

The determination of N is an important demand for several sectors and the analytical features of laser-induced breakdown spectroscopy (LIBS) are very attractive to accomplish this task. In this work, a novel proposal for nitrogen determination was explored considering molecular diatomic emission lines of CN measured by LIBS. As a proof of concept, a method was developed to determine N in biochar-based fertilizers, a highly recalcitrant matrix. The fertilizers were prepared from biochar of eucalyptus pruning residues, peanut skin and fibers of banana tree and the calibration standards were prepared by matrix matching using eucalyptus biochar. Diatomic emission signals of CN at 388.3 nm showed high correlation with the levels of N in standards and samples, suggesting the molecular emission of CN is little affected by the matrix effect. The developed method is accurate since the N levels determined in the samples do not differ statistically from the expected level, with a 95% confidence level. Furthermore, the method using molecular emission is simple and highlights the potential of LIBS for N determination in complex matrices (*e.g.* biochar).

1. Introduction

Nitrogen analysis is required for a wide variety of materials, such as foods, beverages, agricultural products, environmental samples, chemicals, biochemicals, and pharmaceuticals [1]. Therefore, the determination of N is a routine procedure for quality assurance and the concentration is most often accessed using spectrophotometry [2] or Kjeldahl [3]. Both methods require sample preparation, which involves strongly oxidizing reactions and high temperatures. Despite the drastic conditions employed, matrices highly recalcitrant makes sample preparation a very hard task. Therefore, the simplest and quick alternative is the direct analysis.

Laser-induced breakdown spectroscopy (LIBS) is an analytical technique able to perform direct elemental analysis, without chemical reagents and dismissing samples pretreatment. LIBS is based on the measurements of atomic and ionic emission of elemental and diatomic molecular species in a temporary plasma obtained from a high-energy laser pulse. LIBS measurement is extremely fast, demanding usually a few seconds for a single spot analysis [4].

Despite the potential of LIBS for elemental analysis, N determination in solid samples is a challenge analytical task. Due to the high energy of the upper levels of N atom (typically 11 eV) and its high ionization potential (14.53 eV), few strong emission lines of N can be observed in LIBS spectra [5]. Additionally, atmospheric N can interfere in the analysis. Notwithstanding, these drawbacks have been successfully overcome in different ways, allowing the proposition of different methods for the determination of N in soil, using atomic emission lines at 742.36, 744.23, 746.83 nm [6]. Nevertheless, according to Villas-Boas et al. (2019), even the successful efforts in finding an appropriate calibration curve for N determination in soil samples the analysis remains challenging due to matrix effects and LIBS sensitivity [6].

Diatomic molecular emissions correlated with N, such as CN and NH can also be observed in LIBS spectra and has been explored for different purposes, *e.g.* species formation pathways [7], plasma diagnostics [8], normalization of emission signals [9] and identification of organic explosives [10]. However, they remain virtually unexplored especially for quantitative issues. The CN violet system ($B^2\Sigma^+$–$X^2\Sigma^+$), for instance has been investigated as molecular signatures for organic compounds [11–13], however, its exploitation for the purpose of quantitative determination of N has not been reported before.

Considering the above, CN emission bands from violet system were evaluated for N quantitative analysis by LIBS. As a proof of concept, a method was developed for N determination in biochar-based fertilizers, a recent proposal of gradual release fertilizer produced from biomass pyrolysis of agricultural waste [14].

* Corresponding author.
E-mail address: edilene.c.ferreira@unesp.br (E.C. Ferreira).

https://doi.org/10.1016/j.microc.2020.105107
Received 25 April 2020; Received in revised form 28 May 2020; Accepted 29 May 2020
Available online 03 June 2020
0026-265X/ © 2020 Elsevier B.V. All rights reserved.

2. Material and methods

2.1. Samples and calibration standards

Biochar was produced from biomass of eucalyptus pruning waste, peanut shells and banana tree fibers. About 2 g of the biomass were transferred to porcelain crucibles. The crucibles were covered with aluminum foil and a porcelain lid to keep the atmosphere low on oxygen. The crucibles were taken to the muffle for thermochemical conversion of biomass into biochar. The heating program applied consisted of raising the temperature until the maximum of 260 °C and keep it for 60 min. The temperature raise was accomplished in the ratio of 10 °C per minute. At the end of the heating, the samples were allowed to cool inside the muffle to temperatures close to 60 °C and the equilibrium with the room temperature was provided in a fume hood.

Obtained biochar were washed with deionized water aiming to activate sites of the material and eliminate some compounds released during the heating, which could interfere in adsorption process. The washing was carried on using a simple filtration procedure until a clear coloration of the wastewater was observed. Then the material was dried at 100 °C, up to constant mass.

Biochar-based fertilizers were prepared to contain 10% (w/w) of $(NH_4)_2HPO_4$. Sample pellets were prepared by mixing 0.020 g of $(NH_4)_2HPO_4$ and 0.18 g of biochar. The mixtures were homogenized in an agate mortar, and then converted into pellets by applying 10 tons of pressure using a mechanical press (Solab SL – 10/15, Piracicaba, Brazil). The fertilizers from different biochar were produced in triplicate.

Calibration standards were prepared using growing masses of $(NH_4)_2HPO_4$ and 0.10 g eucalyptus biochar. Boric acid was used as a diluting agent to make standards masses up to 300 mg and as a binder [15]. The N levels in the standards were: 0%, 1.05%; 1.43%, 2.15%, 3.54%, 4.94% and 5.98% (w/w). The mixtures were also homogenized and converted into pellets as previously described for the samples. Three pellets were prepared for each standard.

2.2. LIBS analysis

The spectra were acquired using a LIBS system, equipped with a 1064 nm Q-switched Nd:YAG laser (Quantel, Big Sky Ultra 50, Bozeman, USA) operated at 50 mJ maximum power energy with pulse duration less than 8 ns, providing an irradiance around 9.7 GW cm^{-2} at the focal point. The system also includes optical fiber bundle, four spectrometers Ocean Optics (HR2000+, Dunedin, USA), featuring an optical resolution of 0.1 nm (full width at half maximum), and covering a spectral range from 200 nm to 630 nm. The gate time and the Q-switch delay used for spectra acquisition were 1 ms and 2 μs, respectively.

The sample were placed into the sampler, which can be moved in the x and y directions. The pellets surface was adjusted in the focal point of the waist of the laser beam (lens to sample distance equal to 12 cm). A spark discharge system, previously proposed [16], was coupled to the LIBS system aiming to improve detectability. The optimum argon flow to minimize air contributions was evaluated.

Ten emission spectra from each pellet were acquired spreading laser pulses randomly and covering the pellets surface. Each individual spectrum was preprocessed for baseline correction, using an Excel spreadsheet for dealing with spectroscopic and chromatographic data [17], and after they were averaged for each pellet (n = 10) and then for each sample or standard (n = 3). The intensity of the CN emission band at 388.3 nm, was used for the determinations.

To evaluate the accuracy of LIBS method, the N levels in the biochar fertilizers were statistically compared to the expected level, according to the mass of $(NH_4)_2HPO_4$ added in fertilizers preparation.

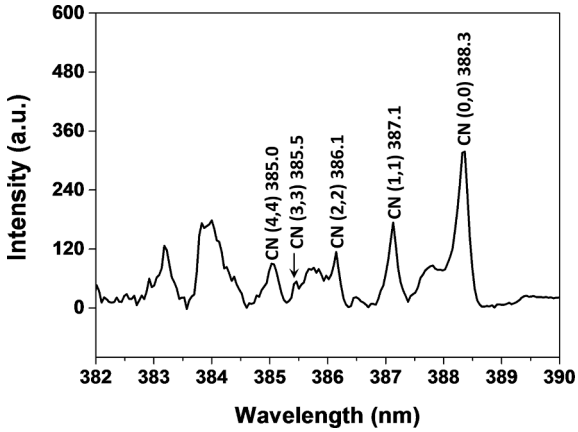


Fig. 1. CN emission bands recorded in biochar fertilizer spectrum.

3. Results and discussion

The configuration of the LIBS system used does not allow observing the CN emission bands, despite the high content of carbon and nitrogen in samples, in addition to the high content of N in atmospheric air. These results corroborate the previous remarks that one of the challenges in determining nitrogen by LIBS is sensitivity [6]. However, when the spark discharge system was coupled to LIBS, molecular spectra corresponding to the CN violet system could be clearly observed in the spectrum of eucalyptus biochar fertilizer (Fig. 1).

In this spectrum, preprocessed for baseline correction, the observed CN bands system is related to (0,0), (1,1), (2,2), (3,3) and (4,4) vibrational transitions, recorded at 388.3, 387.1, 386.1, 385.5, and 385.0 nm, respectively. The spectral profile is similar to that previously reported by Mousavi et al. [12], with the exception of the signal referring to the transition (3.3), whose low intensity allowed background interferences, leading to the signal widening. This type of divergences in terms of relative intensities can occur in the molecular expected profile, since molecular emissions are sensitive to the composition of each single material [18].

Molecular decay is typically slower than atomic and ionic decay, so the acquisition of these signals is favored by longer integration times [19]. Therefore, under the experimental conditions the use of spark discharge, which increases the plasma life time, and the long time for signal integration (1 ms), provided the spectral emergence of the bands of the CN violet system. Increasing the sensitivity of LIBS measures to promote the appearance of atomic N lines has also been studied previously by reducing the pressure in the plasma chamber, increasing the laser energy and varying the delay time [20,21]. Considering the availability of a simple spark discharge device, it was adopted in this proposal to increase sensitivity.

CN specie can be formed by recombination of native sample C and N in the plasma or due to the interaction between atmospheric N and C sample in the plasma [18]. Considering the quantitative aim of this work, argon flow in the sampler chamber of LIBS system was studied to minimize the air contribution for the formation of recombinant CN. The argon flow was evaluated in the range of 0 L min^{-1}, i.e., without flow, to 12 L min^{-1}, boundary condition to avoid plasma turbulence. In Fig. 2 is shown the signal behavior of the most intense CN transition (0,0) in function of argon flow in the sampler chamber.

The greater observed intensity of emission without argon suggests the CN from sample is summed to recombinant CN signals. As the argon flow increases the signals decreases, suggesting progressive N atmospheric removal until its complete elimination at 10 L min^{-1} flow, from which the signal remains nearly constant. Comparisons about argon flows influence point out larger differences in intensities are between 0 mL min^{-1} and 4 mL min^{-1}, suggesting as the air starts to be removed the signal decreases drastically. This result corroborates with the

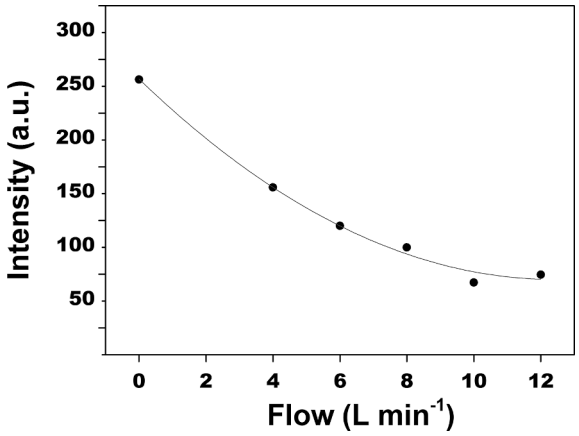


Fig. 2. Influence of argon flow in the signal of CN at 388.3 nm.

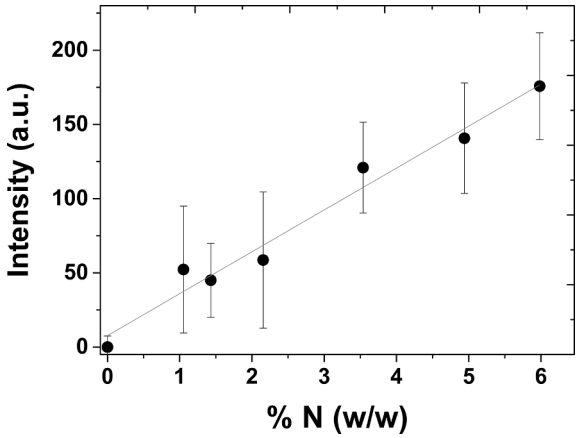


Fig. 3. Analytical curve: CN intensity versus % N (w/w).

previous remarks that atmospheric N emission predominate over N emission originating from a solid target [5].

After fixing argon flow in 10 L min^{-1}, standards and samples were analyzed. To fit a linear model for the analytical curve, correlation between spectral intensities of CN band and %N (w/w) in the standards was evaluated, for each CN band from violet system. The band showing the best linear correlation was the most intense CN band at 388.3 nm (Fig. 1). The obtained analytical curve (Fig. 3) showed good linearity with dynamic linear range from 1.72% to 5.98% N (w/w) and correlation coefficient (r) of 0.97. The limits of detection and quantification calculated according to IUPAC [22] were 0.52% and 1.72% (w/w), respectively.

From the analytical curve, the levels of N were determined in the prepared fertilizers. The obtained values were 1.99 ± 0.45% for peanut shell fertilizer, 2.19 ± 0.85% for fiber of banana tree and 1.78 ± 0.40% for eucalyptus. The comparison among the determined and expected values (2.12% N), do not shows statistical differences at 95% confidence level, indicating the accuracy of proposed method.

Reports about N determination in soil or fertilizer samples by LIBS have employed characteristic and intense N lines, i.e. 742.36 nm, 744.23 nm and 746.83 nm [5,21,23], complex spectral preprocessing and multivariate calibration to enable accurate determination [23-25]. Concerning univariate method, Dong et al. (2013) after fit a linear analytical curve using intensity of atomic emission line at 746.83 nm, conclude the accuracy of quantitative determination is much higher using an internal standard [21]. Furthermore, Morais et al. (2017) also using a univariate model, minimized the severe matrix effects in Ca determination in biochar-based fertilizers, by the normalization of atomic signal using internal standardization [26]. These finds contrast with those observed here since the molecular emission signals of CN were high correlated with N levels in both standards and samples, dispensing spectral corrections and suggesting the diatomic emission was less affected by the matrix effect.

4. Conclusions

A new proposal for nitrogen determination was presented based on monitoring a diatomic emission line of CN, by LIBS. This emission showed high correlation with nitrogen levels in standards and samples. The method expands the LIBS potential for a simple and low-cost nitrogen determination in different matrices, suggesting CN molecular signals is less susceptible to matrix effects.

Concerning biochar-based fertilizers, the recalcitrant features of the material and the difficulties associated with this sample preparation for conventional nitrogen analysis, the developed method is a relevant and low-cost tool, which can be successfully applied in the quality assurance of these fertilizers.

CRediT authorship contribution statement

Samia R. Dib: Investigation, Formal analysis, Data curation. **Maurílio G. Nespeca:** Validation. **Dário Santos Junior:** Resources, Writing - review & editing. **Clovis A. Ribeiro:** Resources. **Marisa S. Crespi:** Resources. **José Anchieta Gomes Neto:** Resources, Writing - original draft. **Edilene C. Ferreira:** Conceptualization, Project administration, Funding acquisition, Writing - review & editing.

Declaration of Competing Interest

The authors declare that they have no known competing financial interests or personal relationships that could have appeared to influence the work reported in this paper.

Acknowledgements

The authors thank the São Paulo Research Foundation (FAPESP, Grants # 2015/24757-9 and 2019/18873-7) for financially supporting this work and the Conselho Nacional de Desenvolvimento Científico e Tecnológico (CNPq) for the researchship to E.C.F (grant # 308200/2018-7) and J.A.G.N (grant # 302414/2017-7).

References

[1] P. Sáez-Plaza, M.J. Navas, S. Wybraniec, T. Michalowsky, A.G. Asuero, Na overview of the Kjeldahl method of nitrogen determination. Part II. Sample preparation, working scale, instrumental finish, and quality control, Crit. Rev. Anal. Chem. 43 (2013) 224–272, https://doi.org/10.1080/10408347.2012.751787.

[2] Z. Marczenko, Separation and Spectrophotometric Determination of Elements, 2nd ed., Ellis Horwood Ltd, Chichester, 1986.

[3] D. Abrams, D. Metcalf, M. Hojjatie, Determination of Kjeldahl nitrogen in fertilizers by AOAC official method 978.02: Effect of copper sulfate as a catalyst, Journal of AOAC International, 97 (2014) 764-767. https://doi.org/10.5740/jaoacint.13-299.

[4] A. W. Miziolek, V. Palleschi, I. Schechter (Eds), Laser-Induced Breakdown Spectroscopy (LIBS), Cambridge University Press, Cambridge, 2006.

[5] R.D. Harris, D.A. Cremers, M.H. Ebinger, B.K. Bluhm, Determination of nitrogen in sand using laser-induced breakdown spectroscopy, Appl. Spectrosc. 58 (2004) 70–775.

[6] P.R. Villas-Boas, M.A. Franco, H.T. Gollany, D.M.B.P. Milori, Applications of laser-induced breakdown spectroscopy for soil characterization, part II: review of elemental analysis and soil classification, Eur. J. Soil Sci. (2019) 1–14, https://doi.org/10.1111/ejss.12889.

[7] J. Serrano, J. Moros, J.J. Laserna, Exploring the formation routes of diatomic hydrogenated radicals using femtosecond laser- induced breakdown spectroscopy of deuterated molecular solids, J. Anal. At. Spectrom. 30 (2015) 2343–2352, https://doi.org/10.1039/c5ja00192g.

[8] D.H. Plemmons, C. Parigger, J.W.L. Lewis, J.O. Hornkohl, Analysis of combined spectra of NH and N_2, Appl. Opt. 37 (1998) 2493–2498, https://doi.org/10.1364/AO.37.002493.

[9] Y. Liu, L. Gigant, M. Baudelet, M. Richardson, Correlation between laser-induced breakdown spectroscopy signal and moisture content, Spectrochim. Acta Part B 73 (2012) 71–74, https://doi.org/10.1016/j.sab.2012.07.009.

[10] P. Lucena, A. Doña, L.M. Tobaria, J.J. Laserna, New challenges and Insights in the detection and spectral identification of organic explosives by laser induced breakdown spectroscopy, Spectrochim. Acta Part B 66 (2011) 12–20, https://doi.org/10.1016/j.sab.2010.11.012.
[11] S. Rai, A.K. Rai, Characterization of organic materials by LIBS for exploration of correlation between molecular and elemental LIBS signals, AIP Adv. 1 (042103) (2011) 1–11, https://doi.org/10.1063/1.3650860.
[12] S.J. Mousavi, M.H. Farsani, S.M.R. Darbani, A. Mousaviazar, M. Soltanolkotabi, A. Eslami Majd, CN and C_2 vibrational spectra analysis in molecular LIBS of organic materials, Appl. Phys. B Lasers Opt. 122 (106) (2016) 1–16, https://doi.org/10.1007/s00340-016-6371-6.
[13] P.K. Tiwari, N.K. Rai, R. Kumar, C.G. Parigger, A.K. Rai, Atomic and molecular laser-induced breakdown spectroscopy of selected pharmaceuticals, Atoms 7 (71) (2019) 1–12, https://doi.org/10.3390/atoms7030071.
[14] D.S. Dias, M.S. Crespi, L.D.M. Torquato, M. Kobelnik, C.A. Ribeiro, Torrefied banana tree fiber pellets having embedded urea for agricultural use, J. Therm. Anal. Calorim. 131 (2018) 705–712, https://doi.org/10.1007/s10973-016-6049-7.
[15] A. Sarkar, D. Alamelu, S.K. Aggarwal, Laser-induced breakdown spectroscopy for determination of uranium inthorium–uranium mixed oxide fuel materials, Talanta 78 (2009) 800–804, https://doi.org/10.1016/j.talanta.2008.12.046.
[16] A.L. Vieira, T.V. Silva, F.S.I. de Sousa, G.S. Senesi, D. Santos Júnior, E.C. Ferreira, J.A. Gomes Neto, Determinations of phosphorus in fertilizers by spark discharge-assisted laser-induced breakdown spectroscopy, Microchem. J. 139 (2018) 322–326, https://doi.org/10.1016/j.microc.2018.03.011.
[17] A.L. Vieira, M.G. Nespeca, W.D. Pavini, E.C. Ferreira, J.A. Gomes Neto, A user-friendly excel spreadsheet for dealing with spectroscopic and chromatographic data, Chemom. Intell. Laborat. Syst. 194 (2019) 1–6, https://doi.org/10.1016/j.chemolab.2019.103816.
[18] Á. Fernández-Bravo, T. Delgado, P. Lucena, J.J. Laserna, Vibrational emission analysis of the CN molecules in laser-induced breakdown spectroscopy of organic compounds, Spectrochim. Acta Part B 89 (2013) 77–83.
[19] S. Trautner, J. Jasik, C.G. Parigger, J.D. Pedarnig, W. Spendelhofer, J. Lackner, P. Veis, J. Heitz, Laser-induced optical breakdown spectroscopy of polymer materials based on evaluation of molecular emission bands, Spectrochim. Acta Part A Mol. Biomol. Spectrosc. 174 (2017) 331–338, https://doi.org/10.1016/j.saa.2016.11.045.
[20] R.D. Harris, D.A. Cremers, M.H. Ebinger, B.K. Bluhm, Determination of nitrogen in sand using laser-induced breakdown spectroscopy, Appl. Spectrosc. 58 (2004) 770–775, https://doi.org/10.1366/0003702041389201.
[21] D.M. Dong, C.J. Zhao, W.G. Zheng, X.D. Zhao, L.Z. Jiao, Spectral characterization of nitrogen in farmland soil by laser-induced breakdown spectroscopy, Spectrosc. Lett. 46 (2013) 421–426, https://doi.org/10.1080/00387010.2012.747542.
[22] L.A. Currie, Detection and quantification limits: origins and historical overview, Anal. Chim. Acta 391 (1999) 127–134, https://doi.org/10.1016/S0003-2670(99)00105-1.
[23] B. Zhang, W. Sha, Y. Jiang, Z. Cui, Quantitative analysis of nitrogen in ammonium phosphate fertilizers using laser-induced breakdown spectroscopy, Appl. Opt. 58 (2019) 3277–3281, https://doi.org/10.1364/AO.58.003277.
[24] A.R. Angkat, K.B. Seminar, M. Rahmat, A. Sutandi, Estimation of soil nitrate (NO_3) level using laser-induced breakdown spectroscopy (LIBS), IOP Conf. Series: Earth Environm. 147 (012045) (2018) 1–6, https://doi.org/10.1088/1755-1315/147/1/012045.
[25] W. Sha, J. Li, W. Xiao, P. Ling, C. Lu, Quantitative analysis of elements in fertilizer using laser-induced breakdown spectroscopy coupled with support vector regression model, Sensors 19 (3277) (2019) 1–14, https://doi.org/10.3390/s19153277.
[26] C.P. Morais, A.I. Barros, D. Santos Júnior, C.A. Ribeiro, M.S. Crespi, G.S. Senesi, J.A. Gomes Neto, E.C. Ferreira, Calcium determination in biochar-based fertilizers by laser-induced breakdown spectroscopy using sodium as internal standard, Microchem. J. 134 (2017) 370–373, https://doi.org/10.1016/j.microc.2017.07.005.

Anexo 16

Atomic Spectroscopy

Article

Spark Discharge-LIBS: Evaluation of One-Point and Multi-Voltage Calibration for P and Al Determination

Alan Lima Vieira,[a] Edilene Cristina Ferreira,[a] Dário Santos Júnior,[b] Giorgio Saverio Senesi,[c] and José Anchieta Gomes Neto[a,*]

[a] São Paulo State University - UNESP, Analytical Chemistry Department, P.O. Box 355, 14801-970, Araraquara - SP, Brazil

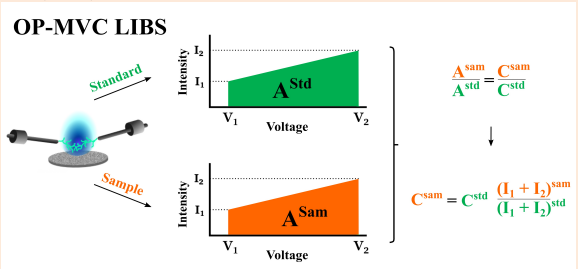
[b] Federal University of São Paulo - UNIFESP, Chemistry Department. 09913-030, Diadema - SP, Brazil

[c] CNR-Istituto per la Scienza e Tecnologia dei Plasmi (ISTP) sede di Bari, Via Amendola, 122/D - 70126 Bari, Italy

Received: *October 31, 2020;* ***Revised:*** *November 12, 2020;* ***Accepted:*** *November 12, 2020;* ***Available online:*** *November 30, 2020.*

DOI: 10.46770/AS.2020.202

ABSTRACT: Spark discharge (SD) laser-induced breakdown spectroscopy (LIBS) is a technique suitable to overcome the low energies of lasers by reheating the plasma, increasing the emission intensities and to perform single-standard calibration. A calibration method called one-point and multi-voltage calibration (OP-MVC), which requires two different voltages applied to both the standard and the sample, is proposed for use with SD-LIBS. The performance of this method was compared to that of the one-point and multi-lines calibration (OP-MLC) and the slope ratio calibration (SRC) methods for LIBS determination of Al in certified reference plant leaves and P in commercial fertilizers. No statistical differences at the 95% confidence level were observed between the Al and P concentrations determined by OP-MVC LIBS for the Al certified values and the P values measured by high-resolution continuum-source flame atomic absorption spectrometry (HR-CS FAAS). The limit of detection (LOD) for P was 0.60 wt% P_2O_5 and 35.1 mg kg^{-1} for Al. The relative standard deviation (n=3) was typically 7% for Al and in the 4 - 10% range for P.



INTRODUCTION

The interest in laser-induced breakdown spectroscopy (LIBS) for elemental analysis has increased greatly in recent years due to its capability to analyze a wide range of samples.[1] However, despite its advantages, the low sensitivity and calibration of this technique are still challenging.[2-4]

Among several approaches attempted to achieve LIBS signal enhancement,[2,3,5,6] spark discharge (SD) was found to be simple and relatively low-cost.[7] Since its first proposal in 1962,[7] SD-LIBS has been used to analyze a variety of samples[8] in various sectors of agriculture[9], such as soil,[10-17] phosphate rock,[10,18] rice,[19] honey,[20] coal[21,22] and onion leaves.[23] For instance, when using the SD method, the signal-to-background (S/B) ratio increased up to 7 times in the analysis of Pb and As in soil,[11] up to 3 times for As, Al, Ba, Ca, Co, Fe, Mg, Pb, Si, Sr, Ti and V in soil,[13] and up to 12 times for P in fertilizer.[18] Furthermore, the detection limit decreased 10 times for Pb, Mg and Sn in soil[15] and improved to 0.028 ppm for Cu in onion leaves.[23]

Besides sensitivity, calibration is also considered a main issue in LIBS analysis due to the matrix effects.[9,24] Several univariate and multivariate calibration methods have been applied to overcome these effects, including partial least squares (PLS),[9,25] artificial neural networks (ANN),[9,25] principal component regression (PCR),[9,25] external calibration (EC),[18,24] internal standardization (IS),[24] calibration-free (CF),[26,27] one-point calibration (OPC),[27,28] CF inverse,[27,29] C-sigma,[27,30] and single-sample calibration (SSC).[31] In particular, the SSC method does not require the calculation of plasma temperature, electron number density or other experimental parameters.[26-30]

The use of a single standard to produce several signal intensities (multi-points), which avoids the preparation of a set of solid standards with a similar matrix to test the samples at different

analyte concentrations, is very attractive. The one-point and multi-line calibration (OP-MLC) method proposed by Hao *et al*.[32] used several wavelengths of Mn, Cr, Ni and Ti to analyze alloy steel, achieving the relative errors of 9, 22, 21 and 36%, respectively. Nunes et al.[33] used the slope ratio calibration (SRC) method[33] to determine B, Ca, Cu Mg, Fe, Mn, P and Zn in plant leaves with an equation equivalent to single-point calibration. An increase of the emission intensities as a function of the applied voltage was observed in the SD-LIBS analysis of Al and Cu in air,[34] As, Pb, Si and Mn in soil,[11,35] Si in silicon crystals,[36] P in fertilizers[18] and Pb and Fe in copper alloys.[37] Quantitative analysis by SD-LIBS usually employs calibration with a fixed single voltage and standards at various concentrations,[9-23] whereas the use of a single standard and various applied voltages has rarely been reported in the literature.

This study aimed to evaluate the performance of one-point and multi-voltage calibration (OP-MVC) for the SD-LIBS determination of Al and P in plant leaves and fertilizers, respectively, in comparison with high-resolution continuum source atomic absorption spectrometry (HR-CS AAS), OP-MLC and SRC. This method required the measurement of the intensities (I) of the standard (C^{std}) and the unknown sample (C^{sample}) at two voltages, so that C^{sample} can be calculated (see Equation 3 below).

EXPERIMENTAL

Samples, standards, reagents and procedures

Six fertilizer samples containing different P concentrations (P_2O_5 wt%) were obtained at a local market in Araraquara city (São Paulo State, Brazil). An amount of 1000 g of each sample was quartered, and aliquots of 250 g were ground manually with a pistil in an agate mortar to obtain a fine powder, which was then dried at 105° C for 12 h. Calcium carbonate and NIST SRM 1568a Rice Flour were employed as blanks for P and Al, respectively, and to calculate the limit of detection (LOD) and the limit of quantification (LOQ). The 1515 Apple Leaves, 1570a Spinach Leaves, 1573a Tomato Leaves and 120c Phosphate Rock standard reference materials (SRM) from the National Institute of Standards and Technology (NIST, Gaithersburg, MD, USA) were employed for the evaluation of calibration and accuracy. Disc pellets of 250 mg powdered fertilizer samples, SRM plant leaves and blanks were prepared daily using the SL-10/15 hydraulic press (Solab, Piracicaba, Brazil), operating at a pressure of 7.5 ton cm^{-2} for 3 min.

For comparative purposes, P was determined by HR-CS AAS after acid digestion of the sample. In particular, 200 mg of each fertilizer sample and phosphate rock SRM was accurately weighed, transferred to a microwave flask, and 3 mL of HCl and HNO_3 solution at a ratio 1:3 (reverse *aqua regia*), 2 mL of deionized water and 1 mL of hydrogen peroxide were added. High purity de-ionized water (resistivity 18.2 MΩ cm) was used to prepare all solutions, obtained with a Millipore Rios 5® reverse osmosis and a Milli-Q Academic® deionizer system (Millipore Corporation, Bedford, MA, USA). Hydrochloric acid, nitric acid, and 30 wt% hydrogen peroxide were purchased from Merck (Darmstadt, Germany).

Digestion was performed in a Multiwave microwave oven (Anton Paar, Graz, Austria). The optimized program involving power/ramp time/hold time consisted in the following steps: step 1, 1000 W/15 min/0 min; step 2, 1000 W/0 min/10 min; step 3, 0 W/0 min/20 min (ventilation). After cooling, the digests were transferred into polypropylene flasks and diluted with deionized water to a final volume of 30 mL.

Instrumentation

The LIBS system used for Al and P determinations consisted of a Q-switched ND:YAG laser (Big Sky Ultra 50, Quantel USA, Bozeman, MT, USA), operating at 1064 nm, 9 ns of pulse duration, 10 Hz repetition rate, energy power of 48.7 ± 0.4 mJ, measured by laser power and energy meter (FieldMaxII-P, Coherent, Inc., Santa Clara, CA, USA). The laser beam was focused onto the sample surface by a plano-convex lens (12-cm focal length), thus producing a spot diameter of about 300 µm, resulting in a laser fluence of *ca*. 69 J cm^{-2} and an irradiance of 0.59 GW cm^{-2} delivered to the sample. The emission spectra were collected by an optical fiber bundle at an angle of 45° with respect to the laser beam and transferred to four spectrometers of the HR2000+ (Ocean Optics, Dunedin, FL, USA), operating at a spectral range from 200 at 620 nm, with optical resolution of 0.5 nm full width at half maximum (FWHM). The analysis was performed using 1-ms integration time and 1-µs Q-switched delay. The LIBS system included an automatic *x-y* direction sample holder and a video camera inside the sampling chamber in order to help the analyst to control the sample position. The laser was rasterized over a sample surface of about 3 mm^2 and broadband spectra from 10 single-pulse ablations were collected and mapped on discrete XY spatial coordinates. All measurements were performed at atmospheric air pressure.

The SD-LIBS system employed two cylindrical, pure tungsten electrodes of 100-mm length and 2.6-mm diameter, with tips arranged at a distance of 4 mm between them and 2 mm above the sample surface. The electrodes were connected to a single-spark generator operating in the voltage range from 2.0 to 4.5 kV. More information about the SD system can be found elsewhere.[18] The peak heights of the atomic lines of Al I at 308.22 nm and P I at 214.91 nm were obtained using Excel spreadsheet "Chromatograms and Spectra Handling"[38] and Microsoft Excel for data processing and calculating the concentrations. A scheme of the experimental setup is shown in Fig. 1.

The concentrations of the sample digests, prepared as described above, were determined by HR-CS AAS using an Analytik Jena ContrAA 300, equipped with a xenon short-arc lamp XBO 301

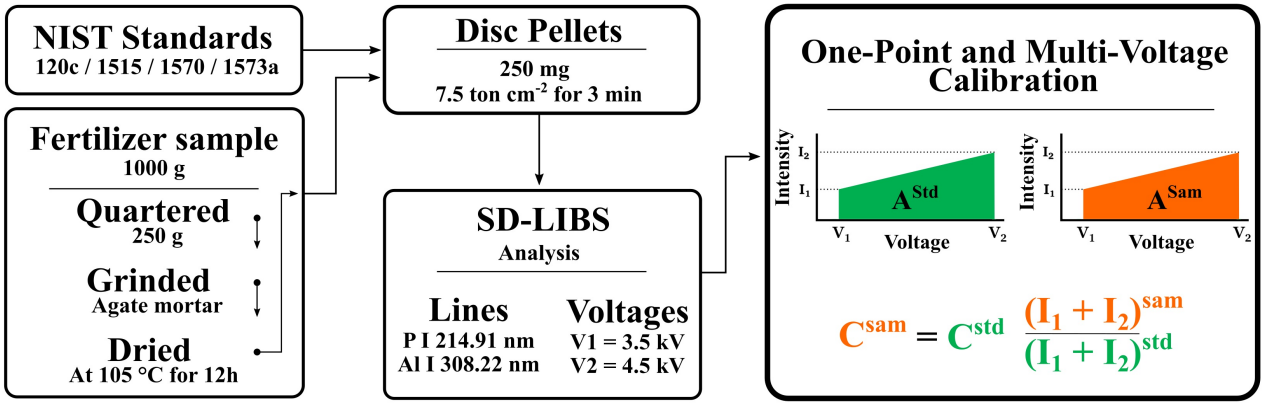


Fig. 1 Scheme of the experiment.

(GLE, Berlin, Germany) and operating in hot-spot mode as the continuum radiation source was used. The instrument was equipped with a high-resolution double-Echelle grating monochromator (< 2 pm per pixel in the far ultraviolet range) and a charge-coupled device (CCD) array detector. All measurements were performed in triplicate using optimized operating conditions.[39]

Fundamental aspects

In atomic emission spectrometry, the emission response at a given wavelength ($I^{ji}_{(\lambda_{ij})}$) is directly related to the analyte concentration (C) and the excited-state transition energy (E_j),[32] according to:

$$I^{ji}_{(\lambda_{ij})} = \frac{FCA_{ji}g_j}{Q(T)} e^{-E_j/k_BT} \quad \text{(Eq. 1)}$$

where F, A_{ji}, g_j, Q(T), k_B, and T are, respectively, the instrumental proportionality constant, transition probability, excited-state degeneracy, partition function, Boltzmann constant and temperature.

Based on this equation, for a certain analyte with the concentration C in a given medium, the emission intensity, I, at a given wavelength, can be described as:

$$I = mC \quad \text{(Eq. 2)}$$

where m is the proportionality constant of the LIBS instrument.

If a calibration standard with a similar matrix is measured by the same instrument in identical plasma conditions, the ratio between the intensities is proportional to the ratio between the respective concentrations, then the concentration of the analyte in the sample can be calculated according to:

$$C^{sam} = C^{std} \frac{I^{sam}}{I^{std}} \quad \text{(Eq. 3)}$$

The proposed OP-MVC method requires that both the standard and the sample be submitted to SD using two different voltages (V_1, V_2) consecutively, so that the two measured intensities, I_1 and I_2, define a rectangular trapeze with an area A, given by:

$$A = \frac{(I_1+I_2).(V_2-V_1)}{2} \quad \text{(Eq. 4)}$$

If the emission intensity is proportional to the concentration, then also its area is. Thus, if the ratio between the intensities in Eq. 3 is replaced by the ratio between the corresponding areas, the concentration of the analyte in the sample can be calculated according to:

$$C^{sam} = C^{std} \frac{(I_1+I_2)^{sam}}{(I_1+I_2)^{std}} \quad \text{(Eq. 5)}$$

The LOD and LOQ can be calculated according to:

$$\text{LOD} = C_{Blk} + 3S_{Blk} \quad \text{(Eq. 6)}$$

$$\text{LOQ} = C_{Blk} + 10S_{Blk} \quad \text{(Eq. 7)}$$

where C_{Blk} and S_{Blk} are, respectively, the average concentration and the standard deviation of 10 measurements of the concentration in the blank samples.[40]

In OP-MVC, the uncertainties of the analyte concentration ($S_{C_{sam}}$) depend on the errors associated to the intensities of both the sample ($S_{I_{sam}}$) and the standard ($S_{I_{std}}$), and on the confidence interval of the CRM standard ($S_{C_{std}}$), which can be estimated by the error propagation according to:

$$\frac{S_{C_{sam}}}{C_{sam}} = \sqrt{\left(\frac{S_{C_{std}}}{C_{std}}\right)^2 + \left(\frac{S_{I_{sam}}}{I_{sam}}\right)^2 + \left(\frac{S_{I_{std}}}{I_{std}}\right)^2} \quad \text{(Eq. 8)}$$

Comparative strategies based on single-standard calibration

The performance of OP-MVC was compared to that of the SRC[33] and OP-MLC[32] methods in determining P in fertilizers and Al in plant materials. In particular, the following equation was used for SRC:

$$C^{Sample} = C^{Std} \frac{b^{Sample}}{b^{Std}} \quad \text{(Eq. 9)}$$

where b_{sample} and b_{std} are the slopes of the standard and the sample, which were obtained using the 5, 10, 15, 20 and 30 cumulative laser pulses with the SD-LIBS operating at 4.5 kV. The analytical lines P I at 214.91 nm and Al I at 308.22 nm were used for P and Al, respectively.

The following equation was used for OP-MLC:

$$C^{Sample} = C^{Std}\ \alpha^{Sample\ .Std} \qquad \text{(Eq. 10)}$$

where $\alpha^{Sample.Std}$ is the slope obtained by plotting the intensities of the sample (y-axis) versus those of the standard (x-axis) measured for different emission lines of the analyte. In particular, the emission lines of P I at 213.62 nm, 214.91 nm and 215.41 nm, and the line of Al I at 308.22 nm, which was selected after considering its lower interference, were employed. However, as OP-MLC requires multiple lines, different wavelengths located at the wing of the Al I core line at 308.22 nm, i.e., 308.01, 308.07, 308.12, 308.17, 308.22 nm, were also used. The SD-LIBS employed 4.5 kV because the Al signals were very low when only LIBS is used.

RESULTS AND DISCUSSION

The P lines profile in the spectra of NIST SRM 120c Phosphate Rock (33.34 ± 0.06 wt% P_2O_5) and the Al lines profile in the spectra of NIST SRM 1515 Apple Leaves (284.5 ± 5.8 mg kg^{-1} Al) acquired by LIBS and SD-LIBS are showed in Fig. 2. Based on earlier information,[18] the P I line at 214.91 nm was selected for P determination in fertilizers, and the Al I line at 308.22 nm was chosen for Al determination in plants. Despite the higher intensity observed for the line of Al I at 309.27 nm, this line was not used due to possible spectral interferences caused by the Mg I lines at 309.10, 309.29 and 309.68 nm.[41] These lines might become critical for samples rich in Mg, such as NIST SRMs 1573a and 1515 which contain 12,000 mg kg^{-1} (not certified) and 2710 ± 120 mg kg^{-1} of Mg, respectively.

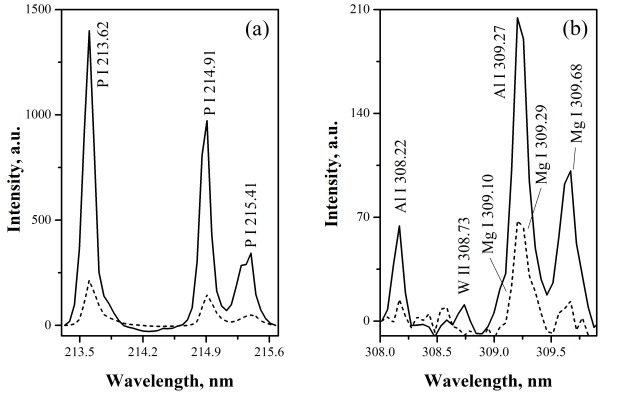


Fig. 2 LIBS (dashed line) and SD-LIBS (continuous line) spectra for (a) P in NIST SRM 120c Phosphate Rock and (b) Al in NIST SRM 1515 Apple Leaves. The voltage applied in SD-LIBS was 4.5 kV.

The effect of the applied voltage at the values of 2.0, 2.5, 3.0, 3.5, 4.0 and 4.5 kV on the emission intensities of the P I line at 214.91 nm and the Al I line at 308.22 nm was evaluated for the NIST SRM 120c and NIST SRM 1515 samples, respectively (Fig. 3). In both cases, the plots of the line intensity against the applied voltage were linear with correlation coefficients (r) of 0.989 and 0.999 for Al and P, respectively. The NIST SRM 1570a and 1573a in the case of Al (Fig. 3a) and all fertilizer samples in the case of P (Fig. 3b) were analyzed only at higher voltages, *i.e.*, 3.5, 4.0 and 4.5 kV, at which the highest line intensity of the analyte, i.e., a greater sensitivity, was achieved. In all cases, for both Al and P, the intensity versus voltage curves were linear with r > 0.97.

The extended temporal evolution of the plasma, and the increase of plasma temperature and electronic density achieved by reheating the plasma, improved the atomization and excitation processes.[10] In particular, the highest increase in the signal intensity for both elements, *i.e.,* 6.7-fold for P (NIST SRM 120c) and 4.4-fold for Al (NIST SRM 1515), was achieved at the maximum applied voltage, *i.e.,* 4.5 kV, which yielded a satisfactory relative standard deviation (RSD) for both Al and P. Thus, further experiments aiming to optimize data collection were carried out at the voltage of 4.5 kV.

Notwithstanding the high content of P in fertilizers and the re-excitation with 4.5-kV high voltage discharge, no self-reversal effect was observed for the peak profiles of P in the concentration range from 4.8 to 33.34 wt% P_2O_5 (Fig. 4a). Furthermore, the plots of the intensity of the emission lines of P I at 213.62, 214.91 and

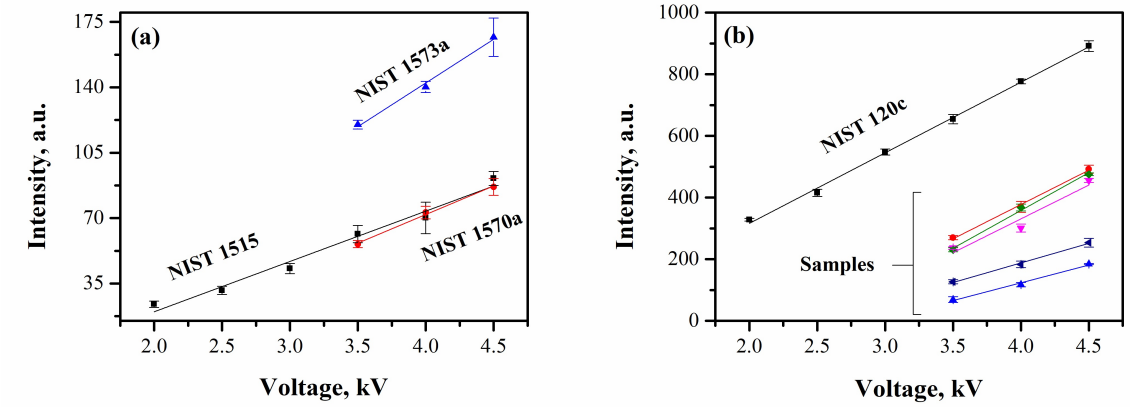


Fig. 3 Plots of line intensity vs. voltage (n = 3) for (a) line Al I at 308.22 nm in three NIST SRM plant leaves and (b) line of P I at 214.91 nm in NIST SRM 120c and fertilizer samples. The error bars represent the standard deviation of the measurements.

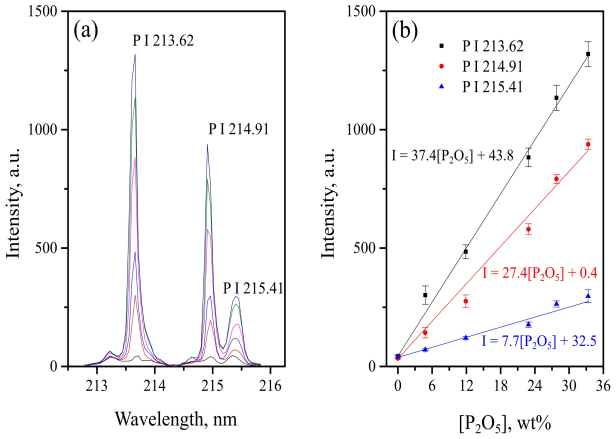


Fig. 4 SD-LIBS spectra of solid standards containing 0 (black), 4.8 (red), 11.9 (light blue), 22.9 (magenta), 27.8 (green) and 33.34 wt% P_2O_5 (dark blue) at an applied voltage of 4.5 kV (a), and (b) linear working range of P I lines at 213.62, 214.91 and 215.41 nm.

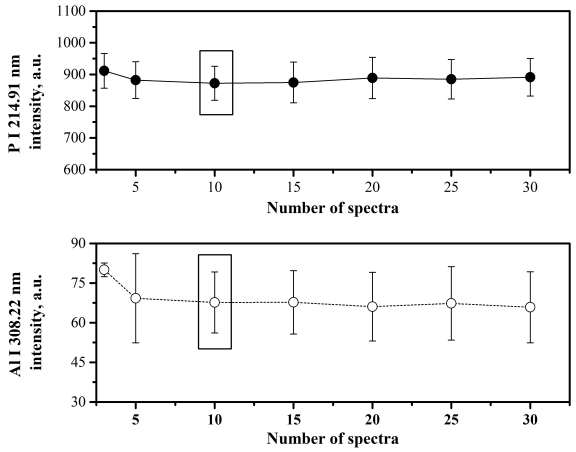


Fig. 5 Effect of the number of replicate spectra on the emission line intensities of Al I at 308.22 nm in NIST 1515 Apple Leaves SRM (○) and P I at 214.91 nm in NIST 120c Phosphate Rock SRM (●) recorded at an applied voltage of 4.5 kV. Circles correspond to the average values and error bars to standard deviations.

215.41 nm versus P concentration yielded straight lines (Fig. 4b) with correlation coefficients ≥ 0.997. As these results were obtained using the maximum voltage discharge, the OP-MVC method yielded emission intensities in the linear range. Generally, SD-LIBS studies do not investigate the influence of re-excitation by high-voltage discharge on self-absorption. The plasma temperature homogeneity increase achieved by SD-LIBS without changing the ablation rate would explain the reduction of P self-absorption in the plasma periphery. A similar effect was observed by Tang *et al.*[42] who used microwave to increase LIBS sensitivity.

The effect of the number of replicate spectra recorded at the emission intensities of P I at 214.91 nm and Al I at 308.22 nm was evaluated by acquiring 3, 5, 10, 15, 20, 25 and 30 spectra for the NIST SRM 120c Phosphate Rock and NIST SRM 1515 Apple Leaves at the voltage of 4.5 kV. The results obtained (Fig. 5) showed that the average intensity for both the Al and P lines remained constant for replicated spectra ≥ 5 and that a satisfactory precision (RSD: 6% for P and 17% for Al) was achieved for replicate spectra ≥ 10. Thus, the total of 10 replicate spectra was chosen for data acquisition as a compromise between precision, sensibility and sample throughput.

After optimization, the proposed calibration method was applied to determine P in fertilizers and Al in plant leaves using one or two voltages. In particular, the NIST SRM 120c Phosphate Rock was used as the unique standard to determine the P content in the five commercial fertilizer samples, which were also analyzed by HR-CS FAAS. The data in Table 1 show good agreement with the paired *t*-test at the 95% confidence level between the data achieved by OP-MVC LIBS and those obtained by HR-CS FAAS. The RSD values for P were in the 4.3 – 9.6% range.

For Al determinations, the NIST SRM 1515 Apple Leaves was used as the unique standard to analyze NIST SRM 1570a Spinach Leaves and NIST SRM 1573a Tomato Leaves, whereas the NIST SRM 1570a Spinach Leaves was used as the unique standard to analyze NIST SRM 1515 Apple Leaves. The results obtained by OP-MVC LIBS were in good agreement with the certified values with a paired *t*-test at the 95% confidence level (Table 1). The recoveries were in the range of 94 – 107% and the RSD values in the 6.0 – 6.9% interval.

The use of two voltages, V1: 3.5 kV and V2: 4.5 kV applied sequentially, achieved good performance in precision and accuracy, which may be attributed to the linear relationship existing between the line intensity and the applied voltage (Fig. 3). Furthermore, the use of three voltages appeared not to alter the results significantly, but it limited the analytical throughput due to the increased time needed to charge the capacitors. Calibration using only one applied voltage at 4.5 kV, which provided the best signal-to-noise ratio, was also tested. For the P and Al data, the relative standard deviations were in the range of 4.3 – 9.5% and 6 – 11%, respectively (Table 1). However, the precision achieved for both P and Al was improved when calibration was performed using two voltages (3.5 and 4.5 kV), which provided also better discrimination between the nominal and the actual applied voltage.

For comparative purposes, the performance of the SRC and OP-MLC methods was also tested for P and Al determination by LIBS (Table 1). The results obtained for Al by OP-MVC were in agreement with those achieved by SRC and OP-MLC at the 95% confidence level, but the RSD values for OP-MVC (in the range of 6.0 – 7.0%) were better than those for SRC and OP-MLC (in the range of 8.3 – 15.8% and 23.0 – 26.7%, respectively). However, the results obtained for P were in agreement with those achieved by SRC, but not by OP-MLC, at the 95% confidence level. The RSD values of P obtained by OP-MVC, SRC and OP-MLC ranged from 4.3 – 9.5%, 4.0 – 14.1% and 0.6 – 15.8%, respectively. Using OP-MVC, SRC and OP-MLC, the LOQs for P (expressed

Table 1. Comparative Results (Mean ± Standard Deviation, n=3) for the Determination of P (wt% P_2O_5) in Fertilizers and Al (mg kg^{-1}) in Plant Leaves Obtained by OP-MVC (with One and Two Voltages) and SRC and OP-MLC Methods

Sample/SRM	Comparative values	OP-MVC		SRC	OP-MLC	Standard used for calibration
		V1 = 4.5 kV	V1 = 3.5 kV V2 = 4.5 kV			
P						
Sample 1	19.0 ± 0.3 [a]	17.3 ± 1.4	17.7 ± 0.9	20.5 ± 2.9	15.0 ± 0.1 [c]	SRM-120c
Sample 2	6.5 ± 0.2 [a]	7.0 ± 0.8	6.9 ± 0.3	6.4 ± 0.4	7.9 ± 0.3 [c]	SRM-120c
Sample 3	17.2 ± 0.4 [a]	16.5 ± 1.6	17.1 ± 1.1	16.2 ± 1.7	14.0 ± 1.3 [c]	SRM-120c
Sample 4	9.2 ± 0.1 [a]	9.1 ± 0.7	9.4 ± 0.9	9.5 ± 1.1	11.4 ± 1.8 [c]	SRM-120c
Sample 5	19.0 ± 0.1 [a]	18.8 ± 1.2	18.5 ± 0.8	19.7 ± 0.8	16.8 ± 1.3 [c]	SRM-120c
Al						
NIST 1570a	310 ± 15 [b]	322 ± 14	316 ± 2	290 ± 46	343 ± 90	NIST 1515
NIST 1515	284.5 ± 5.8 [b]	288 ± 27	280 ± 18	295 ± 25	265 ± 61	NIST 1570a
NIST 1573a	598.4 ± 7.1 [b]	586 ± 56	591 ± 41	579 ± 48	685 ± 183	NIST 1515

[a] Comparative value determined by HR-CS FAAS; [b] Certified values; [c] Not in agreement with comparative values at the 95% confidence level.

as wt% P_2O_5) were, respectively, 2.0%, 2.3% and 2.7%, and for Al (mg kg^{-1}) 117, 126 and 269.

Different LIBS configurations may affect the quality of the data obtained for P using OP-MLC, as the emission line of P I at 213.62 nm may be interfered by those of Cu and Zn, which are commonly present in fertilizers, thus deteriorating the calibration curve obtained for OP-MLC. In particular, the correlation coefficients obtained by plotting the P signal for the sample in the *y*-axis and that of the NIST SRM 120c Phosphate Rock in the *x*-axis varied from 0.946 to 0.998, with the lower values possibly due to these spectral interferences. The significantly higher RSD values obtained by OP-MLC for Al in plant materials with respect to those for P in fertilizers (Table 1) might be due to the much lower content of Al (mg kg^{-1}) compared to P (wt%). Furthermore, the wavelengths employed for Al were located at the wing of the Al I line at 308.22 nm, i.e., the lines at 308.01, 308.07, 308.12, 308.17, and 308.22 nm. Although this procedure is not commonly used for MLC, it was a strategy adopted to overcome the limited number of non-interfered Al I lines. In conclusion, the differences among the results obtained with these various methods might be due to the different instrumental strategies used to increase the signal intensities, such as cumulative laser pulses (SRC), several lines (OP-MLC) and voltages (OP-MVC).

CONCLUSIONS

In this work, SD-LIBS was successfully used in combination with the SSC calibration method of OP-MVC to determine Al and P in plant leaves and fertilizers, respectively, achieving suitable accuracy, precision and LOQs. The required SD extra device used should not be seen as a serious shortcoming as it is a simple, low cost, and rugged tool capable of enhancing the signal intensities for any LIBS system, thus improving the performance especially of those featuring limited sensitivity.

For comparative purposes, the performance of the OP-MVC method was also evaluated with respect to the SRC and OP-MLC methods. Although SRC and OP-MLC are simple and performance calibration methods, they need high sensitivity LIBS systems depending on the specific analyte and sample. Further, SRC can be performed with one emission line, while OP-MLC is limited to elements that feature several lines. In general, all of these calibration methods employ a single solid calibration standard, so that difficulties related to the preparation of several solid standards (*e.g.,* external calibration) with physicochemical properties similar to the samples are minimized.

Finally, the proposed OP-MVC method cannot be considered as limited to LIBS analysis of Al and P in plants and fertilizers, but its performance appears promising to be tentatively extended to other analytes and samples in various matrices.

AUTHOR INFORMATION

Corresponding Author

*J. A. Gomes Neto

Email address: jose.anchieta@unesp.br

Notes

The authors declare no competing financial interest.

ACKNOWLEDGMENTS

The authors thank the São Paulo Research Foundation (FAPESP, Grant # 2019/07537-6) for financially supporting this work and the Conselho Nacional de Desenvolvimento Científico e Tecnológico (CNPq) for the fellowship to A.L.V. (grant# 141977/2016-7), and researchship to J.A.G.N. (grant # 302414/2017-7) and E.C.F. (grant # 308200/2018-7).

REFERENCES

1. S. Musazzi, and U. Perini, *Laser-Induced Breakdown Spectroscopy, Theory and Applications*. Springer-Verlag, Berlin, Germany, 2014.
2. X. Fu, G. Li and D. Dong, *Front. Phys.*, 2020, **68**, 10.3389. https://doi.org/10.3389/fphy.2020.00068
3. Y. Li, D. Tian, Y. Ding, G. Yang, K. Liu, C. Wang and X. Han, *Appl. Spectrosc. Rev.*, 2018, **53**, 1-35. https://doi.org/10.1080/05704928.2017.1352509
4. M. Martinez and M. Baudelet, *Anal. Bioanal. Chem.*, 2020, **412**, 27-36. https://doi.org/10.1007/s00216-019-02195-1
5. D. W. Hahn and N. Omenetto, *Appl. Spectrosc.*, 2012, **66**, 347-419. https://doi.org/10.1366/11-06574
6. Y. Liu, M. Baudelet and M. Richardson, *J. Anal. At. Spectrom.*, 2010, **25**, 1316-1323. https://doi.org/10.1039/C003304A
7. F. Brech and L. Cross, *Appl. Spectrosc.*, 1962, **16**, 59-64.
8. W. D. Zhou, Y. H. Guo and R. R. Zhang, *Front. Phys.*, 2020, **15**, 52201. https://doi.org/10.1007/s11467-020-0969-1
9. J. Peng, F. Liu, F. Zhou, K. Song, C. Zhang, L. Ye and Y. He, *Trends Anal. Chem.*, 2016, **85**, 260-272. https://doi.org/10.1016/j.trac.2016.08.015
10. A. A. Bol'shakov, X. Mao and R. E. Russo, *J. Anal. At. Spectrom.*, 2017, **32**, 657-670. https://doi.org/10.1039/C6JA00436A
11. L. I. Kexue, W. Zhou, Q. Shen, J. Shao and H. Qian, *Spectrochim. Acta. B.*, 2010, **65**, 420-424. https://doi.org/10.1016/j.sab.2010.04.006
12. M. V. Belkov, V. S. Burakov; A. De Giacomo, V. V. Kiris, S. N. Raikov, and N. V. Tarasenko, *Spectrochim. Acta. B.*, 2009, **64**, 899-904. https://doi.org/10.1016/j.sab.2009.07.019
13. K. Li, W. Zhou, Q. Shen, Z. Ren, and B. Peng, *J. Anal. At. Spectrom.*, 2010, **25**, 1475-1481. https://doi.org/10.1039/B922187E
14. V. S. Burakov, S. N. Raikov, N. V. Tarasenko, M. V. Belkov and V. V. Kiris, *J. Appl. Spectrosc.*, 2010, **77**, 595-608. https://doi.org/10.1007/s10812-010-9374-9
15. X. F. Li, W. Zhou, K. Li, H. Qian, R. Huiguo and R. Zhijun, *Opt. Comm.*, 2012, **285**, 54-58. https://doi.org/10.1016/j.optcom.2011.08.074
16. W. Zhou, K. Li, X. Li, H. Qian, J. Shao, X. Fang, P. Xie and W. Liu, *Opt. Lett.*, 2011, **36**, 2961-2963. https://doi.org/10.1364/OL.36.002961
17. X. F. Li, W. D. Zhou and Z. F. Cui, *Front. Phys.*, 2012, **7**, 721-727. https://doi.org/10.1007/s11467-012-0254-z
18. A. L. Vieira, T. V. Silva, F. S. I. de Sousa, G. S. Senesi, D. S. Júnior, E. C. Ferreira and J. A. Gomes Neto, *Microchem. J.*, 2018, **139**, 322-326. https://doi.org/10.1016/j.microc.2018.03.011
19. M. P. Rodríguez, P. M. Dirchwolf, T. V. Silva, R. N. Villafañe, J. A. Gomes Neto, R. G. Pellerano and E. C. Ferreira, *Food Chem.*, 2020, **331**, 127051. https://doi.org/10.1016/j.foodchem.2020.127051
20. M. G. Nespeca, A. L. Vieira, D. Santos Júnior, J. A. Gomes Neto and E. C. Ferreira, *Food Chem.*, 2020, **311**, 125886. https://doi.org/10.1016/j.foodchem.2019.125886
21. Z. Hou, Z. Wang, J. Liu, W. Ni and Z. Li, *Opt. Express*, 2014, **22**, 12909-12914. https://doi.org/10.1364/OE.22.012909
22. S. Sheta, M. S. Afgan, Z. Hou, S. C. Yao, L. Zhang, Z. Li and Z. Wang, *J. Anal. At. Spectrom.*, 2019, **34**, 1047-1082. https://doi.org/10.1039/C9JA00016J
23. A. Jabbar, M. Akhtar, S. Mehmmod, M. Iqbal, R. Ahmed and M. A. Baig, *Spectrochim. Acta B.*, 2019, **162**, 105719. https://doi.org/10.1016/j.sab.2019.105719
24. D. V. Babos, A. I. Barros, J. A. Nóbrega, and E. R. Pereira-Filho, *Spectrochim. Act. B.*, 2019, **155**, 90-98. https://doi.org/10.1016/j.sab.2019.03.010
25. M. Martinez and M. Baudelet, *Anal. Bioanal. Chem.*, 2020, **412**, 27-36. https://doi.org/10.1007/s00216-019-02195-1
26. A. Ciucci, M. Corsi, V. Palleschi, S. Rastelli, A. Salvetti and E. Tognoni, *Appl. Spectrosc.*, 1999, **53**, 960-964. https://doi.org/10.1366/0003702991947612
27. E. Grifoni, S. Legnaioli, G. Lorenzetti, S. Pagnotta, F. Poggialini, and V. Palleschi, *Spectrochim. Acta B.*, 2016, **124**, 40-46. https://doi.org/10.1016/j.sab.2016.08.022
28. G. Cavalcanti, D. Teixeira, S. Legnaioli, G. Lorenzetti, L. Pardini and V. Palleschi, *Spectrochim. Act. B.*, 2013, **87**, 51-56. https://doi.org/10.1016/j.sab.2013.05.016
29. R. Gaudiuso, M. Dell'Aglio, O. De Pascale, A. Santagata and A. De Giacomo, *Spectrochim. Acta B.*, 2012, **74-75**, 38-45. https://doi.org/10.1016/j.sab.2012.06.034
30. C. Aragón and J. A. Aguilera, *J. Quant. Spectrosc. Radiat. Transf.*, 2014, **149**, 90-102. https://doi.org/10.1016/j.jqsrt.2014.07.026
31. R. Yuan, Y. Tang, Z. Zhu, Z. Hao, J. Li, H. Yu, Y. Yu, L. Guo, X. Zeng and Y. Lu, *Anal. Chim. Acta.*, 2019, **1064**, 11-16. https://doi.org/10.1016/j.aca.2019.02.056
32. Z. Q. Hao, L. Liu, R. Zhou, Y. W. Ma, X. Y. Li, L. B. Guo, Y. F. Lu and X. Y. Zeng, *Opt. Express*, 2018, **26**, 22926-22933. https://doi.org/10.1364/OE.26.022926
33. L. C. Nunes, F. R. P. Rocha and F. J. Krug, *J. Anal. At. Spectrom.*, 2019, **34**, 2314-2324. https://doi.org/10.1039/C9JA00270G
34. O. A. Nassef and H. E. Elsayed-Ali, *Spectrochim Acta. B.*, 2005, **60**, 1564-1572. https://doi.org/10.1016/j.sab.2005.10.010
35. K. Li, W. Zhou, Q. Shen, Z. Ren, B. Peng, L. I. Kexue, W. Zhou, Q. Shen, Z. Ren and B. Peng, *J. Anal. At. Spectrom.*, 2010, **25**, 1475-1481. https://doi.org/10.1039/b922187e
36. W. Zhou, X. Su, H. Qian, K. Li, X. Li, Y. Yu and Z. Ren, *J. Anal. At. Spectrom.*, 2013, **28**, 702-710. https://doi.org/10.1039/c3ja30355a
37. Y. Jiang, R. Li and Y. Chen, *J. Anal. At. Spectrom.*, 2019, **34**, 1838-1845. https://doi.org/10.1039/C9JA00169G
38. A. L. Vieira, M. G. Nespeca, W. D. Pavini, E. C. Ferreira and J. A. Gomes Neto, *Chemom. Intell. Lab. Syst.*, 2019, **194**, 103816. https://doi.org/10.1016/j.chemolab.2019.103816
39. M. A. Bechlin, F. M. Fortunato, R. M. Da Silva, E. C. Ferreira, and J. A. Gomes Neto, *Spectrochim. Acta Part B.*, 2014, **101**, 240-244. https://doi.org/10.1016/j.sab.2014.09.012
40. J. Miller, and J. C. Miller, *Statistics and Chemometrics for Analytical Chemistry*. Pearson, Harlow, U.K., 2010.
41. NIST Atomic Spectra Database (https://physics.nist.gov/PhysRefData/ASD/).
42. Y. Tang, J. Li, Z. Hao, S. Tang, Z. Zhu, L. Guo, X. Li, X. Zeng, J. Duan, and Y. Lu, *Opt. Express.*, 2018, **26**, 12121. https://doi.org/10.1364/OE.26.012121

Anexo 17

Vibrational Spectroscopy 112 (2021) 103183

Contents lists available at ScienceDirect

Vibrational Spectroscopy

journal homepage: www.elsevier.com/locate/vibspec

Raman spectroscopy for discriminating transgenic corns

Samia Rodrigues Dib [a], Tiago Varão Silva [a], José Anchieta Gomes Neto [a], Lauro José Moreira Guimarães [b], Ednaldo José Ferreira [c], Edilene Cristina Ferreira [a,*]

[a] São Paulo State University – UNESP, Chemistry Institute, Dep. of Analytical, Physical-Chemical and Inorganic Chemistry, Rua Prof. Francisco Degni, 55, Quitandinha, P.O. Box 355, 14801-970 Araraquara, SP, Brazil
[b] Embrapa Maize & Sorghum, Rodovia MG-424, Km 45, P.O. Box: 285 or 151, 35701-970, Sete Lagoas, MG, Brazil
[c] Embrapa Instrumentation, Rua XV de Novembro, 1.452, Centro, P.O. Box 741, 13560-970 São Carlos, SP, Brazil

ARTICLE INFO

Keywords:
Corn
Genetic modification
Transgenic
Raman spectroscopy
LDA

ABSTRACT

Discrimination of genetically modified organisms is increasingly required by legislation and consumers worldwide. Currently the most commonly used detection methods for identification of transgenic crops are high cost, destructive and time-consuming, so not suitable for fast and extensive application. Raman is a noninvasive and nondestructive spectroscopic technique capable of extracting sample fingerprints. In this paper, Raman spectroscopy and chemometric tools were evaluated for discrimination of transgenic corn. Different spectral preprocessing as well as algorithms for variables selection were evaluated to fit a classifier model based on linear discriminant analysis (LDA). Results showed spectral bands assigned to carbohydrates and carotenoids responsible for classes discrimination. The best classifier achieved 87.5 % of predictive accuracy. These results suggest that genetic differences between evaluated classes are also expressed in their chemical composition, which could be detected using Raman spectroscopy. The developed method is clean, fast and can contribute for establishing normative about genetically modified foods.

1. Introduction

One of the practices in modern agriculture has been adopting new varieties of plant from the arsenal of biotechnology solutions, which includes the genetic transformation, in most of the cases, to facilitate insect and weed control in the field. In this context, some important crops like soybeans, corn, canola, cotton and others have been passed through this process, and the transformed cultivars are called genetically modified (GM) crops or transgenic [1]. There is a vast amount of different transgenics for several crop species, with different genes, and different combination of genes.

GM crops can be tolerant to a specific herbicide or resistant to one or more insects or their larvae. The genetic modification has also the potential to be used to improve nutritional characteristics or to control the absence of intrinsic allergenic compounds, which are conventionally present in the unmodified organism [2]. However, crop protection is one of the main factors for using transgenics, because this kind of genetic technology facilitates field practices and brings positive effects on agricultural yield increase [1].

Corn (*Zea mays* L.) is an important food due to its nutritional properties and its application in the food industry [3]. The constant demand for corn products makes productivity an important requirement as well as corn one of the most target among GM crops.

According to the International Service for the Acquisition of Agri-biotech Applications (ISAA), cultivation of GM crops in 2018 increased *ca.* 1.9 millions hectares compared to 2017, reaching 1917 million hectares worldwide with transgenic crops [4]. Despite the increase in production of GM crops, their acceptability for consumers is still quite questionable, especially with regard to safety making its consumption not fully accepted [5]. Some countries issued normative aiming to control the production and consumption of GMFs (Genetically Modified Foods) [6].

Regulatory demands focused on safety of foods are often accompanied by (or sometimes the starting point) scientific and technological challenges. In this sense, the corn value chain has lacked fast and low cost techniques to be inserted into it for detecting GM crops. The main detection methods for GM products and crops are polymerase chain reaction (PCR) [7], enzyme-linked immunosorbent analysis (ELISA) [8],

* Corresponding author.
E-mail addresses: rdib.samia@gmail.com (S.R. Dib), varao29@yahoo.com.br (T.V. Silva), jose.anchieta@unesp.br (J.A.G. Neto), lauro.guimaraes@embrapa.br (L.J.M. Guimarães), ednaldo.ferreira@embrapa.br (E.J. Ferreira), edilene.c.ferreira@unesp.br (E.C. Ferreira).

https://doi.org/10.1016/j.vibspec.2020.103183
Received 10 September 2020; Received in revised form 28 October 2020; Accepted 5 November 2020
Available online 8 November 2020
0924-2031/© 2020 Elsevier B.V. All rights reserved.

Western blotting [9], two-dimensional electrophoresis [10], microarray analysis [11], mass spectrometry [12], chromatographic protein profiles [13] and electrophoresis [14]. These methods usually have good specificity and high sensitivity, although some disadvantages are observed such as high cost per analysis, destructive sampling and time-consuming procedures, with low scalability potential for insertion in the corn production chain.

Currently, non or minimally destructive analytical techniques combined with chemometric methods have demonstrated success for fast identification of GM crops. Some spectral techniques have been studied including terahertz spectroscopy [15], Laser-induced breakdown spectroscopy [16], infrared spectroscopy [17], near infrared [18], visible/near infrared [19] and multispectral imaging [20].

In addition, Raman spectroscopy, have shown potential for applications in agriculture and food industry [21–25].

The Raman stands out as a candidate tool to be applied to GM crops identification since it is a noninvasive and nondestructive spectroscopic technique capable of providing fingerprints that come from inelastic scattering of light from energy exchange with molecular vibrations in samples.

Although the vibrations of molecules can be explored for sample characterization, other factors, such as physical and chemical properties of the matrix as well as several experimental factors can mask Raman spectrum information. For instance, the low Raman scattering signal, especially when it comes from biological samples, have orders of magnitude lower than intrinsic fluorescence of the organic molecules [26]. In that sense, chemometrics tools aimed at variable selection and fitting of classification models might be a solution to get some hidden spectral signals.

Raman spectroscopic techniques together with chemometric tools have been successfully applied for various purposes [24,27,28]. This promising approach was adopted to develop a new method capable of identify transgenic corn seeds from its conventional counterparts.

2. Materials and methods

2.1. Sample preparation

Seeds samples of corn (*Zea mays* L) were provided by Brazilian Agricultural Research Corporation (Embrapa) from a Research Center for Maize and Sorghum, located in Minas Gerais state, Brazil. The seeds used for analysis were representative of fourteen pairs of transgenic and non-transgenic corn hybrids, totaling 28 samples. The transgenic samples used in this study resulted from the introgression of *Bacillus thuringiensis* genes (cry1A.105 + cry2Ab2), that express resistance to insects (Lepidoptera), and *Agrobacterium spp* gene (c4-epsps), that express tolerance to the glyphosate herbicide. It is important to point that there are lots of other types of transgenic corn, thus, the results are specific for the combination of genes cited above.

Ten seeds were randomly picked for each hybrid species and for each class (transgenic and non-transgenic) from a corn seed storage silo. Sample preparation consisted in cryogenic grinding, which were carried out using a Spex 6800 cryogenic mill (USA). Each isolated seed was introduced into the grinding flask and homogenized using the follow program: 2.0 min of pre-freezing; 3.0 min of grinding and 2.0 min of freezing between the milling steps. This procedure was repeated 10 times for each sample. Each ground seed resulted in a pellet. Pellets were prepared by applying 10 tons of pressure in a mechanical press (Solab SL – 10/15, Piracicaba, Brazil).

2.2. Raman spectra acquisition

Raman spectra were acquired using a portable i-Raman spectrometer (BWS415-785H B & W Tek, Inc., USA) equipped with a near infrared laser operating at 785 nm, with laser spot on sample surface of 85 μm. Spectra comprised the range from 172 to 2700 cm^{-1}, with spectral resolution of 3.5 cm^{-1}. The laser power was 315 mW and the integration time 10 s. For measurements, the probe was mounted using a rod and claw, setting to 1.5 mm between the tip of the probe and the sample surface. Fifty scans were averaged in each spot (measuring point) and five different spots were performed for each pellet.

2.3. Spectral data preprocessing and classification model

Spectral baseline correction by Whittaker filter (WF), Standard Normal Variate transformation (SNV), Normalization (N) and smoothing Savitzky–Golay (SG) [29] with 15-points and second order polynomial, were considered for spectral preprocessing. The spectral preprocessing using WF were applied alone or combined to as follow: WF + SG, WF + SG + SNV, WF + SNV and WF + SG + N (for example, "WF + SG" is sequence of operations, starting by WF and followed by SG). The height of the band at 1456 cm^{-1}, which corresponds to CH_2 vibrations of non-specific structure was used for normalization purposes as previously reported [30].

Linear Discriminant Analysis (LDA) was evaluated to the task of fitting classification models. For this assignment, spectral set were randomly divided into training and testing sets, containing 80 % and 20 % of original samples, respectively. In order to keep the same proportion of transgenic and non-transgenic in the training and testing sets, the sampling process was performed in a stratified way.

Firstly, classification models were fitted using the maximum intensities of spectrum bands in preprocessed spectra. Secondly, aiming to increase the explained variance and reduce the complexity of the fitted models, variable selection was accomplished. The variable selection process was carried out by considering a wrapper approach, ie, by using LDA during the search process (together with the search algorithm), with software default parameters to evaluate the optimal feature subset [31].Six different search algorithms were evaluated: i) BestFirst backward (BF-B), ii) BestFirst forward (BF-F), iii) BestFirst bidirectional (BF-Bi), iv) Genetic algorithm (GA), v) Stepwise True (SW-T) and vi) Stepwise False (SW-F).

LDA-based classifiers obtained from different set of input variables were evaluated according their performances by comparison of their Root Mean Squared Error of Calibration (RMSEC), Root Mean Squared Error of Validation (RMSEV) and accuracy (%).

Spectra preprocessing were carried out using MATLAB® (R2010a) with PLS Toolbox and variable selection and fittings were carried out using WEKA (version 3.6.12) [32].

3. Results and discussion

A preliminary analysis of Raman spectra has indicated the spectral range of 1700 to 2700 cm^{-1} comprised a region of noise and cosmic rays. Therefore, the spectral target for this work was the range between 200 to 1700 cm^{-1}.

Average Raman spectra from non-transgenic and transgenic corn seeds, without preprocessing, are showed in the Fig. 1A. Note that the spectra are similar and intense fluorescence emission masks the Raman signals throughout the spectral region. According to Afseth et al. [26] a mathematical preprocessing is a feasible way to generate reproducible qualitative and quantitative data. Moreover, the baseline correction can remove the effect of fluorescence and other undesirable spectrum fluctuations. Thus, the Whittaker filter baseline correction was evaluated to remove these undesirable effects. This filter works by fitting variable order polynomials and subtracting them from the Raman spectrum. In Fig. 1B are shown the average spectra from transgenic and non-transgenic corn seed obtained by individual spectrum processing by Whittaker filter. Note that after correction a slight difference appears between the classes. In addition, relative standard deviation for the band at 476 cm^{-1} in fifty spectra was estimated in 7 %, after Whittaker filter processing.

Different preprocessing techniques can result in different sets of

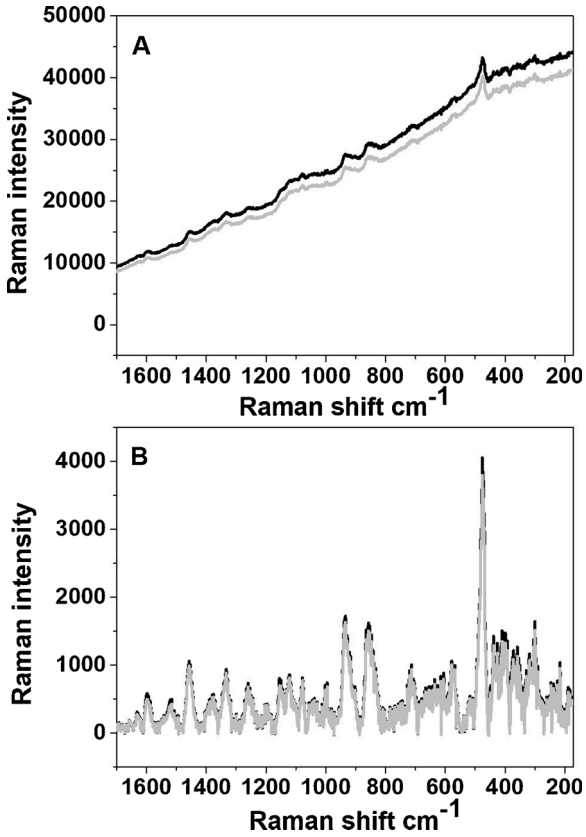


Fig. 1. Averaged spectra of transgenic and conventional corn seeds. A) without preprocessing and B) preprocessed by Whittaker Filter Baseline (▬ transgenic; ▬ non-transgenic).

input variables. Therefore, LDA classification models having as input all identified bands from each single preprocessing were initially fitted. The performance of all fitted models is shown in Table 1.

Models with higher performances (lower RMSEV and high accuracy) were those using the variables of spectra preprocessed by Whittaker filter followed by smoothing Savitzky-Golay (SG) and SNV (Model C) and Whittaker filter followed, smoothing Savitzky-Golay (SG) and Normalization (N) (Model E). The model E provided the smallest prediction error (RMSEV = 0.5747), being, therefore, fixed for the following studies. Average spectra of transgenic and non-transgenic corn preprocessed by WF + SG + N with their 25 assigned bands can be seen in Fig. 2. The assignments of these bands according to different authors is shown in the Table 2. As expected, the major components of corn seeds are carbohydrates, including monomeric sugars and starch. Thus, vibrational bands originate from carbohydrates are prevalent.

Spurious variables, not linked to the investigated phenomenon, might result in accurate models for calibration sets, but showing low performance to validation and test sets. Thus, a variable selection method was carried using different search algorithms. The performance of models fitted using different sets of input variable is shown in Table 3.

Models using variables selected by BF-F, BF-Bi and SW-F showed similar performance to that fitted using all the variables (AV). The worst performance was observed using SW-T, which provided a model able to predict correctly only 37.5 % of samples. However, the models fitted from variables selected by BF-B and GA achieved the lowest RMSEV and highest percentage of correct classifications. The best model was fitted using variables selected by GA, which showed 87.5 % of correct predictions and RMSEV of 0.3689.

All the six search algorithms selected the 1026 cm^{-1} band, which is related to carbohydrates (Table 2). This finding suggests the group of

Table 1
Classification performance provided by the models fitted from all bands visualized in the spectra with different pre-processing.

Model	A	B	C	D	E
Preprocessing	WF	WF + SG	WF + SG + SNV	WF + SNV	WF + SG + N
Spectral bands	15	26	26	15	25
RMSEC	0.2067	0	0	0.3186	0.2511
RMSEV	0.9138	0.7906	0.7071	0.8112	0.5747
Correct classifications	12.5 %	37.5 %	50 %	25 %	50 %

RMSEC = Root Mean Squared Error of Calibration Set; **RMSEV** = Root Mean Squared Error of Validation Set.

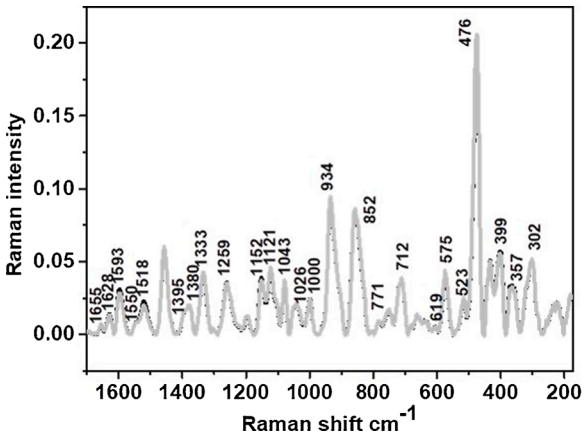


Fig. 2. Averaged spectra of transgenic and conventional corn preprocessed by Whittaker Filter Baseline followed by smoothing Savitzky-Golay (SG) and Normalization (N) by the band height at 1456 cm^{-1} (▬ transgenic; ▬ non-transgenic).

Table 2
Assignments of vibrational bands in the spectra of corn seeds.

Raman shift cm^{-1}	Vibrational Mode	Tentative Assignment	References
302	Amylose, amylopectin, skeletal modes of pyranose ring	carbohydrates	[33]
357	Skeletal modes (ring bending)	carbohydrates	[33]
399	Skeletal modes (ring bending)	carbohydrates	[33]
476	δ(C—C—C)+τ(C—O)	carbohydrates	[30]
523	S−S (gauche-gauche-gauche)	proteins	[34]
575	δ(C—C—O)+τ(C—O)	carbohydrates	[30]
619	δ(C—C—O)	carbohydrates	[30]
712	δ(C—C—O)	carbohydrates	[30]
771	δ(C—C—O)	carbohydrates	[30]
852	δ(C—C—H)+δ(C—O—C)	carbohydrates	[30]
934	δ(C—O—C)+δ(C—O—H)+ν(C—O)	carbohydrates	[30]
1000	ν_3 (C—CH_3 stretching)	carotenoids	[35]
1026	δ(C—O—H)	carbohydrates	[33]
1043	ν(C—O)+ν(C—C)+δ(C—O—H)	carbohydrates	[33]
1079	ν(C—O)+ν(C—C)+δ(C—O—H)	carbohydrates	[33]
1121	ν(C—O)+ν(C—C)+δ(C—O—H)	carbohydrates	[30]
1152	ν(C—O)+ν(C—C)+δ(C—O—H)	carbohydrates	[33]
1259	δ(C—C—H)+δ(O—C—H)+δ(C—O—H)	carbohydrates	[30]
1333	ν(C—O); δ(C—O—H)	carbohydrates	[30]
1380	δ(C—O—H)	carbohydrates	[30]
1395	δ(C—C—H)	carbohydrates	[30]
1518	—C═C —(in plane)	carotenoids	[35]
1550	—C═C —(in plane)	carotenoids	[36]
1593	ν(C—C) aromatic ring+σ(CH)	lignin	[37]
1628	C═C—C (ring)	lignin	[37]
1655	C═O stretching (amide I)	proteins	[34]

Vibrations: ν, stretching; δ, deformation (bending/scissoring); τ, twisting.

Table 3
Evaluation models under different search algorithms for variable selection.

Method	SVs	RMSEC	RMSEV	Correct Classifications (%)
AV	25	0.2511	0.5747	50
BF-B	8	0.3615	0.5077	75
BF-F	2	0.4415	0.5854	50
BF-Bi	2	0.4415	0.5854	50
GA	4	0.4144	0.3689	87.5
SW-F	2	0.4415	0.5854	50
SW-T	11	0.3376	0.6263	37.5

AV = all variables; **BF-B** = Best First backward; **BF-F** = Best First forward; **BF-Bi** = Best First bidirectional; **GA** = Genetic algorithm; **SW-T** = Stepwise True; **SW-F** = Stepwise False; **RMSEV** = Root Mean Squared Error of Validation Set; **RMSEC** = Root Mean Squared Error of Calibration Set; **SVs**= Selected variables.

carbohydrates responsible for this band are likely relevant for discriminating transgenic from non-transgenic corn. According to Cael et al. [33] the band at 1026 cm^{-1} is produced by deformation δ(C—O—H) in a spectral region generally characterized by strong absorbance for all carbohydrates and polysaccharides. The intensity of this band is often sensitive to the degree of hydration of the sample.

Moreover, among the variables set selected by BF-B (523, 619, 712, 852, 1043, 1026, 1518 and 1628 cm^{-1}), 62.5 % are related to carbohydrates and by GA (619, 1026, 1079 and 1518 cm^{-1}), 75 % are related to carbohydrates. The band at 619 cm^{-1}, selected by both search algorithms is related to the bending/scissoring deformation δ(C—C—O) [30]. The carbohydrates responsible for this band are concentrated at the endosperm of corn seed [38]. These results reinforce the importance of such carbohydrates for the discrimination of classes and suggest the genetic modification could cause different expression of in terms of carbohydrates in corn seeds.

The variables selection also suggests that carotenoids are a key group of compounds to distinguish transgenic from non-transgenic corn. The band at 1518 cm^{-1} related to carotenoids (Table 2) was selected by both BF-B and GA, which showed the highest accuracy. According to Osterrothová et al. [35] and Yang et al. [38], the 1518 cm^{-1} band related to the presence of carotenoid can be assigned to in-phase —C═C— bounds (in plane). These compounds are observed in the corn endosperm [38]. The dominant carotenoid in corn seeds is zeaxanthin [39, 40], whose characteristic bands are in agreement with 1518 cm^{-1}. Besides carbohydrates and carotenoids, the model fitted with variables selected by BF-B accounting with bands related to protein (523 cm^{-1}) and lignin (1628 cm^{-1}). However, the best classification model obtained by using variables selected by GA suggest that although the levels of proteins and lignins should change due to genetic modification, carbohydrates and carotenoids better express the modification studied.

4. Conclusions

A novel method based on Raman spectroscopy and chemometric techniques was proposed and evaluated for distinguishing transgenic corn expressing specific *Bacillus thuringiensis* and *Agrobacterium spp* genes. This combination was successful since it provided a model capable of classifying seeds with accuracy greater than 87 %. The wrapper approach for variable selection together with different search algorithms has provided evidence that some classes of compounds can be phenotypic characteristics coming from the genetic modification studied as well as their different amounts can be detected by Raman spectroscopy. Among compounds, carbohydrates and carotenoids played important role. The developed method afforded a simple, fast and Eco-friendly solution, which demands few sample preparation procedures with no chemical waste resulting. The method can be useful for agricultural industry, market demands and others related to food security and nutrition.

CRediT authorship contribution statement

Samia Rodrigues Dib: Investigation, Formal analysis, Writing - original draft. **Tiago Varão Silva:** Formal analysis. **José Anchieta Gomes Neto:** Resources, Writing - review & editing. **Lauro José Moreira Guimarães:** Resources, Writing - review & editing. **Ednaldo José Ferreira:** Conceptualization, Project administration, Methodology, Writing - review & editing. **Edilene Cristina Ferreira:** Conceptualization, Project administration, Supervision, Writing - review & editing.

Declaration of Competing Interest

The authors report no declarations of interest.

Acknowledgements

The authors are grateful to the Coordenação de Aperfeiçoamento de Pessoal de Nível Superior (CAPES) for the doctoral scholarship granted to S. R. D. and Conselho Nacional de Desenvolvimento Científico e Tecnológico (CNPq) for the researchships to E.C.F (grant # 308200/2018-7) and J.A.G.N (grant # 302414/2017-7).

References

[1] C. James, Global status of commercialized biotech/GM Crops in 2017: biotech crop adoption surges as economic benefits accumulate in 22 years, ISAAA, 2017, pp. 1–143, https://doi.org/10.1017/S0014479706343797.
[2] M. Corujo, M. Pla, J. van Dijk, M. Voorhuijzen, M. Staats, M. Slot, A. Lommen, E. Barros, A. Nadal, P. Puigdomènech, J.L. La Paz, H. van der Voet, E. Kok, Use of omics analytical methods in the study of genetically modified maize varieties tested in 90 days feeding trials, Food Chem. 292 (2019) 359–371, https://doi.org/10.1016/j.foodchem.2018.05.109.
[3] B. Shiferaw, M. Smale, H.J. Braun, E. Duveiller, M. Reynolds, G. Muricho, Crops that feed the world 10. Past successes and future challenges to the role played by wheat in global food security, Food Secur. 3 (2011) 307–327, https://doi.org/10.1007/s12571-013-0263-y.
[4] C. James, Brief 54: Global Status of Commercialized Biotech/GM Crops: 2018, Isaaa, 2018. http://www.isaaa.org/resources/publications/briefs/54/default.asp.
[5] M. Rahman, M. Zaman, T. Shaheen, S. Irem, Y. Zafar, Safe use of Cry genes in genetically modified crops, Environ. Chem. Lett. 13 (2015) 239–249, https://doi.org/10.1007/s10311-015-0508-4.
[6] B.M. Maghari, A.M. Ardekani, Genetically modified foods and social concerns, Avicenna J. Med. Biotechnol. 3 (2011) 109–117.
[7] X. Wang, T. Tang, Q. Miao, S. Xie, X. Chen, J. Tang, C. Peng, X. Xu, W. Wei, Z. You, J. Xu, Detection of transgenic rice line TT51-1 in processed foods using conventional PCR, real-time PCR, and droplet digital PCR, Food Control 98 (2019) 380–388, https://doi.org/10.1016/j.foodcont.2018.11.032.
[8] K. Rupula, T. Kosuri, M.Z. Gul, B. Sharma, S.R. Beedu, Immuno-analytical method development for detection of transgenic Cry1Ac protein and its validation, J. Sci. Food Agric. 99 (2019) 6903–6910, https://doi.org/10.1002/jsfa.9976.
[9] A. Razavi, I. Malhotra, A. Ghosh, M. Pusztai-Carey, J. Marks, C. King, Antibodies as epidemiological markers of genetically modified crop exposure: detection of Cry1Ab-specific IgG, Food Agric. Immunol. 28 (2017) 779–788, https://doi.org/10.1080/09540105.2017.1313200.
[10] Y. Tan, J. Zhang, Y. Sun, Z. Tong, C. Peng, L. Chang, A. Guo, X. Wang, Comparative proteomics of phytase-transgenic maize seeds indicates environmental influence is more important than that of gene insertion, Sci. Rep. 9 (2019) 1–11, https://doi.org/10.1038/s41598-019-44748-5.
[11] B. Czepukojc, A. Abuhaliema, A. Barghash, S. Tierling, N. Naß, Y. Simon, C. Körbel, C. Cadenas, N. van Hul, A. Sachinidis, J.G. Hengstler, V. Helms, M.W. Laschke, J. Walter, J. Haybaeck, I. Leclercq, A.K. Kiemer, S.M. Kessler, IGF2 mRNA binding protein 2 transgenic mice are more prone to develop a ductular reaction and to progress toward cirrhosis, Front. Med. 6 (2019) 1–16, https://doi.org/10.3389/fmed.2019.00179.
[12] M.F. Ocaña, P.D. Fraser, R.K.P. Patel, J.M. Halket, P.M. Bramley, Mass spectrometric detection of CP4 EPSPS in genetically modified soya and maize, Rapid Commun. Mass Spectrom. 21 (2007) 319–328, https://doi.org/10.1002/rcm.2819.
[13] J.M. Rodriguez-Nogales, A. Cifuentes, M.C. Garcia, M.L. Marina, Improved methodology for the characterisation of transgenic Bt-11 maize cultivars using RP-HPLC profiles of albumin, globulin, prolamin, and glutelin protein fractions and chemometric analysis, Food Chem. 120 (2010) 1229–1237, https://doi.org/10.1016/j.foodchem.2009.11.069.
[14] S. Patwardhan, S. Dasari, K. Bhagavatula, S. Mueller, S.A. Deepak, S. Ghosh, S. Basak, Simultaneous detection of genetically modified organisms in a mixture by multiplex PCR-Chip capillary electrophoresis, J. AOAC Int. 98 (2015) 1366–1374, https://doi.org/10.5740/jaoacint.15-070.
[15] J. Liu, L. Mao, J. Ku, H. Peng, Z. Lao, D. Chen, B. Yang, Using terahertz spectroscopy to identify transgenic cottonseed oil according to physicochemical

quality parameters, Optik (Stuttg.) 142 (2017) 483–488, https://doi.org/10.1016/j.ijleo.2017.05.103.
[16] X. Liu, X. Feng, F. Liu, J. Peng, Y. He, Rapid identification of genetically modified maize using laser-induced breakdown spectroscopy, Food Bioprocess Technol. 12 (2019) 347–357, https://doi.org/10.1007/s11947-018-2216-0.
[17] G. Alcantara, A. Barison, M. Santos, Assessment of genetically modified soybean crops and different cultivars by Fourier transform infrared spectroscopy and chemometric analysis, Orbital Electron. J. Chem. 2 (2010) 41–52. http://marcos.dfi.ufms.br/index.php/Chemistry/article/view/120.
[18] A.S. Luna, A.P. Da Silva, J.S.A. Pinho, J. Ferré, R. Boqué, Rapid characterization of transgenic and non-transgenic soybean oils by chemometric methods using NIR spectroscopy, Spectrochim. Acta - Part A Mol. Biomol. Spectrosc. 100 (2013) 115–119, https://doi.org/10.1016/j.saa.2012.02.085.
[19] L. Xie, Y. Ying, T. Ying, H. Yu, X. Fu, Discrimination of transgenic tomatoes based on visible/near-infrared spectra, Anal. Chim. Acta 584 (2007) 379–384, https://doi.org/10.1016/j.aca.2006.11.071.
[20] C. Liu, W. Liu, X. Lu, W. Chen, F. Chen, J. Yang, L. Zheng, Non-destructive discrimination of conventional and glyphosate-resistant soybean seeds and their hybrid descendants using multispectral imaging and chemometric methods, J. Agric. Sci. 154 (2016) 1–12, https://doi.org/10.1017/S0021859614001142.
[21] H.J. Butler, F.L. Martin, M.R. Roberts, S. Adams, M.R. McAinsh, Observation of nutrient uptake at the adaxial surface of leaves of tomato (Solanum lycopersicum) using Raman spectroscopy, Anal. Lett. 53 (2020) 1–27, https://doi.org/10.1080/00032719.2019.1658199.
[22] S. Lohumi, H. Lee, M.S. Kim, J. Qin, B.K. Cho, Through-packaging analysis of butter adulteration using line-scan spatially offset Raman spectroscopy, Anal. Bioanal. Chem. 410 (2018) 5663–5673, https://doi.org/10.1007/s00216-018-1189-1.
[23] J. Nogales-Bueno, B. Baca-Bocanegra, A. Rooney, J.M. Hernández-Hierro, H. J. Byrne, F.J. Heredia, Study of phenolic extractability in grape seeds by means of ATR-FTIR and Raman spectroscopy, Food Chem. 232 (2017) 602–609, https://doi.org/10.1016/j.foodchem.2017.04.049.
[24] N. Tena, R. Aparicio, V. Baeten, D.L. García-González, J.A. Fernández-Pierna, Assessment of vibrational spectroscopy performance in geographical identification of virgin olive oils: a world level study, Eur. J. Lipid Sci. Technol. 121 (2019) 1–11, https://doi.org/10.1002/ejlt.201900035.
[25] M.L. Xu, Y. Gao, X.X. Han, B. Zhao, Detection of pesticide residues in food using surface-enhanced raman spectroscopy: a review, J. Agric. Food Chem. 65 (2017) 6719–6726, https://doi.org/10.1021/acs.jafc.7b02504.
[26] N.K. Afseth, V.H. Segtnan, J.P. Wold, Raman spectra of biological samples: a study of preprocessing methods, Appl. Spectrosc. 60 (2006) 1358–1367, https://doi.org/10.1366/000370206779321454.
[27] K. Kucharska-Ambrożej, J. Karpinska, The application of spectroscopic techniques in combination with chemometrics for detection adulteration of some herbs and spices, Microchem. J. 153 (2019) 104278, https://doi.org/10.1016/j.microc.2019.104278.
[28] N.M. Ralbovsky, I.K. Lednev, Raman spectroscopy and chemometrics: a potential universal method for diagnosing cancer, Spectrochim. Acta - Part A Mol. Biomol. Spectrosc. 219 (2019) 463–487, https://doi.org/10.1016/j.saa.2019.04.067.
[29] A. Savitzky, J.E.M. Golay, Smoothing and differentiation of data by simplified least squares procedures, Anal. Chem. 36 (1964) 1627–1639, https://doi.org/10.1021/ac60214a048.
[30] M.R. Almeida, R.S. Alves, L.B.L.R. Nascimbem, R. Stephani, R.J. Poppi, L.F.C. De Oliveira, Determination of amylose content in starch using Raman spectroscopy and multivariate calibration analysis, Anal. Bioanal. Chem. 397 (2010) 2693–2701, https://doi.org/10.1007/s00216-010-3566-2.
[31] K. Ron, G.H. John, Wrappers for feature subset selection Ron, Artif. Intell. 97 (1997) 273–324, https://doi.org/10.1007/978-3-642-39038-8-27.
[32] E. Frank, M.A. Hall, I.A. Witten, The WEKA Workbench. Online Appendix for "Data Mining: Practical Machine Learning Tools and Techniques, 2016.
[33] J.J. Cael, J.L. Koenig, J. Blackwell, Infrared and Raman spectroscopy of carbohydrates. Part VI: Normal coordinate analysis of V-amylose, Biopolymers 14 (1975) 1885–1903, https://doi.org/10.1002/bip.1975.360140909.
[34] A. Rygula, K. Majzner, K.M. Marzec, A. Kaczor, M. Pilarczyk, M. Baranska, Raman spectroscopy of proteins: a review, J. Raman Spectrosc. 44 (2013) 1061–1076, https://doi.org/10.1002/jrs.4335.
[35] K. Osterrothová, A. Culka, K. Němečková, D. Kaftan, L. Nedbalová, L. Procházková, J. Jehlička, Analyzing carotenoids of snow algae by Raman microspectroscopy and high-performance liquid chromatography, Spectrochim. Acta Part A Mol. Biomol. Spectrosc. 212 (2019) 262–271, https://doi.org/10.1016/j.saa.2019.01.013.
[36] F. Adar, Carotenoids—their resonance raman spectra and how they can Be helpful in characterizing a number of biological systems, Spectroscopy 32 (2017) 12–20. http://www.spectroscopyonline.com/carotenoids-their-resonance-raman-spectra-and-how-they-can-be-helpful-characterizing-number-biologic.
[37] L. Sanchez, S. Pant, Z. Xing, K. Mandadi, D. Kurouski, Rapid and noninvasive diagnostics of Huanglongbing and nutrient deficits on citrus trees with a handheld Raman spectrometer, Anal. Bioanal. Chem. 411 (2019) 3125–3133, https://doi.org/10.1007/s00216-019-01776-4.
[38] G. Yang, Q. Wang, C. Liu, X. Wang, S. Fan, W. Huang, Rapid and visual detection of the main chemical compositions in maize seeds based on Raman hyperspectral imaging, Spectrochim. Acta - Part A Mol. Biomol. Spectrosc. 200 (2018) 186–194, https://doi.org/10.1016/j.saa.2018.04.026.
[39] V.U. Ndolo, T. Beta, Distribution of carotenoids in endosperm, germ, and aleurone fractions of cereal grain kernels, Food Chem. 139 (2013) 663–671, https://doi.org/10.1016/j.foodchem.2013.01.014.
[40] H. Schulz, M. Baranska, R. Baranski, Potential of NIR-FT-Raman spectroscopy in natural carotenoid analysis, Wiley Intersci. 77 (2005) 212–221, https://doi.org/10.1002/bip.20215.

Anexo 18

Atomic Spectroscopy

Article

Protected Geographical Identification of Honey by Spark Discharge-assisted Laser-induced Breakdown Spectroscopy

Diana Corina Fechner,[a] Tiago Varão Silva,[b] Maurilio Gustavo Nespeca,[b] Alan Lima Vieira,[b] José Anchieta Gomes Neto,[b] Dário Santos Júnior,[c] Roberto Gerardo Pellerano,[a] and Edilene Cristina Ferreira[b,*]

[a] Instituto de Química Básica y Aplicada del Nordeste Argentino (IQUIBA-NEA), UNNE-CONICET, Facultad de Ciencias Exactas y Naturales y Agrimensura, Av. Libertad 5400, 3400 Corrientes, Argentina

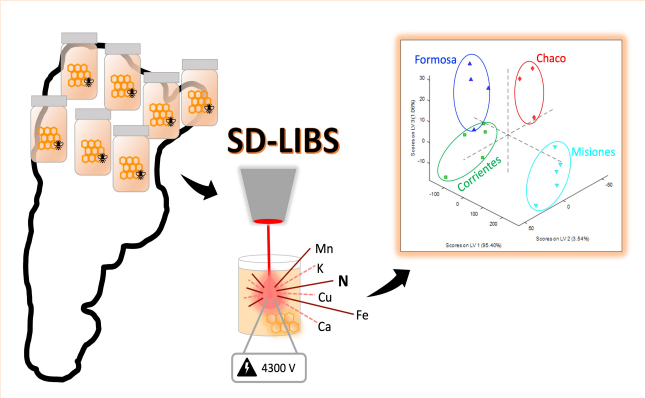
[b] São Paulo State University – UNESP, Chemistry Institute of Araraquara, R. Prof. Francisco Degni 55, 14800-900 Araraquara, SP, Brazil

[c] Department of Chemistry, Federal University of São Paulo - UNIFESP, R. São Nicolau 210, 09913-030, Diadema, SP, Brazil

Received: *March 12, 2021;* ***Revised:*** *April 06, 2021;* ***Accepted:*** *April 06, 2021;* ***Available online:*** *April 07, 2021.*

DOI: 10.46770/AS.2021.022

ABSTRACT: Honey is a natural food that is valued worldwide for its nutritional and therapeutic values. Therefore, authentication of honey according to the geographical origin is a guarantee of the genuine properties. In this article, an evaluation of spark discharge-assisted laser-induced breakdown spectroscopy (SD-LIBS) for certification of the geographical origin of honey is reported. Forty-nine samples of multifloral honey produced in four Argentine provinces were considered. The results showed the best classification performance was obtained using smoothing, generalized least squares weighting (GLSW) and mean centering for spectral preprocessing, added to the k-nearest neighbor (k-NN) or Support Vector Machine (SVM) classification algorithms, which provided 100% of correct classification. More importantly, the results of Partial Least Squares – Discriminant Analysis (PLS-DA) pointed to N, Ca, K, Cu, Fe and Mn as key elements for the certification of geographical origin. In addition, the greatest potential of N stands out for the discrimination of the origin of honey. These findings confirm SD-LIBS as a promising tool for authentication of honey quality, providing a simple, fast and environmentally friendly solution. The method can be useful for industry, the market and others related to food authenticity.



INTRODUCTION

Consumers' lifestyle inquires certificates to prove genuine characteristics of food. Some differentiated foods are labeled by protected geographical identification (PGI) and protected designation of origin (PGO) that requires a premium price for products. Food fraud covers cases where there is a violation of food law, which is intentionally committed to obtain a financial gain through consumer deception.[1]

Honey is the third most adulterated food in the world.[2] Produced by bees from the nectar of plants, honey is a naturally sweet food valued worldwide for its nutritional and therapeutic values[2]. The properties mentioned are intrinsically related to the geographical origin of honey.[3,4] Therefore, authentication of honey according to its origin is an important requirement that demands reliable, fast and reproducible analytical methods.

The method traditionally used to determine botanical and geographical origin of honey is the pollen analysis which reflects the type of vegetation from which the nectar was collected by the bees.[5] The method mentioned is time-consuming and requires great skill and technical experience in pollen morphology.[6] In addition, if honey undergoes a filtration process this type of

analysis becomes infeasible.

In order to simplify the determination of the origin of the honey, methods based on the elemental analysis of the honey composition have been proposed.[7-15] These methods use analytical techniques, such as atomic absorption spectrometry (AAS), inductively coupled plasma optical emission spectroscopy (ICP-OES) and inductively coupled plasma mass spectrometry (ICP-MS) combined with multivariate data analysis. The disadvantages of the aforementioned techniques are the high cost per analysis, since they require gases and high-purity reagents, in addition to the time for the sample pretreatment. Particularly for honey samples, analytical difficulties may arise due to its high carbohydrates content, which influence the performance of the mentioned analytical techniques.[16] Sample pretreatment by wet digestion using concentrated acid and heating[17] or dry ashing followed by ash dissolution in concentrated nitric acid[18] are time-consuming and costly procedures besides not being environmentally friendly. In contrast, the direct analysis of diluted samples using techniques that depend on the nebulization of the sample, such as flame atomic absorption spectrometry (FAAS), ICP-OES and ICP-MS is critically affected by the effects of transport. Considering these disadvantages, direct analysis techniques such as Raman, infrared and some sensors have been explored for classification of honey.[19-22] However, the elemental composition of the samples cannot be accessed by these techniques.

Laser-induced breakdown spectroscopy (LIBS) is an analytical technique capable of performing direct and fast multielement analysis with minimal or no sample preparation, without the use of chemical consumables, such as solvents and gases. LIBS is based on the measurements of atomic and ionic emission of elemental sample constituents excited in a plasma. A single LIBS analysis takes a few seconds to perform. In addition to the elemental analysis, the correlation between spectral fingerprint and other samples properties is also possible.[23,24] Due to its potential, LIBS has been successfully applied to detect food fraud.[25,26] Despite the attractive analytical characteristics, LIBS shows low detectability, which makes some types of application difficult. For this reason, some strategies have been developed to improve the sensitivity of the LIBS, such as the spark discharge-assisted LIBS (SD-LIBS), which increases emission intensities by reheating the plasma.[27]

Recently, Zhao *et al.* (2020)[28] achieved good results for the classification of honey according to geographical origin. The authors used a LIBS system composed by a high-energy laser operating at 532 nm, a high-resolution spectrometer and an intensified detector. In contrast, low-cost LIBS systems have received great attention and expanding the applicability of the technique.[29-30] The low sensitivity and spectral resolution of these instruments have been circumvented using some simple devices to increase sensitivity and applying different spectral processing to extract the appropriate analytical information.[30-32]

In this work, a low-cost LIBS system coupled with a spark-discharge (SD) for authentication of geographical origin of honey was evaluated, taking advantage of the speed and reliability of the LIBS and aiming to provide an accessible device for authentication and traceability of honey.

EXPERIMENTAL

Samples. For this study, forty-nine samples of multifloral honey collected in harvesting season between 2015 and 2016, from four provinces of the Northeast region of Argentina (Fig.1), were used. The extraction and mixing of honey were carried out in an extraction room authorized by the National Service for Agri-food Health and Quality. Each sample corresponded to a composite sample, prepared from the mixture of samples extracted from ten beehives. The use of composite sample was chosen because it provides an unbiased estimation of the population average. Thus, eleven composite samples were obtained from the province of Formosa (F), ten from Chaco (CH), fourteen from Corrientes (C), and fourteen from Misiones (M). The honey samples were stored in polypropylene flasks at room temperature until analysis.

LIBS analysis. The spectra were acquired using a LIBS system designed for direct analysis of solids, which is equipped with a Q-switched laser Nd:YAG 1064 nm Big Sky Ultra 50 (Quantel, Co., Bozeman, MT, USA), an optical fiber bundle, and four spectrometers HR2000+ (Ocean Optics Co., Dunedin, FL, USA), featuring an optical resolution of 0.1 nm (full width at half maximum) and a spectral range from 200 nm to 630 nm. The laser

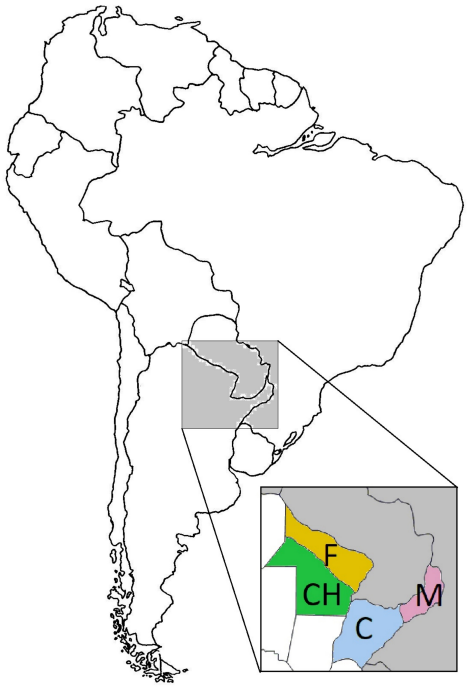


Fig. 1 Geographical location of the Argentine regions producing the studied honey samples.

with pulse duration of 8 ns was operated with a maximum power energy of 50 mJ. The integration time and the Q-Switched delay used for the acquisition of spectra were 1 ms and 2.5 μs, respectively.

The samples were placed in polyethylene sampling flasks until filling out their capacity (around 1 mL). The flask was placed in the sample holder of LIBS system, which can be moved in the x-y directions. The sampling chamber is equipped with video camera to monitor the analyses. A spark discharge device was coupled with LIBS to increase the detectability of emission lines. The spark discharge was obtained using two cylindrical pure tungsten electrodes fixing 4 mm between them and 2 mm above the sample surface. The DC voltage signal was 4300 V. More details on the electric discharge system can be found in Vieira et al. (2018).[33] Twenty spectra were measured for each sample by spreading lasers pulses on the surface of the sample.

Chemometric analysis. All chemometric analysis were performed using MATLAB 2013a (MathWorks Inc., Natick, MA, USA) with PLS toolbox 7.3.1. (Eigenvector Research Inc., WA, USA). The spectral profile of all samples was first evaluated to detect outliers. Spectra showing an anomalous profile, evidenced by the absence of emission signals in any wavelength range, were discarded. Thereafter, each individual spectrum was processed by Whittaker filter for baseline fitting and multiplicative scatter correction (MSC) to normalize the effects of fluctuations, which is common in the LIBS analysis[26,34]. A principal component analysis (PCA) was performed using each preprocessed spectrum. The spectrum that showed scores values beyond the confidence limits (95% level) in the first principal component was excluded. Finally, the spectra corresponding to each sample were averaged. Afterward, the spectrum set was divided into subsets for calibration and validation: two-thirds of the samples were considered for calibration (9 C, 7 CH, 7 F, and 9 M), and one-third for external validation (5 C, 3 CH, 4 F, and 5 M).

Three methods of classification were evaluated, Partial Least Squares Discriminant Analysis (PLS-DA),[35] k-nearest neighbor (k-NN),[36] and Support Vector Machine (SVM).[37] The number of latent variables (LV) used in the PLS-DA model and the number of nearest neighbors (k) were chosen according to the number of correct classifications of the calibration samples during cross-validation. The SVM model was developed using the radial basis kernel type. The values of the SVM parameters (ν and γ) were automatically optimized during cross-validation. The SVMs used for binary classification within a multiclass strategy were based on 0 and 1, with a threshold of 0.5.

The classification methods described were evaluated in combination with the following preprocessing techniques: baseline correction by Whittaker filter, first and second derivatives (15 variables per window), Savitzky-Golay smoothing, MSC by mean, MSC by median, normalization by area, Standard Normal Variate (SNV), Pareto scaling, Poisson scaling, generalized least squares weighting (GLSW), and external parameter orthogonalization (EPO)[38-40]. After the application of each preprocessing, the data were mean centered or autoscaled.

RESULTS AND DISCUSSION

The experimental data were first submitted to the removal of outliers. Thereafter, the remaining spectra were evaluated by PCA, and the scores plot (PC1 *versus* samples) was used as a control chart. Spectra showing scores values out of the confidence limits (95% level) were excluded. The observed outliers may be due to the honey meniscus formed in the sampling flask, which provided different laser focal distance in relation to sample surface, considering the center and the edges of the flask. These differences led to the exclusion of 19% of the spectra. Therefore, the replicates for each sample ranged from 5 to 20. The useful spectra from each sample were adjusted to the baseline, normalized, and averaged.

The classification models were developed using the average spectra of each sample. The first step of the modeling was to determine the most suitable spectral preprocessing for each classification method (PLS-DA, k-NN and SVM). The results of correct classifications for thirteen preprocessing strategies and 30 combinations are shown in Table 1. The mean centering does not influence k-NN and SVM modeling, so this preprocessing was only maintained by convention. Consequently, autoscaling had the same effect as variance scaling using these methods. The combination of smoothing, GLSW, and mean centering provided the highest number of correct classifications for the three methods performed. Since the GLSW attenuates spectral variables that vary in the same class, variables correlated to the classes present greater weight in the modeling. Therefore, this preprocessing was the most important to provide correct classifications. In addition, the Savitzky-Golay smoothing reduced the spectral noise, made emission peaks more defined, and increased model fit. The three methods evaluated for honey classification were able to separate the four classes: the k-NN (k=3) and SVM (ν=0.5, γ=10^{-6}) models provided 100% correct classification for the external validation set, and PLS-DA (9 LV) model provided 94% of correct classification (Table 1).

SVM and k-NN methods do not allow a visualization of the relationship between spectral variables and the class clusters. Thus, the PLS-DA method was used for such visualization and interpretation. The scores plot (Fig. 2) shows the separation of the four honey classes in the first three LVs. The PLS-DA model classified correctly all validation samples, except for a F sample, which was classified as region C honey.

The correlation between the spectral variables and the honey classes was assessed using loading and scores values. This analysis reveals that M samples were separated by the 1st LV (positive values), the CH samples by the 2nd LV (negative values), and the C and F samples were separated by the 3rd LV (C with negative

Table 1. Evaluation of Preprocessing Strategy for Each Classification Method

Preprocessing	Correct Classification					
	PLS-DA		k-NN		SVM	
	Cal	Val	Cal	Val	Cal	Val
MC	87%	46%	33%	57%	46%	45%
BC+MC	84%	46%	33%	57%	64%	53%
1st der+MC	91%	60%	32%	41%	28%	40%
2nd der+MC	87%	60%	29%	26%	36%	58%
Sm+MC	97%	78%	37%	46%	71%	64%
Sm+1st der+MC	94%	75%	42%	46%	50%	50%
Sm+2nd der+MC	91%	55%	37%	52%	36%	40%
MSC(mean)+MC	88%	28%	17%	31%	0%	25%
MSC(median)+MC	88%	52%	31%	33%	53%	36%
Norm.+MC	94%	47%	21%	37%	25%	25%
SNV+MC	88%	23%	17%	31%	17%	20%
GLSW+MC	100%	89%	100%	95%	100%	89%
Sm+GLSW+MC	100%	94%	100%	100%	100%	100%
EPO+MC	100%	59%	42%	56%	33%	35%
Pareto Scaling+MC	100%	88%	24%	36%	61%	62%
Poisson Scaling+MC	100%	69%	27%	31%	33%	40%
AS	100%	71%	37%	40%	64%	62%
BC+AS	100%	74%	32%	23%	0%	20%
1st der+AS	100%	69%	26%	41%	25%	45%
2nd der+AS	100%	74%	32%	51%	0%	15%
Sm+AS	100%	88%	29%	30%	54%	58%
Sm+1st der+AS	100%	69%	33%	51%	25%	50%
Sm+2nd der+AS	100%	69%	33%	46%	36%	45%
MSC(mean)+MC	100%	68%	14%	15%	0%	11%
MSC(median)+MC	100%	46%	17%	45%	0%	10%
Norm+AS	100%	56%	21%	31%	0%	20%
SNV+AS	100%	73%	17%	26%	28%	35%
GLSW+AS	100%	48%	100%	66%	100%	94%
Sm+GLSW+AS	100%	51%	100%	88%	100%	94%
EPO+AS	100%	74%	41%	50%	53%	43%

Note: Calibration set (Cal), external validation set (Val), mean centering (MC), baseline correction by Whittaker filter (BC), first derivative (1st der), second derivative (2nd der), smoothing (Sm), multiplicative scatter correction (MSC), normalization by area (Norm.), standard normal variate (SNV), generalized least squares weighting (GLSW), external parameter orthogonalization (EPO), and autoscaling (AS).

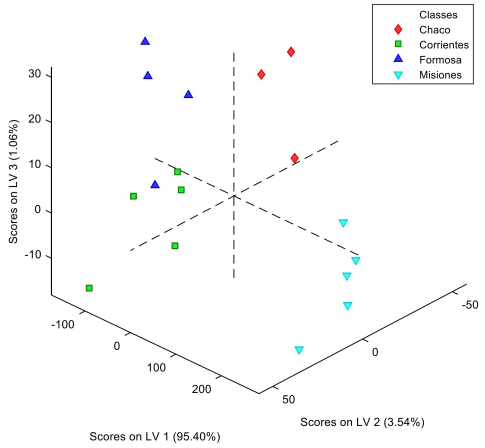


Fig. 2 Score plot of the PLS-DA model (only validation samples).

and F with positive values). The score plot also shows a greater separation of class M from the others, while classes C and F were more similar. These results corroborate the elemental composition of samples (Table 2), obtained by assigning spectral emission lines according to the NIST LIBS database.[41] A typical LIBS spectrum of a honey sample showing the emission lines that influenced class discrimination is shown in Fig. 3.

Class M samples had a relatively lower N content, while C and F samples showed the relatively higher content of this element, suggesting that C and F honeys have a high protein content in contrast to M honey. In addition, the C samples showed the relatively higher Ca content, resulting in the separation of this class by the 3rd LV of the model, and the medium K and Fe content provided the separation of the F samples. The CH samples were

Table 2. Emission Lines Related to Each Class

Class	Peak (nm)	NIST assignments	Intensity among classes
	499.5	N II (499.6 nm)	lowest
	552.9	N I (553.0 nm)	lowest
Misiones	553.5	N II (553.5 nm)	lowest
	567.6	N II (567.6 nm)	lowest
	568.5	N II (568.6 nm)	lowest
	324.7	Cu I (324.7 nm)	highest
Chaco	404.1	Mn I (404.1 nm)	medium
	434.7	Mn II (434.6 nm)	medium
	396.9	Ca II (396.9 nm)	highest
Corrientes	422.8	Ca I (422.7 nm)	highest
	466.2	N I (466.2 nm)	highest
	404.2	K I (404.4 nm)	medium
Formosa	439.7	Fe II (439.8 nm)	medium
	464.3	N II (464.3 nm)	highest

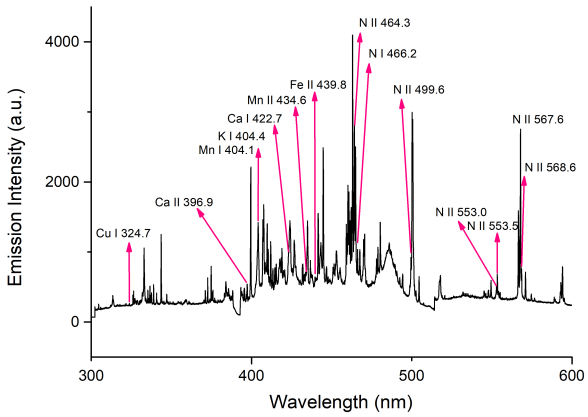


Fig. 3 Typical LIBS spectrum of a honey sample with emission line assignments related to the studied classes.

distinguished from the others by their relative higher levels of Cu and medium levels of Mn, and N did not show significant influence on segregation.

Three class of samples were separated according to the N content, suggesting that N plays a fundamental role in discriminating the geographical origin of honey. According to Imdorf *et al.*,[42] bees feed mainly on nectar and pollen, the latter being the main source of protein for the entire colony. Thus, the supply and quality of pollen, which directly influence the amount of N, could be related to the geographical production of honey. Furthermore, Fechner et al.[10] using ICP-MS data from the same samples used here, obtained a classification method for geographical origin reaching 76% of prediction accuracy. These results suggest that the absence of N in the data set may decrease the accuracy of the predictions. SD-LIBS presented attractive features for authentication of honey in terms of cost and performance, in addition to the ability to measure N, which is not feasible with ICP-MS. Thus, the methods developed provide new horizons for honey quality analysis.

CONCLUSIONS

Authentication of geographical origin of Argentine honey was assessed using a low-cost SD-LIBS and chemometric tools. Adequate spectral preprocessing provided k-NN and SVM models capable of accurately classifying honey according to their production regions. The results suggested N as the most important element to discriminate the studied classes. Complementary contributions from Ca, K, Cu, Fe, and Mn were also important for geographical discrimination of honey. Considering the possibility of measuring N and the importance of this element for geographical discrimination of honey samples, the proposed methods place LIBS in a prominent position in comparison with the conventional atomic techniques generally used for geographical analysis of honey (*e.g.* FAAS, ICP-OES and ICP-MS). Furthermore, the use of SD-LIBS provides fast, clean and direct analysis, providing a low-cost device for the control of food quality.

AUTHOR INFORMATION

Corresponding Author

* E.C. Ferreira

Email address: edilene.c.ferreira@unesp.br

Notes

The authors declare no competing financial interest.

ACKNOWLEDGMENTS

The authors would like to thank Asociación de Universidades Grupo Montevideo for exchange scholarship to D.C.F. and the Conselho Nacional de Desenvolvimento Científico e Tecnológico (CNPq) for the research grant to E.C.F. (308200/2018-7) and Fundação de Amparo à Pesquisa do Estado de São Paulo (FAPESP) grant number 2019/07537-6.

REFERENCES

1. C. European, Food Fraud, https://ec.europa.eu/food/safety/food-fraud_en (accessed 4 April 2019)
2. X. Zhou, M. P. Taylor, H. Salouros, and S. Prasad, *Sci. Rep.*, 2018, **8**, 1–11. https://doi.org/10.1038/s41598-018-32764-w
3. G. Cebrero, O. Sanhueza, M. Pezoa, M. E. Báez, J. Martínez,

M. Báez, and E. Fuentes, *Food Chem.*, 2020, **315**, 126296. https://doi.org/10.1016/j.foodchem.2020.126296

4. S. Đogo Mračević, M. Krstić, A. Lolić, and S. Ražić, *Microchem. J.*, 2020, **152**, 104420. https://doi.org/10.1016/j.microc.2019.104420
5. W. Von Der Ohe, L. Persano Oddo, M. L. Piana, M. Morlot, and P. Martin, *Apidologie*, 2004, **35**, S18–S25. https://doi.org/10.1051/apido:2004050
6. O. Anjos, C. Iglesias, F. Peres, J. Martínez, Á. García, and J. Taboada, *Food Chem.*, 2015, **175**, 128–136. https://doi.org/10.1016/j.foodchem.2014.11.121
7. M. V Baroni, N. S. Podio, R. G. Badini, M. Inga, H. A. Ostera, M. Cagnoni, E. A. Gautier, P. P. García, J. Hoogewerff, and D. A. Wunderlin, *J. Agric. Food Chem.*, 2015, **63**, 4638–4645. https://doi.org/10.1021/jf5060112
8. B. L. Batista, L. R. S. da Silva, B. A. Rocha, J. L. Rodrigues, A. A. Berretta-Silva, T. O. Bonates, V. S. D. Gomes, R. M. Barbosa, and F. Barbosa, *Food Res. Int.*, 2012, **49**, 209–215. https://doi.org/10.1016/j.foodres.2012.07.015
9. G. Di Bella, V. Lo Turco, A. G. Potortı, G. D. Bua, M. R. Fede, and G. Dugo, *J. Food Compos. Anal.*, 2015, **44**, 25–35. https://doi.org/10.1016/j.jfca.2015.05.003
10. D. C. Fechner, M. J. Hidalgo, J. D. Ruiz Díaz, R. A. Gil, and R. G. Pellerano, *Food Biosci.*, 2020, **33**, 483–490. https://doi.org/10.1016/j.fbio.2019.100483
11. J. C. R. García, R. I. Rodríguez, R. M. P. Crecente, J. B. García, S. G. Martín, and C. H. Latorre, *J. Agric. Food Chem.*, 2006, **54**, 7206–7212. https://doi.org/10.1021/jf060823t
12. H. Kaygusuz, F. Tezcan, F. Bedia Erim, O. Yildiz, H. Sahin, Z. Can, and S. Kolayli, *LWT - Food Sci. Technol.*, 2016, **68**, 273–279. https://doi.org/10.1016/j.lwt.2015.12.005
13. A. Terrab, D. Hernanz, and F. J. Heredia, *J. Agric. Food Chem.*, 2004, **52**, 3441–3445. https://doi.org/10.1021/jf035352e
14. I. K. Karabagias, A. P. Louppis, S. Karabournioti, S. Kontakos, C. Papastephanou, and M. G. Kontominas, *Food Chem.*, 2017, **217**, 445–455. https://doi.org/10.1016/j.foodchem.2016.08.124
15. H. Chen, C. Fan, Q. Chang, G. Pang, X. Hu, M. Lu, and W. Wang, *J. Agric. Food Chem.*, 2014, **62**, 2443–2448. https://doi.org/10.1021/jf405045q
16. Z. Vincevica-Gaile, M. Klavins, V. Rudovica, and A. Viksna, *WIT Trans. Ecol. Environ.*, 2011, **167**, 211–220. https://doi.org/10.2495/ST110191
17. S. Silici, O. D. Uluozlu, M. Tuzen, and M. Soylak, *J. Hazard. Mater.*, 2008, **156**, 612–618. https://doi.org/10.1016/j.jhazmat.2007.12.065
18. E. Yarsan, F. Karacal, I. G. Ibrahim, B. Dikmen, A. Koksal, and Y. K. Das, *Bull. Environ. Contam. Toxicol.*, 2007, **79**, 255–258. https://doi.org/10.1007/s00128-007-9034-9
19. C. Maione, F. Barbosa, and R. M. Barbosa, *Comput. Electron. Agric.*, 2019, **157**, 436–446. https://doi.org/10.1016/j.compag.2019.01.020
20. M. Oroian and S. Ropciuc, *Comput. Electron. Agric.*, 2019, **157**, 371–379. https://doi.org/10.1016/j.compag.2019.01.008
21. S. Ghanavati Nasab, M. Javaheran Yazd, F. Marini, R. Nescatelli, and A. Biancolillo, *Chemom. Intell. Lab. Syst.*, 2020, **202**, 104037. https://doi.org/10.1016/j.chemolab.2020.104037
22. D. P. Aykas, M.-L. Shotts, and L. E. Rodriguez-Saona, *Food Control*, 2020, **117**, 107346. https://doi.org/10.1016/j.foodcont.2020.107346
23. T. V. Silva, S. Z. Hubinger, J. A. Gomes Neto, D. M. B. P. Milori, E. J. Ferreira, and E. C. Ferreira, *Spectrochim. Acta Part B At. Spectrosc.*, 2017, **135**, 29–33. https://doi.org/10.1016/j.sab.2017.06.015
24. X. Li, S. Yang, R. Fan, X. Yu, and D. Chen, *Opt. Laser Technol.*, 2018, **102**, 233–239. https://doi.org/10.1016/j.optlastec.2018.01.028
25. B. A. Alfarraj, H. K. Sanghapi, C. R. Bhatt, F. Y. Yueh, and J. P. Singh, *Appl. Spectrosc.*, 2018, **72**, 89–101. https://doi.org/10.1177/0003702817733264
26. G. Bilge, H. M. Velioglu, B. Sezer, K. E. Eseller, and I. H. Boyaci, *Meat Sci.*, 2016, **119**, 118–122. https://doi.org/10.1016/j.meatsci.2016.04.035
27. M. C. Lázaro, C. P. Morais, T. V. Silva, G. S. Senesi, D. Santos Júnior, J. A. Gomes Neto, and E. C. Ferreira, *Anal. Letters*, Accepted. https://doi.org/10.1080/00032719.2020.1833021
28. Z. Zhao, L. Chen, F. Liu, F. Zhou, J. Peng, and M. Sun, *Sensor,* 2020, **20**, 1878. https://doi.org/10.3390/s20071878
29. A. Velásquez-Ferrín, D. V. Babos, C. Marina-Montes, and J. Anzano, *Appl. Spectrosc. Rev.*, 2020, 1–21. https://doi.org/10.1080/05704928.2020.1810060
30. Q. Zeng, F. Deng, Z. Zhu, Y. Tang, B. Wang, Y. Xiao, L. Xiong, H. Yu, L. Guo, and X. Li, *Plasma Sci. Technol.*, 2019, **21**, 034006. https://doi.org/10.1088/2058-6272/aadede
31. Q. Zeng, Z. Zhu, F. Deng, X. Zhu, B. Wang, Y. Xiao, L. Xiong, H. Yu, L. Guo, and X. Li, *Acta Photonica Sin.*, 2018, **47**, 847014. https://doi.org/10.3788/gzxb20184708.0847014
32. G. Nicolodelli, J. Cabral, C. R. Menegatti, B. Marangoni, and G. S. Senesi, *TrAC - Trends Anal. Chem.*, 2019, **115**, 70–82. https://doi.org/10.1016/j.trac.2019.03.032
33. A. L. Vieira, T. V. Silva, F. S. I. de Sousa, G. S. Senesi, D. S. Júnior, E. C. Ferreira, and J. A. G. Neto, *Microchem. J.*, 2018, **139**, 322–326. https://doi.org/10.1016/j.microc.2018.03.011
34. Y. W. Chu, S. S. Tang, S. X. Ma, Y. Y. Ma, Z. Q. Hao, Y. M. Guo, L. B. Guo, Y. F. Lu, and X. Y. Zeng, *Opt. Express*, 2018, **26**, 10119. https://doi.org/10.1364/OE.26.010119
35. M. Barker and W. Rayens, *J. Chemom.*, 2003, **17**, 166–173. https://doi.org/10.1002/cem.785
36. M. A. Sharaf, D. L. Illman, and B. R. Kowalski, *Chemometrics*, Wiley, New York, NY, 1986
37. C.-C. Chang and C.-J. Lin, *Neural Comput.*, 2001, **13**, 2119–2147. https://doi.org/10.1162/089976601750399335
38. R. I. Eigenvector, Eigenvector Research Documentation, http://wiki.eigenvector.com/index.php?title=Advanced_Preprocessing
39. J. A. Da-Col, W. F. C. Dantas, and R. J. Poppi, *Quim. Nova*, 2018, **41**, 345–354. http://dx.doi.org/10.21577/0100-4042.20170149
40. A. Savitzky and J.E.M. Golay, *Anal. Chem.*, 1964, **36**, 1627–1639. http://dx.doi.org/10.1021/ac60214a047
41. A. Kramida, K. Olsen, Y. Ralchenko, and Team, NIST LIBS Atomic Spectra Database Lines Form, https://physics.nist.gov/PhysRefData/ASD/lines_form.html
42. A. Imdorf, M. Rickli, V. Kilchenmann, S. Bogdanov, and H. Wille, *Apidologie*, 1998, **29**, 315–325. https://doi.org/10.1051/apido:19980402

Anexo 19

chemosensors

MDPI

Communication

Phosphorous Determination in Biochar-Based Fertilizers by Spark Discharge-Laser-Induced Breakdown Spectroscopy

Samia Rodrigues Dib [1], Giorgio Saverio Senesi [2,*], Jose Anchieta Gomes Neto [1], Clovis Augusto Ribeiro [1] and Edilene Cristina Ferreira [1]

[1] Department of Analytical, Physical-Chemical and Inorganic Chemistry, Chemistry Institute of Araraquara, São Paulo State University (UNESP), P.O. Box 355, Araraquara 14801-970, Brazil; rdib.samia@gmail.com (S.R.D.); jose.anchieta@unesp.br (J.A.G.N.); clovis.ribeiro@unesp.br (C.A.R.); edilene.c.ferreira@unesp.br (E.C.F.)

[2] CNR, Istituto per la Scienza e Tecnologia dei Plasmi (ISTP) Sede di Bari, Via Amendola 122/D, 70126 Bari, Italy

* Correspondence: giorgio.senesi@cnr.it; Tel.: +39-080-592-9505

Abstract: Biochar-based fertilizers are a new attractive alternative to P supplementation for crops, as they can gradually release the nutrient, avoiding losses and improving soil quality. In this regard, the evaluation of the P amount in biochar-based fertilizers is extremely important for their quality control. Analytical techniques that require sample solubilization are not very efficient for this task, as biochar is difficult to solubilize. Laser-induced breakdown spectroscopy (LIBS) is a promising technique to respond to this demand, as it enables a direct analysis of solid samples, avoiding the complicated process of sample solubilization. In this work, a novel method based on spark discharge (SD) coupled to LIBS was evaluated for P determination in biochar-based fertilizers prepared from three different biomasses. To overcome calibration problems in LIBS analysis, a matrix-matching procedure accomplished by the addition of eucalyptus biochar to calibration standards was used in experiments. This procedure minimized matrix effects and allowed us to achieve a satisfactory accuracy even when applied to similar but different matrices. Furthermore, the developed method is simple, fast, direct, does not generate post-analysis residues and appears appropriate for the quality control of sustainable biochar-based fertilizers and other biochar products.

Keywords: biochar-based fertilizers; P analysis; SD-LIBS; matrix matching

check for updates

Citation: Dib, S.R.; Senesi, G.S.; Gomes Neto, J.A.; Ribeiro, C.A.; Ferreira, E.C. Phosphorous Determination in Biochar-Based Fertilizers by Spark Discharge-Laser-Induced Breakdown Spectroscopy. *Chemosensors* **2021**, *9*, 337. https://doi.org/10.3390/chemosensors9120337

Academic Editors: Damiano Monticelli, Gilberto Binda and Davide Spanu

Received: 3 November 2021
Accepted: 29 November 2021
Published: 30 November 2021

Publisher's Note: MDPI stays neutral with regard to jurisdictional claims in published maps and institutional affiliations.

Copyright: © 2021 by the authors. Licensee MDPI, Basel, Switzerland. This article is an open access article distributed under the terms and conditions of the Creative Commons Attribution (CC BY) license (https://creativecommons.org/licenses/by/4.0/).

1. Introduction

Phosphorus (P) is a macronutrient that plays a fundamental role in the energy metabolism of plants, whereas its deficiency causes reduced plant growth and chlorosis and necrosis in leaves [1]. The deficiency of P in agricultural soils is remediated by the application of phosphate fertilizers that are derived from the extraction, grinding and treatment of igneous or sedimentary rocks and are usually applied in high amounts, although less than 50% of P in them is taken up by plants [2,3]. The non-assimilated P is leached, causing environmental problems, economic losses and contributing to the depletion of limited terrestrial P sources. Thus, controlled-release fertilizers more effectively meet the demand of crops, avoiding the accumulation of P in the environment and minimizing the production cost by the application of a smaller amount of fertilizer [2].

Recently, the possibility of using biochar from different agricultural byproducts to produce controlled-release fertilizers was proposed [4,5]. Furthermore, biochar confers several benefits to agricultural soils, such as an increase in biodiversity and retention of water and nutrients [6,7]. In this context, the International Biochar Initiative (IBI) highlighted the importance of the analytical characterization and certification of biochar products in agriculture [8].

The Association of Official Agricultural Chemists (AOAC) recommends the vanadomolybdate yellow photometric method for P determination in fertilizers, which is based on the stable yellow-colored complex developed when an excess of a molybdate solution is added to an acidified solution of vanadate and orthophosphate [9,10]. Nowadays, faster and more efficient analytical techniques, such as inductively coupled plasma optical emission spectrometry (ICP-OES) and high-resolution continuous-source flame atomic absorption spectrometry (HR-CS FAAS), are used routinely to determine P in fertilizers and other matrices [11,12]. All these techniques, however, require P in solution; thus, solid matrices must be solubilized prior to analysis, which is not a simple task for biochars that are extremely recalcitrant materials [13]. In particular, biochar solubilization generally involves the use of highly oxidizing reagents together with high temperatures and pressures or decomposition in dry conditions using fluxing agents. These procedures increase the analytical time and sample contamination risks and generate chemical residues. Therefore, a method that enables the direct, rapid and waste-free determination of P in biochar would be more efficient to respond to actual analytical demands.

Laser-induced breakdown spectroscopy (LIBS) is a relatively novel, attractive analytical technique that reflects the technological development in analytical chemistry and is expected to be very promising for P determination in agricultural materials [14]. The analytical principle on which LIBS is based consists in the optical emission of species previously excited in a plasma obtained by a pulsed laser beam at nano-to-femtosecond intervals. During the expansion and cooling of the plasma, atoms and ions relax to fundamental energy states emitting light frequencies in the UV-visible-NIR range, which are related to their underlying electronic transitions [15]. The intensity of the emission lines treated with appropriate calibration methods can then provide quantitative information about the elements present in the plasma, i.e., in the sample [15].

LIBS features several analytical advantages including simplicity, reduced sample handling, relatively short analytical times, direct and minimally destructive analysis, and no chemical waste generation. However, this technique presents some as yet unresolved problems, such as low sensitivity and matrix effects, which make it difficult to find appropriate standards for calibration. In particular, the severe matrix effects that affect LIBS measurements, especially in the case of complex matrices such as biochars, are a challenging factor in its analytical application [16]. In particular, Morais et al. (2017) found that the incorporation of Ca^{2+} ions into biochar to produce controlled-release fertilizer changed their original properties, and also those of the calibration standard prepared by simple physical mixing of biochar and Ca^{2+} ions [17]. Thus, an adequate accuracy for Ca predictions was reached by using internal standardization together with matrix matching.

In general, LIBS has high limits of detection (LOD) compared to consolidated analytical techniques such as ICP-OES [15]; thus, the configuration of a classical LIBS system did not allow the detection of P lines. Therefore, to solve this inconvenience, Viera et al. (2018) coupled LIBS to a spark discharge (SD) system to analyze P in various fertilizers [18].

In the context of the emerging demand for biochar products certification for agricultural use, the aim of this study was to attempt the use of SD-LIBS and matrix matching for P determination in different kinds of biochar-based fertilizers.

2. Materials and Methods

2.1. Samples and Calibration Standards

Samples of controlled-release biochar-based fertilizers were prepared from three substrates, i.e., eucalyptus ground leaves and branches, banana fiber and peanut shells, biomasses coming from agricultural tailings in Brazil whose biochar did not contain P level detected by SD-LIBS. To produce the biochar-based fertilizers, approximately 3.0 g of each biomass (raw material) was transferred to Erlenmeyer flasks containing 100 mL of a 2.70 g L^{-1} P solution that was prepared by solubilizing $(NH_4)_2HPO_4$ in high-purity deionized water. The flasks were placed in an incubation chamber at 25 °C and shaken for 24 h with orbital agitation at 150 rpm. Then, the biomasses were separated by filtration and

dried in an oven at 40 °C for 24 h. Successively, approximately 2.0 g of each biomass with incorporated P was transferred to porcelain crucibles that were covered with an aluminum foil to keep the atmosphere with limited oxygen, and submitted to the pyrolysis process in a muffle (under atmospheric conditions) to obtain the biochar-based fertilizer. The heating program consisted of raising the temperature to 260 °C at a rate of 10 °C min^{-1}, and maintaining it for 60 min. Then, the muffle was allowed to cool down to a temperature close to 60 °C, and the crucibles were removed. The second stage of cooling to room temperature was conducted in a gas exhaust hood. The above procedure was repeated three times for each biomass. The samples were then homogenized using an agate mortar and pestle, and aliquots of 300 mg were transferred to a carbon steel mold to make pellets by applying a pressure of 738.8 MPa on the mold using a hydraulic press.

Calibration standards were prepared based on the concept of matrix matching by adding increasing amounts of $(NH_4)_2HPO_4$ to 0.1 g of pure eucalyptus biochar obtained by the same pyrolysis process described above. Cellulose (type 101 Sigmacell) was used as a diluent to bring the standards final weight to 300 mg. The solid standards were then homogenized using an agate mortar and pestle and subjected to a pressure of 10 ton to obtain the pellets. The final content of P in the standards ranged from 0.00% to 11.7% *w*/*w*.

2.2. SD-LIBS Analysis and Validation

Spectra were acquired using a LIBS system equipped with a 1064 nm Q-switched Nd:YAG laser (Quantel, Big Sky Ultra 50, Bozeman, MT, USA) operated at 50 mJ maximum power energy with pulse duration lower than 8 ns, which provided an irradiance of about 9.7 GW cm^{-2} at the focal point. The system also included an optical fiber bundle and four spectrometers Ocean Optics (HR2000+, Dunedin, FL, USA) featuring an optical resolution of 0.1 nm (full width at half maximum) and covering a spectral range from 200 nm to 630 nm. The gate time and the Q-switch delay used for spectra acquisition were 1 ms and 2 μs, respectively.

Each sample pellet was placed into a sampler that could be moved in the x and y directions. The pellets' surface was adjusted in the focal point of the waist of the laser beam (lens to sample distance, 12 cm). A previously used SD system [18] was coupled to the LIBS instrument to improve signal detectability.

Twenty emission spectra were acquired, resulting from 10 laser pulses scattered on both flat faces of each pellet, and individually pre-processed for baseline correction. The average intensities of the P atomic line at 253.55 nm were used.

To assess the accuracy of the proposed method, 100 mg of each fertilizer sample was solubilized using 3.00 mL of HNO_3 70% (*v*/*v*), 2.00 mL of high-purity deionized water and 1.00 mL of H_2O_2 30% (*v*/*v*) in a microwave oven. The digested solutions were then diluted to 20.00 mL, homogenized and analyzed by HR-CS-FAAS. Obtained data were then compared to those achieved by SD-LIBS by applying the paired *t*-test.

3. Results and Discussion

The SD-LIBS spectra measured for the three samples (Figure 1) featured four P atomic lines in the spectral range from 250 to 262 nm. Similar spectra were acquired from the calibration standards (one example is shown in Figure 2 for the standard with 11.7 wt% P). The most intense line at 253.55 nm was chosen as indicator of P concentration, although it was not fully resolved from the line at 253.40 nm, that is, however, also assigned to the analyte (Figure 3).

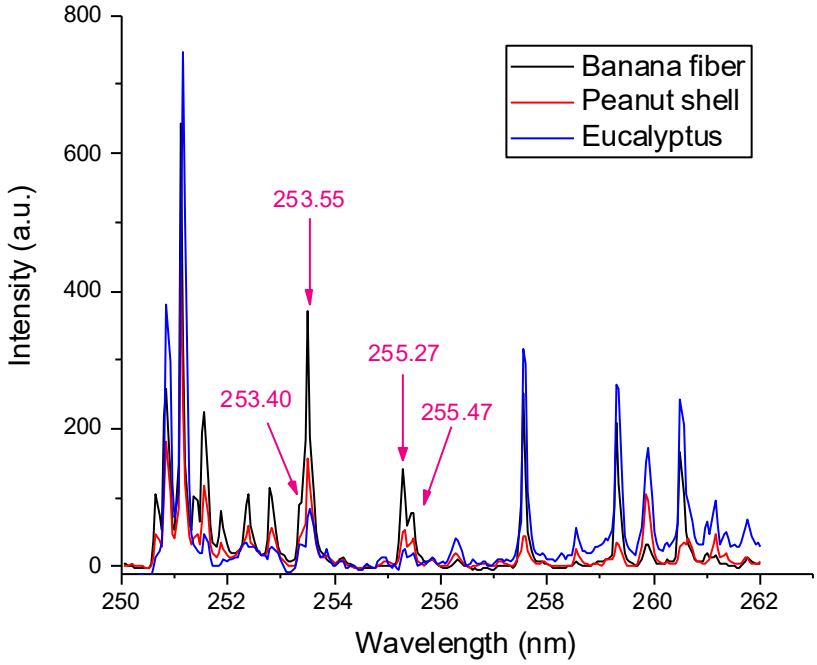


Figure 1. SD-LIBS spectra of the three biochar-based fertilizers with incorporated P in the range from 250 to 262 nm.

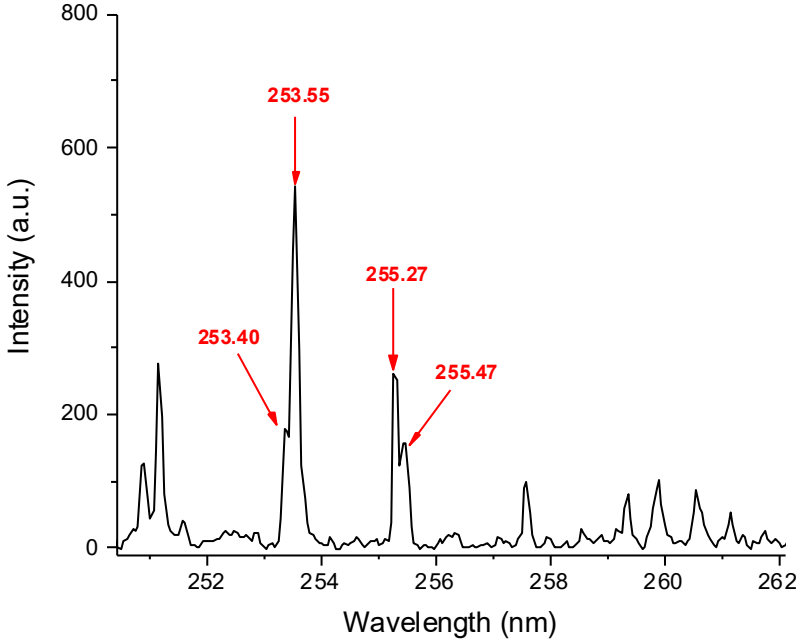


Figure 2. SD-LIBS spectrum of the calibration standard with 11.7 P wt% in the range from 250 to 262 nm.

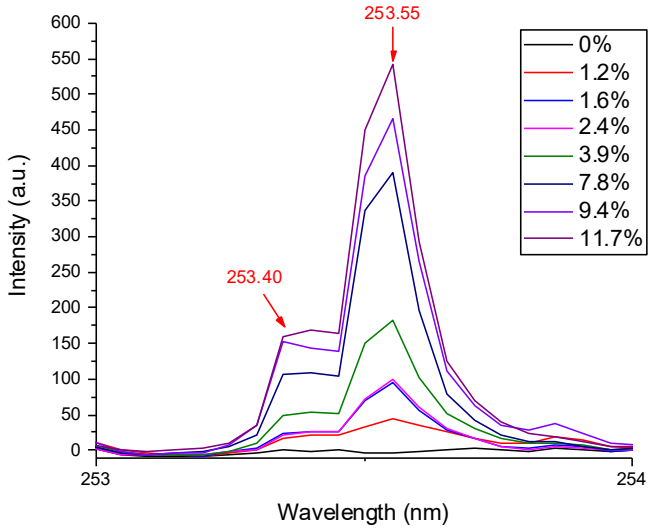


Figure 3. P (I) emission lines at 253.40 and 253.55 nm for the calibration standards.

Although Morais et al. showed that the incorporation of Ca^{2+} ions into biochar changed their original properties, making the fertilizer distinct from pure biochar and also from the calibration standard prepared by physical mixing of eucalyptus biochar and Ca^{2+} [17], the matrix-matching procedure was evaluated here using P. The linear prediction model (analytical curve) fitted by correlating the intensity of the P (I) LIBS line at 253.55 nm and P wt% in the standards achieved a value of $R^2 = 0.9957$ over the linear range from 0.71 to 11.73 wt% P and a sensitivity of 47.835 (Figure 4). The estimated limits of detection and quantification were 0.21 and 0.71 wt% P, respectively. Although R^2 provides an estimate of the strength of the relationship between the signals and the P wt%, it does not provide a formal hypothesis test for this relationship. Thus, the analysis of variance (ANOVA) was applied to validate the correlation. The *p*-value for the global F test was 0.00, less than its level of significance, i.e., 0.05, which confirmed that the value of R^2 was significantly different from zero and the calibration model was efficient for P wt% prediction.

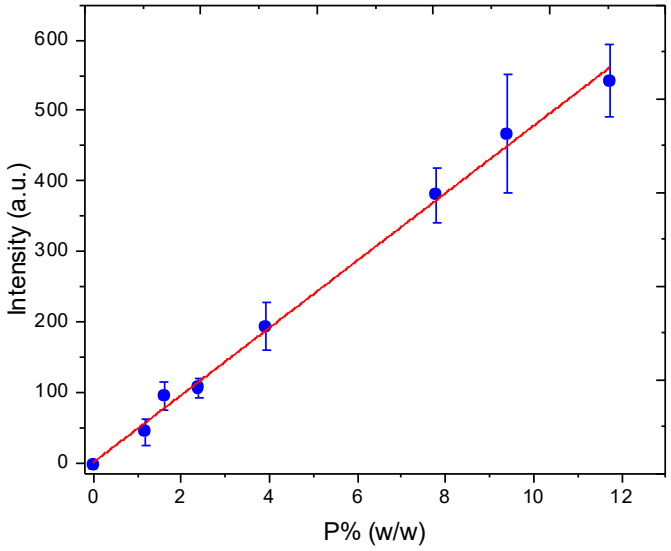


Figure 4. Correlation between the intensities of the P (I) LIBS line at 253.55 nm and P wt% measured by HR-CS-FAAS in the calibration standards (the standard deviation is referred to the mean intensity, calculated for 20 repetitions).

The linear model so obtained was then applied to predict the P wt% level in the three biochar-based fertilizer samples. The predictive capacity of the model with respect to the reference method, and the calculated t-values are shown in Table 1. The student's *t*-test applied to compare the results showed that the P wt% determined by SD-LIBS had no statistical difference from that determined by the reference method at 99% confidence level.

Table 1. P wt% determined by SD-LIBS and the HR-CS-FAAS reference technique in biochar-based fertilizer samples (n = 3 for both methods).

Biochar Fertilizer Source	P wt%		t-Calculated	t-Tabulated (α = 0.005 and DF = 4 **)
	SD-LIBS	HR-CS FAAS		
Eucalyptus	1.30 ± 0.13 *	1.10 ± 0.09	1.461	4.604
Banana fiber	3.71 ± 0.05	3.28 ± 0.24	2.025	
Peanut shells	1.85 ± 0.16	0.98 ± 0.21	3.805	

* Standard deviation of the mean concentration of P (wt%), calculated for three sample repetitions. ** DF—Degrees of freedom.

Unlike the results obtained with Ca by Morais et al. [17], matrix matching for P was adequate to reach a satisfactory accuracy. These results would suggest that Ca and P interact in different ways with biochar and the process that culminates in the excitation of P in LIBS plasma, unlike Ca, was similar for the standards and the samples.

In addition to greater calibration simplicity, the proposed analytical method has built-in the characteristics of LIBS in terms of analytical simplicity, rapid analysis with no chemical waste and little sample preparation, dispensing chemical reagents and the drastic conditions of temperature and pressure, conventionally used. The method also stands out for its cost-effectiveness and for being an eco-friendly solution. However, further studies must be conducted to assess the appropriateness of the calibration strategy for biochar-based fertilizers from different sources.

4. Conclusions

A novel, simple, fast, eco-friendly and non-chemical waste-producing method based on SD-LIBS was proposed for the direct P determination in controlled-release biochar-based fertilizers. A simple procedure of matrix matching using eucalyptus biochar with P added allowed one to reach an adequate accuracy for P determination in fertilizers prepared from three different agricultural residues. Although an evaluation for new fertilizers is required, the method is promising, affording a simple solution for characterization and certification of biochar products and meeting the IBI demands in an ecologically correct and economically viable way.

Author Contributions: Conceptualization, E.C.F. and C.A.R.; Formal analysis, S.R.D.; Data curation, E.C.F.; Writing—original draft preparation, E.C.F.; Writing—review and editing, G.S.S. and J.A.G.N.; Funding acquisition, E.C.F. All authors have read and agreed to the published version of the manuscript.

Funding: This research was funded by São Paulo Research Foundation—FAPESP, Grant number 2015/24757-9 and Conselho Nacional de Desenvolvimento Científico e Tecnológico—CNPq for the research grant to E.C.F., Grant number 308200/2018-7.

Institutional Review Board Statement: Not applicable.

Informed Consent Statement: Not applicable.

Data Availability Statement: Not applicable.

Conflicts of Interest: The authors declare no conflict of interest. The funders had no role in the design of the study; in the collection, analyses, or interpretation of data; in the writing of the manuscript, or in the decision to publish the results.

References

1. Hammond, J.P.; Broadley, M.R.; White, P.J. Genetic responses to phosphorus deficiency. *Ann. Bot.* **2004**, *94*, 323–332. [CrossRef] [PubMed]
2. Rozo, G.; Bohorques, L.; Santamaría, J. Controlled release fertilizer encapsulated by a κ-carrageenan hydrogel. *Polímeros* **2019**, *29*, 1–7. [CrossRef]
3. Zhang, T. *Phosphorus—Recovery and Recycling*, 1st ed.; IntechOpen: London, UK, 2019; p. 104.
4. Quijón, M.E.G. Development of an Urea-Based Controlled-Release Nitrogen Fertilizer Using Biochar as Support Material. Ph.D. Thesis, Universidad de la Frontera, Temuco, Chile, 2013. Available online: https://doctoradorrnn.ufro.cl/wp-content/uploads/2021/01/49-maria-eugenia-gonzalez.pdf (accessed on 24 November 2021).
5. Cen, Z.; Wei, L.; Muthukumarappan, K.; Sobhan, A.; McDaniel, R. Assessment of a biochar-based controlled release nitrogen fertilizer coated with polylactic acid. *J. Soil Sci. Plant Nutr.* **2021**, *21*, 2007–2019. [CrossRef]
6. Atkinson, C.J.; Fitzgerald, J.D.; Hipps, N.A. Potential mechanisms for achieving agricultural benefits from biochar application to temperate soils: A review. *Plant Soil* **2010**, *337*, 1–18. [CrossRef]
7. Fang, Y.; Singh, B.; Singh, B.P.; Krull, E. Biochar carbon stability in four contrasting soils. *Eur. J. Soil Sci.* **2014**, *65*, 60–71. [CrossRef]
8. International Biochar Initiative (IBI). Available online: http://www.biochar-international.org (accessed on 19 July 2021).
9. Hoffman, W.M. AOAC Methods for the determination of phosphorus in fertilizers. *J. AOAC Int.* **1964**, *47*, 420–428. [CrossRef]
10. Hanson, W.C. The photometric determination of phosphorus in fertilizers using the phosphovanado-molybdate complex. *J. Sci. Food Agric.* **1950**, *1*, 172–173. [CrossRef]
11. Yang, W.M.; Boles, R.L.; Mawhinney, T.P. Determination of phosphorus in fertilizers by inductively coupled plasma atomic emission spectrometry. *J. AOAC Int.* **2002**, *85*, 1241–1246. [CrossRef] [PubMed]
12. Welz, B.; Vale, M.G.R.; Pereira, E.R.; Castilho, I.N.B.; Dessuy, M.B. Continuum source atomic absorption spectrometry: Past, present and future aspects—A critical review. *J. Braz. Chem. Soc.* **2014**, *25*, 799–821. [CrossRef]
13. Corazza, G.; Henn, A.S.; Mesko, M.F.; Duarte, F.; Flores, E.; Mello, P. Microwave-induced combustion of coal for further sulfur determination by inductively coupled plasma optical emission spectrometry or ion chromatography. *J. Braz. Chem. Soc.* **2016**, *27*, 1569–1576. [CrossRef]
14. Yu, K.; Ren, J.; Zhao, Y. Principles, developments and applications of laser-induced breakdown spectroscopy in agriculture: A review. *Artif. Intell. Agric.* **2020**, *4*, 127–139. [CrossRef]
15. Miziolek, A.W.; Palleschi, V.; Schechter, I. *Laser-Induced Breakdown Spectroscopy (LIBS): Fundamentals and Applications*, 1st ed.; Cambridge University Press: Cambridge, UK, 2006; pp. 1–40.
16. Radziemski, L.J.; Cremers, D.A. *Laser-Induced Plasmas and Applications*, 1st ed.; Marcel Dekker Inc.: New York, NY, USA, 1989; p. 440.
17. De Morais, C.P.; Barros, A.I.; Júnior, D.S.; Ribeiro, C.A.; Crespi, M.S.; Senesi, G.S.; Neto, J.A.G.; Ferreira, E.C. Calcium determination in biochar-based fertilizers by laser-induced breakdown spectroscopy using sodium as internal standard. *Microchem. J.* **2017**, *134*, 370–373. [CrossRef]
18. Vieira, A.L.; Silva, T.; de Sousa, F.S.I.; Senesi, G.; Júnior, D.S.; Ferreira, E.C.; Neto, J.A.G. Determinations of phosphorus in fertilizers by spark discharge-assisted laser-induced breakdown spectroscopy. *Microchem. J.* **2018**, *139*, 322–326. [CrossRef]